SYNTHESIS AND EVALUATION OF SMALL MOLECULE BASED REACTIVE OXYGEN SPECIES (ROS) GENERATORS

A THESIS

SUBMITTED IN PARTIAL FULFILMENT OF THE REQUIREMENTS

OF THE DEGREE OF

DOCTOR OF PHILOSOPHY

BY

A. DHARMARAJA

20103049

INDIAN INSTITUTE OF SCIENCE EDUCATION AND

RESEARCH PUNE – 411 008

2014

Dedicated to…

My Parents

भारतीय विज्ञान शिक्षा एवं अनुसंधान संस्थान, पुणे
INDIAN INSTITUTE OF SCIENCE EDUCATION AND RESEARCH (IISER), PUNE
(An Autonomous Institution, Ministry of Human Resource Development, Govt. of India)
900 NCL Innovation Park Dr Homi Bhabha Road Pune 411008

Harinath Chakrapani, Ph.D.
Assistant Professor – Chemistry
www.iiserpune.ac.in/~harinath/

CERTIFICATE

Certified that, the work incorporated in the thesis entitled, "***Synthesis and evaluation of small molecule based reactive oxygen species (ROS) generators***" submitted by ***A. Dharmaraja*** was carried out by the candidate, under my supervision. The work presented here or any part of it has not been included in any other thesis submitted previously for the award of any degree or diploma from any other University or institution.

Date: 24th October 2014 **Dr. Harinath Chakrapani**

Pune (MH), India.

DECLARATION

I declare that this written submission represents my ideas in my own words and where others' ideas have been included; I have adequately cited and referenced the original sources. I also declare that I have adhered to all principles of academic honesty and integrity and have not misrepresented or fabricated or falsified any idea/data/fact/source in my submission. I understand that violation of the above will be cause for disciplinary action by the Institute and can also evoke penal action from the sources which have thus not been properly cited or from whom proper permission has not been taken when needed.

Date: 24th October 2014 **A. Dharmaraja**

Pune (MH), India. **20103049**

Table of Contents

General remarks

- ^{1}H NMR spectra were recorded on JEOL ECX 400 or Bruker Avance 500 MHz spectrometer using tetramethylsilane (TMS) as an internal standard. Chemical shifts are expressed in ppm units downfield to TMS.
- ^{13}C NMR spectra were recorded on JEOL ECX 100 or Bruker Avance 125 MHz spectrometer.
- High resolution mass spectrometry (HRMS) was performed on Waters Synapt G2 and Maldi-TOF.
- IR spectra were recorded on Perkin-Elmer 1310 and Perkin-Elmer 1600 FT-IR spectrometers with sodium chloride optics and are measured in cm^{-1}.
- All reactions were monitored by Thin-Layer Chromatography carried out on precoated Merck silica plates (F254, 0.25 mm thickness); compounds were visualized by UV light and staining with anisaldehyde or 2,4-dinitrophenylhydrazine spray.
- All reactions were carried out under nitrogen or argon atmosphere with freshly dried solvents under anhydrous conditions and yields refer to chromatographically homogenous materials unless otherwise stated.
- All evaporations were carried out under reduced pressure on Büchi and Heildoph rotary evaporator below 45 °C unless otherwise specified.
- Silica gel (60-120) and (100-200) mesh were used for column chromatography.
- Materials were obtained from commercial suppliers and were used without further purification.
- Scheme, Figure and Compound numbers in abstract and individual chapters are different.

Abbreviations

Å – Angstrom

Ac – Acetyl

ACN – Acetonitrile

AcOH – Acetic acid

ADP – Adenosine diphosphate

ATP – Adenosine triphosphate

AU – Arbitrary unit

Bn – Benzyl

BnBr – Benzyl bromide

bs – Broad singlet

B. Subtilis – Bacillus subtilis

Calcd – Calculated

Cat – Catalase

CI – Chemical ionization

Conc – Concentrated

d – Days

dd – Doublet of doublet

DCM – Dichloromethane

DIPEA – *N*,*N*-Diisopropylethylamine

DMAP – *N*,*N*-Dimethylaminopyridine

DMF – *N*,*N*'-Dimethyl formamide

DNA – Deoxyribonucleic acid

dt – doublet of triplet

δ – Delta (in PPM)

E. coli – Escherichia coli

eq. – Equivalents

ESI – Electron spray ionization

Et – Ethyl

Et_3N – Triethylamine

EtOH – Ethanol

EtOAc – Ethyl acetate

Et_2O – Diethyl ether

g – Gram

GSH - Glutathione

h – Hour

HPLC – High Performance Liquid Chromatography

HRMS – High-Resolution Mass Spectrometry

Hz – Hertz

IR – Infrared

J – Coupling constant

Kg – Kilogram

m – Multiplet

MDR – Multidrug resistant

Me – Methyl

MeOD – Methanol-D_4

mg – Milligram

MIC – Minimum inhibitory concentration

min. – Minutes

MHz – Megahertz

mL – millilitre

mmol – millimolar

m.p. – Melting point

MS – Mass spectrum

MSSA – Methicillin sensitive *Staphylococcus aureus*

MRSA – Methicillin resistant *Staphylococcus aureus*

Msm – Mycobacterium Smegmatis

Mtb – Mycobacterium tuberculosis

MW – Molecular weight

m/z – Mass to Charge ratio

n-BuLi – *n*-Butyllithium

NMR – Nuclear Magnetic Resonances

P. aeruginosa – *Pseudomonas aeruginosa*

pH – Potential of hydrogen

Py – Pyridine

ppm – Parts per million

R*f* – Retention factor

RT – Room temperature

s – Singlet

SAR – Structure activity relationship

S. aureus – *Staphylococcus aureus*

sat – Saturated

SOD – Superoxide dismutase

t – Triplet

Tb – Tuberculosis

TEA - Triethylamine

TFA – Trifluoroacetic acid

THF – Tetrahydrofuran

TLC – Thin Layer Chromatography

TMS – Tetramethylsilane

UV - ultraviolet

µg – Microgram

µmol – Mmicromolar

µL – Microliter

XDR – Extremely drug resistant

XRD – X-ray diffraction

WT – Wild type (bacterial strain)

Acknowledgements

This is by far the most important part of my thesis. Organic and medicinal chemists often define their achievements in terms of the number of drug scaffolds they have developed or the number of novel reactions they have carried out. Yet, I realize that my greatest achievements have been the professional and personal relationships I have developed that have gotten me to this stage in life. So it is with tremendous gratitude that I write these acknowledgements to show my appreciation to some of the people who have helped me throughout the years.

IISER-Pune is an amazing place to conduct research, and its commitment to excellence is showcased by developments in multidisciplinary research and education. I thank Professor K. N. Ganesh, the Director, IISER-Pune for providing a world class laboratory and state of art instruments to conduct research. Professor Srinivas Hotha and Dr. C. V. Ramana have been my research advisory committee (RAC) board members for whom I owe a lot. Prof. Hotha is a friendly, motivated and fearless glycochemist who is never afraid of thinking big (Arbinoglactan-24 glycosidic units). I cannot begin to describe how much I have learned from Prof. Hotha through all of our discussions. He has had a tremendous influence on how I think of chemistry, and I hope to continue to learn from him in the future. Dr. C. V. Ramana, is One of the famous synthetic organic chemists in National Chemical Laboratory (NCL) – Pune. Dr. C. V. Ramana's critical feedback and research input during my RAC evaluations have helped me in putting extra efforts to precisely plan my research and execute them. I consider myself very fortunate to have had this opportunity to interact with the members of my RAC committee and other distinguished faculty members at IISER-Pune, and I look forward to staying in touch with them.

I would like to extend my thanks to my co-workers in the Hari's group. Satish Malwal has joined just 5 months before me as a first graduate student in the Hari's group; he had been excellent and helped in the initial stages to setup the research facilities together. We have had great and tough times in setting up the lab since we were the first 2 students of Dr. Hari's Lab. My lab juniors Kavita Sharma, Vinayak Khodade, Kundan Singh, R. Sankar, G. Ravikumar, Amogh Kulkarni were really good and supportive at maintaining

the lab standards and arranging new facilities. Kavita is coolest and cheerful in the lab, works really well, and sincerely takes care of her lab responsibilities. Among the members, I got opportunities to work with Vinayak, Sankar, Ravi and Amogh. More than they learned from me, I benefitted a lot from them, I was highly impressed by their motivation and interest in research. Kundan is good at lab and highly excited all the times. Myself and Kundan used to go out for playing and tasting cuisines around Pune. We have got highly motivated under graduate students Rohan Kumbhare, Sarath Chandra and Charu Jain to work in our lab for their summer internships, they keep the playful atmosphere in lab. All our group members have kept a pleasant and lively lab atmosphere in which I could work effectively and without noticing 5 years of time passed like few days. New additions to the list of Dr. Hari's graduate students, Ajaykumar Sharma and Preeti Chauhan are highly motivated and I am sure they will keep the cheerful lab atmosphere. Our advisor has high standards for his graduate students because he is fortunate enough to have enthusiastic and energetic members like them. The friendships I have developed with the entire Hari's group will last a lifetime. It is such a supportive environment for conducting research.

My special thanks to Dr. Pinaki talukdar and his group for their support when I first came to IISER-Pune. We had our group meetings together and fruitful discussions with Dyaneshwar, Sharad and Dinesh. IISER-Pune faculty members Dr. Srivatsan helped me in setting up HPLC and DNA damage assays, and Dr. Jayakannan supported and provided the facility of cyclic voltammetry and taught me the result interpretations. I thank all faculty members of chemistry for their constant support and encouragements duing my stay at IISER-Pune. I thank Dr. Mayurika Lahiri from Department of Biology, IISER-Pune, who has helped me learning biological assays when I was anxious about learning biological sciences. Dr. Mithali, Payal, Libi, Abhinav, Surojit and Satish from Dr. Mayurika's lab were really supportive and helping. On this occasion, I should acknowledge our collaborators, Dr. Badrinath, NISER-Bhubaneswar for providing anticancer activities for my first ROS project, Dr. Sriram, BITS-hyderabad for anti-mycobacterial studies of my second ROS project and Dr. Amit Singh and Priyanka Tyagi for their efforts in studying the mechanisms of ROS in inhibiting Mycobacterium

tuberculosis. I am genuinely grateful to collaborators, as we would not have successfully directed our research on ROS without their support.

Over the years at IISER-Pune I have been blessed with many good friends. Anantharaj had been with me from the starting of my PhD, he is quite, cool, skillful, hard worker and difficult to write his qualities. He is one of the close friends of mine and I am sure will continue his friendship for my life time. Shivaji is from Lab 102, is the highly motivated, hardworking and inspirational personality, I am fortunate to have his friendship. We used to go to Gym together and give competitions but never bothered who is winning, we have organized many touring events like trekking and all old memories will be there with us forever, I should thank him for keeping me in the circle and had a wonderful time. I thank the support and encouragement I received from friends of IISER-Pune, Pramod, Wilbee, Bijoy, Maidul, Venki, Balu, Tushar, Maroti, Anupam, Arun, etc.

My roommates Gopal, Ganesh, Kiran, Satheesh and Rajesh were so cooperative during our two years of stay outside IISER-Pune, all are telugu natives and I got an excellent opportunity to learn telugu, what a wonderful language, Satheesh played the best part in teaching me. Ganesh needs a special mentioning as me and Ganesh were again roommates in IISER-hostel, I am really fortunate to have these people in my life. Shivashankar, Sureshkumar, Manikandan, Manoharan, Vijayakanth, Ananthakumar, Rajasekar, Balamurugan from IISER-pune, have arranged Chithirai sanagamam functions for tamil new year celebrations, I thank them for creating a joyful atmosphere, had a wonderful time with them at IISER.

Sports at IISER-Pune had been a great entertainment for me; IISER students have given me opportunities to participate in all the sports events conducted at IISER – IPL (IISER-Premier league tournaments), IISM (Inter-IISER Sports meet), IBL (IISER-Badminton League) and Kreeda Jung in Cricket, volleyball, badminton, table tennis and carom. I thank all those who made my walk at IISER a playful journey, in particular the team "ALCHEMIST", and players, Dr. Sandip, Dr. Amar, Dr. Prakash, Dr. Sachin, Trimbak, and all others. A special mentioning to Dr. Srivatsan (Cricket), Dr. Vaidhyanathan (Badminton) and Dr. Srinivas Hotha (Badminton) at their age I am not sure even I would be half-enthusiastic as they are now in sports, great inspiration.

At this point, I would like to thank my colleagues and friends who helped me before I came to IISER-Pune. Dr. Malathi, Dr. Manikandan and Dr. Balu Uphade from Dow Chemical Int. Pvt. Ltd., were really inspiring and encouraged me to join IISER-Pune for PhD, and I have got a lot advice on planning my activities. Dr. Malathi needs a special citing here, She is a multi-talented individual, quite talkative and an excellent friend of mine, proof read my thesis, a great thanks to her and family for their support. Dr. Kannan and Sangeetha kannan are like my family members, always Kannan has been with me (while playing, reading, working etc), I have shared all the moments with him and many times he had been the one to know first, who has helped me tremendously in writing my thesis. Mohan Raj is not just my friend, as a senior he had taught me experimental science during my M.Sc at Bharathidasan University. Professor K. Panchanatheswaran was my MSc thesis supervisor and a great teacher, an inspirational personality I always keep him in my heart. I am fortunate to have Dr. Sivanesan, T. Rajasekaran and Venkatesh as my best friends who have been highly encouraging and motivating all through my studies. My Friends (from NCL) Dr.Mallikarjuna, Dr. Khaja, Dr. Pradeep, Dr. Vijayanand, Dr. Eshwar, Dr. Ramanujam, (from Bharathidasan University) Dr. Lalitha, Dr. Josekavita, Dr. Baby, Dr. Suguna, Dr. Krishnamoorythy, Dr. Mothi Dr. Jabadurai, all difficult to take every names and all of them were extremely good and helped me each stage along my carrier.

I must thank the most important people in my life, my family. I am nothing without them. My Dad, Allimuthu. K., is my role model in life. I need to thank him for developing my insatiable passion for pursuing knowledge. He has also taught me the value of hard work and humility. If I end up being one tenth the man that my father is, I will be a great man. My mother, Thangammal, is the backbone of our family. She has sacrificed everything to ensure that I would always be able to strive for my goals. She deserves this Ph.D. as much as I do. All my family members uncles, aunties, sister (Punitha), brothers (Chandru and Lingan) and Jothi are my strength and support all my life.

Now that I have thanked my teachers, my co-workers, my friends, and my family, I must thank the only person in this world who seems to fit in all of these categories. How do I even begin to thank Dr. Harinath Chakrapani (Hari) - my research advisor. I have never had a difficult time saying anything to him. So it is ironic that I am having difficulty in

expressing my gratitude. How can I thank a person who has done everything in his power to make sure that I succeed in life. I'm getting emotional just thinking about it. Intellectually, Hari has been an ideal advisor. I met him in the spring of 2010, from the day I joined I have changed to a great deal, but I am still learning so much from him. There is no doubt in my mind that I will be a student of Dr. Hari for the remainder of my life. As an advisor, he has always encouraged me to explore my ideas, and he has always guided me in the right direction. Hari's work ethic is inspiring, and his uncontrollable excitement for chemistry is contagious. Hari's eagerness towards multiplying collaborations to produce high quality scientific results, punctuality, foresight, practicality, focus while writing and willingness to learn are some qualities I always admire. Whenever I was losing motivation for a project, I knew that a five minute conversation with him would be enough to inspire me. Dr. Hari is known as a prolific, brilliant chemist (physical Organic Chemistry). His intellect is only surpassed by his humility. And he is by far the hardest working person I know, we used to work many late nights and Hari is also an amazing friend. He has always been there to congratulate me on the happiest days of my life, and he has always been the first one to pick me up on the most difficult days of my life. I am able to sit here today and write my acknowledgements because of Hari's support. Although the occasion of my thesis defense marks the end of my time as a member of Hari's group, it also marks the beginning of a lifelong friendship. Finally, I thank the almighty God for blessing me with strength and courage to pursue my dreams during this entire journey.

A. Dharmaraja

****

ABSTRACT

Nearly all aerobic organisms use oxygen for respiration. Electrons released during respiration from redox enzymes are accidentally abstracted by O_2 to produce superoxide ($O_2^{\bullet-}$), which is subsequently converted to hydrogen peroxide (H_2O_2). In the presence of trace metal ions such as Fe^{2+} or Cu^{+}, H_2O_2 can produce the highly reactive hydroxyl radical ($OH^{\bullet}$). Together, these species can react with the majority of biomacromolecules such as DNA, proteins and lipids, causing oxidative damage and are hence called reactive oxygen species (ROS). It is therefore not surprising that ROS are generated in immune cells to combat invading pathogens as a protective mechanism. Recently, ROS have been shown to sensitize infectious pathogens to clinical antibiotics suggesting that ROS-generating drugs could be used as antibacterials. With the rapid rise in bacteria acquiring drug resistance to most commercial antibiotics, development of new interventional strategies to help overcome drug resistance is critical. This however requires developing methodologies for the controlled generation of ROS. Although there are few methods available, none of them are suited for reliable ROS generation. Here, three distinct approaches for controlled ROS generation will be presented. First, a series of dihydrobenzoquinones were evaluated as sources of $O_2^{\bullet-}$ in physiological pH. These compounds are expected to undergo an enolization in buffer to produce a 1,4-dihydroxyarene, which are known to react with oxygen to generate ROS. In this series, ROS generation was found to depend in part on the propensity of the "keto" form of the dihydrobenzoquinone to enolize thus providing a structural handle to regulate rates of ROS generation. Having established the utility of these compounds to generate ROS in cell-free systems, we investigated the ability of these compounds to permeate cells to elevate ROS. Using an array of techniques, we provide evidence for these compounds to enhance ROS in bacteria including mycobacteria. We next exploited the utility of the ROS generator as an adjuvant to sensitize a Gram negative bacterium, *E. coli* to aminoglycoside antibiotics such as kanamycin and gentamycin. Next, a methodology for ROS generation triggered by a bacterial enzyme was developed. This enzyme activated ROS generator was found to permeate cells and enhance ROS levels inside bacteria. A spatiotemporally controlled generation of ROS was observed with this enzyme triggered ROS generator. Our comparative data suggests that this compound is better suited for the

enhancement of intracellular ROS than the routinely used ROS sources. Finally, two scaffolds for thiol activated ROS generation were synthesized and studied. Here, an enhanced induction of oxidative stress is expected through depletion of intracellular antioxidant thiols and concomitant ROS generation. This synergestic effect was anticipated to be lethal to drug resistant bacteria. When tested, we found that a majority of the compounds were highly potent *in vitro* inhibitors of methicillin resistant *Staphylococcus aureus* supporting this as a viable strategy to overcome bacterial drug resistance.

CHAPTER 1: INTRODUCTION

1.1. Oxygen:

Oxygen is an element present in the second row of the periodic table positioned next to nitrogen (N) and before fluorine (F).[1] In its molecular form oxygen exists as a colorless, odorless and tasteless gaseous diatomic molecule (O_2), and it constitutes 20.8 % by volume of the atmospheric gases and 87% of seawater by weight.[2] Oxygen is a common element in the Earth's crust (47%) and the third most abundant element in the universe ranked next to hydrogen and helium.[2] Oxygen constitutes most of the living organisms. Biomolecules like nucleic acids, proteins, carbohydrates and fats contain oxygen (Figure 1.1).[2]

Figure 1.1. Oxygen containing biomolecules

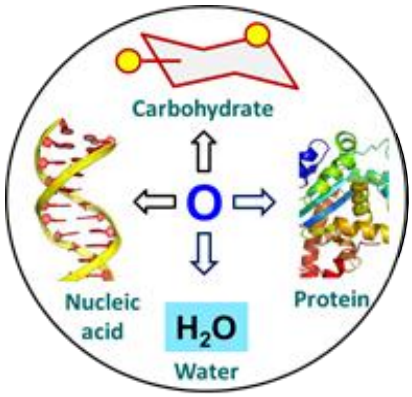

Oxygen is central to life because nearly all aerobic organisms breathe oxygen for their survival.[3] During photosynthesis, oxygen is continuously replenished in the atmosphere by the conversion of water to oxygen using sunlight as an energy source (Scheme 1.1).[4] Converse to photosynthesis, during respiration, aerobic organisms use oxygen for metabolism to produce energy, this is one of the most important biological applications of O_2.[5] In the process of cellular respiration oxygen catabolizes the biomacromolecules such as carbohydrates and proteins to carbon dioxide and produces energy, which is utilized for the needs of cellular activities in living organisms (Scheme 1.1).[6-8]

Scheme 1.1. Natural process of oxygen production during photosynthesis and its utilization during respiration for metabolism in eukaryotes

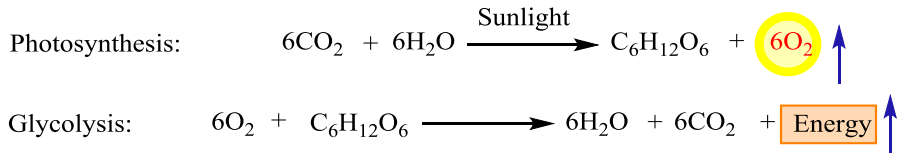

1.2. Respiration in mitochondria:

Mitochondrion, a cellular organelle found in eukaryotes, is the house of adenosine triphosphate (ATP). ATP is produced as a product of glycolysis (glucose is being oxidized to CO_2), fatty acid oxidation and amino acid oxidation.[9] Cells use ATP as an energy source for their cellular functions, so ATP is also called as cellular energy currency.[9] ATP is synthesized *via* oxidative phosphorylation of adenine diphosphate (ADP) in mitochondrial electron transport chain (ETC) during respiration (Figure 1.2).[9] ETC consists of a multi-enzyme complex, where a four electron reduction of oxygen to water occurs by controlled redox reactions and followed by release of energy. Mainly, four enzyme complexes are found to be involved in transferring electrons, *viz.*, complex I) Nicotinamide adenine dinucleotide (NADH) dehydrogenase, complex II) succinate dehydrogenase, complex III) cytochrome complex (Cyt C) and complex IV) cytochrome C oxidase. In addition to these enzyme complexes, ubiquinone (Q) and cytochrome C are found in the ETC as electron carriers (Figure 1.2).[7,9]

Figure 1.2. Mitochondrial electron transport chain

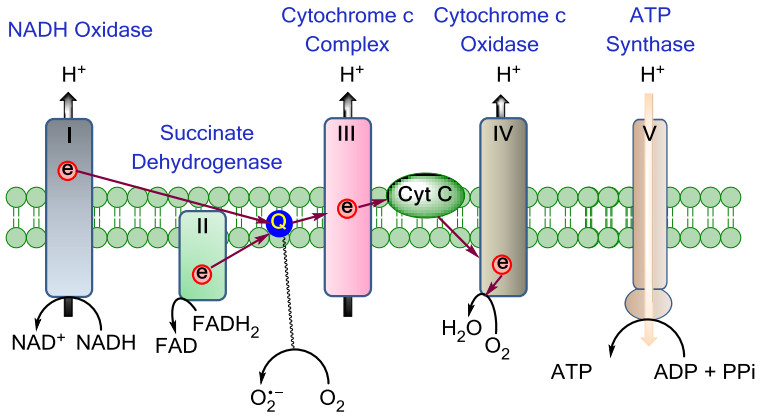

Complex I: Nicotinamide adenine dinucleotide (NADH) dehydrogenase enzyme is a large enzyme with 42 different polypeptide chains including six iron-sulfur (Fe-S) clusters and a flavin mononucleotide (FMN) containing flavoprotein (Figure 1.2). Complex I catalyzes a reversible oxidation of reduced nicotinamide adenine dinucleotide, NADH to NAD^+ and gives out two electrons and two protons (Scheme 1.2).[10] As NADH is not permeable through inner mitochondrial membrane, the electrons are transferred to ubiquinone, a fat soluble quinone, which is present in the ETC and subsequently the protons are pumped into the inner membrane space through complex I.[10]

Scheme 1.2. Oxidation of NADH to NAD^+ in respiratory complex I

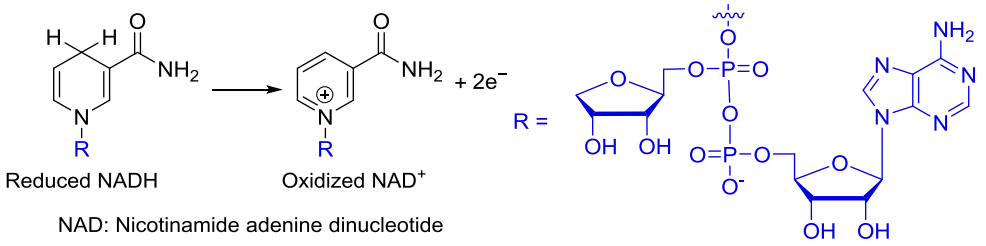

NAD: Nicotinamide adenine dinucleotide

Complex II: Enzyme complex II contains succinate dehydrogenase and is found in the citric acid cycle as the only membrane bound enzyme (Figure 1.2). At this stage of ETC, succinate is oxidized to fumarate, during the process flavin mono- and di-nucleotides are reduced to FMN and FAD, respectively (Scheme 1.3).[11] These reduced flavin adenine nucleotides, are oxidized and the freed electrons are carried by ubiquinone. The complex contains a heme group with a binding site for ubiquinone, which carries the electrons from complex II and transfers to cytochrome C.[11]

Scheme 1.3. Oxidation of $FADH_2$ to FAD in respiratory complex II

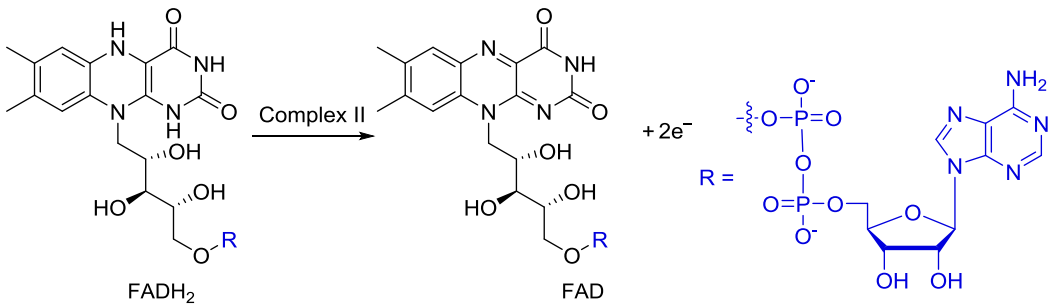

FAD: Flavine adenine dinucleotide

Ubiquinone: This is also called as Co-enzyme Q_{10} (Q_{10}), a lipid soluble 1,4-benzoquinone with a long isoprenoid side chain. Q_{10} undergoes one electron- as well as two electron- reduction. Addition of the first electron leads to the formation of ubiquinone radical intermediate and addition of the second electron produces a 1,4-diol, ubiquinol (Scheme 1.4). This diol carries electrons from complex I and II to cytochrome C oxidase (complex III). Ubiquinone is a highly diffusible small molecule in the inner mitochondrial membrane (Figure 1.2). It carries both electrons and protons, thus playing a central role in coupling electron flow to the proton movement.[12-14]

Scheme 1.4. Reduction of ubiquinone to ubiquinol by electron transfer from respiratory complexes I and II

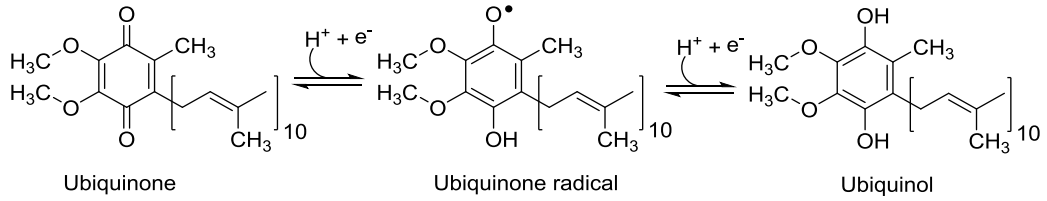

Complex III: The third respiratory complex III is the cytochrome C complex, which transfers the electrons from ubiquinol to cytochrome C in the inner membrane space; upon this reaction ubiquinone is regenerated (Scheme 1.5). A functional core of complex III has 3 subunits, viz., cytochrome C with two hemes, Fe-S protein and cytochrome with its heme (Figure 1.2). In complex III electrons are transferred from two electron transferring quinone to one electron transferring cytochrome C.[15] Cytochrome C is a small protein found in the intermembrane space, where the molecule accepts an electron from complex III and transfers to the respiratory complex IV.[15]

Scheme 1.5. Electrons transfer from ubiquinol to cytochrome C in enzyme complex III

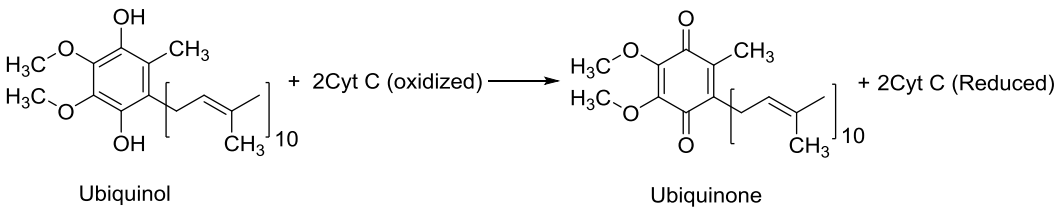

Complex IV: Complex IV is a large protein with 13 subunits positioned in the inner mitochondrial membrane. Subunit I contains two heme groups and subunit II has binuclear copper complex coordinated with -SH groups of the cysteine residues (Figure 1.2). Electron transfer from cytochrome C to oxygen in the respiratory enzyme complex IV is the final step of the electron transport chain (Scheme 1.6). Only one electron is transferred at a time to carry out the complete four electron reduction of O_2 to H_2O. During the entire process all the partially reduced oxygen intermediates are tightly regulated.[9]

Scheme 1.6. Four electron reduction of O_2 to H_2O in enzyme complex IV

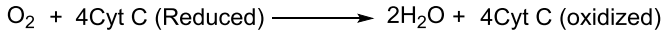

Complex V: The synthesis of ATP from ADP and phosphate (Pi), catalyzed by the ATP synthase in the inner membrane, which is driven by proton motive force (Figure 1.2). Energy released from enzyme complexes I – IV is conserved by the proton motive force. Approximately 200 kJ/mol of energy is released per pair of electron transfer and the energy utilized for the ATP synthesis is 50 kJ/mol (Scheme 1.7).[7,9]

Scheme 1.7. ATP synthesis catalyzed by ATP synthase in mitochondria

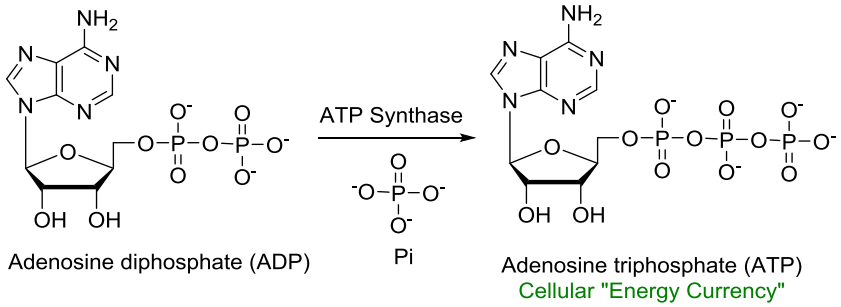

During cellular respiration, glucose is oxidized to carbon dioxide (CO_2) to produce 30 molecules of ATP per glucose molecule. It is a thermodynamically favoured process as oxidation of glucose to CO_2 has a high standard free energy of $\Delta G°$ is equal to`–2840 kJ/mol.[7] In the ETC, O_2 is converted into H_2O through a $4e^-$ reduction process and the energy released is used for ATP synthesis. Oxygen is reduced by a sequential one-electron transfer process in the mitochondrial electron transport chain to water. Succinate

dehydrogenase enzyme complex-II in the mitochondrial ETC is not linked with the inner mitochondrial membrane, which usually transfers electrons to ubiquinone. During this process electrons are leaked from ETC and directly transferred to oxygen and produce reduced oxygen species. Apart from enzyme complex II, reduced ubiquinone (ubiquinol) and enzyme complexes I and III also have been identified to transfer electrons directly to oxygen inadvertently to generate partially reduced oxygen species. For example, premature reduction of oxygen by one electron produces superoxide radical anion, $O_2^{\bullet -}$. Subsequent divalent reduction forms peroxide, O_2^{2-}, which then can react with trace metal ions present in biological systems to generate $OH^{\bullet}$ radical. All these species are known to oxidatively damage biomacromolecules such as DNA, proteins and lipids, thus collectively called as reactive oxygen species (ROS).[12,16,17]

1.3. Reactive Oxygen Species (ROS):

Reactive oxygen species is a collective term used for defining highly reactive molecules which can either be neutral or radical species containing oxygen. Some of the examples are: singlet oxygen $^1O_2$, superoxide radical anion $O_2^{-\bullet}$, hydrogen peroxide H_2O_2, hydroxyl radical $OH^{\bullet}$, organoperoxyl radical $ROO^{\bullet}$, hypochlorite anion OCl^-, and peroxynitrite anion $ONOO^-$ (Scheme 1.8A).[18,19] These species are known to oxidize biomacromolecules such as DNA, proteins and lipids and enhance stress called oxidative stress, inside the cells (Scheme 1.8B). Among these, ROS, $O_2^{-\bullet}$, H_2O_2 and $OH^{\bullet}$ are frequently formed during cellular respiration.[12,18,20,21]

Scheme 1.8. (A). General scheme for ROS production; (B). Damaging effects of ROS to biomacromolecules

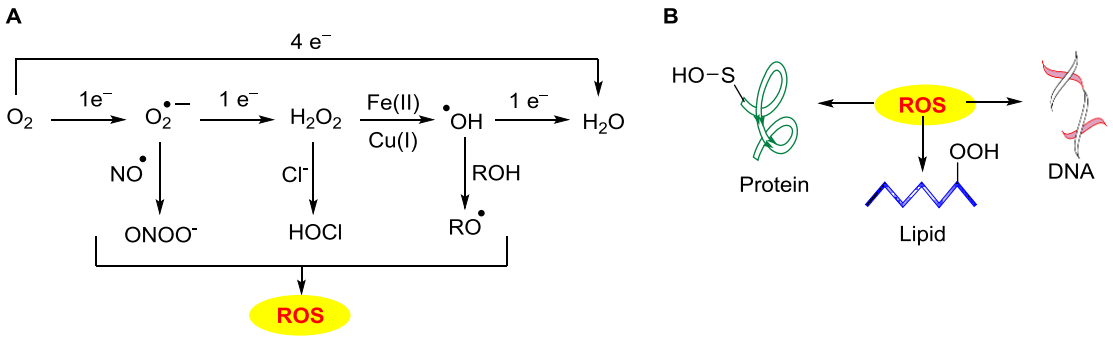

Figure 1.3. Electronic configuration of oxygen and its reduced species.

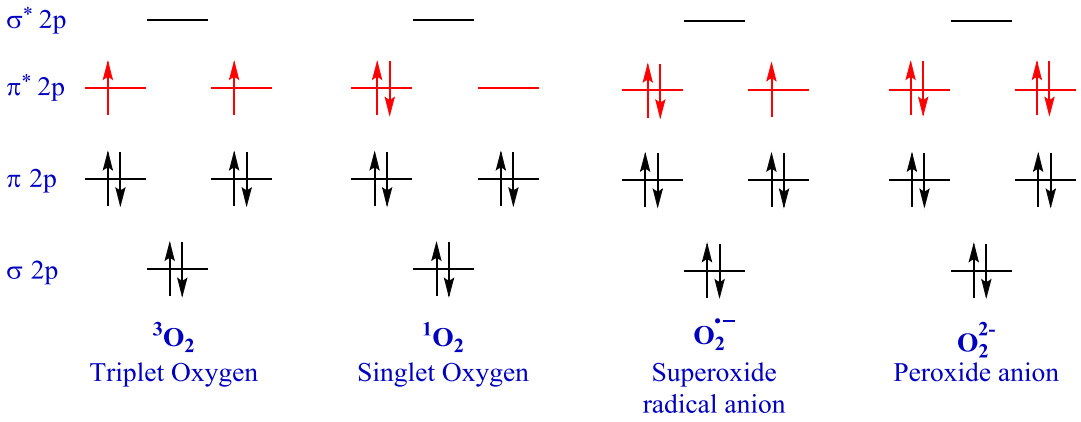

1.3.1. Molecular oxygen, $^3O_2$:

Oxygen is a neutral molecule with two unpaired electrons occupying the π* 2p orbitals with parallel spins in its ground state called triplet state (Figure 1.3). Diamagnetic molecules with empty π* orbitals are more reactive than the half-filled paramagnetic molecules. Thus molecular oxygen is relatively less reactive than the diamagnetic form, the singlet oxygen $^1O_2$.[22]

1.3.2. Singlet oxygen, $^1O_2$:

The electrons in the π* 2p orbitals of molecular O_2 are paired to give a diamagnetic neutral species, singlet oxygen $^1O_2$ (Figure 1.3). This is formed when oxygen is exposed to ultra-violet (UV) irradiation (photochemical process).[23,24] Chemically, a reaction of H_2O_2 with sodium hypochlorite (NaOCl) is used to generate singlet oxygen, $^1O_2$ (Scheme 1.9), which is highly reactive and unstable (half-life in microseconds). $^1O_2$ is acting as a photosensitizer in photodynamic therapy (PDT) for skin, liver and lung cancers. Literature evidence suggests that $^1O_2$ causes oxidative damage to biomacromolecules such as iron-sulfur (Fe-S) cluster proteins by oxidation and lipid peroxidation and hence, classified under the category of ROS.[22-24]

Scheme 1.9. Singlet oxygen generations by photochemical and chemical methods

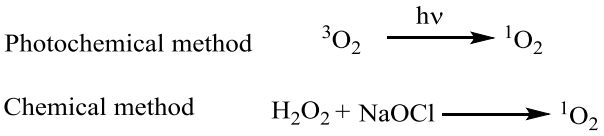

1.3.3. Superoxide radical anion, $O_2^{\bullet-}$:

The paramagnetic superoxide ($O_2^{\bullet-}$) radical anion is formed by the addition of an electron to π* 2p orbital of the oxygen molecule (Figure 1.3). This is a radical anion with one unpaired electron in its valence shell and the oxidation number of oxygen in $O_2^{\bullet-}$ is –½. Inadvertent transfer of electrons from ubiquinone and ETC complex-II during mitochondrial respiration produces $O_2^{\bullet-}$ in cells. Mainly, $O_2^{\bullet-}$ is produced in inner mitochondrial membrane, through one electron reduction of oxygen by NADH dehydrogenase in the respiratory chain, or a catalytic enzymatic oxidation by cytochrome P450 or CYP_{450}.[22,25-27] $O_2^{\bullet-}$ is unstable and highly reactive in its free form, but this is trapped as a stable potassium salt, KO_2 and commercially sold in this form (Scheme 1.10). A reaction of molten potassium with molecular oxygen produces potassium superoxide (KO_2).[28] $O_2^{\bullet-}$ has a high reduction potential of +0.94 V in comparison to other oxidative species (-0.16 for O_2 and +0.38 for H_2O_2), thus expected a slow reactivity, despite that, oxidative damage caused by $O_2^{\bullet-}$ to Fe-S cluster proteins are well documented.[25,29,30] A diffusion controlled reaction of nitric oxide ($NO^{\bullet}$) radical with $O_2^{\bullet-}$ produces peroxynitrite anion ($ONOO^-$), which is in equilibrium with peroxynitrous acid (ONOOH), has a half-life of 1–3 s, and generates $^{\bullet}OH$ radical and nitrogen dioxide (N_2O) upon decomposition.[19,22] $ONOO^-$ is a highly reactive ROS, reported to induce oxidative damage to most of the biomolecules including DNA, proteins and lipids.[26]

Scheme 1.10. Synthesis of potassium superoxide (KO_2)

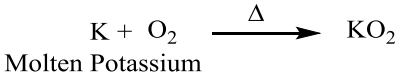

1.3.4. Hydrogen peroxide, H_2O_2:

A one electron reduction of $O_2^{\bullet-}$ leads to the formation of hydrogen peroxide (H_2O_2), which is a neutral diamagnetic molecule with completely filled π* 2p orbital and the oxidation number of oxygen in H_2O_2 is -1 (Figure 1.3). This ROS is relatively stable when compared with other ROS, commercially available, and can be stored at 2 to 8 °C for long periods of time, but at 30 °C, its estimated half-life is reduced to 10 h .[8,29-31] Industrially H_2O_2 is produced by a palladium catalyzed reduction of 2-ethyl-9,10-anthraquinone to form the corresponding hydroquinone and subsequent exposure to oxygen (Scheme 1.11).[32] In cells, dismutation of $O_2^{\bullet-}$ by a family of superoxide dismutase enzymes leads to the formation of H_2O_2.[22,33] Although highly diffusible through biological membranes, the toxicity of H_2O_2 to cells is reported to be sub-lethal at low concentrations (sub micro molar level), but at elevated concentrations (milli molar level) could result in damage to DNA and Fe-S cluster proteins.[31,34,35] A trace amount of metal ions such as copper(I) or iron(II) can catalyze the formation of $OH^{\bullet}$ from H_2O_2.[36,37]

Scheme 1.11. Industrial production of hydrogen peroxide (H_2O_2)

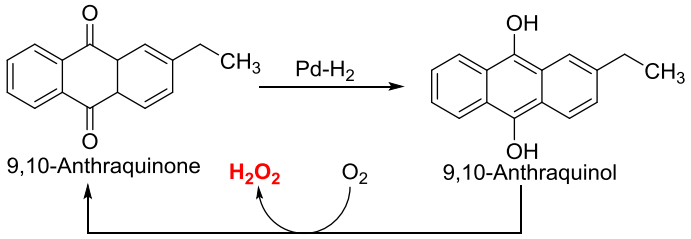

1.3.5. Hydroxyl radical, $^{\bullet}OH$:

Homolytic cleavage of H_2O_2 upon UV irradiation leads to the formation of $OH^{\bullet}$ radical. Also, in the Fenton reaction H_2O_2 is reduced to $OH^{\bullet}$ and water at the expense of oxidation of ferrous ion, Fe (II) to ferric ion, Fe (III). In cells, Fe(II) is generated through the Haber-Weiss process, by a reaction of $O_2^{\bullet-}$ with Fe(III) (Scheme 1.12).[38] $OH^{\bullet}$ is one of the highly reactive ROS with a half-life in nanoseconds.[36,37] A diffusion controlled reactivity of $OH^{\bullet}$ causes oxidative damage at minimum concentrations in nucleic acids, mainly in DNA. The damaging effects of $OH^{\bullet}$ to proteins are caused by oxidation of tyrosine and thiol containing amino acids such as cysteine and methionine which affects

the protein structure and functions. In the case of lipids, an oxidative damage is caused by $OH^{\bullet}$ through initiation of a chain reaction such as lipid peroxidation. These harmful effects of $OH^{\bullet}$ radical to all biomolecules could lead to cell death.[22,37,39]

Scheme 1.12. Hydroxyl radical formation ($OH^{\bullet}$) from H_2O_2 by Fenton reaction

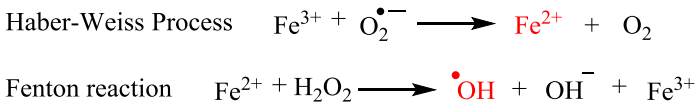

1.3.6. Other reactive oxygen species (ROS):

Hypochlorite and peroxyl radicals are capable of inducing oxidative stress in side cells. HOCl is a product of H_2O_2 reacting with chloride ion (Cl^-) in cells and one of the highly reactive species in physiological conditions. Peroxyl radicals such as hydroperoxyl radical and organo peroxyl radicals are mainly involved in lipid peroxidation and produced by a reaction of H_2O_2 and $OH^{\bullet}$ with lipids. These ROS are generated in very low levels in cells, so the precise roles of these ROS in biological systems are barely understood.[18,30]

1.4. Molecular Effects of ROS in Biological Systems:

Scheme 1.13. ROS generation in biological systems.

ETC: Electron transport chain; NOX: NADPH oxidase; SOD: Superoxide dismutase; MPO: Myeloperoxidase.

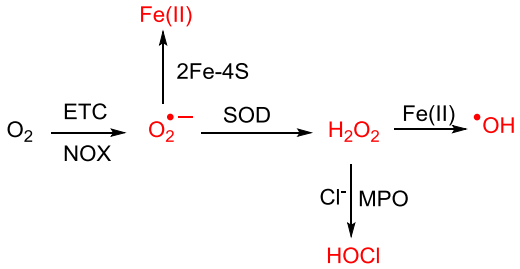

In cells, superoxide ($O_2^{\bullet -}$) is generated by 1 e^- transfer to O_2 either from ETC or by NADPH oxidase (NOX) enzyme. $O^{\bullet -}$ is known to damage the Iron-sulfur cluster protein (Fe-S) in cells and Fe(II) is released into the extracellular matrix and as an effect,

inactivates the Fe-S protein function.[20,26] This $O_2^{\bullet-}$ species undergoes a dismutation to H_2O_2 in a buffer or catalyzed by a family of enzymes called superoxide dismutase (SOD) (Scheme 1.13). H_2O_2 is reactive towards a variety of functional groups in biomolecules; for example, thiol of the cysteine containing proteins is oxidized to form sulfenic acids. This inturn can undergo further oxidations by second and third equivalent of H_2O_2 to form sulfenic and then sulfonic acids, respectively (Scheme 1.14a).[12,20,21,40,41]

Next, $OH^{\bullet}$ radical is generated by a metal (Fe(II) or Cu(I)) mediated reduction of H_2O_2 through Fenton reaction (Scheme 1.13). Hydroxyl radical directly reacts with DNA and causes oxidative damage which is often irreversible causing mutations in the DNA sequence.[12,20] The reactive sites for DNA damage are sugar backbone and nucleobases. In ribose, C-4′ tertiary radical is generated and subsequent uncontrolled reactions lead to DNA degradation or mutations. Among the nucleobases guanine is a highly reactive base and 8-oxoguanine is formed during its reaction with $OH^{\bullet}$. Another nucleobase called thymine undergoes addition reaction with $OH^{\bullet}$, forms thymine radical species (Scheme 1.14b) and induces mutations in DNA. Proteins are found to be damaged by $OH^{\bullet}$, mainly thiol containing amino acids including methionine residues are oxidized to form methionine sulfoxides by $OH^{\bullet}$ radical. Protein carbonyls are generated by a reaction of $OH^{\bullet}$ with amino acids such as lysine, arginine, proline and histidine at the carboxylic acid functional group and oxidation of histidine residues in protein produces 2-oxo-histidines (Scheme 1.14a).[21,40]

Formation of hypochlorus acid from H_2O_2 in cells is catalyzed by an enzyme myeloperoxidase (MPO). This species is reactive towards biomolecules and found to oxidize cysteine residues of protein to cysteine sulfenic acid and tyrosine to chlorotyrosine. HOCl is much more reactive (3×10^7 M^{-1}, s^{-1}) than H_2O_2 (0.9 M^{-1}, s^{-1}) as observed in oxidizing glutathione (Scheme 1.14a).

Hydroxyl radical, $^{\bullet}OH$, is the source for generation of hydroperoxyl or organoperoxyl radicals, which can oxidatively damage lipids by oxidation and lipid peroxidation.[40] (Scheme 1.14c)

Scheme 1.14. Molecular effects of ROS in biological systems.

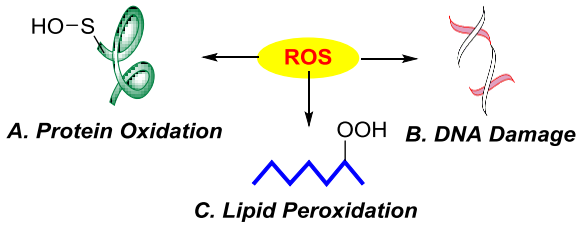

A. Oxidative reactions of ROS with amino acids in proteins

Hydrogen peroxide (H_2O_2):

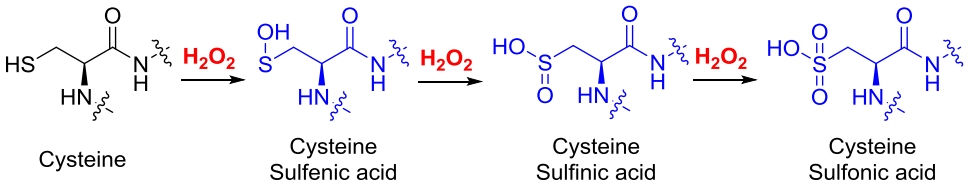

Hydroxyl radical ($^{\bullet}OH$):

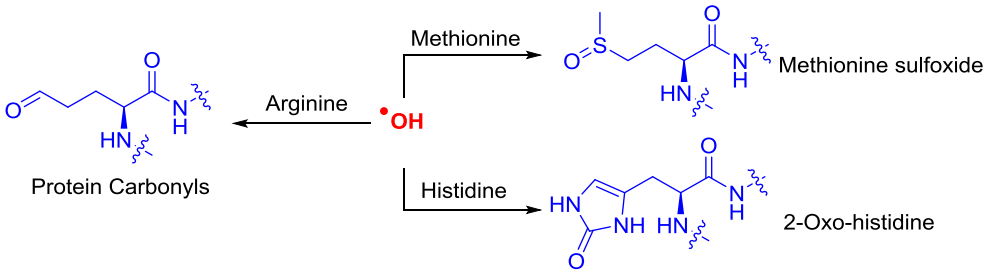

Hypochlorus acid (HOCl):

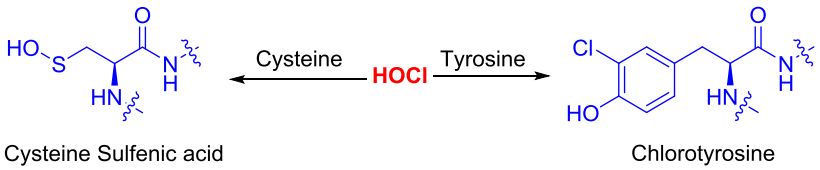

B. Oxidative DNA damage by $^{\bullet}OH$ and $ROO^{\bullet}$:

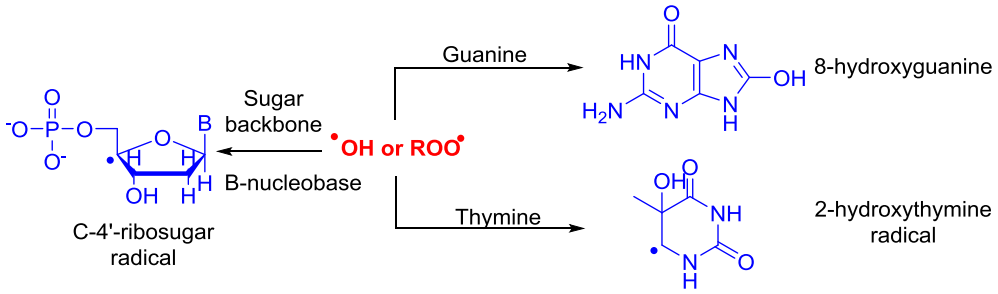

C. Oxidative reactions of ROS with lipids:

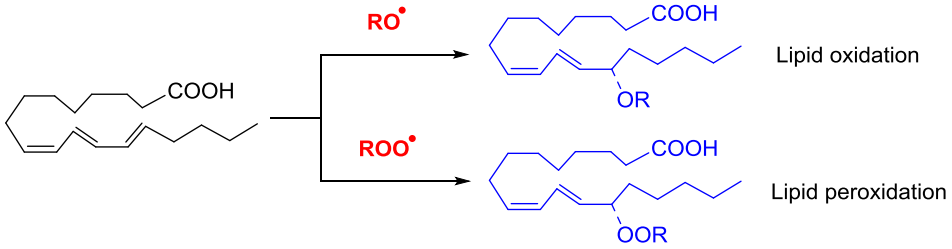

Together a majority of these ROS are known to oxidatively damage biomolecules to different extents depending on the reactivity of ROS. As discussed below, elaborate antioxidant as well as repair systems are typically present to counter these damaging effects of ROS. However, irreparable damage caused by ROS in biomacromolecules leads to cell damage and death.

1.5. Antioxidant Systems:

Aerobic organisms are continuously exposed to an oxidative environment and are prone to undergo oxidative damage by ROS. As an evolution, cells have developed a strong antioxidant response to these ROS, mainly by small molecule cellular thiols such as cysteine (Cys) and glutathione (GSH).[42] These reduced thiols are important for the maintenance of cellular redox homeostasis which works through neutralization of ROS. During the homeostasis process reduced thiols such as GSH undergo a dimerization to form glutathione dimer (GS-SG), which is reduced back in the cells by reducing enzymes such as glutathione reductase.

Scheme 1.15. Antioxidant system for controlling the level of ROS

ETC: Electron transport chain; NOX: NADPH oxidase; SOD: Superoxide dismutase; Cat: Catalase; GPO: Glutathione peroxidase; MPO: Myeloperoxidase; GSH: Glutathione; AA: Amino acids.

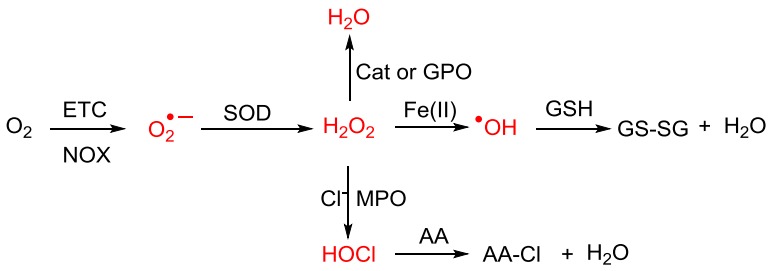

Due to the spin restrictions for the addition of electrons in triplet oxygen, one electron reduced species superoxide ($O_2^{\bullet-}$) should be the first ROS generated from O_2.[43,44] A family of metal cofactored superoxide dismutase are found in cells as antioxidant systems to control the level of $O_2^{\bullet-}$ production in cells (Scheme 1.15). Some examples are, manganese superoxide dismutase (MnSOD), copper superoxide dismutase (CuSOD), and iron superoxide dismutase (FeSOD). These SODs are found to quench $O_2^{\bullet-}$ by dismutation into H_2O_2 and O_2 (Scheme 1.15). Next, H_2O_2 is converted to O_2 and water, mainly, by catalase and glutathione peroxidase enzymes.[42] Sensor proteins such as OxyR, hydroperoxidase I (KatG), and peroxiredoxin (AhpC) are expressed in cells to detect the level of H_2O_2 generated in cells. OxyR is an enzyme activated upon exposure to H_2O_2 via oxidation of a cysteine-199 residue in OxyR, and induces more than 20 antioxidants to scavenge H_2O_2.[45-48] Other antioxidants are KatG and AhpC which is also found to act through oxidation of the cysteine residue in the enzymes.[42] Upon detection of any excess H_2O_2 production in cells, these enzymes activate an array of antioxidant systems to control the intracellular H_2O_2 levels (Scheme 1.15). Further, H_2O_2 can react with trace amount of metal ions to generate $OH^{\bullet}$, a highly reactive ROS. The reduced thiols present in excess in cells such as cysteine and glutathione traps the $OH^{\bullet}$ to protect the cellular components from the oxidative damaging effects (Scheme 1.15).[22,42]

1.6. ROS During Immune Response:

Due to the aforementioned damaging effects of ROS in biomolecules, ROS are generated deliberately by the immune cells including macrophages and neutrophilsin the presence of pathogens.[18,22,40,42] The immune system can be divided into two types: 1) innate immune system, formed by multicellular organisms and 2) acquired immune system, mostly found in vertebrates. T-cells and B-cells play important roles in acquired immunity by antigen-antibody reaction, whereas the innate immune system contains macrophages, neutrophils and dendritic cells, which are primary prophylactic systems working by eliminating one-self.[49] ROS and reactive nitrogen species (RNS) are generated immediately after the recognition of any invading foreign bodies such as virus and bacteria (Scheme 1.16). NOX proteins are the main source inducing ROS production in macrophages for phagocytic killing of invading pathogens.[50-52] Nitric oxide synthase (NOS) is an enzyme responsible for generating nitric oxide, a RNS during immune response, where arginine is converted into citrulline for the production of NO by NOS catalysis.[53-55]

Scheme 1.16. Phagocytosis of bacteria during immune response in cells

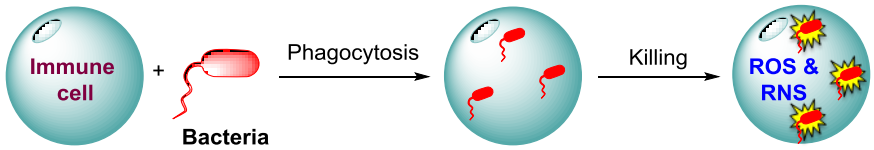

1.7. Enhancement of ROS:

Mimicking biological systems and enhancing the level of ROS in cells by systems biology or chemical approaches have been considered as potential strategies to target bacterial infections. ROS is produced invariably in all aerobic organisms; however they have evolved antioxidant systems to counteract oxidative stress.[42] Bacteria have evoled with strong antioxidant response, but enhancing the level of endogenous ROS could affect the bacteria survival.[56] Either impairing antioxidant systems or enhancing the endogenous levels of ROS in bacteria could be useful strategies to increase oxidative damage for bacterial growth inhibition.

1.7.1. Impairing antioxidant systems:

Bacteria with impaired antioxidant systems are more sensitive to ROS and antibiotics. In *E.coli* mutations were induced to deplete SOD levels on the genes of antioxidant MnSOD and FeSOD enzymes. These SOD deficient mutants were found to be highly sensitive when subjected to treatment with paraquat, a superoxide generating small organic molecule, during reaction with oxygen. Conversely, when the bacteria were cultured in anaerobic conditions no effect in the growth was observed, thus proving a vital role for SOD in protecting bacteria against enhanced oxidative attack by ROS.[57] Catalase is an enzyme expressed in cells as a major antioxidant for the scavenging of H_2O_2. A detailed study of the effect of H_2O_2 on the growth of catalase deficient mutants of *E. coli* was reported. When compared with wild type *E. coli* bacterium, catalase null mutants were identified to be 50-60 fold more sensitive to H_2O_2.[58] Catalase is one of the most important antioxidant systems present in cells for the protection from harmful effects of H_2O_2.[58,59] *RecA* is a gene expressed as a response to DNA damage in cells. RecA mutants of *E. coli* were found to be 6-7 folds more sensitive to H_2O_2 than the wild type *E. coli*.[58]

Not just Gram negative bacteria, *Staphylococcus aureus*, a Gram positive bacterium also has shown to be sensitive to ROS when its antioxidant system is impaired. *S. aureus* is an infective pathogen associated with community and hospital acquired skin infections, which has been known to affect around a million each year. Staphyloxanthine is a pigment found in *S. aureus* and it is an important virulence factor identified to promote resistance against ROS and host-immune system (Figure 1.4). Staphyloxanthine quenches ROS such as $O_2^{\bullet-}$, H_2O_2, and HOCl generated by the innate immune systems. Thus, inhibition of staphyloxanthine biosynthesis could increase the levels of endogenous ROS that could be lethal to the bacterium. As the staphyloxanthine biosynthesis is a close resemblance to cholesterol biosynthesis, a series of cholesterol biosynthetic inhibitors were evaluated to inhibit the staphyloxanthine biosynthesis and the BPH-652 was found to inhibit at nano molar concentrations (inhibitory concentration, K_i = 1.5 nm). An increased susceptibility of *S. aureus* was observed when BPH-652 was co-treated with H_2O_2 (Figure 1.4).

Figure 1.4. Stuctures of staphyloxanthine and its inhibitor BPH-652

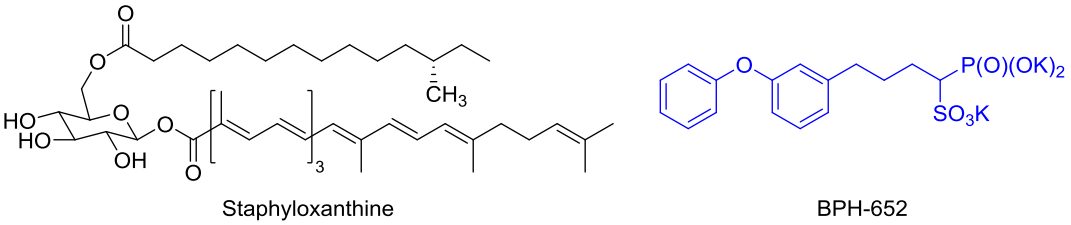

Thus, impairing the antioxidant system in Gram positive and Gram negative bacteria was found to sensitize bacteria to ROS and antibiotics.[60]

1.7.2. Enhancement of endogenous ROS levels:

Another way of interfering or even inhibiting bacterial growth is by increasing endogenous ROS thereby increasing the oxidative damage for the inhibition of bacteria. Flavins and flavoproteins in their reduced forms react with molecular O_2 to produce ROS such as $O_2^{\bullet-}$ and H_2O_2 by sequential $1e^-$ reduction process (Scheme 1.17).[61]

Scheme 1.17. ROS generation from oxidation of flavins during reaction with O_2

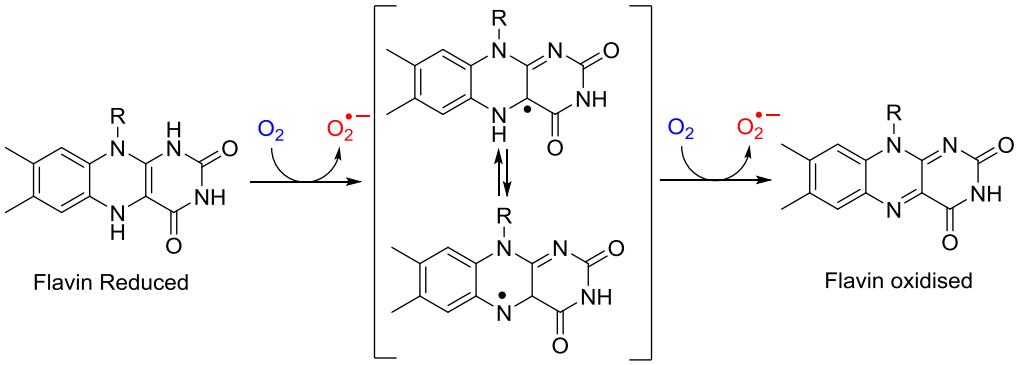

Flavoproteins such as flavodoxin, flavoredoxin, flavin dehydrogenase (acyl CoA dehydrogenase) DT-diaphorase, and flavin monooxygenase are known to react with molecular oxygen to generate ROS.[25,61,62] Each enzyme has different rate of reactivity with oxygen for ROS generation, the stability of the flavin radical determining the type of ROS generated. Unstable radical species reacts faster with oxygen and $O_2^{\bullet-}$ is found to be the major ROS generated, whereas more stable flavin radical is found to generate

H_2O_2 as a major ROS.[62] In *E. coli* NADH is another cofactor undergoing oxidation to generate ROS in cells catalyzed by NADH-oxidase enzyme.[33,63]

An emerging research field in biomedical engineering is systems biology, where complex interactions of cell components and their functions are studied. Systems biology based approach for studying complex enzymatic interactions and the metabolic products has led to advances in biotechnology and microbiology.[56] Using this approach, a genome scale metabolic models were created for predicting the increase in intracellular ROS production in bacteria. In this metabolic pathway 133 reactions that involve ROS generation were identified and in addition 266 ROS producing reactions were also found. For example, SOD for H_2O_2 production were included for the *in silico* analysis. Specific gene deletion analyses provided information about pathways involving ROS enhancement in bacterium. To validate the findings experimentally, genetic mutations (incorporation or deletion of 21 identified genes) were successfully carried out and the analysis of metabolic by-product showed a predictable enhancement of ROS in *E. coli*. Next, bacterial mutants deficient of antioxidants were found to be highly sensitive when treated with oxidants such as H_2O_2, NaOCl and menadione, whereas the wild type bacterium *E. coli* was resistant. A significantly enhanced sensitivity of mutants to H_2O_2 suggested the utility of enhancement of ROS as a method to target bacterial inhibition.[56]

Traditional antibiotics have largely independent mechanisms for their bactericidal activities, and hence if bacteria develop resistance to one antibiotic, typically remain sensitive to others. For example, β-lactam antibiotics (such as ampicillin, amoxicillin etc.) are known to inhibit bacterial cell wall biosynthesis, quinolone antibiotics (norfloxacin, ciprofloxacin etc.) are DNA gyrase inhibitors and amino acid biosynthesis in bacteria is inhibited by aminoglycoside antibiotics (Kanamycin, gentamycin etc.).[64] However, a common mechanism of bactericidal activity for traditional antibiotics was proposed as an enhancement intracellular ROS in bacteria along with their individual targets for bactericidal activity.[65] Although this concept was disputed by few independent reports,[66-68] ROS was used as an adjuvant to potentiate the antibacterial activity of the commercial antibiotics.[56,69] Thus, enhancing intracellular ROS was considered as a potential strategy to target bacterial infection.

Using the systems biology approach toxicity of $OH^{\bullet}$ generated from silver ion in silver nitrate ($AgNO_3$) to a Gram negative bacterium, *E. coli* was studied. Detection of $OH^{\bullet}$ generated from Ag^{+} treated bacteria was carried out using hyroxyphenylfluorescein (HPF) based fluorescence assay, further confirmed by quenching of this fluorescence using thiourea, a standard quencher of $OH^{\bullet}$.[69] A series of mutants such as SOD-A, a superoxide overproducing mutant and iron import gene mutants were incubated with Ag^{+} and the growth profile was monitored. A significant inhibition of bacterial growth suggests the utility of ROS as antibacterial agents. In addition, Ag^{+} was also found to enhance the killing efficacy of the bacterial antibiotics both *in vitro* and *in vivo*.[69]

Scheme 1.18. Antibacterial agents acting by ROS generation mechanism

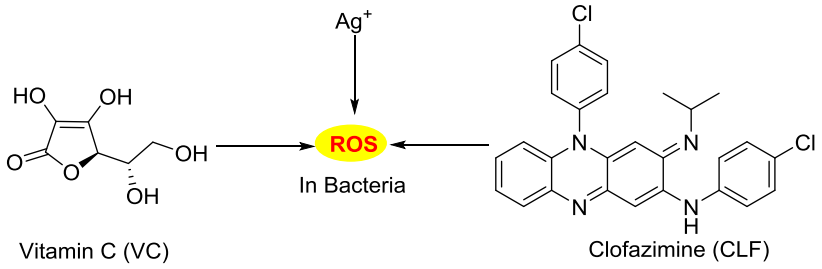

Mycobacterium tuberculosis (*Mtb*) is the causative agent of tuberculosis and is one of the highly infective pathogens. One third of the world population is infected by *Mtb* as estimated by World health organization (WHO).[70] Vitamin C (VC) is a known antioxidant and one of the essential nutrients for mammals.[71] VC is shown to reduce the ferric ion (Fe^{3+}) and increase the level of free ferrous ions (Fe^{2+}) in the extracellular medium. The free $Fe^{(2+)}$ can react with O_2 and generate $O_2^{\bullet -}$, H_2O_2 and highly reactive $^{\bullet}OH$ by Haber-Weiss process and Fenton reaction (Scheme 1.18).[38] VC (4 mM) was shown to enhance the ROS levels and found to be lethal to *Mtb*. Addition of deforaxamine, a Fe^{2+} chelator along with VC showed no effect in the bacterial growth, providing evidence for Fe^{2+} mediated ROS generation for bacterial inhibition. Due to thick waxy cell wall *Mtb* is considered to be one of the difficult pathogens to treat and is shown to be sensitive to enhanced oxidative stress.[72]

Clofazimine (CLF) is a commercial drug used for the treatment of leprosy, a chronic infection caused by *mycobacterium leprae*. The mechanism of action exerted by CLF is

proposed to generate intracellular ROS and induce oxidative stress.[73,74] A bioreduction of CLF by NADH-oxidoreductase, which is present in the ETC, leads to reduced CLF and a concomitant reaction with O_2 produces ROS (Scheme 1.18). As a support of ROS generation, bacterium was found to be less sensitive to CLF when cultured in antioxidants supplemented medium.[73,74] Thus the development of ROS based antibacterial agents might have therapeutic potential against Gram positive and Gram negative bacteria and also could serve as an adjuvant to enhance the efficacy of commercially used antibiotics.

1.8. ROS in Cancer and Aging:

Mitochondrion is the main source of endogenous ROS production in cells. A sub lethal level of ROS is always maintained in cells for proliferation, cell survival and signaling.[12,21,22,40] Cancer cells are characterized for producing higher levels of reactive oxygen species when compared to normal cells. This property is due to enhanced metabolism in cancer cells. As a response to enhanced ROS, reduced thiols such as glutathione are also over expressed in cancer cells to maintain the redox homeostasis.[75-78] A considerable body of evidences suggest an established correlation of enhancement of ROS with mutagenesis. Ironically, controlled generation of ROS above the normal level can induce apoptosis (programmed cell death, a controlled process) or necrosis (uncontrolled damage of cellular components leading to cell death) in cancer. Thus disturbing the redox hemeostasis by increasing the level of ROS in cancer is considered as a potential strategy to eliminate cancer.[79-81]

Figure 1.5. Structures of ROS based anticancer agents

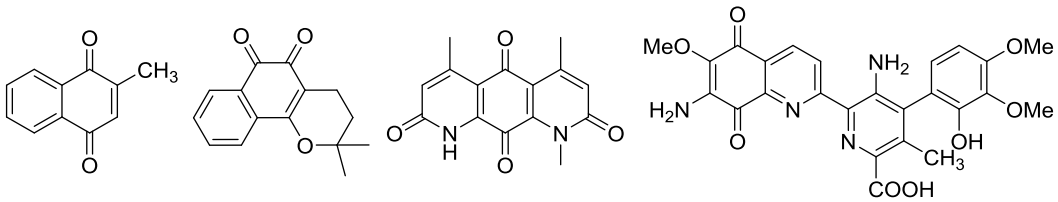

Bioreductively activated ROS generators such as menadione,[82-87] deoxynyboquinone,[88,89] β-lapachone,[90,91] mitomycin C,[92,93] and streponigrin[94,95] were

developed as anticancer agents (Figure 1.5). Indiscriminate damage caused by ROS were used to support free radical theory of aging and the effects of ROS were considered cumulative and random. It was proposed that accumulation of ROS in mitochondria causes mutations in mitochondrial DNA (mtDNA); as a consequence rapidly aging phenotypes could be produced. However, no alteration in the level of ROS was identified when experiments were carried out in mitochondria *ex vivo*, declining the theory of oxidative damage for aging. Ironically, when the levels of ROS in mitochondria depleted, delay in the onset of aging was observed. While the role of ROS in aging process is puzzling with coupled evidences, involvement of ROS such as superoxide and hydrogen peroxide in cell regulation and activation of prosurvival signals for increasing the life span of cells are known. Thus ROS is not just mediating aging but also involved in cell maturation and survival, the harmful effect is due to compromised signaling.[12,41,50,96,97] Thus, the link between ROS and cancer has been widely understood and accepted, but its antibacterial effects and its effects on aging are being investigated.[50,75,79,81,88,89,98]

1.9. Sources of ROS and Their Limitations:

Although the sensitivity of bacteria to ROS is well documented, only limited sources of reliable ROS generators are available. We have classified them into two types of ROS sources used: 1) direct sources of ROS (self-decomposing), 2) enzymatically activated ROS generators.

1.9.1. Direct sources of ROS:

Potassium superoxide is used as a source of $O_2^{\bullet -}$ for most of the extracellular assays. However, due to its poor cell permeability this is not suitable for intracellular assays.[25] H_2O_2 is frequently used as a hospital disinfectant as it is freely cell permeable unlike $O_2^{\bullet -}$. However, the potential limitation is the absence of structural handle to control reactivity.[99] The organic derivative of H_2O_2 is *tert*-butyl hydroperoxide (*t*-BuOOH), used for the induction of oxidative stress in cells to study the effects of enhanced oxidative stress in biological pathways, mainly in cancer. The sluggishness of *t*-BuOOH in decomposition to generate a radical under physiological conditions is a concern.[100-102] Sodium hypochlorite is another ROS used in conjunction with H_2O_2 for sterilization of

surgical apparatus from bio-contaminants. Similar to $O_2^{\bullet -}$, sodium hypochlorite also has issues with cell permeability (Figure 1.6).[20,21] Unless these species are generated in intracellular environment or produced by cell permeable sources, studying the effects or the role of ROS in biological systems would be complicated.

Figure 1.6. Self decomposing sources of ROS

KO_2	H_2O_2	*tert*-BuOOH	NaOCl
Potassium Superoxide	Hydrogen peroxide	*tert*-butyl hydroperoxide	Sodium hypochlorite

1.9.2. Enzymatically activated ROS generators:

1.9.2A. Bioreductive activation for ROS generation:

Menadione and flavin are known to generate ROS and the mechanism is proposed through an enzymatic reductive activation in biological systems. Menadione is a 2-methyl derivative of 1,4-naphthoquinone which is reduced to 1,4-diol by DT-diapharase also known as NADH-dehydrogenase, using NADH co-factor as an electron source. The product 1,4-diol is highly reactive and upon exposure to molecular O_2 generates ROS and the parent quinone (Menadione) is regenerated (Scheme 1.19). Although the compound is used for cell based studies, it has poor solubility in aqueous media. The bioreduction product 1,4-diol(ate) reacts rapidly with O_2 to generate ROS. In addition to its poor aqueous solubility inability to provide temporal control over ROS generation is a significant drawback.[80,103,104]

Scheme 1. 19. Bioreduction of menadione by DT-diapharase for ROS generation

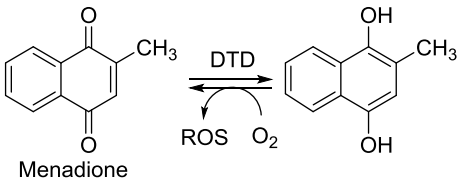

DTD: DT-Diaphorase enzyme

Flavin is a class of isoalloxazine derivatives found in many biological sources such as flavin mononucleotide (FMN), flavin dinucleotide (FAD), and in many flavoproteins.

The reduced form of flavins are known to react with molecular O_2 to generate ROS, the reduction of flavin moiety is mediated by NOX enzyme (Scheme 1.20). Poor cell permeability of flavins limits the utility of flavins for intracellular ROS generation.[61,62,105-107]

Scheme 1. 20. ROS generation from flavin mediated by NOX enzymes

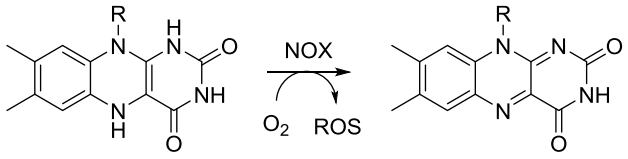

NOX: NADH-Oxidase enzyme

1.9.2B. Generation of ROS by enzymatic oxidation:

Xanthine and xanthine oxidase are routinely used for extracellular $O_2^{-\bullet}$ production. The reaction consists of oxidation of xanthine is which catalyzed by the enzyme xanthine oxidase and the reduced product is $O_2^{-\bullet}$. This is an efficient method for rapid $O_2^{-\bullet}$ generation (Scheme 1.21). However, poor cell permeability of xanthine as well as superoxide radical anion raises the concern over the suitability of this method for intracellular applications.[25]

Scheme 1.21. Superoxide, $O_2^{-\bullet}$ generation from xanthine, catalysed by xanthine oxidase

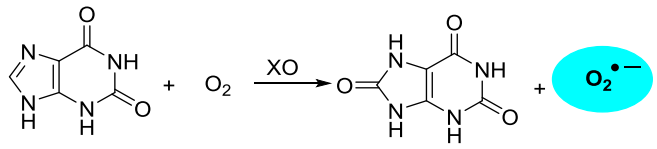

H_2O_2 is generated enzymatically by glucose oxidase catalyzed oxidation of glucose. This is highly selective and a rapid generation of H_2O_2 is observed by this enzymatic oxidation (Scheme 1.22).

Although the aforementioned methods are widely used, they all suffer from limitations. For example, X + XO generates superoxide only outside the cell. The

substrate for glucose oxidase is widely present and would be unsuitable for site-directed delivery of ROS.

Scheme 1.22. Glucose oxidase mediated H_2O_2 generation by oxidation of glucose

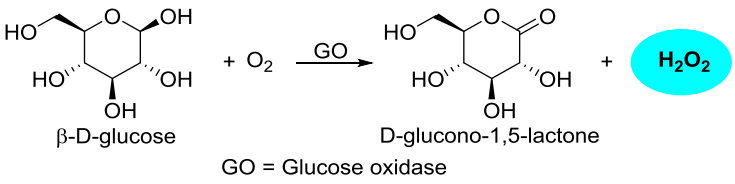

Considering the limitations with the available sources of ROS, new sources with desirable properties, such as stability, structural control, temporal control and site selectivity for biological studies are necessary. Despite the known importance of ROS in biochemical and biological systems, organic sources for reliable ROS generation are limited.

In this thesis, in Chapter 2, we describe the identification of a new scaffold for ROS generation in aerobic buffers and explore the utility of ROS generators to enhance ROS levels within bacteria. Further, we report the study of substituent effects on this scaffold for tunable ROS generation. In Chapter 3, for a site directed delivery of ROS, a bacterial enzyme, nitroreductase activated intracellular ROS generation is demonstrated using a pro-ROS generator and its potential to sensitize *E. coli* to antibiotics is evaluated. Finally, we have shown a thiol activated ROS generation for depletion of antioxidant thiol in cells and subsequent enhancement of ROS to target drug resistant bacteria in Chapter 4.

1.10. References:

1. *CRC Handbook of Chemistry and Physics*. 92nd ed.; CRC Press: 2011; Vol. 2011.
2. Emsley, J.; *Nature's Building Blocks: An A-Z Guide to the Elements*. Oxford, England, UK: Oxford University Press: 2001.
3. Ligeza, A.; Tikhonov, A. N.; Hyde, J. S.; Subczynski, W. K. Oxygen permeability of thylakoid membranes: electron paramagnetic resonance spin labeling study. *Biochim. Biophys. Acta* **1998,** 1365, 453-463.
4. Lyons, T. W.; Reinhard, C. T.; Planavsky, N. J. The rise of oxygen in Earth/'s early ocean and atmosphere. *Nature* **2014,** 506, 307-315.
5. Boiteux, A.; Hess, B. Design of glycolysis. *Philos. Trans. R Soc. Lond. B Biol. Sci.* **1981,** 293, 5-22.
6. Meléndez-Hevia, E.; Waddell, T. G.; Shelton, E. D. Optimization of molecular design in the evolution of metabolism: the glycogen molecule. *Biochem. J.* **1993,** 295, 477-483.
7. David, L. N. A., L Lehninger; Michael, M Cox. *Lehninger principles of biochemistry*. 5 ed.; New York : W.H. Freeman, ©2008.
8. Imlay, J. A. How oxygen damages microbes: Oxygen tolerance and obligate anaerobiosis. In *Adv. Microb. Physiol.*,, Academic Press: 2002; Vol. Volume 46, pp 111-153.
9. Babcock, G. T.; Wikstrom, M. Oxygen activation and the conservation of energy in cell respiration. *Nature* **1992,** 356, 301-309.
10. Brandt, U. Proton-translocation by membrane-bound NADH:ubiquinone-oxidoreductase (complex I) through redox-gated ligand conduction. *Biochim Biophys Acta* **1997,** 16, 1-2.
11. Yankovskaya, V.; Horsefield, R.; Törnroth, S.; Luna-Chavez, C.; Miyoshi, H.; Léger, C.; Byrne, B.; Cecchini, G.; Iwata, S. Architecture of Succinate Dehydrogenase and Reactive Oxygen Species Generation. *Science* **2003,** 299, 700-704.
12. Finkel, T.; Holbrook, N. J. Oxidants, oxidative stress and the biology of ageing. *Nature* **2000,** 408, 239-247.

13. Turrens, J. F.; Alexandre, A.; Lehninger, A. L. Ubisemiquinone is the electron donor for superoxide formation by complex III of heart mitochondria. *Arch. Biochem. Biophys.* **1985,** 237, 408-414.
14. Ernster, L.; Dallner, G. Biochemical, physiological and medical aspects of ubiquinone function. *Biochim. Biophys. Acta* **1995,** 1271, 195-204.
15. Zito, F.; Finazzi, G.; Delosme, R.; Nitschke, W.; Picot, D.; Wollman, F. A. *The Qo site of cytochrome b6f complexes controls the activation of the LHCII kinase*. 1999; Vol. 18, p 2961-2969.
16. Lee, S.; Tak, E.; Lee, J.; Rashid, M. A.; Murphy, M. P.; Ha, J.; Kim, S. S. Mitochondrial H2O2 generated from electron transport chain complex I stimulates muscle differentiation. *Cell Res.* **2011,** 21, 817-834.
17. Murphy, M. P. How mitochondria produce reactive oxygen species. *Biochem. J.* **2009,** 417, 1-13.
18. Fang, F. C. Antimicrobial reactive oxygen and nitrogen species: Concepts and controversies. *Nat. Rev. Microbiol.,* **2004,** 2, 820-832.
19. Szabo, C.; Ischiropoulos, H.; Radi, R. Peroxynitrite: biochemistry, pathophysiology and development of therapeutics. *Nat. Rev. Drug Discov.* **2007,** 6, 662-680.
20. Imlay, J. A. The molecular mechanisms and physiological consequences of oxidative stress: lessons from a model bacterium. *Nat. Rev. Microbiol.* **2013,** 11, 443-454.
21. Winterbourn, C. C. Reconciling the chemistry and biology of reactive oxygen species. *Nat. Chem. Biol.* **2008,** 4, 278-286.
22. Kalyanaraman, B. Teaching the basics of redox biology to medical and graduate students: Oxidants, antioxidants and disease mechanisms. *Redox Biol.* **2013,** 1, 244-257.
23. Adam, W.; Kazakov, D. V.; Kazakov, V. P. Singlet-Oxygen Chemiluminescence in Peroxide Reactions. *Chem. Rev.* **2005,** 105, 3371-3387.
24. Schweitzer, C.; Schmidt, R. Physical Mechanisms of Generation and Deactivation of Singlet Oxygen. *Chem. Rev.* **2003,** 103, 1685-1758.

25. Imlay, J. A.; Fridovich, I. Superoxide Production by Respiring Membranes of Escherichia Coli. *Free Radic. Res. Comms.* **1991,** 12, 59-66.
26. Fridovich, I. Superoxide radical: An endogenous toxicant. *Ann. Rev. Pharmacol. Toxicol.,* **1983,** Vol. 23, 239-257.
27. Imlay, J. A.; Fridovich, I. Assay of metabolic superoxide production in Escherichia coli. *J. Biol. Chem.,* **1991,** 266, 6957-6965.
28. Jackson C, B.; Werner R, C. Manufacture and Use of Potassium Superoxide. In handling and uses of the alkali metals, Americal Chemical Society: 1957; Vol. 19, pp 174-177.
29. Imlay, J. A. Iron-sulphur clusters and the problem with oxygen. *Mol. Microbiol.,* **2006,** 59, 1073-1082.
30. Imlay, J. A. The molecular mechanisms and physiological consequences of oxidative stress: Lessons from a model bacterium. *Nat. Rev. Microbiol.,* **2013,** 11, 443-454.
31. Kumar, S. R.; Imlay, J. A. How Escherichia coli tolerates profuse hydrogen peroxide formation by a catabolic pathway. *J. Bacteriol.,* **2013,** 195, 4659-4679.
32. Campos-Martin, J. M.; Blanco-Brieva, G.; Fierro, J. L. G. Hydrogen Peroxide Synthesis: An Outlook beyond the Anthraquinone Process. *Angew. Chem. Int. Ed.* **2006,** 45, 6962-6984.
33. Korshunov, S.; Imlay, J. A. Two sources of endogenous hydrogen peroxide in Escherichia coli. *Mol. Microbiol.* **2010,** 75, 1389-1401.
34. Waghray, M.; Cui, Z.; Horowitz, J. C.; Subramanian, I. M.; Martinez, F. J.; Toews, G. B.; Thannickal, V. J. Hydrogen peroxide is a diffusible paracrine signal for the induction of epithelial cell death by activated myofibroblasts. *FASEB J.,* **2005,** 19, 854-856.
35. Kamsler, A.; Segal, M. Hydrogen peroxide as a diffusible signal molecule in synaptic plasticity. *Mol. Neurobiol.,* **2004,** 29, 167-178.
36. Wardman, P. Fluorescent and luminescent probes for measurement of oxidative and nitrosative species in cells and tissues: Progress, pitfalls, and prospects. *Free Radical Biol. Med.,* **2007,** 43, 995-1022.

37. Wrona, M.; Patel, K.; Wardman, P. Reactivity of 2',7'-dichlorodihydrofluorescein and dihydrorhodamine 123 and their oxidized forms toward carbonate, nitrogen dioxide, and hydroxyl radicals. *Free Rad. Biol. Med.,* **2005,** 38, 262-270.

38. Haber, F.; Weiss, J. The Catalytic Decomposition of Hydrogen Peroxide by Iron Salts. *Proc. Royal Soc. Lond. A* **1934,** 147, 332-351.

39. Gutteridge, J. M. C.; Halliwell, B. The role of superoxide and hydroxyl radicals in the degradation of DNA and deoxyribose induced by a copper-phenanthroline complex. *Biochem. Pharmacol.,* **1982,** 31, 2801-2805.

40. Dickinson, B. C.; Chang, C. J. Chemistry and biology of reactive oxygen species in signaling or stress responses. *Nat. Chem. Biol.* **2011,** 7, 504-511.

41. Stadtman, E. R. Protein oxidation and aging. *Free Radical Res.* **2006,** 40, 1250-1258.

42. Imlay, J. A. Cellular defenses against superoxide and hydrogen peroxide. *Annu. Rev. Biochem.* **2008,** 77, 755-76.

43. Fridovich, I. Superoxide radical: an endogenous toxicant. *Annu. Rev. Pharmacol. Toxicol.* **1983,** 23, 239-57.

44. Taube, H. Mechanisms of oxidation with oxygen. *J. Gen. Physiol.* **1965,** 49, 29-52.

45. Seaver, L. C.; Imlay, J. A. Alkyl Hydroperoxide Reductase Is the Primary Scavenger of Endogenous Hydrogen Peroxide in Escherichia coli. *J. Bacteriol.* **2001,** 183, 7173-7181.

46. Christman, M. F.; Storz, G.; Ames, B. N. OxyR, a positive regulator of hydrogen peroxide-inducible genes in Escherichia coli and Salmonella typhimurium, is homologous to a family of bacterial regulatory proteins. *Proc. Natl. Acad. Sci. USA* **1989,** 86, 3484-3488.

47. Choi, H.-J.; Kim, S.-J.; Mukhopadhyay, P.; Cho, S.; Woo, J.-R.; Storz, G.; Ryu, S.-E. Structural Basis of the Redox Switch in the OxyR Transcription Factor. *Cell* **2001,** 105, 103-113.

48. Aslund, F.; Zheng, M.; Beckwith, J.; Storz, G. Regulation of the OxyR transcription factor by hydrogen peroxide and the cellular thiol‚ÄìÄîdisulfide status. *Proc. Natl. Acad. Sci. USA* **1999,** 96, 6161-6165.

49. Murphy, Michael P.; Siegel, Richard M. Mitochondrial ROS Fire Up T Cell Activation. *Immunity* 38, 201-202.
50. Kohchi, C.; Inagawa, H.; Nishizawa, T.; Soma, G. ROS and innate immunity. *Anticancer Res.* **2009,** 29, 817-821.
51. West, A. P.; Shadel, G. S.; Ghosh, S. Mitochondria in innate immune responses. *Nat. Rev. Immunol.* **2011,** 11, 389-402.
52. Yang, Y.; Bazhin, A. V.; Werner, J.; Karakhanova, S. Reactive oxygen species in the immune system. *Int. Rev. Immunol.* **2013,** 32, 249-270.
53. Fukumura, D.; Kashiwagi, S.; Jain, R. K. The role of nitric oxide in tumour progression. *Nat. Rev. Cancer* **2006,** 6, 521-534.
54. Wink, D. A.; Hines, H. B.; Cheng, R. Y. S.; Switzer, C. H.; Flores-Santana, W.; Vitek, M. P.; Ridnour, L. A.; Colton, C. A. Nitric oxide and redox mechanisms in the immune response. *J. Leukoc. Biol.* **2011,** 89, 873-891.
55. Bogdan, C. Nitric oxide and the immune response. *Nat. Immunol.* **2001,** 2, 907-916.
56. Brynildsen, M. P.; Winkler, J. A.; Spina, C. S.; MacDonald, I. C.; Collins, J. J. Potentiating antibacterial activity by predictably enhancing endogenous microbial ROS production. *Nat. Biotech.* **2013,** 31, 160-165.
57. Carlioz, A.; Touati, D. Isolation of superoxide dismutase mutants in Escherichia coli: is superoxide dismutase necessary for aerobic life? *Embo J.* **1986,** 5, 623-630.
58. Loewen, P. C. Isolation of catalase-deficient Escherichia coli mutants and genetic mapping of katE, a locus that affects catalase activity. *J. Bacteriol.* **1984,** 157, 622-626.
59. Hebrard, M.; Viala, J. P.; Meresse, S.; Barras, F.; Aussel, L. Redundant hydrogen peroxide scavengers contribute to Salmonella virulence and oxidative stress resistance. *J. Bacteriol.* **2009,** 191, 4605-4614.
60. Liu, C. I.; Liu, G. Y.; Song, Y.; Yin, F.; Hensler, M. E.; Jeng, W. Y.; Nizet, V.; Wang, A. H.; Oldfield, E. A cholesterol biosynthesis inhibitor blocks Staphylococcus aureus virulence. *Science* **2008,** 319, 1391-1394.

61. Massey, V. Activation of molecular oxygen by flavins and flavoproteins. *J. Biol. Chem.* **1994,** 269, 22459-22462.

62. Siddens, L. K.; Krueger, S. K.; Henderson, M. C.; Williams, D. E. Mammalian flavin-containing monooxygenase (FMO) as a source of hydrogen peroxide. *Biochem. Pharmacol.* **2014,** 89, 141-147.

63. Messner, K. R.; Imlay, J. A. The Identification of Primary Sites of Superoxide and Hydrogen Peroxide Formation in the Aerobic Respiratory Chain and Sulfite Reductase Complex of Escherichia coli. *J. of Biol. Chem.* **1999,** 274, 10119-10128.

64. Walsh, C. Molecular mechanisms that confer antibacterial drug resistance. *Nature* **2000,** 406, 775-781.

65. Kohanski, M. A.; Dwyer, D. J.; Hayete, B.; Lawrence, C. A.; Collins, J. J. A Common Mechanism of Cellular Death Induced by Bactericidal Antibiotics. *Cell* **2007,** 130, 797-810.

66. Ezraty, B.; Vergnes, A.; Banzhaf, M.; Duverger, Y.; Huguenot, A.; Brochado, A. R.; Su, S. Y.; Espinosa, L.; Loiseau, L.; Py, B.; Typas, A.; Barras, F. Fe-S cluster biosynthesis controls uptake of aminoglycosides in a ROS-less death pathway. *Science* **2013,** 340, 1583-1587.

67. Keren, I.; Wu, Y.; Inocencio, J.; Mulcahy, L. R.; Lewis, K. Killing by bactericidal antibiotics does not depend on reactive oxygen species. *Science* **2013,** 339, 1213-1216.

68. Liu, Y.; Imlay, J. A. Cell death from antibiotics without the involvement of reactive oxygen species. *Science* **2013,** 339, 1210-1213.

69. Morones-Ramirez, J. R.; Winkler, J. A.; Spina, C. S.; Collins, J. J. Silver Enhances Antibiotic Activity Against Gram-Negative Bacteria. *Sci. Transl. Med.* **2013,** 5, 190ra81.

70. Fauci, A. S.; Alston, B.; Barry, C. E.; Augustine, A. D.; Fenton, M. J.; Handley, F. G.; Holland, S. M.; Huebner, R. E.; Jacobs, G.; Laughon, B.; Lehrman, S.; Makhene, M.; Mason, R. M.; Olivier, K. N.; Polis, M. A.; Prevots, D. R.; Sizemore, C.; Spinelli, B. A.; Taylor, K.; Touchette, N. A.; Via, L. E. Multidrug-resistant and extensively drug-resistant tuberculosis: The National Institute of

Allergy and Infectious Diseases research agenda and recommendations for priority research. *J. Infect. Dis.* **2008,** 197, 1493-1498.

71. Padayatty, S. J.; Katz, A.; Wang, Y.; Eck, P.; Kwon, O.; Lee, J. H.; Chen, S.; Corpe, C.; Dutta, A.; Dutta, S. K.; Levine, M. Vitamin C as an antioxidant: evaluation of its role in disease prevention. *J. Am. Coll. Nutr.* **2003,** 22, 18-35.
72. Vilchèze, C.; Hartman, T.; Weinrick, B.; Jacobs Jr, W. R. Mycobacterium tuberculosis is extraordinarily sensitive to killing by a vitamin C-induced Fenton reaction. *Nat. Commun.,* **2013,** 4:1881, 1-10.
73. Yano, T.; Kassovska-Bratinova, S.; Teh, J. S.; Winkler, J.; Sullivan, K.; Isaacs, A.; Schechter, N. M.; Rubin, H. Reduction of Clofazimine by Mycobacterial Type 2 NADH:Quinone Oxidoreductase: A pathway for the generation of bactericidal levels of reactive oxygen species. *J. Biol. Chem.* **2011,** 286, 10276-10287.
74. Lee, S. J.; Wegner, S. A.; McGarigle, C. J.; Bierer, B. E.; Antin, J. H. *Treatment of Chronic Graft-Versus-Host Disease With Clofazimine*. 1997; Vol. 89, p 2298-2302.
75. D'Autreaux, B.; Toledano, M. B. ROS as signalling molecules: mechanisms that generate specificity in ROS homeostasis. *Nat. Rev. Mol. Cell Biol.* **2007,** 8, 813-824.
76. Cook, J. A.; Pass, H. I.; Iype, S. N.; Friedman, N.; DeGraff, W.; Russo, A.; Mitchell, J. B. Cellular Glutathione and Thiol Measurements from Surgically Resected Human Lung Tumor and Normal Lung Tissue. *Cancer Res.* **1991,** 51, 4287-4294.
77. Godwin, A. K.; Meister, A.; O'Dwyer, P. J.; Huang, C. S.; Hamilton, T. C.; Anderson, M. E. High resistance to cisplatin in human ovarian cancer cell lines is associated with marked increase of glutathione synthesis. *Proc. Natl. Acad. Sci. USA* **1992,** 89, 3070-3074.
78. Chen, X.; Zhou, Y.; Peng, X.; Yoon, J. Fluorescent and colorimetric probes for detection of thiols. *Chem. Soc. Rev.* **2010,** 39, 2120-2135.
79. Lopez-Lazaro, M. Dual role of hydrogen peroxide in cancer: Possible relevance to cancer chemoprevention and therapy. *Cancer Lett.* **2007,** 252, 1-8.

80. Keyes, S. R.; Rockwell, S.; Sartorelli, A. C. Modification of the Metabolism and Cytotoxicity of Bioreductive Alkylating Agents by Dicoumarol in Aerobic and Hypoxic Murine Tumor Cells. *Cancer Res.* **1989,** 49, 3310-3313.

81. Trachootham, D.; Alexandre, J.; Huang, P. Targeting cancer cells by ROS-mediated mechanisms: a radical therapeutic approach? *Nat. Rev. Drug Discov.* **2009,** 8, 579-591.

82. Keyes, S. R.; Rockwell, S.; Sartorelli, A. C. Modification of the metabolism and cytotoxicity of bioreductive alkylating agents by dicoumarol in aerobic and hypoxic murine tumor cells. *Cancer Res.* **1989,** 49, 3310-3313.

83. Chen, Q.; Cederbaum, A. I. Menadione cytotoxicity to Hep G2 cells and protection by activation of nuclear factor-kappaB. *Mol. Pharmacol.* **1997,** 52, 648-657.

84. Vallis, K. A.; Wolf, C. R. Relationship between the adaptive response to oxidants and stable menadione-resistance in Chinese hamster ovary cell lines. *Carcinogenesis* **1996,** 17, 649-654.

85. Beck, R.; Verrax, J.; Dejeans, N.; Taper, H.; Calderon, P. B. Menadione reduction by pharmacological doses of ascorbate induces an oxidative stress that kills breast cancer cells. *Int. J. Toxicol.* **2009,** 28, 33-42.

86. Chlebowski, R. T.; Dietrich, M.; Akman, S.; Block, J. B. Vitamin K3 inhibition of malignant murine cell growth and human tumor colony formation. *Cancer Treat Rep.* **1985,** 69, 527-532.

87. Prasad, K. N.; Edwards-Prasad, J.; Sakamoto, A. Vitamin K3 (menadione) inhibits the growth of mammalian tumor cells in culture. *Life Sci.* **1981,** 29, 1387-1392.

88. Parkinson, E. I.; Bair, J. S.; Cismesia, M.; Hergenrother, P. J. Efficient NQO1 Substrates are Potent and Selective Anticancer Agents. *ACS Chem. Biol.* **2013,** 8, 2173-2183.

89. Bair, J. S.; Palchaudhuri, R.; Hergenrother, P. J. Chemistry and Biology of Deoxynyboquinone, a Potent Inducer of Cancer Cell Death. *J. Am. Chem. Soc.* **2010,** 132, 5469-5478.

90. Li, Y.; Sun, X.; LaMont, J. T.; Pardee, A. B.; Li, C. J. Selective killing of cancer cells by beta -lapachone: direct checkpoint activation as a strategy against cancer. *Proc. Natl. Acad. Sci. USA* **2003,** 100, 2674-2678.

91. Pink, J. J.; Planchon, S. M.; Tagliarino, C.; Varnes, M. E.; Siegel, D.; Boothman, D. A. NAD(P)H:Quinone oxidoreductase activity is the principal determinant of beta-lapachone cytotoxicity. *J. Biol. Chem.* **2000,** 275, 5416-5424.

92. Shi, K.; Wang, D.; Cao, X.; Ge, Y. Endoplasmic Reticulum Stress Signaling Is Involved in Mitomycin C(MMC)-Induced Apoptosis in Human Fibroblasts via PERK Pathway. *PLoS ONE* **2013,** 8, e59330.

93. Kim, K. K.; Lange, T. S.; Singh, R. K.; Brard, L.; Moore, R. G. Tetrathiomolybdate sensitizes ovarian cancer cells to anticancer drugs doxorubicin, fenretinide, 5-fluorouracil and mitomycin C. *BMC Cancer* **2012,** 12, 1471-2407.

94. Troxell, B.; Xu, H.; Yang, X. F. Borrelia burgdorferi, a Pathogen That Lacks Iron, Encodes Manganese-dependent Superoxide Dismutase Essential for Resistance to Streptonigrin. *J. Biol. Chem.* **2012,** 287, 19284-19293.

95. Bolzan, A. D.; Bianchi, M. S. Genotoxicity of streptonigrin: a review. *Mutat. Res.* **2001,** 488, 25-37.

96. Logan, A.; Shabalina, I. G.; Prime, T. A.; Rogatti, S.; Kalinovich, A. V.; Hartley, R. C.; Budd, R. C.; Cannon, B.; Murphy, M. P. In vivo levels of mitochondrial hydrogen peroxide increase with age in mtDNA mutator mice. *Aging Cell* **2014,** 13, 765-768.

97. Liochev, S. I. Reactive oxygen species and the free radical theory of aging. *Free Radical Biol. Med* **2013,** 60, 1-4.

98. Raha, S.; Robinson, B. H. Mitochondria, oxygen free radicals, disease and ageing. *Trends in Biochem. Sci.* **2000,** 25, 502-508.

99. Kalghatgi, S.; Spina, C. S.; Costello, J. C.; Liesa, M.; Morones-Ramirez, J. R.; Slomovic, S.; Molina, A.; Shirihai, O. S.; Collins, J. J. Bactericidal Antibiotics Induce Mitochondrial Dysfunction and Oxidative Damage in Mammalian Cells. *Sci. Transl Med.* **2013,** 5, 192ra85.

100. Bellomo, G.; Jewell, S. A.; Thor, H.; Orrenius, S. Regulation of intracellular calcium compartmentation: studies with isolated hepatocytes and t-butyl hydroperoxide. *Proc. Natl. Acad. Sci. USA* **1982,** 79, 6842-6846.

101. Koubek, E.; Haggett, M. L.; Battaglia, C. J.; Ibne-Rasa, K. M.; Pyun, H. Y.; Edwards, J. O. Kinetics and Mechanism of the Spontaneous Decompositions of Some Peroxoacids, Hydrogen Peroxide and t-Butyl Hydroperoxide. *J. Am. Chem. Soc.* **1963,** 85, 2263-2268.

102. Latour, I.; Demoulin, J. B.; Buc-Calderon, P. Oxidative DNA damage by t-butyl hydroperoxide causes DNA single strand breaks which is not linked to cell lysis. A mechanistic study in freshly isolated rat hepatocytes. *FEBS Lett.* **1995,** 373, 299-302.

103. Chen, Q.; Cederbaum, A. I. Menadione Cytotoxicity to Hep G2 Cells and Protection by Activation of Nuclear Factor-ŒʃB. *Mol. Pharmacol.* **1997,** 52, 648-657.

104. Brynildsen, M. P.; Winkler, J. A.; Spina, C. S.; MacDonald, I. C.; Collins, J. J. Potentiating antibacterial activity by predictably enhancing endogenous microbial ROS production. *Nat. Biotechnol.,* **2013,** 31, 160-165.

105. Massey, V.; Strickland, S.; Mayhew, S. G.; Howell, L. G.; Engel, P. C.; Matthews, R. G.; Schuman, M.; Sullivan, P. A. The production of superoxide anion radicals in the reaction of reduced flavins and flavoproteins with molecular oxygen. *Biochem. Biophys. Res. Commun.* **1969,** 36, 891-897.

106. Bruice, T. C.; Yano, Y. Radical mechanisms for 1,5-dihydro-5-methylflavine reduction of carbonyl compounds. *Journal of the American Chemical Society* **1975,** 97, 5263-5271.

107. Eberlein, G.; Bruice, T. C. One and two electron reduction of oxygen by 1,5-dihydroflavins. *Journal of the American Chemical Society* **1982,** 104, 1449-1452.

CHAPTER 2.1: DESIGN, SYNTHESIS AND EVALUATION OF DIHYDROQUINONES AS REACTIVE OXYGEN SPECIES (ROS) GENERATORS

2.1.1. Introduction:

Generation of reactive oxygen species (ROS) plays crucial role in different areas of pathology and physiology. ROS such as superoxide, $O_2^{\bullet -}$, hydrogen peroxide, H_2O_2 and hydroxyl radicals, $^{\bullet}OH$ are produced by reduction of oxygen in electron donor redox centers in cells (Scheme 2.1.1A). Mitochondria can produce $O_2^{\bullet -}$and H_2O_2 in cells, which can get converted into $^{\bullet}OH$ by Fe^{2+} in the Fenton reaction.[1-4] Damaging effects of ROS at elevated concentrations to biomacromolecules such as DNA, protein and lipids are well documented (Scheme 2.1.1B).[1-3] Immune system produces ROS in a highly controlled fashion to counteract invading pathogens during pathogenesis. A scaffold based on organic small molecules that generate ROS in a programmed manner inside cells could be a mimic to immune system for enhancement of intracellular ROS to target pathogens.

Scheme 2.1.1. (A) Reactive oxygen species (ROS) are generated through reduction of oxygen; (B) ROS can damage biomacromolecules such as proteins and DNA.

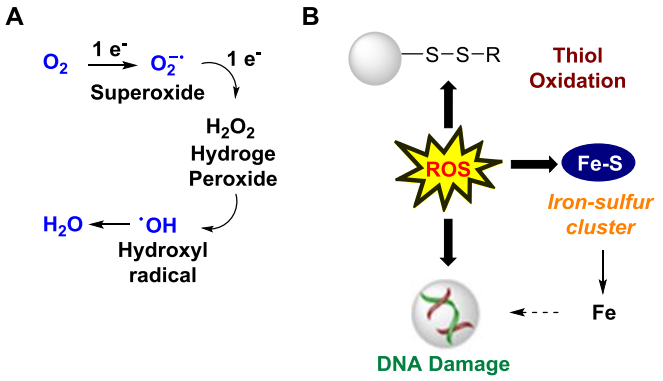

Scheme 2.1.2 Bioreduction of 1,4-quinones to hydroquinones and ROS generation upon exposure to oxygen

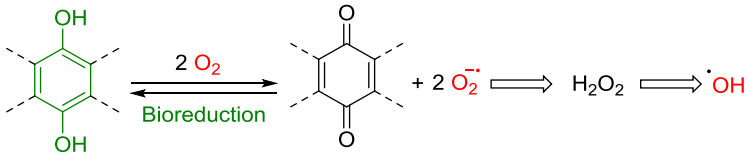

Quinones are ubiquitous in nature and constitute an important class of natural product that is involved in electron transport chain and photosynthesis in plants, fungi and bacteria. Quinones are well known sources of ROS, where these undergo a bioreduction to generate 1,4-diol (hydroquinone) and subsequent exposure to oxygen produces ROS such as $O_2^{\bullet -}$ and H_2O_2 (Scheme 2.1.2).[5-7] Quinones such as 1,4-naphthoquinone, 2-methyl-1,4-naphtoquinone, juglone, plumbagin, 1,2-naphthoquinone, 2-methylanthraquinone, 9, 10-phenanthraquinone and acenaphthenquinone (Figure 2.1.1) were studied for their ability to generate ROS in cells and consequent damaging effects to DNA.[8,9]

Figure 2.1.1. Structures of quinone based ROS generators

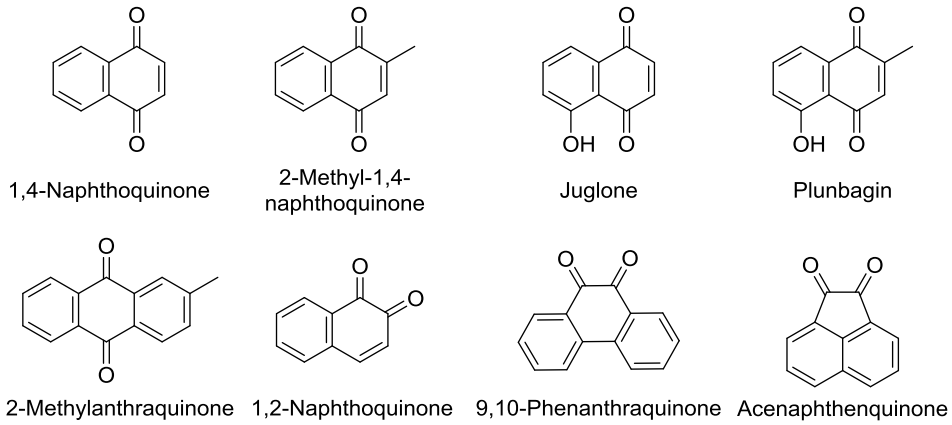

Industrial production of H_2O_2 is initiated by *in situ* catalytic hydrogenation of anthraquinone to produce 9,10-dihydroxyanthracene, which then spontaneously reacts with molecular oxygen to produce H_2O_2, presumably through the intermediacy of superoxide anion (Scheme 2.1.3).[10]

Scheme 2.1.3. Anthraquinone process for the production of H_2O_2.

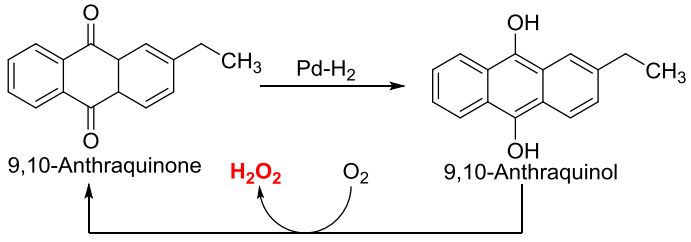

However, there are just a few reliable methods for the controlled generation of ROS *in vivo*. It is anticipated that such a strategy would not only facilitate investigating the roles of ROS in bacterial responses to antibiotics but could help with the development of novel therapeutic agents to overcome drug resistance as well. Our design of ROS sources was based on the observation that aromatic 1,4-diols react with molecular oxygen to produce H_2O_2. Aromatic quinols themselves are not good candidates as H_2O_2 generators due to their susceptibility to undergo aerobic oxidation, difficulty of isolation. Furthermore, these diols do not have a structural handle to modulate rates of ROS generation. Instead, we considered surrogates of hydroquinone, 2,3-dihydro-1,4-benzoquinones (**A**) as potential ROS generators (Scheme 2.1.4). Conversion of **A** to its tautomer 1,4-dihydroxynaphthalene (**B**) might occur under physiological pH; the diol **B** can undergo aerobic oxidation to give **C** with concomitant production of superoxide and H_2O_2 as inorganic products (Scheme 2.1.4). Ring size "n" and functional groups X and Y provide structural handles to modulate ROS generation profiles through perturbation of the keto-enol equilibrium (Table 2.1.1).

Scheme 2.1.4. Compounds of type **A** tautomerize to **B**, which can react with oxygen to generate superoxide and H_2O_2 as the inorganic products with concomitant formation of **C**. Bioreduction of quinone **C** and further redox cycling might also produce ROS.

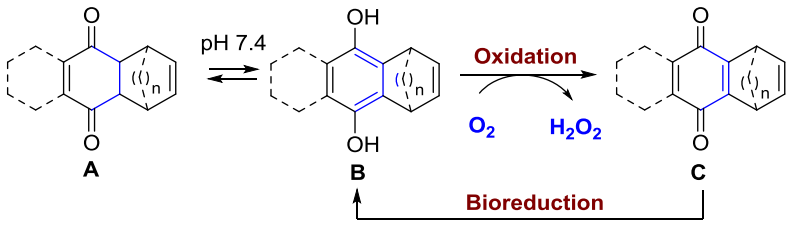

1,4-Quinones such as **C** are candidates for bioreduction by enzymes such as NADPH: cytochrome P450 reductase to generate quinol **B**, which can react with oxygen to produce ROS.[11-15] Thus, the use of **A** as a candidate for intracellular oxidation[16-18] with concomitant introduction of reactive oxygen species could act in conjunction with introduction of quinone **C**, and together result in perturbation of intracellular redox equilibrium (Scheme 2.1.4).

2.1.2 Results and Discussion:

2.1.2.1 Synthesis, characterization and ROS generation studies in buffer:

In order to test our hypothesis that 2,3-dihydro-1,4-benzoquinones are candidates for ROS generation, compounds **1-8** were synthesized from commercially available 1,4-naphthoquinones and 1,3-dienes in yields ranging from 58-87% (Table 2.1.1). Starting from 1,4-benzoquinone, compounds **9-12** were synthesized in excellent yields after reacting with either 1,3-cyclopentadiene or 1,3-cyclohexadiene (Scheme 2.1.5).

Table 2.1.1. Synthesis of **1-8** by a [4 + 2] cycloaddition.

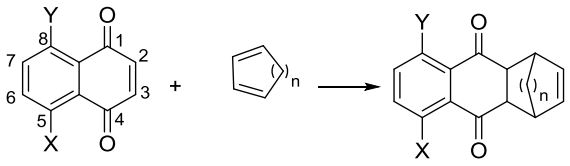

Entry	X	Y	n	Product	Yield (%)
1	H	H	1	**1**	87
2	H	H	2	**2**	81
3	OH	H	1	**3**	80
4	OH	H	2	**4**	78
5	OH	OH	1	**5**	83
6	OH	OH	2	**6**	71
7	OBn	H	1	**7**	58
8	OBn	H	2	**8**	72

In order to test whether **1-12** were sources of ROS, these compounds were incubated in pH 8.0 buffer under ambient aerobic conditions and their ability to generate superoxide ($O_2^{\bullet-}$) was evaluated using a luminol based chemiluminescence assay. A reaction of luminol with $O_2^{\bullet-}$ leads to nitrogen extrusion and simultaneous formation of excited state species of 3-aminobenzene-1,2-dicarboxylate. Returning of the excited state species to

ground state emits light (luminescence), and the emission is recorded as a measure of superoxide generated during the reaction (Scheme 2.1.6).

Scheme 2.1.5. Synthesis of **9-12** from benzoquinone.

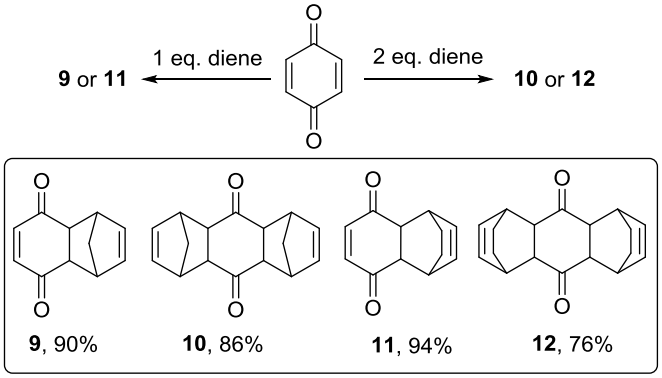

Scheme 2.1.6. Reaction of luminol with superoxide radical ($O_2^{\bullet -}$)

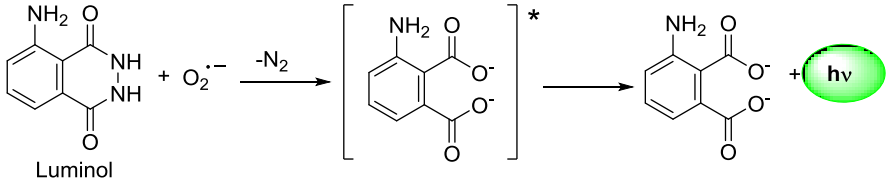

Using this luminol assay, superoxide generated by **1-12** during 30 min in pH 8.0 was evaluated (Figure 2.1.2).[19] A wide range of superoxide levels were observed with **1-12** and **4** was found to be the best superoxide generator amongst **1-12** (Figure 2.1.2). The intermediacy of superoxide was also confirmed by complete abrogation of luminescence attributable to this species in the presence of superoxide dismutase (SOD), an enzyme that catalyzes the decomposition of superoxide to oxygen and hydrogen peroxide. Hydrogen peroxide, the less reactive and more stable ROS, is formed by a $1e^-$ transfer to superoxide (Scheme 2.1.1A). The amount of H_2O_2, generated during 30 min incubation of **1-12** in pH 7.4 was estimated using a xylenol orange-based colorimetric assay (Figure 2.1 3).[20,21] Compounds **4** and **6** were the best hydrogen peroxide generators amongst analogues **1-12** (Table 2.1.2, entries 4 and 6).

Figure 2.1.2. Superoxide detection: Superoxide generated during incubation of **1-12** (5 μM) in pH 8.0 buffer at 37 ºC for 30 min was estimated by a luminol-based chemiluminescence assay.

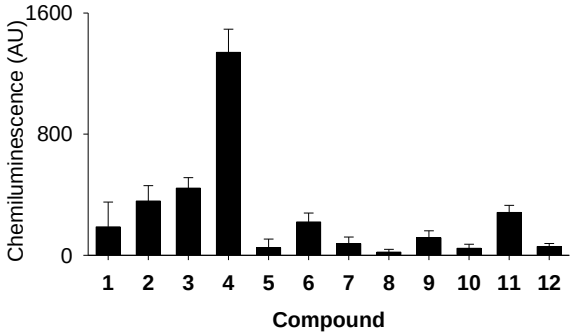

Table 2.1.2. H_2O_2 yields during incubation of **1-12** in pH 7.4.

Entry	Compd	H_2O_2, pH 7.4 (%)[a]
1	**1**	5.1
2	**2**	5.1
3	**3**	8.7
4	**4**	11.1
5	**5**	4.0
6	**6**	11.1
7	**7**	4.7
8	**8**	6.0
9	**9**	4.1
10	**10**	1.9[c]
11	**11**	10.4
12	**12**	5.0[c]

[a]H_2O_2 generated during incubation of **1-12** (5 μM) in pH 7.4 buffer at 37 ºC during 30 min was estimated by a xylenol orange-based colourimetric assay. We found no significant colour formation in the presence of catalase suggesting the generation of H_2O_2. [c]Calculated based on 2 mol H_2O_2 from 1 mol of compound.

Figure 2.1.3. Hydrogen peroxide estimation: Hydrogen peroxide generated during incubation of **1**-**12** (5 μM) in pH 7.4 buffer for 30 min at 37 ºC was estimated using xylenol orange-based colorimetric assay.

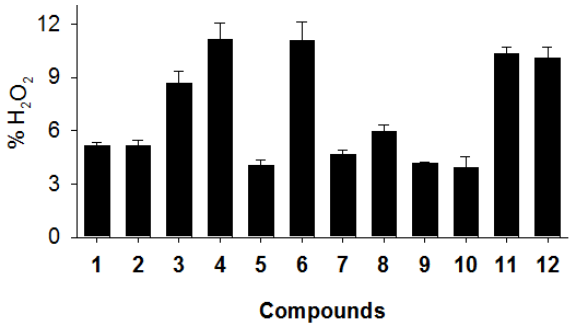

Figure 2.1.4. DNA damage assay: (a) Reaction mixtures (20 μL) contained 100 ng of Form I DNA in pH 8.0 phosphate buffer (100 mM) and compounds were incubated at 37 °C for 6 h: CTR: untreated control; Lane 1, 50 μM **1** + Fe(II); Lane 2, 50 μM **2** + Fe(II); Lane 3, 50 μM **3** + Fe(II); Lane 4, 50 μM **4** + Fe(II); Lane 5, 50 μM **5** + Fe(II); Lane 6, 50 μM **6** + Fe(II); Lane 7, 50 μM **7** + Fe(II); Lane 8, 50 μM **8** + Fe(II); Lane 9, 50 μM **9** + Fe(II); Lane 10, 50 μM **10** + Fe(II); Lane 11, 50 μM **11** + Fe(II); Lane 12, 50 μM **12** + Fe(II). Nicked DNA is represented by II. (b) Relative nuclease activity is with respect to untreated control and is defined as the ratio of Form II (nicked) to Form I (supercoiled plasmid) and is obtained by digitized image analysis.

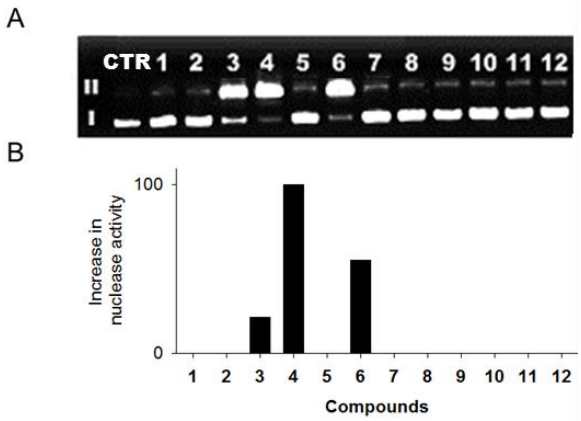

Hydroxyl radical is perhaps the most reactive of the ROS generated *in vivo* and is produced through Fenton-type chemistry in the presence of metal ions. Hydroxyl radical

causes extensive damage to biomacromolecules such as DNA.[22-24] Nuclease activity of **1-12** was estimated using a pBR322 supercoiled plasmid DNA-based assay.[25] In the presence of Fe(II) and compounds **1-12** at 50 μM concentrations during 6 h, nick induction was observed in nearly all compounds tested (Figure 2.1.4a). We found no evidence for nick induction in the absence of Fe(II) suggesting the involvement of hydroxyl radical in mediating the observed nuclease activity.

Again, **4** was found to be the best DNA damage-inducing agent with nearly 70-fold increase in nuclease activity in comparison with control (Figure 2.1.4b) followed by **6** (54-fold) and **3** (33-fold). Compounds **3**, **4** and **6** were also amongst the best superoxide and hydrogen peroxide generators of **1-12** suggesting a role for the proximal hydroxyl group. Several reports have shown a strong intramolecular H-bonding in 3-hydroxyketones (Scheme 2.1.7).[26] For example, H-atom exchange is documented in 9-hydroxyphenalenone leading to delocalization of π-electrons (inset, Scheme 2.1.7). The O···O bond distance in the case of 9-hydroxyphenalenone was found to be 2.486 Å.[26]

Scheme 2.1.7. Strong intramolecular H-bonding results in delocalization of π-electrons of 9-hydroxyphenalenone.

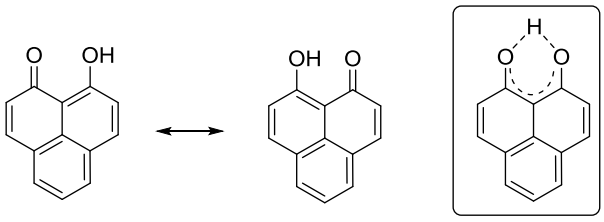

Figure 2.1.5. Crystal structures: ORTEP diagrams for (a) **4** and (b) **6** shows intramolecular H-bonding between the H-atom of the hydroxyl group and the carbonyl oxygen.

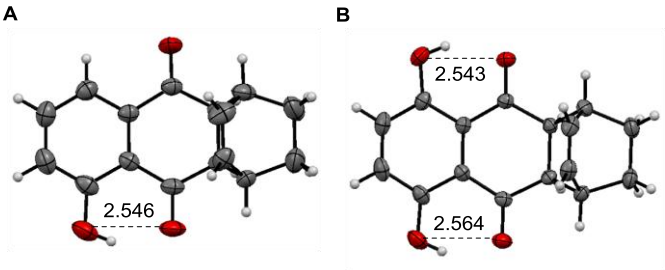

We found evidence for intramolecular H-bonding by X-ray diffraction analysis of crystalline **4** and **6** and obtained O···O bond distances as ~2.54 Å (Figure 2.1.5). Thus, delocalization of the π-electrons (**4B**) through H-exchange between **4** and **4A** (Scheme 2.1.8) might be predicted.

Scheme 2.1.8. Intramolecular H-bonding might result in rearrangement of **4** to **4A**; structure **4B** is a representation of the expected π-electron delocalization.

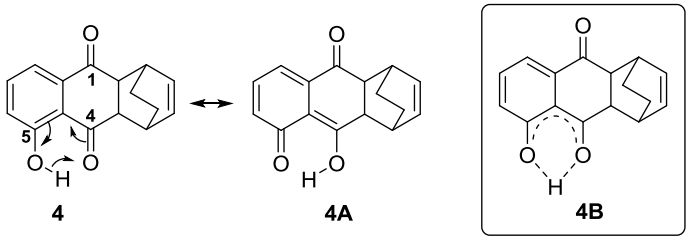

Figure 2.1.6. IR stretching frequencies for selected compounds prepared in this study.

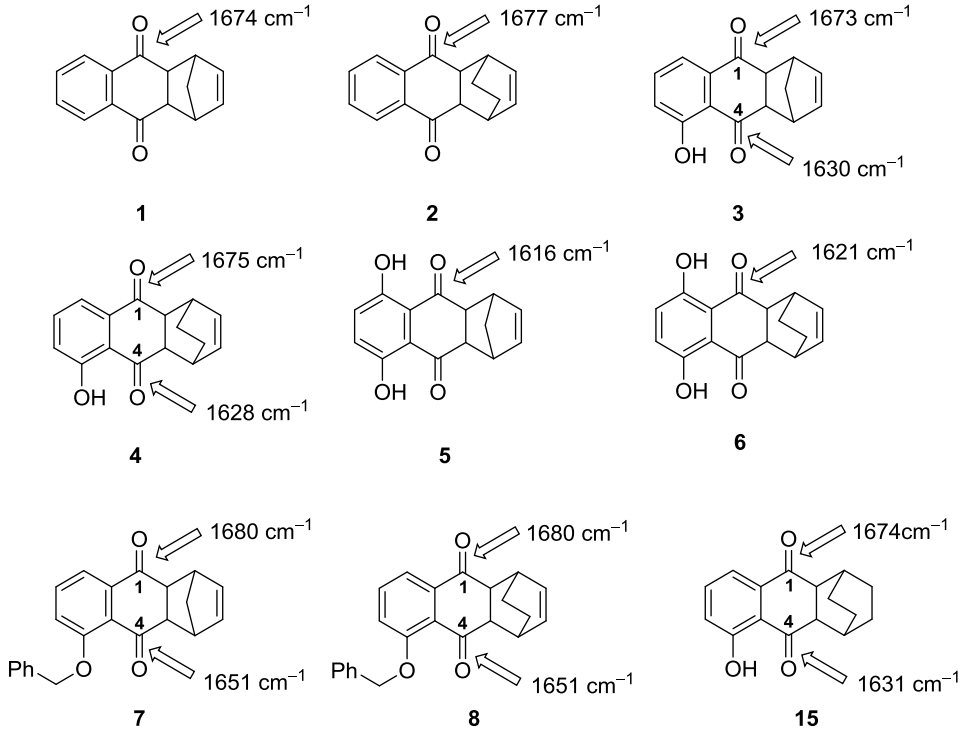

A possible consequence of delocalization is the lengthening of the carbonyl of C-1 in **4** in comparison with C-4 of **4** (Figure 2.1.5a). Indeed, X-ray diffraction analysis shows

C-1···O bond distance as 1.218 Å while the C-4···O bond distance was found to be 1.235 Å (Figure 2.1.5a). A similar elongation of the C···O bond (1.24 Å) was observed for **6** (Figure 2.1.5b). Lengthening of the carbonyl of C-1 in **4** was also confirmed by IR spectroscopy. The $\nu_{C=O}$ for **1** and **2** were experimentally determined as 1674 and 1677 cm^{-1}, respectively (Figure 2.1.6). The C-4 $\nu_{C=O}$ for **3** and **4** were significantly diminished as 1630 and 1628 cm^{-1}, respectively (Figure 2.1.6). Similarly, in the cases of **5** and **6**, $\nu_{C=O}$ were found as 1616 and 1621 cm^{-1}, respectively (Figure 2.1.6). The C-1 carbonyls of **3** and **4** were comparable with **1** and **2** suggesting that intramolecular H-bonding leads to significant reduction of the carbonyl double bond character. Removal of H-bonding capability by introduction of a benzyl group results in a higher stretching frequency: C-4 $\nu_{C=O}$ for **8** was found as 1651 cm^{-1} (Figure 2.1.6).

Scheme 2.1.9. Proposed mechanism for generation of ROS during incubation of 2,3-dihydro-1,4-benzoquinones in pH 7.4 buffer.

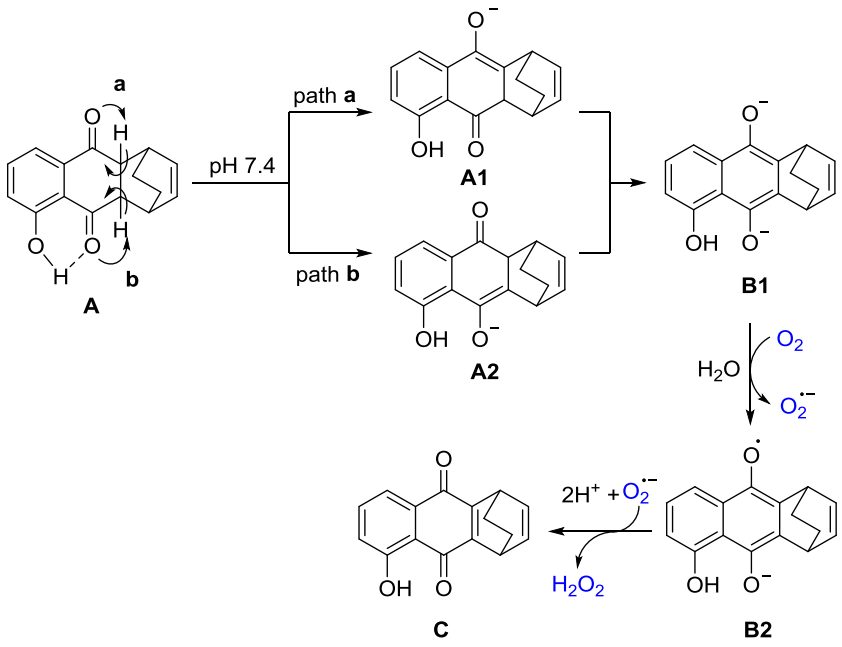

The following mechanism for ROS generation during incubation of **4** was considered. Keto-enol tautomerism produces enolates **A1** (path **a**) and/or **A2** (path **b**), which then rearranges to give **B1**, which can react with oxygen to generate superoxide by a 1 e^- transfer to produce **B2** (Scheme 2.1.9).[27-29] **B2** can further transfer an additional electron

to superoxide to produce hydrogen peroxide and the quinone **C** (Scheme 2.1.9).[26-28] Energy minimizations on **2**, **4**, **6** and **8** using DFT-B3LYP-631G (d,p) were carried out and an electron density map were generated. Here, we found an increased electronegativity (–0.556 versus –0.480) on the oxygen of carbonyls adjacent to a hydroxyl group (Figure 2.1.7). This result supports a preferential enolization at C-3, C-4 (path **b**) in comparison with C1-C2 (path **a**, Scheme 2.1.9).

Figure 2.1.7. Calculated electronegativities for **2**, **4**, **6** and **8**.

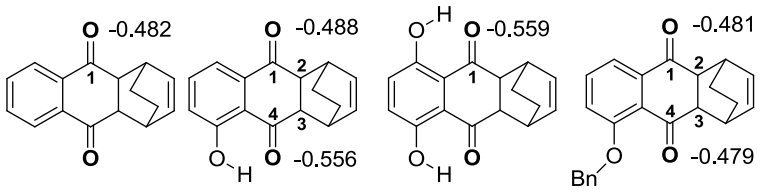

As enolization of **3** would result in the formation of a double bond attached to a 5-membered ring, placing an olefin adjacent to a five-membered ring might be less favourable than a six-membered ring (angle strain) in the case of **4**. Perhaps, relative ease of enolization of **4** in comparison with **3** might help explain the higher levels of ROS generation from **4** (Figure 2.1.2, Table 2.1.2, Figure 2.1.3). A similar trend was seen in the cases of **5** and **6** as shown in Table 2.1.2, entries 5,6. As the juglone derivative **4** was the best generator of superoxide and H_2O_2 amongst **1**-**12** (Figure 2.1.2, Figure 2.1.3, Table 2.1.2), further studies were carried out on compound **4**.

2.1.2.2. Studies on ROS generation and mechanisms of compound 4:

A time course experiment for superoxide generation from **4** was conducted. A gradual increase in the level of superoxide over a period of 30 min was measured using luminol based chemiluminescence assay. Superoxide generation profile of **4** was compared with a derivative of **4**, in which 5-OH group protected with benzyl group, **8**, in which significantly a lower level of superoxide generation was observed from **8** proving further the importance of hydrogen bonding to promote superoxide generation. A standard method for superoxide generation is enzymatic oxidation of xanthine by xanthine oxidase (X+XO). We found a sharp rise in the chemiluminescence as an evidence for superoxide generation within 5 min of incubation and slow decay in the level of superoxide was

recorded. A slow and steady generation of superoxide in cells is necessary to study intracellular effects of superoxide, which cannot be achieved with X+XO based enzymatic method and thus, compound **4** is better suited for intracellular studies than X+XO (Figure 2.1.8A).

Figure 2.1.8. Measurement of superoxide generation from **4** and **8** in pH 8.0 phosphate buffer at 37 °C. (A) Time course of $O_2^{-\bullet}$ generation during incubation in pH 8.0 buffer over 30 min was studied by a luminol chemiluminescence assay (B) A high performance liquid chromatograph (HPLC)-based dihydroethidium (DHE) assay was used to infer generation of $O_2^{\bullet-}$ after incubation of compounds (50 µM) in pH 8.0 buffer for 1 h. 2-Hydroxyethidium (2-OH-E^+), which is exclusively formed by the reaction of $O_2^{\bullet-}$ with DHE elutes at 28.6 min, and ethidium E^+, which is formed by non-specific oxidation of DHE elutes at 29.5 min.(Figure 2.1.8B)

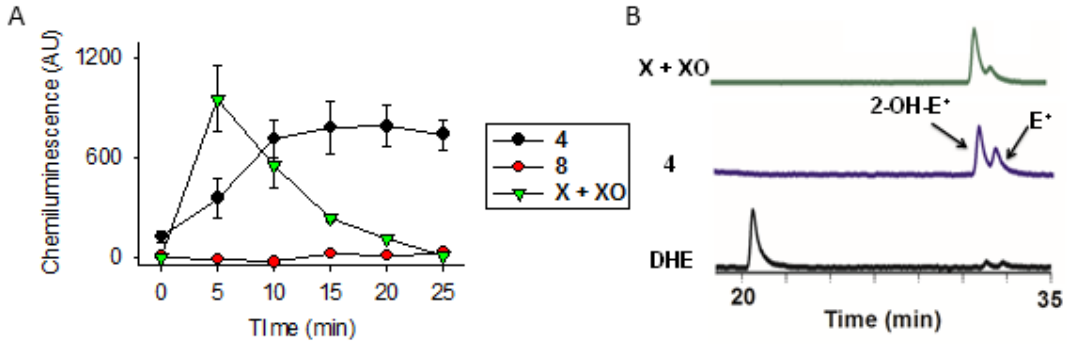

Scheme 2.1.10. A scheme for formation of 2-OH-E^+ and E^+ during reaction of DHE with ROS

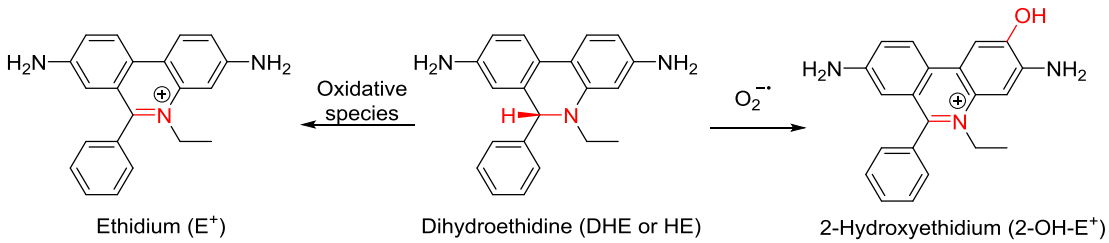

A dihydroethidium (DHE) based HPLC analysis was used to infer superoxide generation independently. DHE is a fluorescent probe regularly used for intracellular ROS detection.[30-32] A reaction of DHE with superoxide produces 2-hydroxyethidium (2-

OH-E^+) as a specific oxidized product which is fluorescent whereas the non-specific oxidation of DHE with other ROS produces fluorescent ethidium (E^+) dye (Scheme 2.1.10). Both these oxidized products elute in different retention times under HPLC conditions. This fluorescence based HPLC method is widely used for the detection of superoxide as well as other oxidative species generation.[30-32]

An authentic sample of DHE was injected in HPLC which indicated a peak at 20.8 min, an addition of X+XO to DHE in pH 7.4 phosphate buffer generated a new peak at 30.8 min corresponding to 2-OH-E^+ indicating superoxide is a major product, and a small peak at 31.6 min was identified as E^+ as an evidence for the formation of other oxidative species in minor proportions (Figure 2.1.8B). A similar experiment was carried out for **4** with DHE in pH 7.4 phosphate buffer. After incubation for 60 min at 37 °C the reaction mixture was injected in HPLC to find a neat conversion of DHE to 2-OH-E^+ (as a major product) and E^+ (Figure 2.1.8B). Evidence for formation of both the oxidized species (2-OH-E^+ and E^+) were obtained from mass spectral analysis. This experiment authenticates the generation of superoxide from **4** in buffer under physiological conditions.

Figure 2.1.9. Decomposition studies and estimation of H_2O_2 from **4.** (A) HPLC traces of incubation of **4** in pH 7.4 buffer during 12 h shows complete conversion of **4** to **18**; (B) Estimation of H_2O_2 generated during incubation with 10 µM of the compound **4** in pH 7.4 phosphate buffer was estimated using an Amplex Red® fluorescence assay.

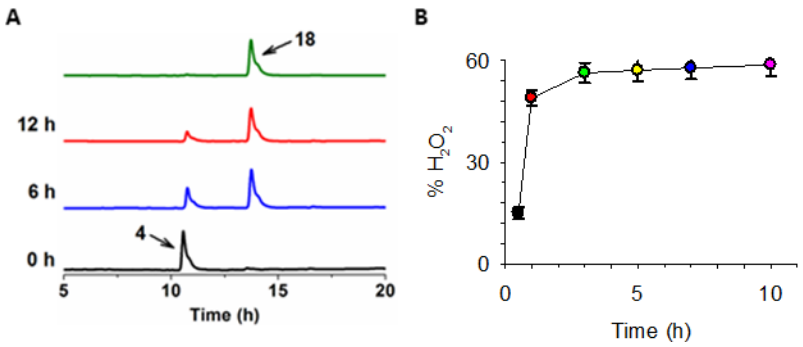

Next, HPLC mediated decomposition study was carried out to identify the product formed during the reaction of **4** in aerobic buffer. Compound **4** was incubated in pH 7.4 aerobic buffer at 37 °C, and the decomposition profile was monitored using HPLC analysis. After 12 h of reaction in buffer, nearly complete disappearance of the peak for **4**

at 10.6 min was observed with concomitant formation of a new peak at 13.8 min (Figure 2.1.9A). The expected decomposition product is **18**, which is the oxidized derivative of **4**. Independently we have synthesized **18** by a reported procedure (Scheme 2.1.11)[33] and the decomposition product of **4** was identified by comparing the HPLC trace of authentic compound **18**. A nearly complete conversion of **4** to **18** was found in 12 h which was followed using HPLC analysis (Figure 2.1.9a).

Simultaneously, a time course for H_2O_2 generation from **4** was recorded for 12 h in pH 7.4 buffer using Amplex Red assay. Amplex red is a non-fluorescent colorless substrate, highly sensitive to H_2O_2 (10 picomoles in 100 µL volume detection limit). A H_2O_2 selective enzyme, horse radish peroxidase (HRP) & catalyzed reaction of Amplex red with H_2O_2 at 1:1 stoichiometry, produces resorufin, a highly fluorescent dye. In this reaction, HRP catalyzes the formation of OH radical from H_2O_2 and a reaction of OH radical with Amplex Red produces resorufin (Scheme 2.1.12). A maximum H_2O_2 yield of 58% was quantified from compound **4** after 6 h and almost no change in the level was observed in the next 6 h (Figure 2.1.9b). Thus, **4** offers a temporal control over generation of ROS such as superoxide and H_2O_2 in buffer, hence proving to be a promising candidate for cellular studies.

Scheme 2.1.11. Synthesis of **18** from **4** and **19** from **15**

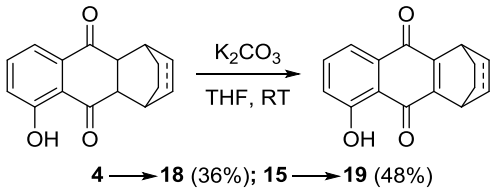

Scheme 2.1.12. A scheme for oxidation of non-fluorescent Amplex Red® by H_2O_2 to fluorescent resorufin in the presence of horse radish peroxidase (HRP) enzyme

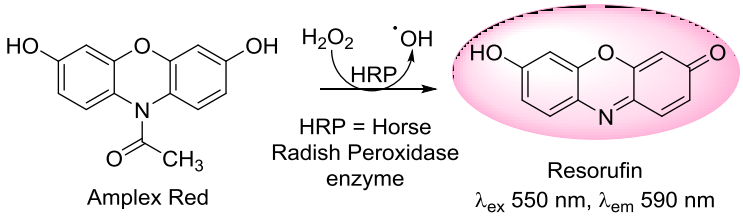

2.1.2.3. Extracellular and intracellular ROS generation studies in bacteria:

Having established ROS generation in aerobic buffer using a series of 2,3-dihydronaphthoquinone based small organic molecules we have tested the compounds for their ability to generate ROS in two different bacterial cultures *viz*., a Gram negative bacterium, *Escherichia coli* (*E. coli*) and a Gram positive bacterium *Mycobacterium smegmatis* (*Msm*).

2.1.2.3.1. ROS generation studies in Escherichia coli (E. coli):

Due to its bi-layered cell wall with peptidoglycan and phospholipid, *E. coli* a Gram-negative bacterium, is one of the most difficult bacterium to inhibit. Cell permeability of a drug has been a primary challenge. *E. coli* has evolved with strong antioxidant response to counteract intracellular ROS induced by immune system for its survival. However, many recent reports have demonstrated that enhancement of intracellular ROS can sensitize this bacterium to antibiotics.[34-37] In this context, first the ability of the compounds to generate H_2O_2 in the presence of *E. coli* bacterium was studied using Amplex Red® based fluorescence assay. Using this assay extracellular H_2O_2 generation from **4** was recorded by incubating **4** (100 μM) with *E. coli* for 1 h at 37 °C, a maximum yield of 20 μM (20%) of H_2O_2 was measured after 1 h. Thus the ability of compound **4** to generate ROS in extracellular medium in the presence of bacterium was inferred. When the negative control **8** was tested, as expected no significant level of H_2O_2 generation was observed (Figure 2.1.10b).

Next, the ability of the compounds to permeate cells to generate ROS intracellularly was studied using two independent assays, namely, DHE assay and DCF-DA assay. Firstly, DHE assay was carried out for the detection of intracellular superoxide production in *E. coli* with **4** using HPLC attached with a fluorescent detector. Bacterial control showed unreacted DHE with diminished levels of 2-OH E^+ and E^+, upon the treatment of **4** and DHE with bacterium, significant increase in the peak intensity for 2-OH E^+ and E^+ was seen, this result is consistent with increase in intracellular superoxide production (Figure 2.1.10A).

Figure 2.1.10. ROS generation studies with bacteria: (A) HPLC traces of assay for intracellular $O_2^{\bullet-}$ production using a dihydroethidium (DHE) assay in *E. coli*. Incubation with the compounds (50 µM) was for 30 min and DHE levels indicate un-oxidized dye while 2-OH-E^+ formed is an indicator for $O_2^{\bullet-}$ production and E^+ is indicative of increase in oxidative species. (B) Estimation of hydrogen peroxide (H_2O_2) generated during incubation of *E. coli* with 50 µM of the compound in pH 7.4 was estimated using an Amplex Red® fluorescence assay. Student T-test performed on this data provided a P value of <0.001. (C) Increase in intracellular oxidative species upon treatment of *E.coli* with **4** and **8** was determined by a 2,7-dichlorodihydrofluorescein-diacetate (DCFH-DA)-based fluorescence assay and DMSO (0.5%) was used as control (Figure 2.1.10 B). Increase in intracellular fluorescence is obtained with respect to DMSO control. Student T-test performed on this data provided a P value of <0.001.

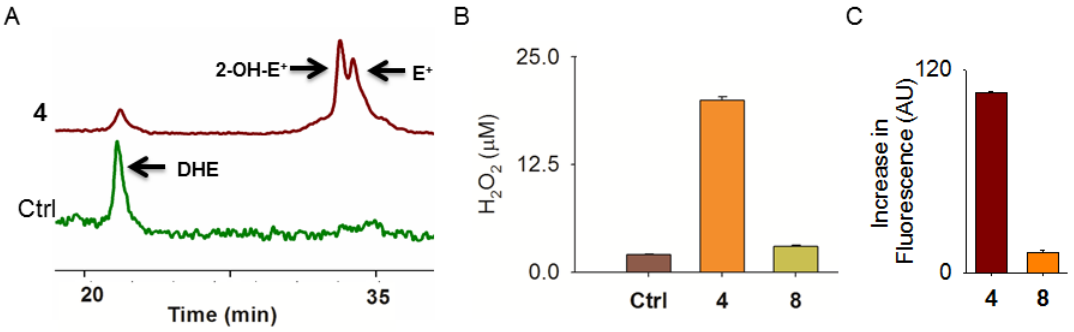

Scheme 2.1.13. A scheme for oxidation of non-fluorescent $DCFH_2$-DA by ROS to fluorescent dye

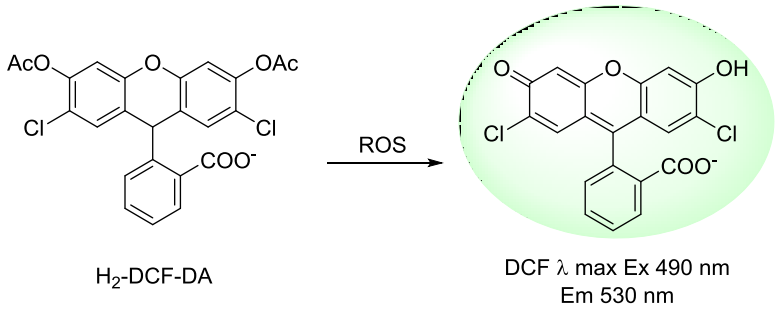

H_2-DCF-DA

DCF λ max Ex 490 nm
Em 530 nm

Further evidence for cell permeability of compounds and intracellular ROS generation was obtained using 2,7-dichlorodihydrofluorescein-diacetate ($DCFH_2$-DA)-based fluorescence assay. $DCFH_2$-DA is a weakly fluorescent cell permeable dye, which reacts efficiently with OH radical and to some extent with H_2O_2, and the fluorescence

turns on when $DCFH_2$-DA is oxidized by these ROS. When compound **4** was incubated with $DCFH_2$-DA treated *E. coli,* a significant increase in the fluorescence intensity was observed, while bacterial control alone did not show any enhanced fluorescence emission (Figure 2.1.10C). In support of fluorescence emission only by intracellular ROS generation, compound **8**, a negative control for ROS generation was incubated with pre-treated *E. coli* with DCF dye; only negligible level of fluorescence enhancement was observed (Figure 2.1.10C). These results suggest that, compound is capable of permeating *E. coli* and produce ROS inside cells to enhance the level of intracellular ROS.

2.1.2.3.1. ROS generation in Mycobacterium smegmatis (Msm):

Tuberculosis (TB) remains a leading cause of morbidity and mortality in much of the world.[38,39] *Mycobacterium tuberculosis* (*Mtb*), the etiological agent of this infectious disease, is a highly adaptive pathogen and possesses a nearly impenetrable cell wall thus making it an extremely difficult pathogen to kill.[39] Due to its thick waxy cell wall containing a peptidoglycan layer, cell permeability is being a major challenge in drug discovery for *Mtb.* The anti-mycobacterial activity exhibited by vitamin C was attributed to intracellular enhancement of ROS. Thus, enhancing intracellular ROS has a potential to target *Mtb*.[40]

Next, we sought to study the ROS generators prepared in this study to permeate mycobacterium cell wall to generate ROS inside cells. Since *Mtb* is a contagious pathogen, we performed our studies with *Mycobacterium smegmatis* (*Msm*) a non-pathogenic model bacterium comes under the class of mycobacterium. Amplex Red fluorescence assay was used to determine extracellular H_2O_2 generation from **4** in *Msm*, a yield of 6.8 % H_2O_2 was quantified after 60 min of incubation (Table 2.1.3, entry 1). We envisaged that the removal of external double bond in **4** could perturb the enolization and subsequent reaction with oxygen to generate ROS. An analogue of **4** was synthesized by a palladium catalyzed hydrogenation reaction and obtained **15** in 81% yield (Table 2.1.4, entry 3). Then, we have treated **15** with *Msm* for 60 min and measured to find an improved H_2O_2 yield of 11.1 % in comparison with its structural analogue **4** (Table 2.1.3, entry 5). Next, we have synthesized the reduced analogues of **1**, **3**, **5** & **6** using similar

experimental conditions to obtain compounds **13**, **14**, **16** & **17** in yields ranging from 78 – 95% (Table 2.1.4, entries 1, 2, 4 & 5). Extracellular H_2O_2 produced from **14** and **15** in *Msm* after 60 min were better than **4** (Table 2.1.3, entries 3, 4). During the decomposition of **15** for ROS generation, **19** resulted as an oxidized product and this was confirmed by comparing the HPLC traced of reaction mixture of **15** in buffer with authentic **19** independently synthesized (Scheme 2.1.11). No ROS generation is expected from **19** in buffer, consistently **19** did not produce any extracellular H_2O_2 during its incubation with *Msm.*

Table 2.1.3. H_2O_2 yields during incubation of **4, 13-17**, **19** in the presence of *Msm*

Entry	Compd	Extracell. H_2O_2 (%)[a]
1	**4**	6.8
2	**13**	2.5
3	**14**	8.2
4	**15**	11.1
5	**16**	2.7
6	**17**	3.8
7	**19**	-

[a]Extracell.= Extracellular, Amplex Red fluorescence assay was used for the measurement of H_2O_2 from compounds (50 μM) with *Msm.*

Generation of intracellular ROS from **13-17** were assayed using a HPLC based DHE assay, which is highly selective for the detection of intracellular $O_2^{\bullet-}$. During a reaction of DHE with $O_2^{\bullet-}$, 2-Hydroxyethidium (2-OH-E^+) is formed as an exclusive product, which elutes at 28.6 min and a non-specific oxidation of DHE leads to the formation of ethidium E^+, which elutes at 29.5 min. Compounds (50 μM) were incubated with DHE in *Msm* for 30 min and a peak at 21.6 min indicates unoxidized DHE, while 2-OH-E^+ formed is an indicator for $O_2^{\bullet-}$ production and E^+ is indicative of increase in oxidative species (Figure 2.1.11).

Table 2.1.4. Synthesis of **13-17** by palladium catalyzed hydrogenation

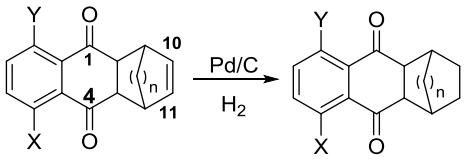

Entry	X	Y	n	Product	Yield (%)
1	H	H	1	**13**	91
2	OH	H	1	**14**	78
3	OH	H	2	**15**	81
4	OH	OH	1	**16**	87
5	OH	OH	2	**17**	95

Figure 2.1.11. Dihydroethidium (DHE) assay with *wt-Msm*: HPLC traces of assay for intracellular $O_2^{-\bullet}$ production using a dihydroethidium (DHE) assay in *Mycobacterium smegmatis* (*Wt-Msm*).

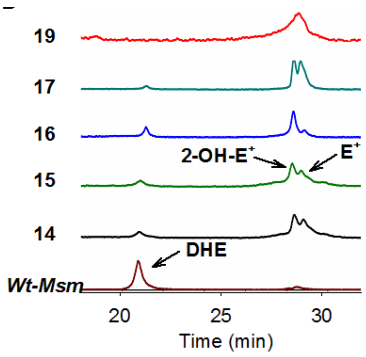

Thus, we have synthesized a library of 2,3-dihydro-1,4-naphtoquinones, and the compounds were found to enhance the extracellular H_2O_2 levels when treated with two of the highly challenging bacteria *E.coli* and *Mycobacterium*. We have demonstrated the compounds ability to permeate bacterial cell wall to enhance intracellular ROS levels.

2.1.2.4. Antimicrobial properties of ROS generators:

When tested for the inhibitory potential of **4** and **13-17** against *E. coli*, we observed no effect on the bacterial growth, suggesting the compounds are non-toxic to *E. coli* even at 100 μM and the model bacterium is capable of tolerating the enhanced intracellular ROS

levels. Recently, ROS based sources were reported to sensitize bacteria to commercially used antibiotics, called as adjuvants. Adjuvants can be defined as the compound themselves may not have antimicrobial properties, but during co-treatment with antibiotics they enhance the efficacy of antibiotics for bacterial inhibition. Hence, it was predicted that compound **4** can act as an adjuvant to commercial antibiotics to inhibit bacterial growth at lower concentrations.

Table 2.1.5. Minimum inhibitory concentration (MIC) of **4**, Kanamycin, Gentamycin, Menadione and H_2O_2 with *E. coli* and fold increase in the inhibitory effect

Entry	Compound	MIC in μM[a]	Fold increase[b]
1	**4**	>250	-
2	**8**	>250	-
3	Kanamycin	16.5	-
4	Gentamycin	4.2	-
5	**4** (50 μM) + Kanamycin	4.1	4
6	**4** (50 μM) + Gentamycin	0.5	8
7	**8** (50 μM) + Kanamycin	16.5	0
8	**8** (50 μM) + Gentamycin	4.1	0
9	Menadione	>250	-
10	H_2O_2	> 250	-
11	Menadione (250 μM) + Kanamycin	16.5	0
12	H_2O_2 (250 μM) + Kanamycin	8.2	2

[a]Minimum inhibitory concentration (MIC) is the lowest concentration required to inhibit >99% of the bacterial growth; [b]Fold increase in MIC of compounds in combination with antibiotics was compared with MIC of antibiotic control

Aminoglycoside antibiotics are effective inhibitors of *E. coli* and their mechanism of action is through the inhibition of amino acid biosynthesis. However, a lower level of ROS generation in cells was reported during treatment of aminoglycoside antibiotics such as kanamycin and gentamycin. Ototoxicity and nephrotoxicity are associated with prolonged treatment of aminoglycoside antibiotics are major issues and require suitable adjuvants to reduce the effective dose levels by enhancing antibiotic efficacy.[42-44] Next,

we have tested the inhibitory potential of the aminoglycoside antibiotics against *E. coli*. Kanamycin was found to have 16.5 μM of minimum inhibitory concentration (MIC) for more than 99% inhibition of *E. coli* (Table 2.1.5, entry 3) and gentamycin was effective at 4.2 μM (Table 2.1.5, entry 4). When the compound **4** (50 μM) was co-treated with kanamycin and gentamycin a significant enhancement in their inhibitory potential was observed. For kanamycin 4 fold (4.1 μM, Table 2.1.5, entry 5) and for gentamycin 8 fold (0.5 μM, Table 2.1.5, entry 6) enhancement in MICs' were observed. Menadione (MD) is regularly used for mimicking intracellular ROS environment. When the *E. coli* bacterium was exposed to 250 μM of MD, no effect on the growth of bacterium was observed (Table 2.1.5, entry 9), and the co-treatment of MD with kanamycin also did not show any enhanced sensitivity (Table 2.1.5, entry 10). H_2O_2 itself was tested for disturbing the bacterial growth, even at 250 μM concentration of H_2O_2 bacteria were growing as efficiently as the untreated control (Table 2.1.5, entry 10). However, addition of 250 μM of H_2O_2 with kanamycin did sensitize the bacterium and a 2 fold reduction in the MIC (8.2 μM) was observed (Table 2.1.5, entry 12). Here, **4** (50 μM) was identified to sensitize bacterium to aminoglycoside antibiotics at 5 fold lesser concentration than H_2O_2 (250 μM). Further, **4** was identified as an efficient, cell permeable ROS generator, better suited for studying the effects of enhancement of intracellular ROS generation at low concentrations than the currently used organic small molecule, MD, which is used in millimolar concentrations.[45] Here, we have identified a new scaffold for effective and spontaneous ROS generation in buffer as well as in intracellular environment and studied the potency as an adjuvant to traditional antibiotics such as kanamycin and gentamycin for the inhibition of a Gram- negative bacterium *E coli*.

These ROS generators were tested for their ability to inhibit the growth of *Mycobacterium tuberculosis* (*Mtb*), which is the causative agent of tuberculosis affects a million each year. From our studies, many of these ROS generators were found to inhibit growth of *Mtb* - including multidrug resistant (MDR), extremely drug resistant (XDR) strains of *Mtb* with less than 1 μg/mL of minimum inhibitory concentration (Data for Mtb was obtained from Dr. Sriram and Dr. Amit Singh). Further studies on the precise mechanism of these ROS generators to inhibit *Mtb* are underway.

2.1.3. Conclusion:

In this Chapter 2.1, we have presented design and synthesis of 2,3-dihydro-1,4-benzoquinones as surrogates of hydroquinone. These compounds undergo a keto-enol tautomerism to react with molecular oxygen to produce ROS such as superoxide, H_2O_2 and OH radical mediated by Fe^{2+}. The capability of these compounds to generate ROS in buffer as well as in extracellular medium is studied using independent assays. Among the compounds tested, compounds **4**, **14** and **15** were found to generate higher levels of ROS. Evidence for cell permeability of compounds and enhancement of intracellular ROS levels also studied using two independent assays, DHE assay (for superoxide) and DCFH-DA assay (oxidative species). Having established cell permeable highly efficient ROS generators, we have shown the utility of **4** as an adjuvant to aminoglycoside antibiotics for the inhibition of Gram-negative bacterium *E. coli*, efficiency of **4** was better than currently used sources of ROS, H_2O_2 and menadione. *Mycobacterium tuberculosis* (*Mtb)*, is one of the highly challenging pathogens to treat. Due to its thick waxy cell wall, many of the drug candidates have compromised cell permeability in *Mtb*. However, *Mtb* has been shown to be sensitive to ROS suggesting that enhancement of intracellular ROS could be a viable strategy to target *Mtb*. Initially, evidence for compound's ability to generate extracellular and intracellular ROS was obtained using DHE and Amplex Red® assays. Then, the inhibitory potential of these ROS generators were tested against virulent strain of *Mtb* H_{37}Rv. Many of the compounds (**4**, **15** and **19**) were found to be highly potent and lead compound **14** was identified to inhibit *Mtb* at less than 1 μg/mL of MIC (0.76 μg/mL). Further studies on these compounds mechanism of *Mtb* inhibition are in progress. Taken together, we have identified small organic molecule based sources of cell permeable and spontaneous ROS generators, and applied as an adjuvant to aminoglycoside antibiotics for bacterial growth inhibition.

2.1.4. Experimental and Characterization Data

2.1.4.1. General:

All reactions were conducted under nitrogen atmosphere. All the chemicals were purchased from commercial sources and used as received unless stated otherwise. Dichloromethane (DCM), toluene and tetrahydrofuran (THF) for reaction were used as dried, and petroleum ether and ethyl acetate (EtOAc) for chromatography were distilled before use. Column chromatography was performed on Merck silica gel (100–200 mesh). ^{1}H and ^{13}C spectra were recorded on JEOL 400 MHz (or 100 MHz for ^{13}C) spectrometers using either residual solvent signals as an internal reference ($CDCl_3$ δ_H, 7.24 ppm, δ_C 77.1 ppm) or an internal tetramethylsilane (δ_H = 0.00, δ_C = 0.0). Chemical shifts (δ) are reported in ppm and coupling constants (*J*) in Hz. The following abbreviations are used: m (multiplet), s (singlet), br s (broad singlet), d (doublet), t (triplet) dd (doublet of doublet) and dt (doublet of triplet). High-resolution mass spectra were obtained from HRMS-ESI-Q-Time of Flight LC/MS or MALDI TOF/TOF analyzer (Applied Biosystems 4800 Plus). FT-IR spectra were obtained using NICOLET 6700 FT-IR spectrophotometer as KBr disc and reported in cm^{-1}. Melting point was measured using a VEEGO melting point apparatus; all melting points were measured in open glass capillary and values are uncorrected. High performance liquid chromatography (HPLC) was performed on a Dionex ICS-3000 model or a Metrohm 882 compact IC plus instrument equipped with a Phenomenex C-18 reverse phase column (250 × 4.6 mm, 5μm). Fluorimetric, luminometric and spectrophotometric measurements were performed using Thermo Scientific Varioscan microwell plate reader.

2.4.1.2. Experimental Section

Compounds **1**[46], **2**[33,47], **3**[48,49], **4**[33,47], **5**[50,51], **9**[52], **10**[53,54], **11**[55,57] **12**,[53], **13**[57] and **18**[33] have been previously reported and analytical data that we collected were consistent with the reported values.

2.1.4.3. General procedure for [4 + 2] cycloaddition with 1, 3-cyclopentadiene.

To a solution of 1,4-naphthoquinone (**20**, 1.0 mmol) in dichloromethane (10 mL), freshly distilled 1,3-cyclopentadiene (**25**, 1.2 mmol) was added and the reaction mixture was stirred at room temperature. The reaction progress was monitored by thin layer

chromatography (TLC). After completion of the reaction the volatiles were evaporated under reduced pressure to obtain crude product, which was purified by silica gel column chromatography using solvent system of ethyl acetate (1→ 5 %) and petroleum ether to afford pure material.

2.1.4.4 – General procedure for [4 + 2] cycloaddition with 1, 3-cyclohaxadiene.

To a solution of the 1,4-naphthoquinone (**20**, 1.44 mmol) in toluene (10 mL), freshly distilled 1,3-cyclohexadiene (**26**, 1.72 mmol) was added and the mixture was refluxed for 12 h. Upon complete consumption of the starting material (TLC analysis), the reaction mixture was evaporated to dryness under reduced pressure to obtain crude product. The crude material was purified by silica gel column chromatography using ethyl acetate (1→5 %) and petroleum ether solvent system to obtain pure material.

5,8-Dihydroxy-1,4,4a,9a-tetrahydro-1,4-ethano-9,10-anthraquinone (6).

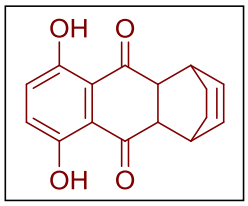

Starting from 5,8-dihydroxy-1,4-naphthoquinonoe (**22** 100 mg, 0.53 mmol), **6** was isolated as a bright yellow crystalline solid (101 mg, 71%): mp 133 – 135 °C; FT-IR (ν_{max}, cm^{-1}): 3437, 1629, 1569, 1417, 1351, 1185, 1112, 1021, 808; ^{1}H NMR (400 MHz, $CDCl_3$): δ 12.59 (s, 2H), 7.19 (s, 2H), 6.19 (dd, *J* = 3.2, 6.1 Hz, 2H), 3.36 (d, *J* = 1.4 Hz, 2H), 3.15 (s, 2H), 1.77 (dd, *J* = 5.5, 13.2 Hz, 2H), 1.40 (dd, *J* = 4.2, 11.8 Hz, 2H); ^{13}C NMR (100 MHz, $CDCl_3$): 203.6, 155.9, 133.8, 128.4, 114.7, 49.7, 36.2, 24.9; Elemental analysis for $C_{16}H_{14}O_4$ calcd. C, 71.10; H, 5.22. Found C, 71.28; H, 5.03; HRMS (MALDI) for $[C_{16}H_{14}O_4+K]^+$: calcd., 309.0529; Found: 309.0168.

5-benzyloxy-1,4,4a,9a-tetrahydro-1,4-methano-9,10-anthraquinone (7).

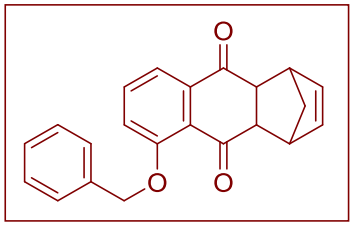

Starting from 5-benzyloxy-1,4-naphthoquinone (**23**, 50 mg, 0.19 mmol), **7** was isolated as a pale yellow semi-solid (36 mg, 58%): FT-IR (ν_{max}, cm^{-1}): 2927, 2858, 1642, 1574, 1416, 1346, 1279, 1119, 1023, 976; ^{1}H NMR (400 MHz, $CDCl_3$): δ 7.49-7.54 (m, 4H), 7.37-7.40 (m, 2H), 7.28-7.32 (m, 1H), 7.20-7.22 (m, 1H), 6.06 (dd, *J* = 2.8, 5.6 Hz, 1H), 5.99 (dd, *J* = 2.8, 5.6 Hz, 1H),

5.20 (dd, *J* = 12.3, 20.9 Hz, 2H), 3.58 (d, *J* = 13.1 Hz, 2H), 3.46 (dq, *J* = 3.5, 12.5 Hz, 2H), 1.55 (dt, *J* = 1.7, 8.7 Hz, 1H), 1.47 (d, *J* = 8.6 Hz, 1H); ^{13}C NMR (100 MHz, $CDCl_3$): δ 198.5, 196.6, 157.8, 138.8, 136.5, 136.3, 135.8, 134.4, 128.8, 128.0, 126.9, 126.2, 119.2, 119.0, 71.0, 51.6, 50.5, 48.7, 48.1, 47.8; HRMS (ESI) for $[C_{22}H_{18}O_3+Na]^+$: calcd., 353.1154; Found: 353.1157.

5-benzyloxy-1,4,4a,9a-tetrahydro-1,4-ethano-9,10-anthraquinone (8). Starting from 5-benzyloxy-1,4-naphthoquinone (**23**, 200 mg, 0.76 mmol), **8** was isolated as a yellowish white semi-solid (189 mg, 72%): FT-IR (ν_{max}, cm^{-1}): 2936, 2863, 2374, 1645, 1577, 1416, 1346, 1283, 1242, 1182, 1113, 1020, 911; ^{1}H NMR (400 MHz, $CDCl_3$): δ 7.49-7.53 (m, 4H), 7.36-7.40 (m, 2H), 7.28-7.32 (m, 1H), 7.19 (m, 1H), 6.09-6.19 (m, 2H), 5.20 (d, *J* = 8.0 Hz, 2H), 3.29-3.34 (m, 2H), 3.21 (s, 2H), 1.70 (d, *J* = 7.6 Hz, 2H), 1.38 (d, *J* = 8.8 Hz, 2H); ^{13}C NMR (100 MHz, $CDCl_3$): δ 198.2, 196.2, 157.3, 138.7, 136.3, 134.3, 134.2, 133.5, 128.8, 128.0, 126.9, 126.3, 119.0, 118.8, 71.0, 52.1, 51.1, 34.4, 33.6, 24.8, 24.7; HRMS (ESI) for $[C_{23}H_{20}O_3+Na]^+$: calcd., 367.1310; Found: 367.1311.

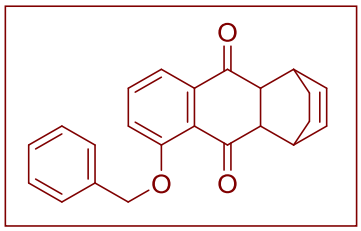

2.1.4.5. General procedure for palladium catalyzed hydrogenation reaction:

To a 25 mL round bottom flask containing tetrahydrofuran (THF, 6 mL), compound (1 mmol) was added followed by Pd/C (5 mol%); the reaction mixture was flushed with hydrogen gas using a balloon and stirred under hydrogen atmosphere at room temperature for 2 h. Upon complete consumption of starting material (TLC analysis), the reaction mixture was filtered through a celite bed and washed with THF of 10 mL. The resulting filtrate was evaporated under reduced pressure and washed with *n*-pentane (3 × 3 mL) to obtain pure product.

5-Hydroxy-1,2,3,4,4a,9a-hexahydro-1,4-methano-9,10-anthraquinone (14). Starting from **3** (120 mg, 0.50 mmol), **14** was isolated as a yellow crystalline solid (102 mg, 91%): mp 139 – 141 °C; FT-IR (ν_{max}, cm^{-1}): 3450, 2943, 2937, 1667, 1633, 1578, 1456, 1416, 1355, 1304, 1263, 1230, 1168, 1067; ^{1}H NMR (400 MHz, $CDCl_3$): δ 12.79 (s, 1H),

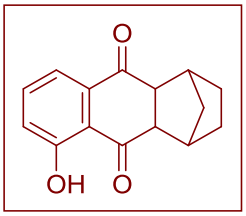

7.61-7.68 (m, 2H), 7.26 (dd, *J* = 0.9, 8.0 Hz, 1H), 3.21 (dd, *J* = 4.7, 10.8 Hz, 1H), 3.12 (dd, *J* = 4.8, 10.8 Hz, 1H), 3.01 (d, *J* = 13 Hz, 2H), 1.45-1.60 (m, 4H), 1.13-1.20 (m, 2H); ^{13}C NMR (100 MHz, $CDCl_3$): δ 206.4, 198.4, 162.1, 137.5, 135.5, 124.1, 118.3, 118.2, 50.3, 50.0, 43.9, 43.8, 39.3, 24.9, 24.8; HRMS (ESI): calcd. for $[C_{15}H_{14}O_3+Na]^+$: 265.0841; Found: 265.0845.

5-hydroxy-1,2,3,4,4a,9a-hexahydro-1,4-ethano-9,10-anthraquinone (15).

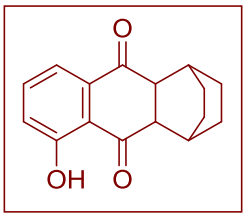

Starting from **4** (100 mg, 0.39 mmol), **15** was obtained as a yellow crystalline solid (82 mg, 81%): mp 90 – 92 °C; FT-IR (ν_{max}, cm^{-1}): 3448, 2939, 2860, 1662, 1630, 1574, 1418, 1351, 1261, 1163, 1113; ^{1}H NMR (400 MHz, $CDCl_3$): δ 12.74 (s, 1H), 7.61-7.68 (m, 2H), 7.26 (dd, *J* = 1.7, 7.8 Hz, 1H), 3.17 (dd, *J* = 2.8, 10.7 Hz, 1H), 3.07 (dd, *J* = 3.0, 10.7 Hz, 1H), 2.36 (d, *J* = 13.7 Hz, 2H), 1.70-1.76 (m, 4H), 1.38-1.42 (m, 4H); ^{13}C NMR (100 MHz, $CDCl_3$): δ 206.3, 198.4, 162.0, 137.4, 135.2, 123.8, 118.2, 48.6, 48.1, 30.3, 30.0, 25.9, 25.8, 22.0, 21.9; Elemental analysis for $C_{16}H_{16}O_4$calcd.: C, 74.98; H, 6.29. Found C, 75.29; H, 6.12; HRMS (MALDI) for $[C_{16}H_{16}O_3+Na]^+$: calcd., 279.0997; Found: 279.0840.

5,8-dihydroxy-1,2,3,4,4a,9a-hexahydro-1,4-methanoanthracene-9,10-dione (16).

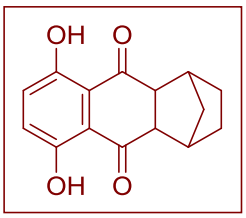

Starting from **5** (150 mg, 0.59 mmol), **16** was isolated as a yellow crystalline solid (132 mg, 87%): mp 138 – 140 °C; FT-IR (ν_{max}, cm^{-1}): 3440, 3088, 2950, 2876, 1620, 1451, 1360, 1310, 1205, 1072, 1023, 934; ^{1}H NMR (400 MHz, $CDCl_3$): δ 12.78 (s, 2H), 7.24 (s,2H), 3.13 (s, 2H), 2.98 (s, 2H), 1.45-1.58 (m, 4H), 1.16-1.19 (m, 2H); ^{13}C NMR (100 MHz, $CDCl_3$): 205.0, 156.0, 129.1, 114.9, 49.7, 44.0, 39.3, 24.8; HRMS (ESI) for $[C_{15}H_{14}O_4+H]^+$: calcd., 259.0970; Found: 259.0972.

5,8-dihydroxy-1,2,3,4,4a,9a-hexahydro-1,4-ethanoanthracene-9,10-dione (17).

Starting from **6** (150 mg, 0.56 mmol), **17** was isolated as a rosy red crystalline solid (143 mg, 95%): mp 152 – 154 °C; FT-IR (ν_{max}, cm^{-1}): 3441, 3080, 2935, 2863, 1604, 1488,

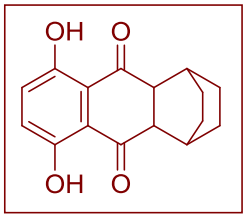

1453, 1370, 1314, 1211, 1029, 951; ^{1}H NMR (400 MHz, $CDCl_3$): δ 12.75 (d, *J* = 1.6 Hz, 2H), 7.26 (d, *J* = 1.4 Hz, 2H), 3.10 (s, 2H), 2.36 (s, 2H), 1.72-1.74 (m, 4H), 1.42-1.44 (m, 4H); ^{13}C NMR (100 MHz, $CDCl_3$): 205.0, 155.8, 128.8, 114.5, 48.0, 30.3, 25.7, 21.9; HRMS (ESI) for $[C_{16}H_{16}O_4+H^+]$: calcd., 273.1121; Found: 273.1125.

2.1.4.6–Synthesis of 5-hydroxy-2,3,4a,9a-tetrahydro-1,4-ethano-9,10-anthraquinone (19)

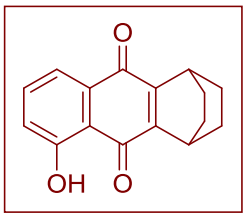

In a 25 mL round bottom flask compound **15** (100 mg, 0.39 mmol) was dissolved in chloroform ($CHCl_3$, 5 mL) and DBU (50 μL, 0.33 mmol) was added drop wise to the above solution. The reaction mixture was stirred at room temperature for 20 min, complete conversion of the starting material was followed by thin layer chromatography (TLC). The reaction mixture was evaporated under reduced pressure to obtain crude product. The crude product was passed through a silica plug (5 cm) to obtain an orange yellow crystalline solid (29 mg, 48%): mp 141 – 143 °C; FT-IR (ν_{max}, cm^{-1}): 3419, 2938, 2867, 1621, 1440, 1361, 1286, 1236, 1178, 1103, 1022, 969; ^{1}H NMR (400 MHz, $CDCl_3$): δ 12.19 (s, 1H), 7.6 (dd, *J* = 1.2, 7.5 Hz, 1H), 7.56 (t, *J* = 8.0 Hz, 1H), 7.21 (dd, *J* = 1.2, 8.3 Hz, 1H), 3.52 (s, 2H), 1.78 (d, *J* = 7.5 Hz, 4H), 1.34 (d, *J* = 7.6 Hz, 4H); ^{13}C NMR (100 MHz, $CDCl_3$): δ 187.1, 181.1, 161.5, 151.9, 150.4, 135.9, 132.6, 124.1, 119.1, 115.2, 27.1, 26.3, 25.3, 25.2.; HRMS (ESI) for $[C_{16}H_{14}O_3+Na]^+$: calcd., 255.1021; Found: 255.1020.

2A.5.5 Stability studies of compound 4.

To a 5 mL glass vial compound **4** (500 μL, 10 mM) was reacted with potassium phosphate buffer (450 μL, 100 mM) under an air balloon at 37 °C. Each time 500 μL of the reaction mixture was diluted to 5 mL using CH_3CN: H_2O (1:1 v/v) and injected into high performance liquid chromatography at different time intervals during 14 h. An authentic sample of **18** was injected as a control.

2A.5.6 Computational calculations.

The DFT calculations are being performed with the Gaussian 03 program and are analyzed with the help of the GaussView program. The geometries of the model compounds are optimized using the 6-31G basis set, at the DFT level, and these calculations are mainly carried out in the framework of the Becke–Lee–Yang–Parr [B3LYP] functional. Isoelectronic molecular electrostatic potential surfaces (EPS) are plotted by the computer program GaussView. The Mulliken charge density distributions derived from periodic quantum calculation with density functional theory and B3LYP/6-31G(d,p) geometry. Atomic coordinates for compounds **4** and **6** were taken from crystallographic information file (CIF) obtained from the respective X-ray crystal structure data.

2.1.4.7 Crystallographic data:

Crystals of compounds **4** and **6** were grown by slow evaporation from a solution of ethylacetae / hexane (25:75 v/v). A single crystal was mounted in a loop with a small amount of the mother liquor. The X-ray data were collected at 296 K temperature on a Bruker AXS SMART APEX CCD diffractometer using MoKα radiation (λ = 0.71073 Å).

Compound **4**, (**C**$_{16}$H$_{14}$O$_3$) an orange yellow crystalline needle, ω-scans (θ = 28.91°), for a total number of 3181 independent reflections with a space group *P(-1)* , a = 6.536(4), b = 10.053(1), c = 10.130(1) Å, α = 67.597 (3), β = 79.986(2), γ = 82.187 (2), V = 604.26(15) Å^3, triclinic *P-1*, Z = 2 for chemical formula C$_{16}$H$_{14}$O$_3$.ρ calcd = 1.398 g cm^{-3}, μ = 0.096 mm^{-1}, F(000) = 268.14, *Rint* = 0.0511 for 2161 reflections and *w*R = 0.1591 (for 3136) reflections. The structure was obtained by direct methods using SHELXS-97. All non-hydrogen atoms were refined anisotropically. The hydrogen atoms were fixed geometrically in the idealized position and refined in the final cycle of refinement as riding over the atoms to which they are bonded. The final R value was 0.0511 (wR = 0.1591) for 2161, S = 0.997.

Compound **6**, (C$_{16}$H$_{14}$O$_5$); yellow crystal, ω-scans (θ = 28.68°), for a total number of 3103 independent reflections with a space group *P(-1)*, a = 6.410(3), b = 9.943(7), c = 10.590(5) Å, α = 113.766 (2), β = 90.148(2), γ = 97.772(2), V = 610.93(13) Å^3, triclinic

P-1, Z = 2 for chemical formula $C_{16}H_{14}O_5$. ρ calcd = 1.469 g cm^{-3}, μ = 0.106 mm^{-1}, *F*(000) = 284.0, *Rint* = 0.0388 for 2825 reflections and *w*R = 0.1158 (for 3103) reflections. The structure was obtained by direct methods using SHELXS-97. All non-hydrogen atoms were refined anisotropically. The hydrogen atoms were fixed geometrically in the idealized position and refined in the final cycle of refinement as riding over the atoms to which they are bonded. The final *R* value was 0.0388 (*wR* = 0.1158) for 2825, *S* = 1.045.

2.1.4.8. Luminol assay for superoxide estimation:[19,59]

A luminol stock solution (4 mM) was prepared by dissolving 7.1 mg of luminol in 10 mL of 30 μM sodium hydroxide solution. To a 96-microwell plate, compound (5 μM) in quintuplicate was incubated with 180 μL of potassium phosphate buffer (100 mM, pH 8.0) and 5 μL of luminol stock solution (4 mM, in 30 μM sodium hydroxide) for 30 min at RT and luminescence was measured using microwell plate reader. As a positive control superoxide ($O_2^{\bullet-}$) was generated from the enzymatic reaction of xanthine oxidase (0.1 U/mL) and hypoxanthine (1 mM in phosphate buffer pH 8.0) in the presence of 5 units catalase as a scavenger for H_2O_2; for compound **4** superoxide estimation was done in the presence of H_2O_2 scavenger (catalase, 5 units) as well. Superoxide dismutase (SOD from Bovine erythrocytes, sigma), 10 U/mL was prepared in 1 mM phosphate buffer (1 mM in phosphate buffer pH 7.8. The complete quenching of luminescence was observed during the addition of SOD.

2.1.4.9. Dihydroethidium (DHE) assay[30-32]

A stock solution of dihydroethidium (1.12 mg, 3.55 μmol) was prepared in DMSO (355 μL) and stored in the dark at –20 ºC until its use. A stock solution of the compound (10 μL, 10 mM) and DHE (10 μL of 10 mM) were reacted in acetonitrile: phosphate buffer of pH 7.4 (1:1, v/v, 100 mM, final volume 100 μL) for 3 h at 37 ºC. The reaction mixture was diluted to 100 μM using acetonitrile: phosphate buffer of pH 7.4 (1:1, v/v, to a final volume of 1 mL). The reaction mixture was filtered (0.22 μm) and injected (25 μL) in an Agilent high performance liquid chromatograph (HPLC) attached with a fluorescence detector (excitation at 356 nm; emission at 590 nm). The column used was Zorbax SB C-

18 reversed phase column (250 mm × 4.6 mm, 5 μm), the mobile phase was water: acetonitrile containing 0.1% trifluoroacetic acid and a gradient starting with 10: 90 to 30: 70 → 0 – 45 min, 0: 100 → 45 – 50 min, 0: 100 → 50 – 55 min, 10: 90 → 55 – 60 min was used with a flow rate of 0.5 mL/min. Under these conditions literature report indicate that if superoxide is produced, a peak for 2-hydroxyethidium (2-OH-E^+,), which elutes at 30.9 min, would be observed.[29-31] When other oxidative species are generated, ethidium (E^+) is formed. Again, according to literature reports E^+ elutes at 31.7 min (Figure 2.1.8).[29-31] We independently confirmed the formation of 2-OH-E^+ and E^+ by mass spectrometry. Hypoxanthine (10 μL, 1 mM) and xanthine oxidase (5 μL of 0.02 U/mL) were mixed in phosphate buffer (pH 7.4, 100 mM) along with DHE (10 μL of 10 mM, 100 μM final concentration) for 2 h and served as a positive control.

2.1.4.10. Estimation of hydrogen peroxide:[20,60]

Xylenol orange (1.25 mM) stock solution was prepared by dissolving 9.5 mg (12.5 μmol) in 10 mL of de-ionised water. This solution was diluted 10-fold using de-ionised water to get a 125 μM stock solution. A 1 M solution of sorbitol (1.82 g, 1 mol in 10 mL dI water) was also prepared and diluted to produce 100 mM stock solution. A 250 mM ferrous ammonium sulphate (FAS) solution was prepared by dissolving 980.3 mg of FAS in 10 mL of 2.5 M sulphuric acid. This solution was further diluted 10-fold by using 2.5 M sulphuric acid for the final stock solution of FAS (25 mM). Xylenol orange and sorbitol stock solutions were mixed together in a ratio of 1:1 (v/v) and to this 100:1 (v/v) FAS stock solution was added to obtain the final FOX stock solution, which is used for the hydrogen peroxide estimation. A calibration was generated with hydrogen peroxide. Hydrogen peroxide estimation experiments were performed in 96-microwell plates. Compound (5 μM) in triplicate was incubated at pH 7.4 with potassium phosphate buffer (20 μL, 0.5% acetonitrile for solubility) for 30 min. FOX reagent (180 μL) was added to the above, incubated for 30 min at room temperature (25 °C) for the color development and the absorbance (586 nm) was measured using a Thermo Scientific Varioscan microwell plate reader.

Catalase from Bovine liver (1.03 mg) was dissolved in 1.0 mL of de-ionized water to obtain 2000 U/mL stock solution. 10 mL of catalase stock solution was added to 30 min

reaction mixture of compound 13 (5 mM) in phosphate buffer (pH 7.4); After 5 min, FOX reagent (180 μL) was added and reacted for 30 min at RT, measured the absorbance at 586 nm. We found no significant color formation in the presence of catalase confirming the production of H_2O_2.

2.1.4.11 Supercoiled plasmid DNA cleavage:

DNA cleavage was analyzed by the conversion of pBR322 circular DNA to open circular and/or linear forms. Briefly, pBR322 DNA (100 ng) was incubated with compound in the presence of 1 eq. of $FeCl_2$ in 1 mM phosphate buffer (pH 8.0), in a final volume of 20 μL, the solutions were incubated at 37 °C for 6 h. The solutions were mixed with bromophenol blue (0.25 wt.%) and 1X GelRed™ (2 μL), this mixture was loaded in a 1.0% agarose gel (0.5 g in 50 mL of 1x TAE (40 mM Tris-acetate buffer containing 1 mM EDTA, pH 8.0)) and immediately subjected to electrophoresis in a horizontal slab gel apparatus containing 1x TAE buffer as medium for 40 min under constant 95 V. After electrophoresis, the DNA was visualized under GBOX Syngene UV-transilluminator, photographed using Genesnap-7.04. Image analysis for quantifying the amount of DNA damage was done using Syngene-gene tools software, where the pixels of bands were quantified and analyzed.

2.1.4.12. Extracellular hydrogen peroxide estimation in *E. coli*:[61]

E. coli (EC2065) was cultured in 5 mL of Luria Bertani (LB) medium at 37 ºC for 16 h and centrifuged to aspirate out the medium and re-suspended to an O.D of 1.0 with fresh LB medium. A stock solution of the compound in DMSO (0.5%) was added so that the final concentration was 100 μM. After incubation for 1 h, the bacterial suspension was centrifuged and the extracellular media was separated. To the media (divided in several 50 μL portions in a 96-well microplate), 50 μL of a premixed solution of 10-acetyl-3,7-dihydroxyphenoxazine or Amplex Red® (prepared by following manufacturer's protocol from Invitrogen) was added and incubated at RT for 25 min before measuring the fluorescence using a microtiter plate reader (excitation 550 nm; emission 590 nm). A calibration curve with known concentrations of hydrogen peroxide was generated (Figure 2.1.16) in LB medium and was used to quantify hydrogen peroxide produced during

incubation of test analytes. Data presented are an average of three independent experiments.

2.1.4.13. Intracellular superoxide detection in *E. coli*.[30-32]

Escherichia Coli (EC2065) was cultured in 5 mL of Luria Bertani (LB) medium at 37 ºC for 16 h. The cultured bacteria were centrifuged to aspirate out the medium and re-suspended to an O.D of 1.0 with fresh LB medium. This bacterial solution was incubated with 250 μM of compound and 50 μM of dihydroethidium for 30 min in dark by covering the falcon tube in an aluminum foil. The suspension was centrifuged to aspirate out any excess of the compound and/or DHE in the medium. The collected bacterial pellet was re-suspended with acetonitrile and the cells were lysed using a probe sonicator for 3 min on ice. The cell lysate was then removed by centrifugation and the supernatant acetonitrile was separated and stored at −20 ºC before injecting in HPLC. The HPLC method used was as described previously.[30-32]

2.1.4.14. Estimation of intracellular oxidative species - $DCFH_2$-DA assay in *E. Coli*.[62]

Escherichia Coli (EC2065) was cultured in 5 mL of Luria Bertani (LB) medium at 37 ºC for 16 h. The cultured bacteria were centrifuged to aspirate out the medium and re-suspended in LB medium of O.D adjusted to 1.0 The bacterial medium was incubated with 200 μM of 2′,7′-dichlorodihydrofluorescein diacetate ($DCFH_2$-DA) a weakly fluorescent dye for 60 min. Next, centrifugation of the bacterial suspension followed by removal of extracellular media to remove any excess DCFH2-DA was carried out. The collected bacterial pellet was re-suspended with LB medium and 100 μL aliquots were placed in triplicate in wells of sterile flat bottom 96-well microtiter plates. A final concentration of 100 μM compound in DMSO (0.5%) was added in each well and incubated for 60 min; bacterial solution with 0.5% DMSO was used as the control. The fluorescence of oxidized green fluorescent 2′,7′-dichlorofluorescein (DCF) was measured (excitation, 490; emission, 520 nm). $DCFH_2$DA is reported to be more reactive with $^{\bullet}OH$ in comparison with other ROS.[62,63]

2.1.4.15. Extracellular H_2O_2 generation in *Mycobacterium smegmatis*:[64]

The 10-acetyl-3,7-dihydroxyphenoxazine (Amplex red) solution was used to estimate hydrogen peroxide. The Amplex red solution was prepared by following the manufacturer's protocol from invtirogen-Amplex red hydrogen peroxide assay kit (100 μM Amplex red reagent and 0.2 U/mL HRP (Horse Radish Peroxidase enzyme) in 50 mM PBS (phosphate buffered saline). Using hydrogen peroxide a calibration curve was generated. The cultured *Mycobacterium smegmatis* MC^2155 was centrifuged to aspirate out the media and re-suspended in LB medium of 5 mL. The bacterial medium was incubated with a final concentration of 50 μM compound in DMSO (0.5%) was placed in each well and incubated for 60 min, bacterial solution with 0.5% DMSO was used as the control. To the 96-microwell plate 50 μL of Amplex red solution was added and incubated at room temperature for 30 min. Fluorescence of resulting Amplex red dye reaction (resorufin) was measured by exciting at 550 nm and the emission was collected at 590 nm.

2.1.4.16. Intracellular superoxide detection in *Mycobacterium smegmatis*:[30-32]

Mycobacterium smegmatis MC^2155 were inoculated in a ten milliliter 60 hours cultures, grown from single colonies in Dubos medium monitored by measuring OD_{600} 0.1 - 0.5. The cultured bacteria was centrifuged to aspirate out the media and re-suspended in Lysogeny broth (LB) medium of 5 mL. This bacterial solution was incubated with 50 μM of compound and 50 μM of dihydroethidine (DHE) for 30 min in dark by covering the falcon tube in an aluminum foil. The suspension was centrifuged to aspirate out any excess of the compound and/or DHE in the medium. The collected bacterial pellet was re-suspended with acetonitrile and the cells were lysed using a probe sonicator for 3 min on ice. The cell lysate was then removed by centrifugation and the supernatant acetonitrile was separated and stored at −20 ºC before injecting in HPLC. The HPLC method used was as described previously.[30-32]

2.1.4.17. Intracellular ROS generation in *Mycobacterium smegmatis*:

Mycobacterium smegmatis MC^2155 were inoculated in a ten milliliter 60 hours cultures, grown from single colonies in Dubos medium (middle brook-M7H9) monitored by

measuring OD_{600} 0.1 - 0.5. The cultured bacteria was centrifuged to aspirate out the media and re-suspended in M7H9 medium of 5 mL. The bacterial medium was incubated with 200 μM of 2′,7′-dichlorodihydrofluorescein diacetate ($DCFH_2$-DA) a pre-nonfluorescent dye for 60 min followed with centrifugation to aspirate out the $DCFH_2$-DA loading LB medium. The collected bacterial pellet was re-suspended with LB medium and 100 μL aliquots were placed in triplicate in wells of sterile flat bottom 96-well microtiter plates. A final concentration of 50 μM compound **15** in DMSO (0.5%) was added in each well and incubated for 60 min; bacterial solution with 0.5% DMSO was used as the control. The fluorescence of oxidized green fluorescent 2′,7′-dichlorofluorescein (DCF) was measured by exciting at 490 nm and the emission was collected at 530 nm wavelength.

2.1.4.18. Determination of minimum inhibitory concentration.

The Minimum Inhibitory Concentration (MIC) assay is used to determine the inhibitory potential of a compound against bacterial pathogens. To determine the MIC, the microbroth dilution technique is commonly used as recommended by National Committee for Clinical Laboratory Standards.[63] For this, a fixed bacterial inoculum (5×10^5 CFU/mL) is added into a series of test wells in a microtitre plate that contain various concentrations of compound under test. Following a period of incubation (37 ºC, 18-20 h), the wells are examined for growth. The lowest concentration of antibiotic that inhibits growth of the organism, as detected visually is designated as the MIC.

2.1.4.19. Bacterial strains and culture conditions:

Gram positive (*Staphylococcus aureus* – SA5021 and *Bacillus subtilis* – BS2063) and Gram negative (*Escherichia coli* – EC2065, *Salmonella typhimurium* – ST2501, *Klebsiella pneumonia* – KP2957 and *Pseudomonas aeruginosa* – PA5029). The bacteria were grown in freshly prepared nutrient broth (NB) at 37 ºC for 14-16h. *Mycobacterium smegmatis* - MC^2155, was cultured in middlebrook 7H9 media at 37 °C for 60 h

2.1.4.20 Drug stock preparation:

Ampicillin and kanamycin were dissolved in sterile de-ionized water; chloramphenicol, rifampicin and test compounds were prepared in DMSO; ciprofloxacin was dissolved in 0.2 N HCl and diluted with sterile de-ionized water.

2.1.4.21. MIC experiment protocol:

Briefly, subculture 1 of bacterium was streaked in an agar plate and grown at 37 ºC for overnight. An agar slant subculture 2 was prepared by streaking isolated colonies from subculture 1 agar plate. From the slant 2-3 colonies were isolated, grown in 5 mL of LB medium (except *E. coli* B strain, 5% NaCl nutrient broth was used) for 1-2 h (OD_{625} of 0.08 – 0.13, 1×10^8 cfu/mL). A dilution of logarithmic phase culture to 1×10^6 cfu/mL was performed and 50 μL were aliquoted into a 96-well microtiter plate. In another 96 well plate antibiotics and test compounds were taken as 2 fold of treatment concentration in LB medium (maximum of 2% DMSO solution). A concentration range 0.2 to 100 μM of **14** and **15** in LB (2% DMSO) were added to the above bacterial medium. Ampicillin, kanamycin, ciprofloxacin, rifampicin and chloramphenicol concentrations ranging from 0.06 to 32 μg/mL were used as positive controls. Broth control was used to verify any medium contamination with other organisms, bacterial growth control was with 2% DMSO. Verification agar plate was streaked with 1000 fold dilute bacterial medium of the growth control. After 16-18 h of incubation at 37 ºC inhibition was visualized and also O.D (optical density) was measured at 625 nm using Thermo Varioscan microplate reader to determine the extent of bacterial growth inhibition. The assay was validated by checking broth and growth controls; and the verification agar plates were counted to be ~ 40 to 65 individual colonies (within the limits of 50 ± 30 CFU). The MIC (minimum inhibitory concentration) of the commercial antibiotics observed was in the prescribed range of CLSI values.[65]

2.1.4.22. Adjuvant Studies:

Growth inhibition studies in the presence of additives were performed by co-treatment of aminoglycosides including kanamycin, gentamicin and streptomycin independently with the additive. A premixed media of LB with 50 μM of the additive (in 2% DMSO) was used for bacterial dilution, and plated in a 96 well plate before adding the antibiotics, remaining protocol was followed as mentioned above. Data presented here are results of three independent experiments.[65]

2.1.5 – Spectral Charts

^{1}H NMR Spectrum (400 MHz, $CDCl_3$) of Compound **6**

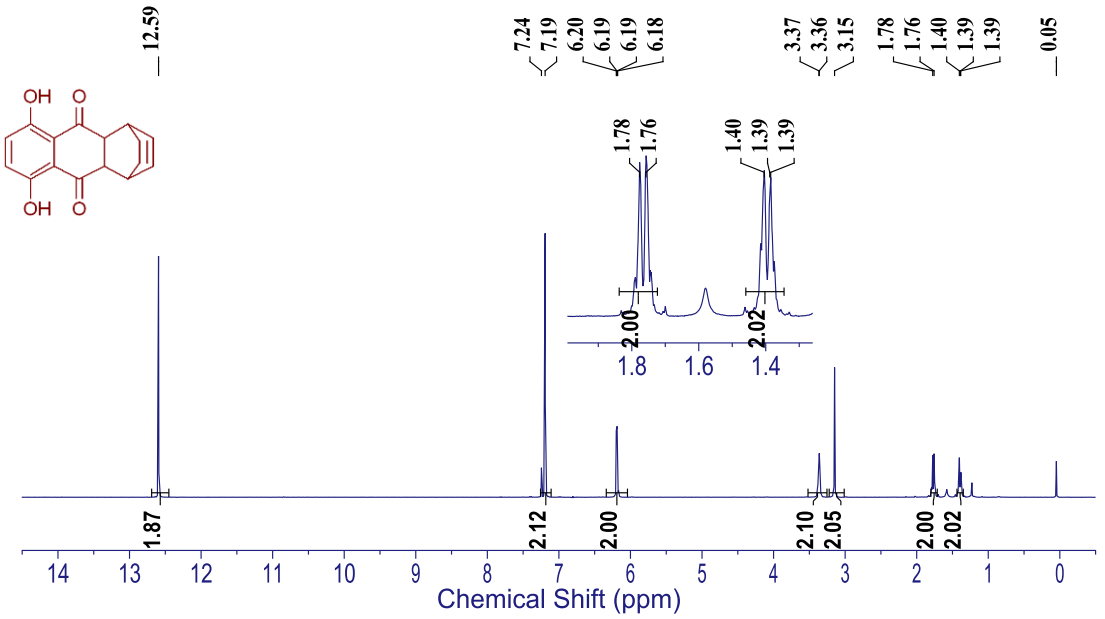

^{13}C NMR Spectrum (100 MHz, $CDCl_3$) of Compound **6**

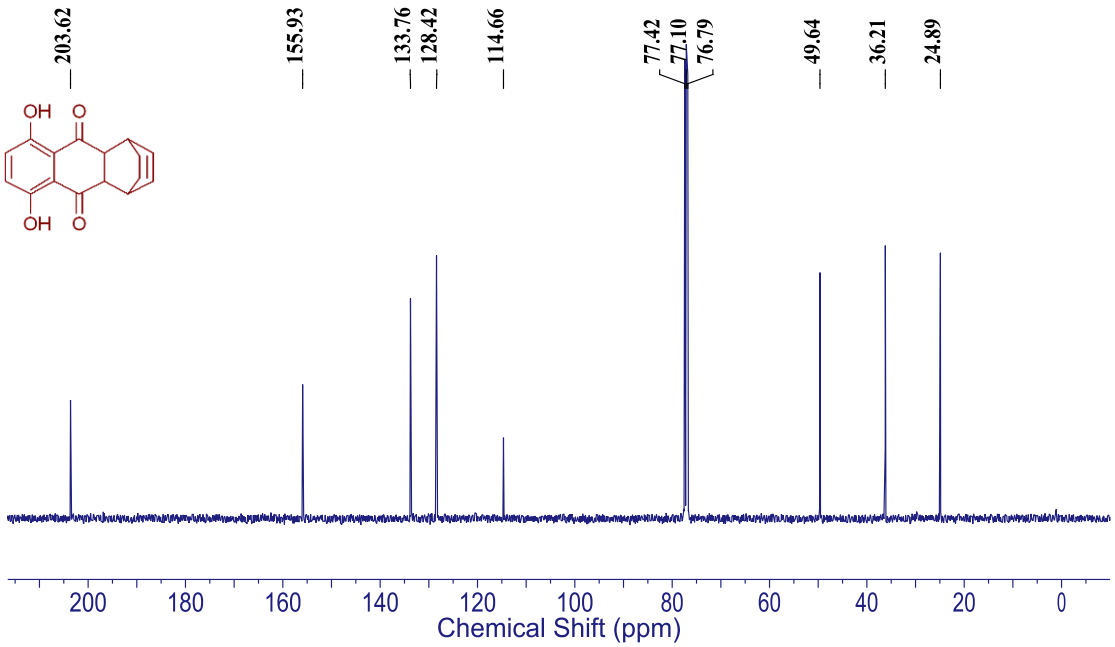

^{1}H NMR Spectrum (400 MHz, $CDCl_3$) of Compound **7**

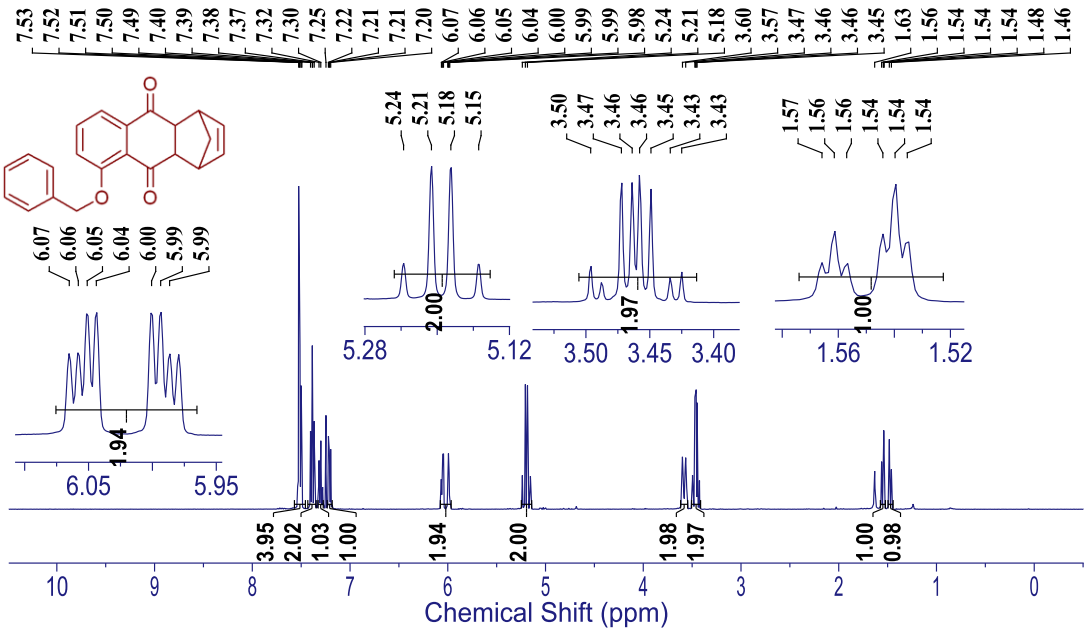

^{13}C NMR Spectrum (100 MHz, $CDCl_3$) of Compound **7**

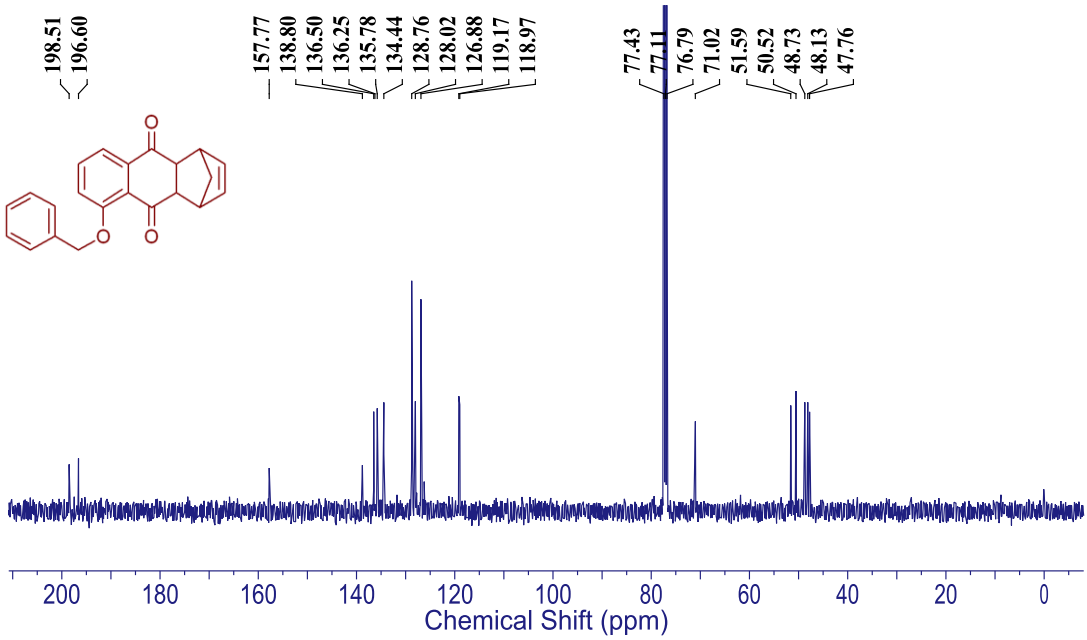

^{1}H NMR Spectrum (400 MHz, $CDCl_3$) of Compound **8**

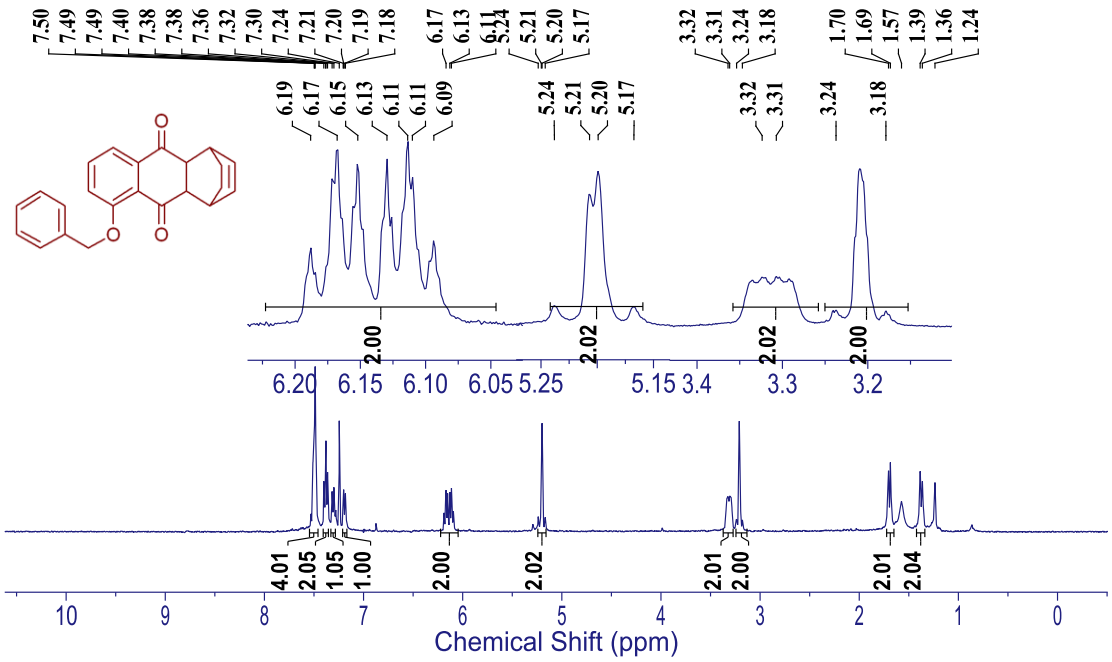

^{13}C NMR Spectrum (100 MHz, $CDCl_3$) of Compound **8**

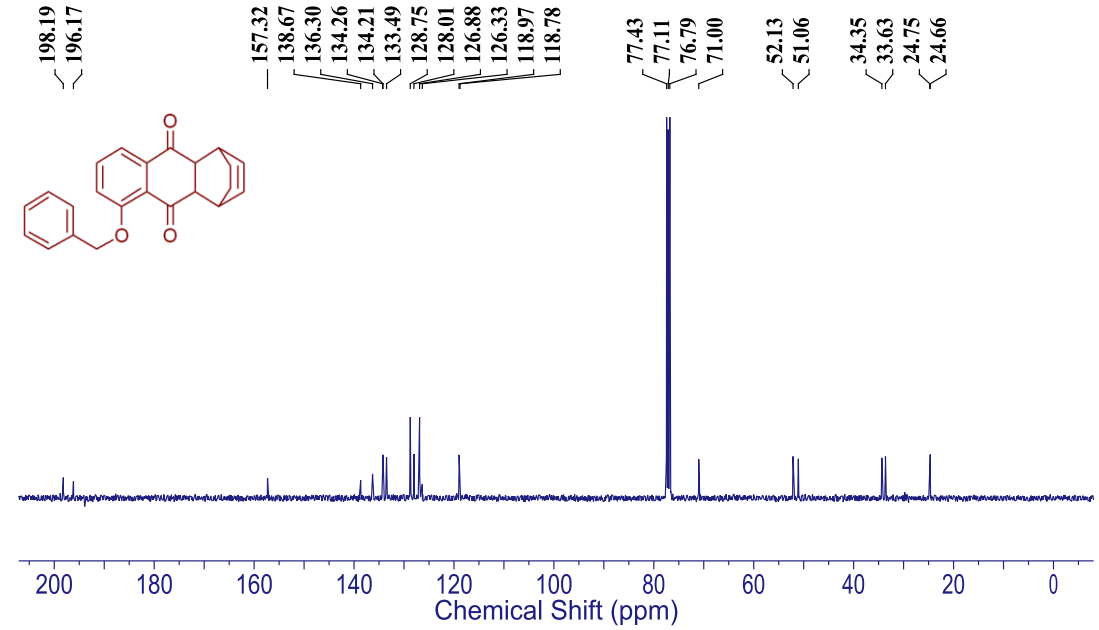

^{1}H NMR Spectrum (400 MHz, $CDCl_3$) of Compound **14**

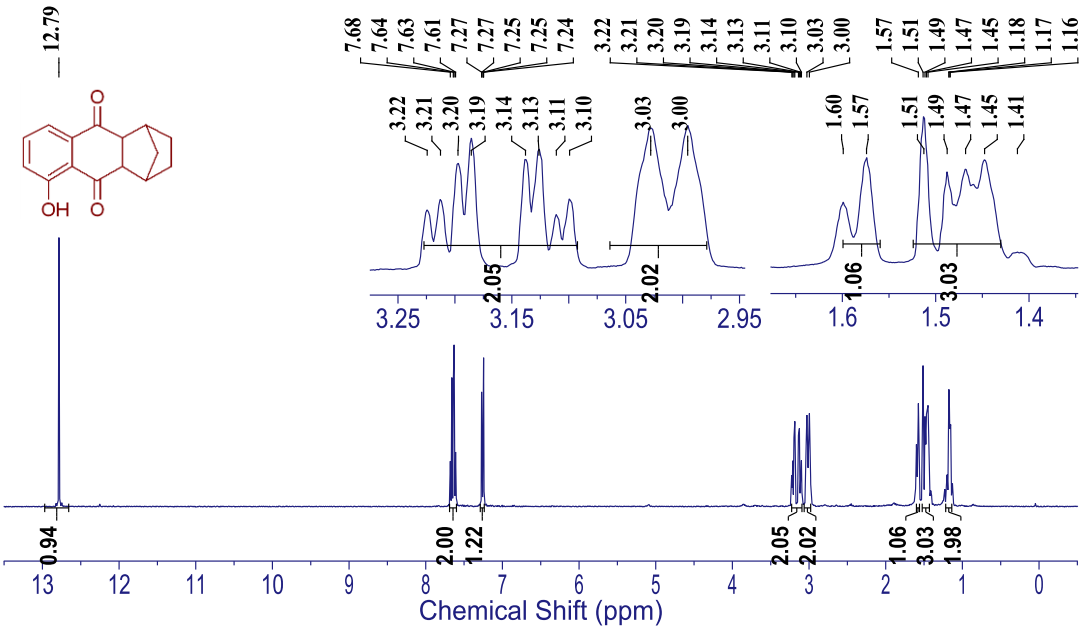

^{13}C NMR Spectrum (100 MHz, $CDCl_3$) of Compound **14**

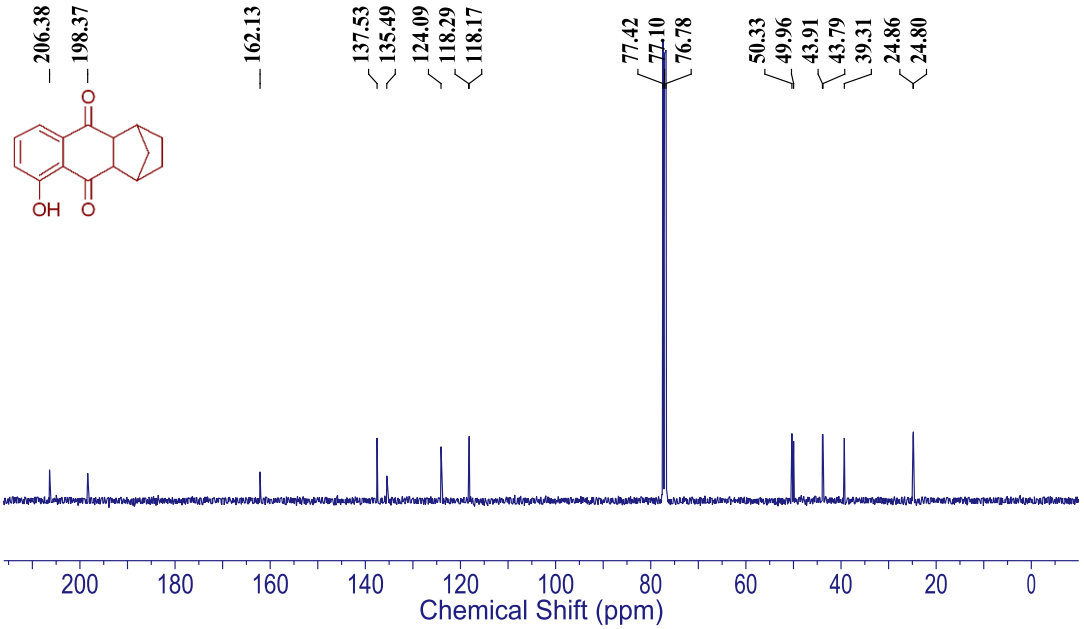

^{1}H NMR Spectrum (400 MHz, $CDCl_3$) of Compound **15**

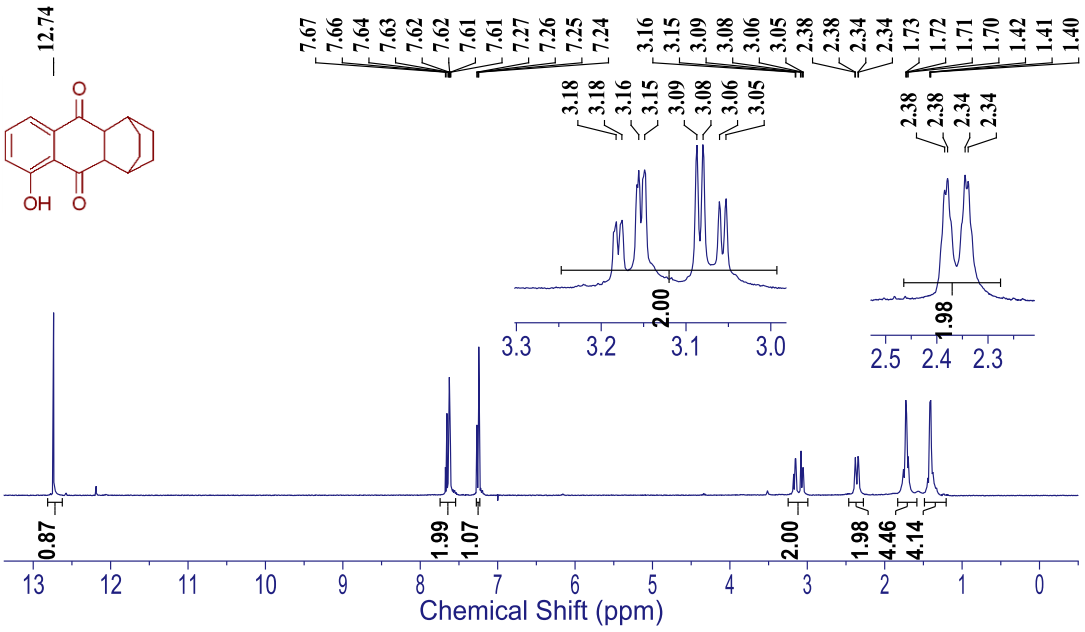

^{13}C NMR Spectrum (100 MHz, $CDCl_3$) of Compound **15**

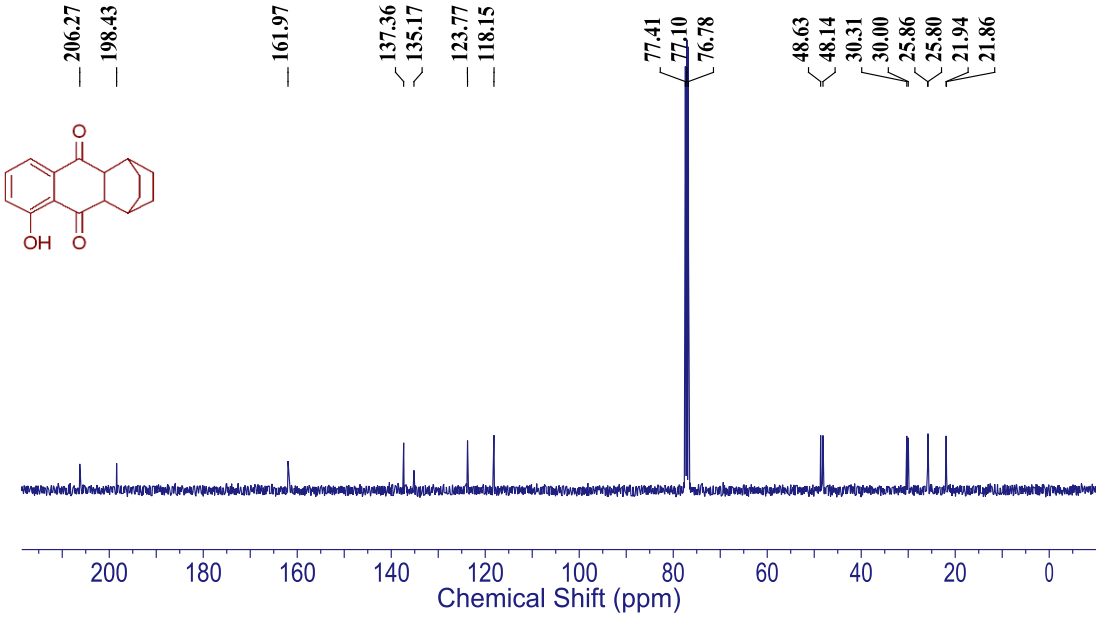

^{1}H NMR Spectrum (400 MHz, $CDCl_3$) of Compound **16**

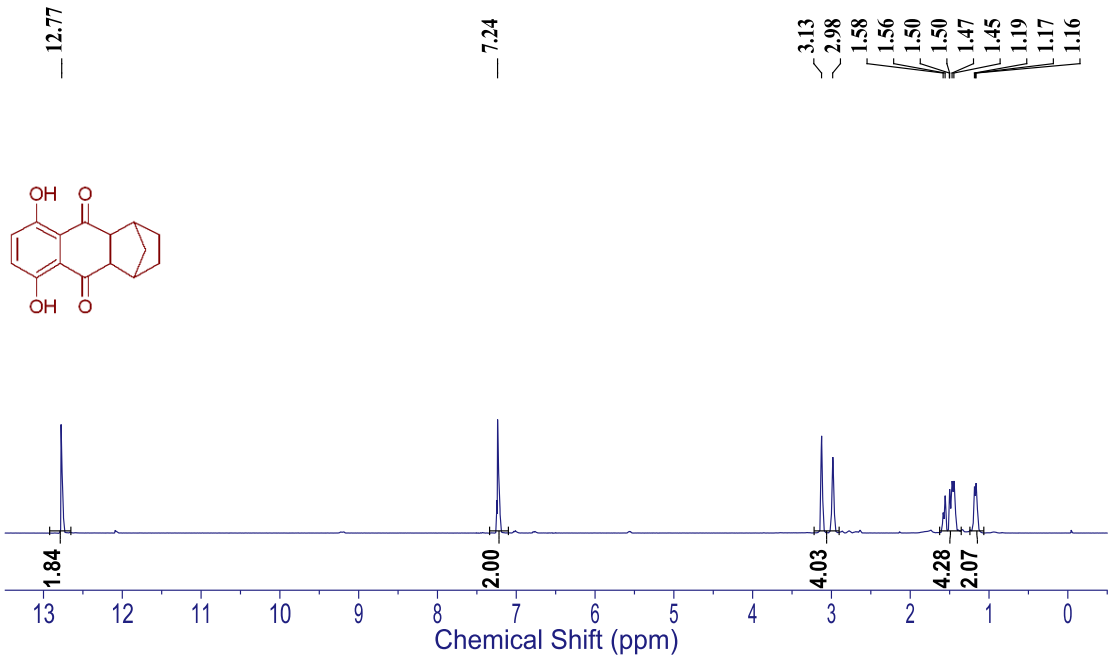

^{13}C NMR Spectrum (100 MHz, $CDCl_3$) of Compound **16**

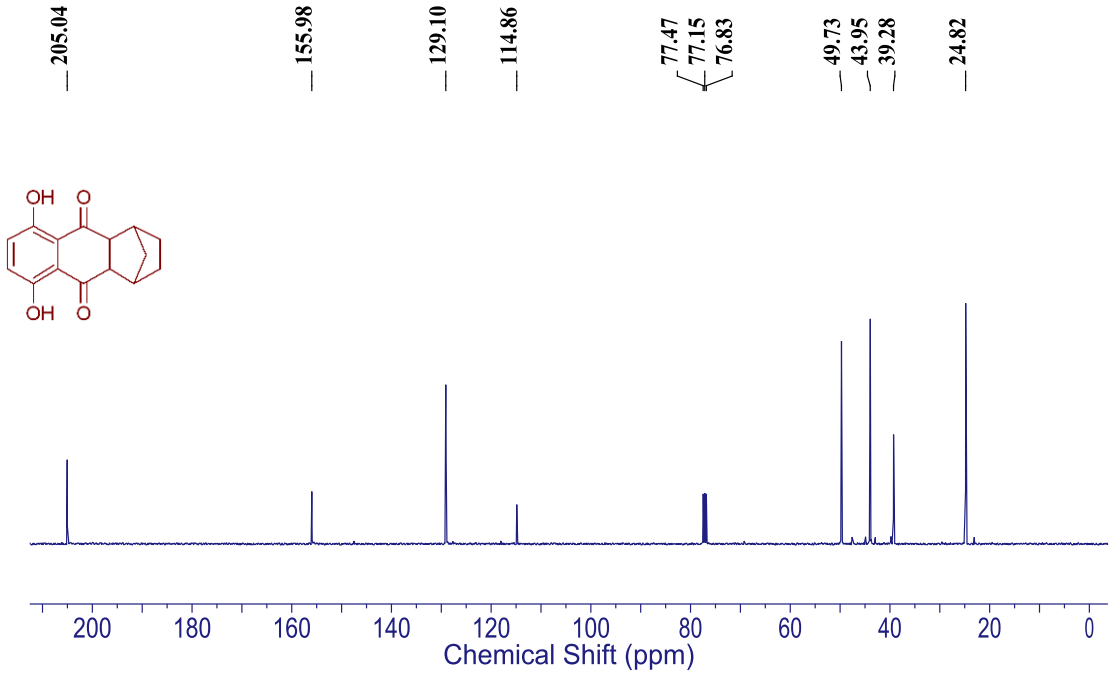

^{1}H NMR Spectrum (400 MHz, $CDCl_3$) of Compound **17**

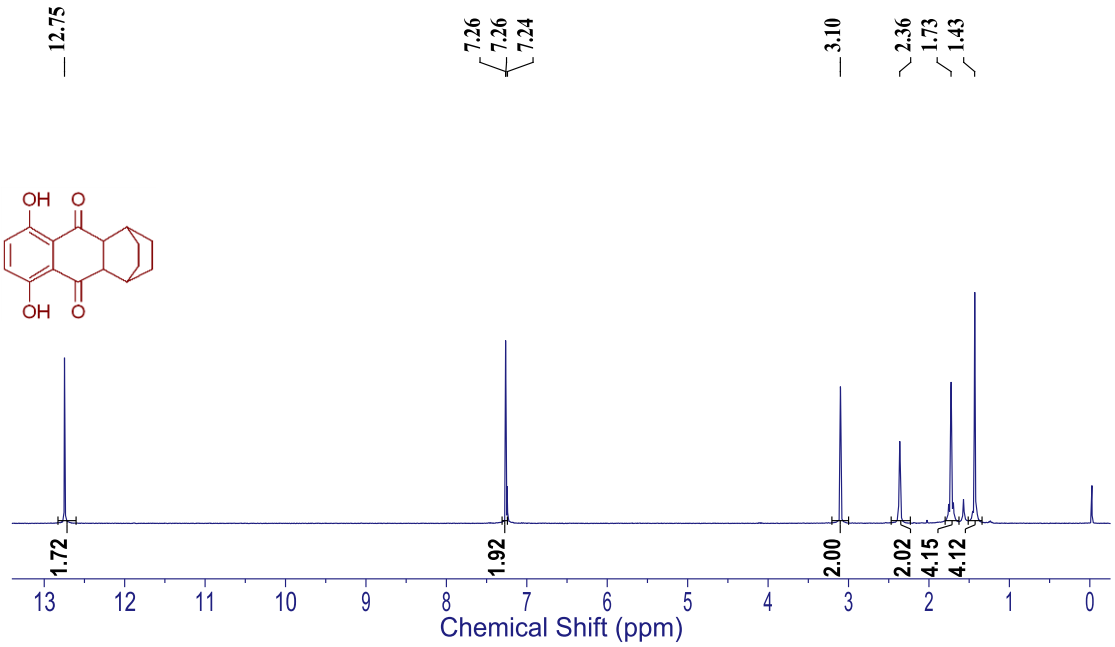

^{13}C NMR Spectrum (100 MHz, $CDCl_3$) of Compound **17**

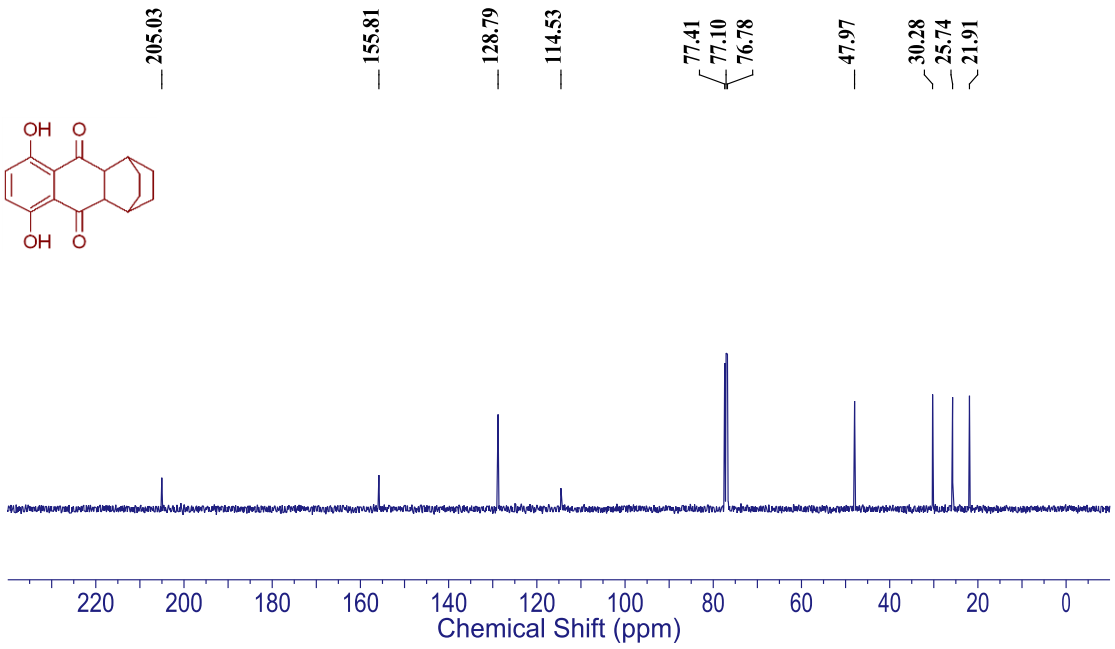

2.1.6. References:

1. Witte, M. E.; Geurts, J. J. G.; de Vries, H. E.; van der Valk, P.; van Horssen, J. Mitochondrial dysfunction: A potential link between neuroinflammation and neurodegeneration? *Mitochondrion* **2010,** 10, 411-418.
2. Sundaresan, M.; Yu, Z. X.; Ferrans, V. J.; Irani, K.; Finkel, T. Requirement for generation of H2O2 for platelet-derived growth factor signal transduction. *Science* **1995,** 270, 296-9.
3. Murphy, M. P. How mitochondria produce reactive oxygen species. *Biochem. J.* **2009,** 417, 1-13.
4. Shang, Y.; Zhang, L.; Jiang, Y.; Li, Y.; Lu, P. Airborne quinones induce cytotoxicity and DNA damage in human lung epithelial A549 cells: The role of reactive oxygen species. *Chemosphere* **2014,** 100, 42-49.
5. Parkinson, E. I.; Bair, J. S.; Cismesia, M.; Hergenrother, P. J. Efficient NQO1 Substrates are Potent and Selective Anticancer Agents. *ACS Chem. Biol.* **2013,** 8, 2173-2183.
6. Bair, J. S.; Palchaudhuri, R.; Hergenrother, P. J. Chemistry and Biology of Deoxynyboquinone, a Potent Inducer of Cancer Cell Death. *J. Am. Chem. Soc.* **2010,** 132, 5469-5478.
7. Beck, R.; Verrax, J.; Dejeans, N.; Taper, H.; Calderon, P. B. Menadione reduction by pharmacological doses of ascorbate induces an oxidative stress that kills breast cancer cells. *Int. J. Toxicol.* **2009,** 28, 33-42.
8. Monks, T. J.; Hanzlik, R. P.; Cohen, G. M.; Ross, D.; Graham, D. G. Quinone chemistry and toxicity. *Toxicol. Appl. Pharmacol.* **1992,** 112, 2-16.
9. Klaus, V.; Hartmann, T.; Gambini, J.; Graf, P.; Stahl, W.; Hartwig, A.; Klotz, L.-O. 1,4-Naphthoquinones as inducers of oxidative damage and stress signaling in HaCaT human keratinocytes. *Arch. Biochem. Biophys.* **2010,** 496, 93-100.
10. Campos-Martin, J. M.; Blanco-Brieva, G.; Fierro, J. L. G. Hydrogen Peroxide Synthesis: An Outlook beyond the Anthraquinone Process. *Angew. Chem. Int. Ed.* **2006,** 45, 6962-6984.
11. Blanchard, J. S. Quinone reductase reaction catalyzed by streptococcus faecalis NADH peroxidase. *Biochemistry¬Æ* **1995,** 34, 6621-6627.

12. Colucci, M. A.; Couch, G. D.; Moody, C. J. Natural and synthetic quinones and their reduction by the quinone reductase enzyme NQO1: From synthetic organic chemistry to compounds with anticancer potential. *Organic and Biomolecular Chemistry* **2008,** 6, 637-656.
13. Guo, W.; Reigan, P.; Siegel, D.; Zirrolli, J.; Gustafson, D.; Ross, D. The bioreduction of a series of benzoquinone ansamycins by NAD(P)H:quinone oxidoreductase 1 to more potent heat shock protein 90 inhibitors, the hydroquinone ansamycinss. *Mol. Pharmacol.* **2006,** 70, 1194-1203.
14. Segura-Aguilar, J.; Metodiewa, D.; Welch, C. J. Metabolic activation of dopamine o-quinones to o-semiquinones by NADPH cytochrome P450 reductase may play an important role in oxidative stress and apoptotic effects. *Biochimica et Biophysica Acta - General Subjects* **1998,** 1381, 1-6.
15. Hillard, E. A.; de Abreu, F. C.; Ferreira, D. C. M.; Jaouen, G.; Goulart, M. O. F.; Amatore, C. Electrochemical parameters and techniques in drug development, with an emphasis on quinones and related compounds. *Chemical Communications* **2008**, 2612-2628.
16. Farhana, A.; Guidry, L.; Srivastava, A.; Singh, A.; Hondalus, M. K.; Steyn, A. J. Reductive stress in microbes: implications for understanding Mycobacterium tuberculosis disease and persistence. *Adv. Microb. Physiol.* **2010,** 57, 43-117.
17. Lipinski, B. Evidence in support of a concept of reductive stress. *Br. J. Nutr.* **2002,** 87, 93-4; discussion 94.
18. Meena, R. C.; Thakur, S.; Nath, S.; Chakrabarti, A. Tolerance to thermal and reductive stress in Saccharomyces cerevisiae is amenable to regulation by phosphorylation-dephosphorylation of ubiquitin conjugating enzyme 1 (Ubc1) S97 and S115. *Yeast* **2011,** 28, 783-93.
19. Trung Pham, H.; Marquetty, C.; Pasquier, C.; Hakim, J. Luminol assay for microdetermination of superoxide dismutase activity: Its application to human fetal blood. *Anal. Biochem.,* **1984,** 142, 467-472.
20. Dharmaraja, A. T.; Dash, T. K.; Konkimalla, V. B.; Chakrapani, H. Synthesis, thiol-mediated reactive oxygen species generation profiles and anti-proliferative activities of 2,3-epoxy-1,4-naphthoquinones. *MedChemComm* **2012,** 3, 219 - 224.

21. Gay, C.; Collins, J.; Gebicki, J. M. Hydroperoxide assay with the ferric-xylenol orange complex. *Analytical Biochemistry* **1999,** 273, 149-155.
22. Gutierrez, P. L. The metabolism of quinone-containing alkylating agents: free radical production and measurement. *Front Biosci.* **2000,** 5, D629-638.
23. Hajas, G.; Bacsi, A.; Aguilerra-Aguirre, L.; German, P.; Radak, Z.; Sur, S.; Hazra, T. K.; Boldogh, I. Biochemical identification of a hydroperoxide derivative of the free 8-oxo-7,8-dihydroguanine base. *Free Radical Biology and Medicine* **2012,** 52, 749-756.
24. Halliwell, B. Superoxide-dependent formation of hydroxyl radicals in the presence of iron salts is a feasible source of hydroxy radicals in vivo. *Biochemical Journal* **1982,** 205, 461-463.
25. Khodade, V. S.; Dharmaraja, A. T.; Chakrapani, H. Synthesis, reactive oxygen species generation and copper-mediated nuclease activity profiles of 2-aryl-3-amino-1,4-naphthoquinones. *Bioorganic & Medicinal Chemistry Letters* **2012,** 22, 3766-3769.
26. Bruice, T. C.; Yano, Y. Radical mechanisms for 1,5-dihydro-5-methylflavine reduction of carbonyl compounds. *Journal of the American Chemical Society* **1975,** 97, 5263-5271.
27. Eberlein, G.; Bruice, T. C. One and two electron reduction of oxygen by 1,5-dihydroflavins. *Journal of the American Chemical Society* **1982,** 104, 1449-1452.
28. Kemal, C.; Chan, T. W.; Bruice, T. C. Reaction of 3O2 with dihydroflavins. 1. N3,5-Dimethyl-1,5-dihydrolumiflavin and 1,5-dihydroisoalloxazines. *Journal of the American Chemical Society* **1977,** 99, 7272-7286.
29. Georgiou, C. D.; Papapostolou, I.; Grintzalis, K. Superoxide radical detection in cells, tissues, organisms (animals, plants, insects, microorganisms) and soils. *Nat. Protoc.,* **2008,** 3, 1679-1692.
30. Zielonka, J.; Vasquez-Vivar, J.; Kalyanaraman, B. Detection of 2-hydroxyethidium in cellular systems: A unique marker product of superoxide and hydroethidine. *Nat. Protoc.,* **2008,** 3, 8-21.
31. Zhao, H.; Joseph, J.; Fales, H. M.; Sokoloski, E. A.; Levine, R. L.; Vasquez-Vivar, J.; Kalyanaraman, B. Detection and characterization of the product of

hydroethidine and intracellular superoxide by HPLC and limitations of fluorescence. *Proc. Natl. Acad. Sci.,* **2005,** 102, 5727-5732.

32. Valderrama, J. A.; Espinoza, O.; Gonz√°lez, M. F.; Tapia, R. A.; Rodr√≠guez, J. A.; Theoduloz, C.; Schmeda-Hirschmann, G. Studies on quinones. Part 40: Synthesis and cytotoxicity evaluation of anthraquinone epoxides and isomerization products. *Tetrahedron* **2006,** 62, 2631-2638.
33. Kalghatgi, S.; Spina, C. S.; Costello, J. C.; Liesa, M.; Morones-Ramirez, J. R.; Slomovic, S.; Molina, A.; Shirihai, O. S.; Collins, J. J. Bactericidal Antibiotics Induce Mitochondrial Dysfunction and Oxidative Damage in Mammalian Cells. *Sci. Transl Med.* **2013,** 5, 192ra85.
34. Brynildsen, M. P.; Winkler, J. A.; Spina, C. S.; MacDonald, I. C.; Collins, J. J. Potentiating antibacterial activity by predictably enhancing endogenous microbial ROS production. *Nat. Biotechnol.,* **2013,** 31, 160-165.
35. Hebrard, M.; Viala, J. P.; Meresse, S.; Barras, F.; Aussel, L. Redundant hydrogen peroxide scavengers contribute to Salmonella virulence and oxidative stress resistance. *J. Bacteriol.* **2009,** 191, 4605-14.
36. Liu, C. I.; Liu, G. Y.; Song, Y.; Yin, F.; Hensler, M. E.; Jeng, W. Y.; Nizet, V.; Wang, A. H.; Oldfield, E. A cholesterol biosynthesis inhibitor blocks Staphylococcus aureus virulence. *Science* **2008,** 319, 1391-4.
37. Fauci, A. S.; Alston, B.; Barry, C. E.; Augustine, A. D.; Fenton, M. J.; Handley, F. G.; Holland, S. M.; Huebner, R. E.; Jacobs, G.; Laughon, B.; Lehrman, S.; Makhene, M.; Mason, R. M.; Olivier, K. N.; Polis, M. A.; Prevots, D. R.; Sizemore, C.; Spinelli, B. A.; Taylor, K.; Touchette, N. A.; Via, L. E. Multidrug-resistant and extensively drug-resistant tuberculosis: The National Institute of Allergy and Infectious Diseases research agenda and recommendations for priority research. *J. Infect. Dis.* **2008,** 197, 1493-1498.
38. Gandhi, N. R.; Moll, A.; Sturm, A. W.; Pawinski, R.; Govender, T.; Lalloo, U.; Zeller, K.; Andrews, J.; Friedland, G. Extensively drug-resistant tuberculosis as a cause of death in patients co-infected with tuberculosis and HIV in a rural area of South Africa. *Lancet* **2006,** 368, 1575-1580.

39. Gomez, J. E.; McKinney, J. D. M. tuberculosis persistence, latency, and drug tolerance. *Tuberculosis (Edinb)* **2004,** 84, 29-44.

40. Gonzalez Iii, L. S.; Spencer, J. P. Aminoglycosides: A practical review. *Am. Fam. Physician,* **1998,** 58, 1811-1820.

41. Vilchèze, C.; Hartman, T.; Weinrick, B.; Jacobs Jr, W. R. Mycobacterium tuberculosis is extraordinarily sensitive to killing by a vitamin C-induced Fenton reaction. *Nat. Commun.,* **2013,** 4:1881, 1-10.

42. Boehme, D. E.; Vincent, K.; Brown, O. R. Oxygen and toxicity inhibition of amino acid biosynthesis. *Nature* **1976,** 262, 418-420.

43. Ezraty, B.; Vergnes, A.; Banzhaf, M.; Duverger, Y.; Huguenot, A.; Brochado, A. R.; Su, S. Y.; Espinosa, L.; Loiseau, L.; Py, B.; Typas, A.; Barras, F. Fe-S cluster biosynthesis controls uptake of aminoglycosides in a ROS-less death pathway. *Science* **2013,** 340, 1583-1587.

44. Brynildsen, M. P.; Winkler, J. A.; Spina, C. S.; MacDonald, I. C.; Collins, J. J. Potentiating antibacterial activity by predictably enhancing endogenous microbial ROS production. *Nat. Biotech.* **2013,** 31, 160-165.

45. Keshavaraja, A.; Ramaswamy, A. V.; Pandey, B.; Hegde, V. R.; Kumar, P.; Ravindranathan, T. Eine yttriumhaltige starke Lewis-Säure zur heterogenen Katalyse der Diels-Alder-Reaktion. *Angewandte Chemie* **1995,** 107, 2333-2336.

46. Carreno, M. C.; Garcia Ruano, J. L.; Urbano, A. Asymmetric Diels-Alder reactions of (S)-2-(p-tolylsulfinyl)-1,4-naphthoquinones. *The Journal of Organic Chemistry* **1992,** 57, 6870-6876.

47. Blokzijl, W.; Blandamer, M. J.; Engberts, J. B. F. N. Diels-Alder reactions in aqueous solutions. Enforced hydrophobic interactions between diene and dienophile. *Journal of the American Chemical Society* **1991,** 113, 4241-4246.

48. Stork, G.; La Clair, J. J.; Spargo, P.; Nargund, R. P.; Totah, N. Stereocontrolled Synthesis of (¬±)-12a-Deoxytetracycline. *Journal of the American Chemical Society* **1996,** 118, 5304-5305.

49. Fari√±a, F.; Paredes, M. C.; Stefani, V. Polycyclic hydroxyquinones : XXIV Diels-alder reactions of 5-amino-8-hydroxy-1,4-naphthoquinone. Novel

transcycloaddition reactions with derivatives of 1,4-dihydro-1, 4-methanoanthracene-9,10-dione. *Tetrahedron* **1986,** 42, 4309-4318.

50. Hayakawa, K.; Aso, M.; Kanematsu, K. Site-selective Diels-Alder reactions of 1,4,5,8-naphthodiquinones with anthracenes and successively with cyclopentadiene: electronic effects vs. steric effects. *The Journal of Organic Chemistry* **1985,** 50, 2036-2040.
51. Pandey, B.; Dalvi, P. V. Photo-induced exo-selective Diels-Alder reactions. *Angewandte Chemie (International Edition in English)* **1993,** 32, 1612-1613.
52. Rathore, R.; Kochi, J. K. Isolation of novel radical cations from hydroquinone ethers. Conformational transition of the methoxy group upon electron transfer. *Journal of Organic Chemistry* **1995,** 60, 4399-4411.
53. Valiulin, R. A.; Arisco, T. M.; Kutateladze, A. G. Strained to the limit: When a cyclobutyl moiety becomes a thermodynamic sink in a protolytic ring-opening of photogenerated oxetanes. *Organic Letters* **2010,** 12, 3398-3401.
54. Eastgate, M. D.; Buono, F. G. Mechanistic insight into the palladium-catalyzed 1,4-oxidation of 1,3-dienes to 1,4-dicarboxy-alk-2-enes. *Angewandte Chemie - International Edition* **2009,** 48, 5958-5961.
55. Mori, K.; Hara, T.; Mizugaki, T.; Ebitani, K.; Kaneda, K. Hydroxyapatite-bound cationic ruthenium complexes as novel heterogeneous Lewis acid catalysts for Diels-Alder and aldol reactions. *Journal of the American Chemical Society* **2003,** 125, 11460-11461.
56. Ogasawara, Y.; Uchida, S.; Yamaguchi, K.; Mizuno, N. A Tin-tungsten mixed oxide as an efficient heterogeneous catalyst for C-C Bond Bond-Forming reactions. *Chemistry - A European Journal* **2009,** 15, 4343-4349.
57. Menter, J. M.; Filipescu, N. Photochemical detection of intramolecular energy transfer between nonconjugated chromophores in rigid model compounds. *J. Chem. Soc. (B)* **1970**, 464-468.
58. Bensinger, R. E.; Johnson, C. M. Luminol assay for superoxide dismutase. *Analytical Biochemistry* **1981,** 116, 142-145.

59. Cho, Y. S.; Kim, H. S.; Kim, C. H.; Cheon, H. G. Application of the ferrous oxidation–xylenol orange assay for the screening of 5-lipoxygenase inhibitors. *Anal. Biochem.* **2006,** 351, 62-68.

60. Zhou, M.; Diwu, Z.; Panchuk-Voloshina, N.; Haugland, R. P. A Stable Nonfluorescent Derivative of Resorufin for the Fluorometric Determination of Trace Hydrogen Peroxide: Applications in Detecting the Activity of Phagocyte NADPH Oxidase and Other Oxidases. *Anal. Biochem.,* **1997,** 253, 162-168.

61. Wardman, P. Fluorescent and luminescent probes for measurement of oxidative and nitrosative species in cells and tissues: Progress, pitfalls, and prospects. *Free Rad. Biol. Med.,* **2007,** 43, 995-1022.

62. Wrona, M.; Patel, K.; Wardman, P. Reactivity of 2',7'-dichlorodihydrofluorescein and dihydrorhodamine 123 and their oxidized forms toward carbonate, nitrogen dioxide, and hydroxyl radicals. *Free Rad. Biol. Med.,* **2005,** 38, 262-270.

63. Zhou, M.; Diwu, Z.; Panchuk-Voloshina, N.; Haugland, R. P. A Stable Nonfluorescent Derivative of Resorufin for the Fluorometric Determination of Trace Hydrogen Peroxide: Applications in Detecting the Activity of Phagocyte NADPH Oxidase and Other Oxidases. *Analytical Biochemistry* **1997,** 253, 162-168.

64. Szatrowski, T. P.; Nathan, C. F. Production of Large Amounts of Hydrogen Peroxide by Human Tumor Cells. *Cancer Res.* **1991,** 51, 794-798.

65. CLSI. Performance standards for antimicrobial suceptibility testing; twenty second supplement,. *National Committee for Clinical Laboratory Standards (NCCLS), M100-22* **2012,** 32.

CHAPTER 2.2: SUBSTITUENT EFFECTS ON REACTIVE OXYGEN SPECIES (ROS) GENERATION BY HYDROQUINONES

2.2.1 Introduction:

In chapter 2.1, we described small molecule based reactive oxygen species (ROS) generators in aerobic buffer. Hydroquinones or 1,4-dihydroxyarenes occupy an important position among the small molecule based ROS generators. These diols can transfer 1 e^- to oxygen to produce $O_2^{\bullet -}$, which is subsequently converted to hydrogen peroxide, H_2O_2 (Scheme 2.2.1).

Scheme 2.2.1. Generation of superoxide, $O_2^{\bullet -}$ from hydroquinone enolate upon reaction with molecular O_2

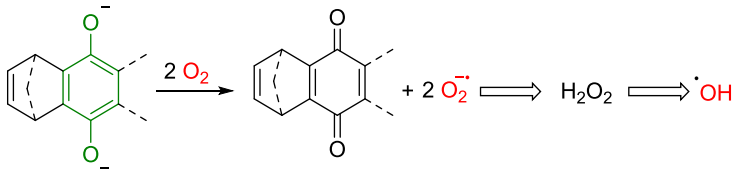

Design and synthesis of a library of 2,3-dihydro-1,4-naphthoquinones and their evaluation for ROS generation was presented in Chapter 2.1.[1] A mechanism for ROS generation from these compounds involved enolization as the first step that produces an aromatic 1,4-diol, which is known to react with oxygen to produce $O_2^{\bullet -}$. Although a majority of these 2,3-dihydro-1,4-naphthoquinones were efficient ROS generators there are no structural handle to fine tune the ROS generation profile (Scheme 2.2.2).

Scheme 2.2.2. A scheme for ROS generation from 2,3-dihydro-1,4-naphthoquinone derivatives.

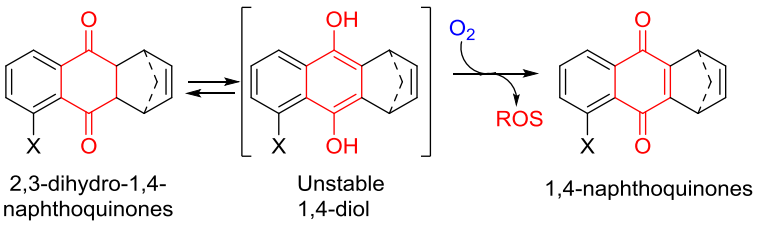

Furthermore, substituent effects on stabilizing the enol and subsequent reaction with O_2 is poorly understood. Thus, we hypothesized that introducing substituents near carbonyl group on dihydrobenzoquinones (keto form, Scheme 2.2.3) might affect its stability by increasing the propensity to enolize. We hypothesized that tautomerization of the hydroquinone was the key step for ROS generation and accordingly, placing substituents on the aryl ring might perturb the position of the equilibrium of tautomers possibly offering opportunities to tune ROS generation (Scheme 2.2.3). These tools would allow us to study the differences in inhibitory effects of ROS generation profiles.

Scheme 2.2.3. 6-Aryl-2,3-dihydro-1,4-benzoquinones equilibrate with their corresponding diols.

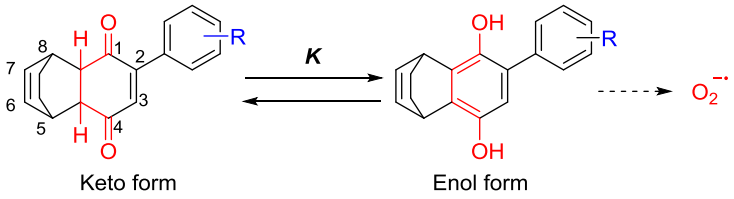

2.2.2. Results and Discussion:

2.2.2.1. Synthesis and characterization:

In order to synthesize the designed scaffold 6-aryl-2,3-dihydrobenzoquinone, substituted *p*-benzoquinones **27-38** were first synthesized using a silver nitrate catalyzed arylation of 1,4-benzoquinone with substituted arylboronic acids with electron releasing and withdrawing functional groups (Table 2.2.1, entries 1- 12)[2]. A reaction of phenylboronic acid with 1,4-benzoquinone produced 2-phenyl-1,4-benoquinone (**27**) in 88% yield. Under similar conditions 2-aryl-1,4-benzoquinone derivatives with electron donating methyl (**28**) and methoxy (**29** & **38**) substituents on the aryl ring were obtained in yields ranging from 41-63 % (Table 2.2.1, entries 2,3, 12). Similarly, halogenated derivatives such as bromo (**30**), chloro (**31**) and fluoro (**32**) derivatives of 2-phenyl-1,4-benzoquinone were synthesized by a reaction of corresponding arylboronic acids with 1,4-benzoquinone (Table 2.2.1, entries 4-6). Introduction of electron withdrawing groups such as 4-acetyl (**33**), 4-nitro (**34**), 4-formyl (**35**), 3-nitro (**36**) and 3-formyl (**37**) on 2-

phenyl-1,4-benzoquinone were carried out by a reaction of respective arylboronic acids with 1,4-benzoquinone (Table 2 2.1, entries 7-11).

Table 2.2.1. Synthesis of 2-aryl-1,4-benzoquinones (**27**-**38**)

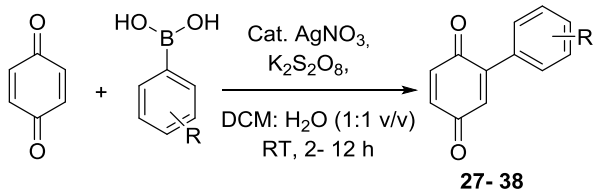

27- 38

Entry	Reactant	Product	% Yield
1	Ph	**27**	88
2	4-MePh	**28**	59
3	4-MeOPh	**29**	63
4	4-BrPh	**30**	69
5	4-ClPh	**31**	74
6	4-FPh	**32**	76
7	4-AcPh	**33**	66
8	4-NO_2Ph	**34**	14
9	4-CHOPh	**35**	60
10	3-NO_2Ph	**36**	39
11	3-CHOPh	**37**	49
12	2-MeOPh	**38**	41

Next, **5, 27**-**38** were independently reacted with 1,3-cycohexadiene to produce the Diels-Alder adducts (**11**, **39**-**50**) in yields ranging from 67-95% (Table 2.2.2, entries 1-13). ^{1}H nuclear magnetic resonance (^{1}H-NMR) spectroscopy study conducted on **39** showed that this compound exclusively existed in the keto form (**39a**) as evidenced by signals for the hydrogens of α- and β- (bridgehead) to the C=O, which appeared in the range 3.0–3.4 ppm (Figure 1). A similar result was recorded for the 4-methyl as well as 4-methoxyphenyl derivatives **40** and **41** (Figure 1) suggesting no major effect of introduction of an electron donating group on the position of the equilibrium.

Table 2.2.2. Synthesis of hydroquinones **39**-**50**

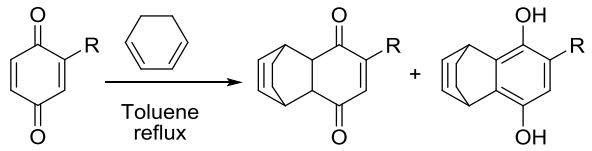

5, 27-38 **11, 39a-50a** **39b-50b**

Entry	Reactant	R	Product	% Yield
1	**5**	H	**11**	70
2	**27**	Ph	**39a**	73
3	**28**	4-MePh	**40a**	66
4	**29**	4-MeOPh	**41a**	74
5	**30**	4-BrPh	**42** (**42a** + **42b**)	81
6	**31**	4-ClPh	**43** (**43a** + **43b**)	95
7	**32**	4-FPh	**44** (**44a** + **44b**)	66
8	**33**	4-AcPh	**45 (45a** + **45b**)	84
9	**34**	4-NO_2Ph	**46b**	47
10	**35**	4-CHOPh	**47b**	81
11	**36**	3-NO_2Ph	**48** (**48a** + **48b**)	67
12	**37**	3-CHOPh	**49b**	87
13	**38**	2-MeOPh	**50a**	70

Next, ^{1}H NMR spectrum for the 4-bromo derivative **42** was recorded and this compound was found to exist predominantly in its keto form **42a**. In addition, a set of peaks at 4.2–4.5 ppm for the bridgehead hydrogens of the enol form **42b** was also observed (Figure 2.2.1). The major tautomer was the keto form **42a** estimated as 93% (Figure 2.2.1). A similar result was recorded for **44**, **45**, **46** (Figure 2.2.1) and **48** and these compounds were found to have 27-89% keto forms (Table 2.2.3, entries 6-8, 11). Compounds **46**, **47** and **49** with electron withdrawing substituents were found to exist nearly exclusively in the enol forms **46b**, **47b** and **49b** in solution (Table 2.2.3, entries 9, 10, 12). The aryl derivative **50** with a 2-methoxy substituent was found to behave similar

to the 4-methoxy derivative **41** and only the keto form **50a** could be detected (Table 2.2.3, entry 13).

Figure 2.2.1. Portions of ^{1}H NMR spectra of **39**, **41**, **42**, **45** and **47**. Compounds **39a** and **41a** were nearly exclusive equilibrium components while evidence for a mixture was seen in the cases of **41** and **45** with **41a** and **45a** being the major isomers. In the case of **47**, we found no evidence for the keto isomer **47a** and the enol form **47b** was the major component. Arrows indicate the characteristic C-H bridgehead signals for the enol isomer.

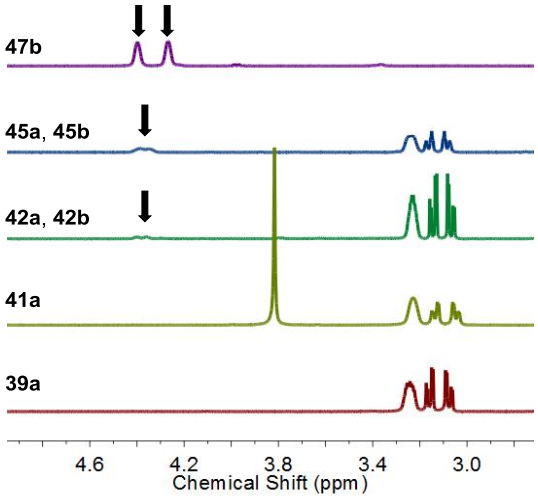

Based on the ratios of the keto and enol forms, an equilibrium constant for enolization K_{eq} was calculated (Table 2.2.3). Using these K_{eq}, a Hammett plot was constructed, a moderate linear correlation (R^2 = 0.6751) was observed with σ and an overall reaction constant ρ of +3.6 was obtained (Figure 2.2.2a).[3] In order to estimate the resonance contribution to the position of the equilibrium, a similar plot was constructed with σ^+ and a ρ value of +2.37 was obtained but with better linearity (R^2 = 0.7420, Figure 2.2.2b).[4] This result suggests that the position of the equilibrium was dictated more by resonance effects than by induction. Thus, electronic effects of the adjacent aryl ring significantly perturb the 2,3-dihydro-1,4-benzoquinone-hydroquinone equilibrium in an organic medium and is in favor of the enol tautomer in the presence of electron withdrawing groups. Previous reports of such equilibria in related β-diketones such as benzoylacetones

and benzoylcyclohexanones indicate that electron deficient keto forms are stabilized by the electron releasing groups. Conversely, the presence of electron withdrawing groups resulted in domination by the enol form, possibly by destabilization of the keto form or by stabilizing relatively electron rich enols. Although the magnitude of the reaction constant ρ derived from σ^+ and equilibrium constants was significantly lower (0.6 – 0.9[5-7]) in the aforementioned studies than the ρ that we find in this study, the sign was positive supporting similar trends in stability of keto and enol forms.

Figure 2.2.2. Plot of log (K_X/K_H) for keto-enol equilibria of 2,3-dihydrobenzoquinones versus Hammett substitution constant a) σ,[3] obtained reaction constant ρ = 3.60; R^2 = 0.6751; b) σ^+,[4] obtained reaction constant ρ = 2.37; R^2 = 0.7420.

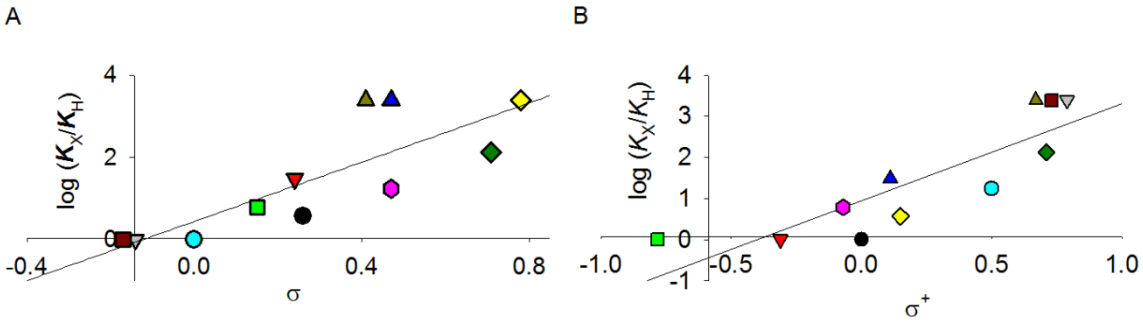

Under basic conditions, the keto form is expected to undergo an enolization to produce the 1,4-diol and this could be used to understand the substituents' effect on the rate of enolization in basic media. Hence, **39** which predominantly exists in the keto form **39a** was exposed to NaOD (0.2 equiv, pH = 10.0) and NMR spectrum was recorded after 15 min (Figure 2.2.3a). We found nearly complete disappearance of **39a** presumably to the enolate form as suggested by characteristic peaks for the bridgehead hydrogens indicated by arrows in Figure 2.2.3a. A similar experiment conducted with **41a** showed that in the same time period, 62% of **41a** remained supporting that electron donating groups decreased the propensity of the ketone to enolize (Figure 2.2.3b). Complete enolization was however observed in 1 h. A similar experiment conducted with **42** (93:7; **42a**:**42b**) and **45** (77:23; **45a**:**45b**) showed complete conversion to the corresponding enolate in 15 min. When **47b** was exposed to NaOD, we did not observe any significant change in the

pattern of ^{1}H NMR signal for the bridgehead hydrogens of **47b** (indicated by arrow, Figure 2.2.3c).

Table 2.2.3. Keto-enol tautomers (%), equilibrium constants (K_{eq}) and Hammett parameters

Entry	Compd	% Keto[a]	% Enol[a]	K_{eq}[b]	σ[c]	σ^{+}[d]
1	**11**	100	n.d.	0.0204[e]	-	-
2	**39**	100	n.d.	0.0204[e]	0	0.00
3	**40**	100	n.d.	0.0204[e]	-0.14	-0.31
4	**41**	100	n.d.	0.0204[e]	-0.17	-0.78
5	**42**	93	7[f]	0.0753	0.26	0.15
6	**43**	62[b]	38	0.6129	0.24	0.11
7	**44**	89	11[f]	0.1235	0.15	-0.07
8	**45**	74	26[f]	0.3513	0.47	0.50
9	**46**	n.d.	100[f]	49	0.78	0.79
10	**47**	n.d.	100[f]	49	0.47	0.73
11	**48**	27	73[f]	2.703	0.71	0.71
12	**49**	n.d.	100	49[e]	0.41	0.67
13	**50**	100	n.d.	0.0204	-	-

[a]% keto and enol forms were estimated by ^{1}H NMR spectroscopy in $CDCl_3$ unless otherwise indicated (spectra were recorded on a 400 MHz NMR spectrometer); [b]K_{eq} was estimated by ratio of peaks corresponding to α- and β-hydrogens to the C=O (for the keto form) and the bridgehead hydrogens for the enol form; [c]Hammett parameters were obtained from ref. 33; [d]Hammett parameters were obtained from ref. 34; [e]Estimated by considering 98% of the major tautomer; [f]experiment was conducted in DMSO-d_6; n.d. = not detected

Figure 2.2.3. Keto-enol tautomerization of **39**, **41** and **47** with sodium deutroxide (NaOD, 0.2 equiv in DMSO–d_6, pH = 10.0) was studied using ^{1}H NMR spectroscopy. Portions of ^{1}H NMR spectra displayed here are before and 15 min after addition of NaOD, (a) **39** alone and **39** + NaOD; (b) **41** alone and **41** + NaOD; and (c) **47** alone and **47** + NaOD. Arrows indicate the characteristic C-H bridgehead signals for the enol isomer.

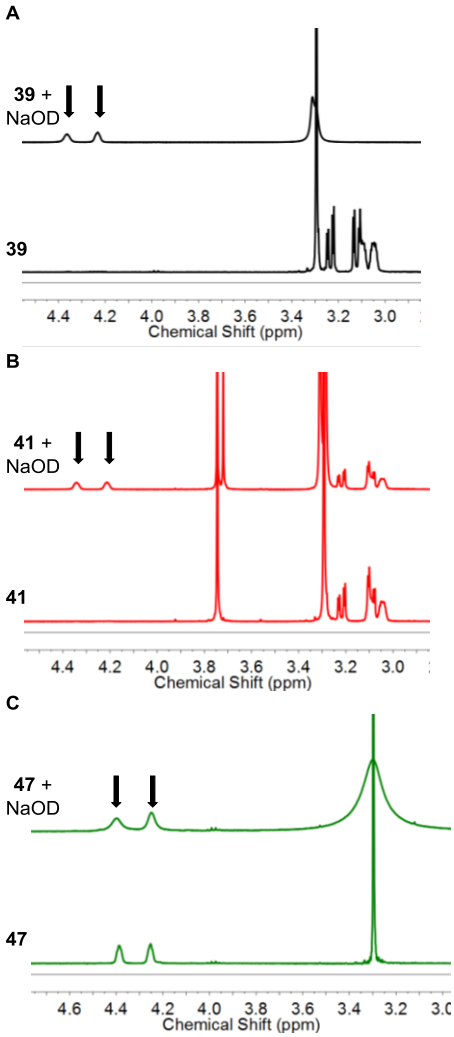

2.2.2.2. Stability studies in buffer:

In ambient aerobic buffer, the hydroquinone is expected to rapidly react with oxygen to produce the corresponding 1,4-benzoquinone while the 2,3-dihydro-1,4-benzoquinone

would be expected to tautomerize to the corresponding hydroquinone and then undergo oxidation. Accordingly, the hydroquinone is expected to be more reactive in ambient aerobic buffer. When **11** was dissolved in pH 7.4 buffer: acetonitrile (1:1, v/v), we find nearly 32% of compound remaining after 60 min from HPLC analysis (Table 2.2.3, entry 1). When a similar experiment was conducted with **39**, 74% of the compound remained after 1 h (Table 2.2.3, entry 3). The time course of decomposition of **39** was recorded and nearly 15% of compound remained after 8 h (Figure 2.2.4a); curve fitting to a first order reaction gave a rate constant of 0.28 h^{-1} (R^2 = 0.9875) and a half-life ($t_{1/2}$) of 2.49 h.

Figure 2.2.4. Decomposition studies on **39** and **47**: Time course of decomposition of (a) **39** (1 mM, k_{39} = 0.28 h^{-1}, R^2 = 0.9875) and (b) **47** (1 mM, k_{47} = 1.48 h^{-1}, R^2 = 0.9546) in acetonitrile: pH 7.4 buffer (1:1 ratio, v/v) based on HPLC analysis.

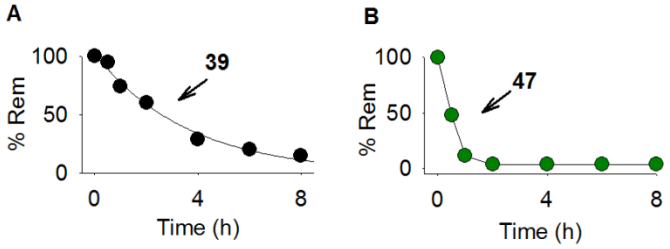

Compounds **40a** and **41a** with electron donating groups were found to have comparable decomposition profiles after 1 h (Table 2.2.3, entries 3, 4). In the cases of compounds **42-45** and **48** which existed as mixtures of keto and enol forms in organic media, the % remaining in these cases was calculated based on the keto form and ranged from 18-57%, all lower in comparison with **39a** (Table 2.2.3, entries 5-8, 11). In addition, compounds **46b** and **47b** were 90% decomposed in 1 h while the 40% of the formyl derivative **49b** remained in the same time period (Table 2.2.3, entries 9, 10, 12). Under these conditions, a first order rate constant k = 1.48 h^{-1} (R^2 = 0.9546) was recorded for decomposition of **47b**. The half-life of this compound was estimated as 0.47 h, which is lower in comparison with **39a** (Figure 2.2.4b). Taken together, these results suggest that the enol form in buffer was significantly less stable in comparison with the keto form.

Decomposition of 6-phenyl-2,3-dihydro-1,4-benzoquinone **39a** in pH 7.4 buffer was monitored by HPLC showed concurrent formation of the oxidized product **51**. We have

independently synthesized **51** by reacting **39a** with K_2CO_3 in THF under atmospheric conditions (Scheme 2.2.4). Similarly, compounds **52** and **53** were synthesized from the corresponding 6-aryl-2,3-dihydro-1,4-benzoquinones **41a** and **45a** respectively. The product of decomposition 6-aryl-2,3-dihydro-1,4-benzoquinones (**41a**, **42a**+**42b** and **45a**+**45b**) in aerobic buffer was validated by comparing the HPLC traces of respective benzoquinones **51**-**53**.

Scheme 2.2.4. Synthesis of **51**-**53**.

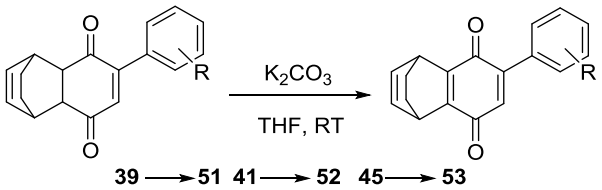

2.2.2.3. Studies on Generation of ROS:

The decomposition product of hydroquinone in aerobic buffer is benzoquinone and a simultaneous direct $1e^-$ transfer to O_2 should produce superoxide $O_2^{\bullet-}$. We studied the level of superoxide ($O_2^{\bullet-}$) generated from **39**–**50** in buffer using a reported chemiluminescence assay.[8] All compounds **39**–**50** (10 μM) were independently incubated in pH 8.0 buffer for 25 min, following which addition of luminol and measurement of chemiluminescence was carried out. Results of this assay confirms that **39**-**50** were capable of generating $O_2^{\bullet-}$ in buffer.

Figure 2.2.5. Estimation of H_2O_2 generation from **39** and **47**: Time course of H_2O_2 generated from (a) **39** (10 μM) and (b) **47** (10 μM) during 6 h in pH 7.4 buffer measured using Amplex Red® based fluorescence assay.

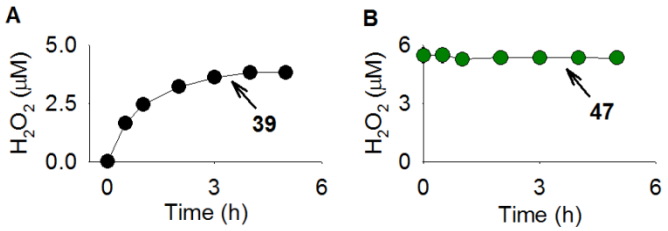

Table 2.2.4. % Compound remaining and H_2O_2 from **11, 39-50** in pH 7.4 phosphate buffer

Entry	Compound	% remaining[a]	H_2O_2 (μM)[b]
1	**11**	32	1.16
2	**39**	74	1.66
3	**40**	60	0.75
4	**41**	86	1.07
5	**42**	25	0.85
6	**43**	52	3.67
7	**44**	57	2.65
8	**45**	17	2.44
9	**46**	9.6	1.59[d]
10	**47**	11.4	5.42
11	**48**	18	3.55
12	**49**	40	3.55
13	**50**	70	0.45

[a]The compound (1 mM) was incubated in pH 7.4 phosphate buffer for 60 min at 37 °C under ambient aerobic conditions and HPLC was used to determine % compound remaining; [b]The compound (10 μM) was incubated in pH 7.4 buffer under ambient aerobic conditions for 60 min and H_2O_2 was assayed by an Amplex Red® fluorescence assay; [d]HPLC analysis of this reaction mixture showed multiple unidentified products suggesting possible side reactions or collateral consumption of starting material possibly contributing to diminished yield of H_2O_2.

Addition of an electron to $O_2^{\bullet-}$ would lead to the formation of H_2O_2, which was assayed using a commercially available Amplex Red® reagent.[9] Compound **39a**, which predominantly existed in its keto form, generated H_2O_2 during 6 h with a yield of 3.95 μM (Figure 2.2.5a). On the other hand, an exclusive enol isomer **47b** is stable in organic media, generated H_2O_2 rapidly upon dissolution in buffer (Figure 2.2.5b). All compounds tested were found to generate H_2O_2 and in a majority of the cases, we find that the

presence of an electron withdrawing substituent enhanced ROS generation. This result is in consistent with enolization being the critical step in ROS production and once formed, the enolate reacts rapidly with O_2 to generate ROS. However, a decreased yield of H_2O_2 was observed for strong electron withdrawing 4-nitrophenyl derivative **46**. We have examined the decomposition of **46** in buffer using a HPLC analysis, we found multiple uncharacterized products formed, perhaps ROS might get quenched by a cross reaction with **46** or with resultant organic product and hence showing a diminished H_2O_2 yield in buffer.

2.2.3. Conclusion

Taken together, we provide evidence for predictably tuning keto-enol tautomerism in dihydrobenzoquinones by varying substituent electronic effects. The position of the equilibrium appears to have significant effects on ROS generation ability. Compounds with dominant enol forms were better ROS generators. Most tools for ROS generation offer certain level of temporal control. For example, xanthine-xanthine oxidase is used for the generation of superoxide $O_2^{\bullet-}$ and glucose-glucose oxidase is used to generate H_2O_2, both the enzymatic methods generate ROS as a burst. H_2O_2 itself is used for studying the effect of induced oxidative stress in mammalian cells[10-12] and in bacteria at higher concentrations.[13] An organic hydrogen peroxide derivative, *tert*-butylhydroperoxide (TBHP) is widely used as a model compound to investigate the mechanisms of cellular damage by oxidative stress although TBHP is sluggish in its decomposition in buffer.[14-16] Taken together we provide evidence for predictably tuning keto–enol tautomerism in dihydrobenzoquinones by varying substituent electronics and the position of this equilibrium significantly affects ROS generation.

2.2.4. Experimental and Characterization Data:

Compounds **12**,[17] **39**[18] and **27**–**38**[2,19] have been previously reported and analytical data that we recorded were consistent with the reported values.

2.2.4.1. General procedure for [4 + 2] cycloaddition with 1, 3-cyclohaxadiene.

To a solution of the 1,4-benzoquinone (1.44 mmol) in toluene (10 mL), freshly distilled 1,3-cyclohexadiene (1.72 mmol) was added and the mixture was refluxed for 12 h. Upon complete consumption of the starting material (TLC analysis), the reaction mixture was evaporated to dryness under reduced pressure to obtain crude product. The crude material was purified by silica gel column chromatography using ethyl acetate (1→5 %) and petroleum ether solvent system to obtain pure material.

6-(4-Methylphenyl)-1,4,4a,8a-tetrahydro-1,4-ethanonaphthalene-5,8-dione (40a).

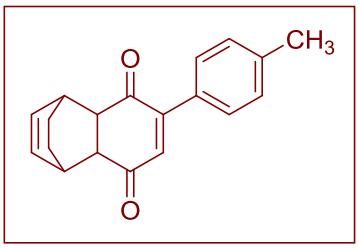

Starting from **28** (150 mg, 0.76 mmol), **40a** was isolated as a pale yellow solid (174 mg, 66%): mp 116 – 118 °C; FT-IR (ν_{max}, cm^{-1}): 2927, 2861, 1743, 1681, 1653, 1516, 1462, 1208, 1029; ^{1}H NMR (400 MHz, $CDCl_3$): δ 7.30 (d, *J* = 8.2 Hz, 2H), 7.20 (d, *J* = 8.0 Hz, 2H), 6.74 (s, 1H), 6.15 – 6.31 (m, 2H), 3.21 – 3.27 (m, 2H), 3.15 (dd, *J* = 2.5, 9.3 Hz, 1H), 3.06 (dd, *J* = 2.5, 9.3 Hz, 1H), 2.37 (s, 3H), 1.69 – 1.76 (m, 2H), 1.34 – 1. 69 (m, 2H); ^{13}C NMR (100 MHz, $CDCl_3$): δ 199.6, 198.9, 151.7, 140.6, 137.7, 133.8, 133.4, 130.5, 129.3, 128.8, 50.7, 50.2, 35.6, 35.5, 24.8, 21.5; Elemental analysis for $C_{19}H_{18}O_2$ calcd., C, 81.99; H, 6.52. Found, C 81.71; H, 6.42; HRMS (ESI) for $[C_{19}H_{18}O_2+Na]^+$: calcd., 301.1204; Found: 301.1194.

6-(4-Methoxyphenyl)-1,4,4a,8a-tetrahydro-1,4-ethanonaphthalene-5,8-dione (41a).

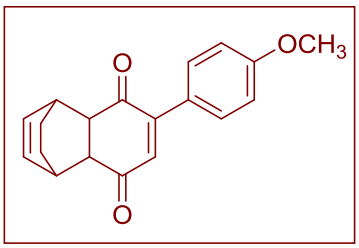

Starting from **29** (100 mg, 0.47 mmol), **41a** was isolated as an orange yellow solid (101 mg, 74%): mp 121 – 123 °C; FT-IR (ν_{max}, cm^{-1}): 2928, 2859, 1743, 1678, 1652, 1515, 1462, 1258, 1023; ^{1}H NMR (400 MHz, $CDCl_3$): δ 7.39 (d, *J*

= 8.7 Hz, 2H), 6.90 (d, *J* = 8.7 Hz, 2H), 6.72 (s, 1H), 6.18 – 6.33 (m, 2H), 3.82 (s, 3H), 3.23 (s, 2H), 3.13 (dd, *J* = 2.1, 9.3 Hz, 1H), 3.05 (dd, *J* = 2.1, 9.3 Hz, 1H), 1.72 (d, *J* = 6.9 Hz, 2H), 1.38 (d, *J* = 7.8 Hz, 2H); ^{13}C NMR (100 MHz, $CDCl_3$): δ 199.5, 199.2, 161.4, 151.0, 136.7, 133.8, 133.4, 130.5, 125.6, 114.1, 55.5, 50.8, 50.1, 35.5, 35.4, 24.9; Elemental analysis for $C_{19}H_{18}O_3$ calcd., C, 77.53; H, 6.16. Found, C, 77.64; H, 5.82; HRMS (ESI) for $[C_{19}H_{18}O_3+Na]^+$: calcd., 317.1153; Found: 317.1149.

6-(4-Bromophenyl)-1,4,4a,8a-tetrahydro-1,4-ethanonaphthalene-5,8-dione (42a).

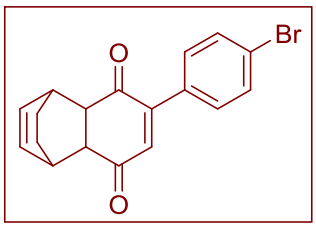

Starting from **30** (500 mg, 1.9 mmol), **42a**+**42b** was isolated as a pale yellow solid (531 mg, 81%): mp 132 – 134 °C; FT-IR (ν_{max}, cm^{-1}): 3531, 2920, 2873, 1741, 1651, 1460, 1339, 1201, 1073; ^{1}H NMR (400 MHz, $CDCl_3$): δ 7.50 – 7.54 (m, 2H), 7.24 – 7.27 (m, 2H), 6.69 – 6.77 (m, 1H), 6.19 – 6.28 (m, 2H), 3.23 (dd, *J* = 2.5, 5.0 Hz, 2H), 3.15 (d, *J* = 2.5 Hz, 1H), 3.13 (d, *J* = 2.5 Hz, 1H), 1.66 – 1.79 (m, 2H), 1.33 – 1.46 (m, 2H); ^{13}C NMR (100 MHz, $CDCl_3$): δ 199.3, 198.4, 150.5, 138.4, 133.9, 133.4, 132.3, 132.1, 131.8, 130.9, 130.5, 124.8, 50.6, 50.2, 35.6, 35.5, 24.8; Elemental analysis for $C_{18}H_{15}BrO_2$ calcd. C, 62.99; H, 4.41. Found, C, 63.21; H, 4.09; HRMS (ESI) for $[C_{18}H_{15}BrO_2+Na]^+$: calcd., 365.0152; Found: 365.0152.

6-(4-Chlorophenyl)-1,4,4a,8a-tetrahydro-1,4-ethanonaphthalene-5,8-dione (43a).

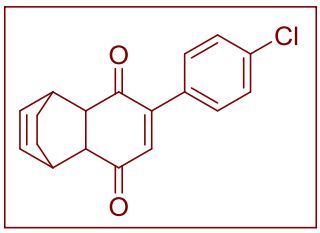

Starting from **31** (300 mg, 1.4 mmol), **43a**+**43b** was isolated as a yellow solid (391 mg, 95%): mp 149 – 151 °C; FT-IR (ν_{max}, cm^{-1}): 3581, 3422, 3055, 2952, 2869, 1742, 1653, 1467, 1259, 1040; ^{1}H NMR (400 MHz, DMSO-d_6): δ 7.41 – 7.45 (m, 4H), 6.82 (s, 1H), 6.12 – 6. 23 (m, 2H), 3.23 (dd, *J* = 2.4, 9.5 Hz, 1H), 3.01 – 3.13 (m, 3H), 1.67 (d, *J* = 8.2 Hz, 2H), 1.20 – 1.40 (m, 2H); ^{13}C NMR (100 MHz, DMSO-d_6): δ 199.2, 198.4, 150.4, 138.4, 133.9, 133.4, 130.6, 130.2, 129.4, 128.7, 113.3, 63.8, 50.6, 50.2, 35.6, 35.5, 25.0, 24.8 (a mixture of keto (62%) and enol (38%) tautomers); Elemental analysis for $C_{18}H_{15}ClO_2$ calcd., C, 72.36; H, 5.06. Found, C, 72.61; H, 4.58; HRMS (ESI) for $[C_{18}H_{15}ClO_2+Na]^+$: calcd., 321.0658; Found: 321.0656.

6-(4-Fluorophenyl)-1,4,4a,8a-tetrahydro-1,4-ethanonaphthalene-5,8-dione (44a).

Starting from **32** (300 mg, 1.48 mmol), **44a**+**44b** was isolated as a yellow semi-solid (277 mg, 66%): FT-IR (ν_{max}, cm^{-1}): 3567, 2961, 1742, 1695, 1652, 1513, 1462, 1220, 1157; ^1H NMR (400 MHz, $CDCl_3$): δ 7.36 – 7.41 (m, 2H), 7.03 – 7.12 (m, 2H), 6.72 (s, 1H), 6.24 (dd, *J* = 3.4, 4.3 Hz, 2H), 3.22 - 3.27 (m, 2H), 3.14 (dd, *J* = 2.5, 9.3 Hz, 1H), 3.06 (dd, *J* = 2.5, 9.3 Hz, 1H), 1.67 – 1.78 (m, 2H), 1.32 – 1.43 (m, 2H); ^{13}C NMR (100 MHz, $CDCl_3$): δ 199.3, 198.6, 165.2, 162.7, 150.4, 138.2, 133.9, 133.3, 131.0, 130.9, 115.8, 115.6, 113.5, 50.6, 50.2, 35.6, 35.5, 24.8; HRMS (ESI) for $[C_{18}H_{15}FO_2+Na]^+$: calcd., 305.0953; Found: 305.0957.

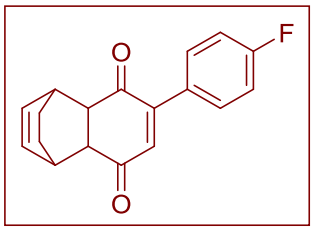

6-(4-Acetylphenyl)-1,4,4a,8a-tetrahydro-1,4-ethanonaphthalene-5,8-dione (45a).

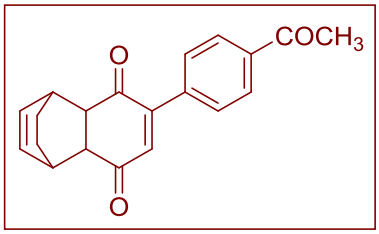

Starting from **33** (500 mg, 2.2 mmol), **45a**+**45b** was isolated as a yellow solid (566 mg, 84%): mp 127 – 128 °C; FT-IR (ν_{max}, cm^{-1}): 3563, 2980, 2862, 1742, 1659, 1519, 1461, 1354, 1170, 1044; ^1H NMR (400 MHz, $CDCl_3$): δ 7.95 (dd, *J* = 2.1, 8.4 Hz, 2H), 7.46 (dd, *J* = 1.8, 8.3 Hz, 2H), 6.76 (d, *J* = 2.2 Hz, 1H), 6.25 (dd, *J* = 2.5, 4.8 Hz, 2H), 3.04 – 3.30 (m, 4H), 2.59 (d, *J* = 2.2 Hz, 3H), 1.73 (d, *J* = 7.4 Hz, 2H), 1.38 (d, *J* = 8.1 Hz, 2H); ^{13}C NMR (100 MHz, $CDCl_3$): δ 199.3, 198.3, 197.6, 150.6, 144.4, 139.1, 134.0, 133.4, 129.2, 129.1, 128.4, 127.5, 50.6, 50.2, 35.7, 35.5, 26.8, 24.8; Elemental analysis for $C_{20}H_{18}O_3$ calcd. C, 78.41; H, 5.92. Found, C, 78.09; H, 5.57; HRMS (ESI) for $[C_{20}H_{18}O_3+Na]^+$: calcd., 329.1153; Found: 329.1154.

NMR data of enol tautomer, **6-(4-acetylphenyl)-1,4-dihydro-1,4-ethanonaphthalene-5,8-diol (45b)**:

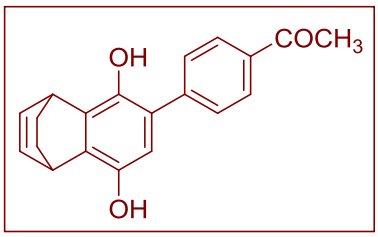

^1H NMR (400 MHz, DMSO-d_6): δ 8.73 (s, 1H), 7.99 (s, 1H), 7.91 (d, *J* = 8.3 Hz, 2H), 7.57 (d, *J* = 7.8 Hz, 2H), 6.42 – 6.49 (m, 3H), 4.39 (s, 1H), 4.26 (s, 1H), 2.54 (s, 3H), 1.40 (d, *J* = 8.1 Hz, 2H), 1.28 (d, *J* = 9.6 Hz, 2H);

^{13}C NMR (100 MHz, DMSO-d_6): δ 198.05, 145.1, 145.0, 140.9, 135.8, 135.6, 135.0, 134.2, 132.0, 129.9, 128.4, 126.1, 113.7, 33.7, 33.3, 27.2, 25.4, 25.3.

6-(4-Nitrophenyl)-1,4-dihydro-1,4-ethanonaphthalene-5,8-diol (46b).

Starting from **34** (100 mg, 0.41 mmol), **46b** was isolated as a pale yellow semi-solid (64 mg, 47%): FT-IR (ν_{max}, cm^{-1}): 3517, 3452, 2936, 2869, 1741, 1653, 1517, 1460, 1196, 1021; ^{1}H NMR (400 MHz, DMSO-d_6): δ 8.79 (s, 1H), 8.17 – 8.20 (m, 3H), 7.69 (d, J = 8.7 Hz, 2H), 6.49 (s, 1H), 6.44–6.46 (m, 2H), 4.40 (s, 1H), 4.26 (s, 1H), 1.40 (d, J = 7.6 Hz, 2H), 1.27 (d, J = 9.9 Hz, 2H); ^{13}C NMR (100 MHz, DMSO-d_6): δ 172.8, 166.1, 147.3, 146.1, 145.2, 140.9, 135.7, 135.6, 134.4, 132.9, 130.7, 125.0, 123.6, 113.6, 33.7, 33.4, 25.3, 25.1; HRMS (ESI) for $[C_{18}H_{15}NO_4+H]^+$: calcd., 310.1079; Found: 310.1078.

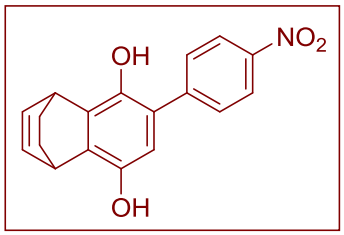

6-(4-Formylphenyl)-1,4-dihydro-1,4-ethanonaphthalene-5,8-diol (47b).

Starting from **35** (150 mg, 0.71 mmol), **47b** was isolated as a pale yellow solid (168 mg, 81%): mp 193 – 195 °C; FT-IR (ν_{max}, cm^{-1}): 3568, 2930, 2862, 1743, 1684, 1598, 1551, 1520, 1461, 1266, 1067, 1020; ^{1}H NMR (400 MHz, DMSO-d_6): δ 9.96 (s, 1H), 8.73 (s, 1H), 8.03 (s, 1H), 7.86 (d, J = 8.2 Hz, 2H), 7.65 (d, J = 8.1 Hz, 2H), 6.37 – 6.58 (m, 3H), 4.40 (s, 1H),4.26 (s, 1H), 1.40 (d, J = 7.9 Hz, 2H), 1.28 (d, J = 8.9 Hz, 2H); ^{13}C NMR (100 MHz, DMSO- d_6): δ 193.2, 146.6, 145.1, 140.9, 135.7, 135.6, 134.5, 134.3, 132.3, 130.3, 129.7, 126.0, 113.7, 33.7, 33.3, 25.4, 25.3; HRMS (ESI) for $[C_{19}H_{16}O_3+H]^+$: calcd., 293.1177; Found: 293.1173.

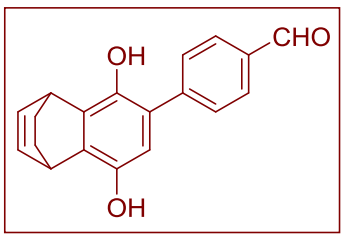

6-(3-Nitrophenyl)-1,4-dihydro-1,4-ethanonaphthalene-5,8-diol (48).

Starting from **36** (100 mg, 0.46 mmol), **48a**+**48b** was isolated as a yellow solid (96 mg, 67%): mp 163 – 165 °C; FT-IR (ν_{max}, cm^{-1}): 3615, 2928, 1741, 1688, 1517, 1421, 1339, 1272, 1154; ^{1}H NMR (400 MHz, DMSO-d_6) δ 8.78 (s, 1H), 8.27 – 8.32 (m, 1H), 8.17 (s, 1H), 8.07 (dd, J = 1.8, 8.1 Hz, 1H), 7.82 – 7.88 (m, 1H), 7.62 (t, J = 8.0 Hz, 1H), 6.46 (dd, J = 9.1, 12.9 Hz,

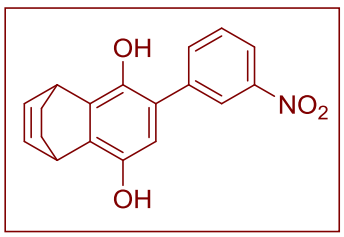

3H), 4.39 (s, 1H), 4.26 (s, 1H), 1.40 (d, *J* = 8.0 Hz, 2H), 1.22 – 1.31 (m, 2H); ^{13}C NMR (100 MHz, DMSO-d_6): δ 199.2, 198.4, 148.8, 148.0, 145.2, 141.6, 140.8, 139.2, 136.1, 135.9, 135.7, 135.6, 135.4, 134.3, 134.1, 132.4, 130.4, 130.0, 124.9, 124.7, 124.3, 124.2, 121.4, 113.5, 50.4, 50.1, 34.8, 33.7, 33.3, 25.4, 25.3, 24.7, 24.6 (a mixture of keto: enol (27: 73) tautomers); HRMS (ESI) for $[C_{18}H_{15}NO_4+Na]^+$: calcd., 332.0899; Found: 332.00898.

6-(3-Formylphenyl)-1,4-dihydro-1,4-ethanonaphthalene-5,8-diol (49b).

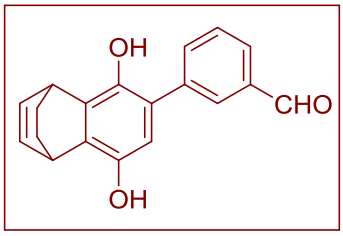

Starting from **37** (400 mg, 1.88 mmol), **49b** was isolated as a yellow solid (477 mg, 87%): mp 158 – 160 °C; FT-IR (ν_{max}, cm^{-1}): 3455, 3323, 2913, 2865, 1833, 1742, 1675, 1514, 1459, 1288, 1146, 1071; ^{1}H NMR (400 MHz, DMSO-d_6): δ 10.00 (s, 1H), 8.72 (s, 1H), 8.00 (s, 1H), 7.97 (s, 1H), 7.76 (dd, *J* = 1.4, 7.6 Hz, 2H), 7.56 (t, *J* = 7.6 Hz, 1H), 6.45 – 6.48 (m, 3H), 4.40 (s, 1H), 4.27 (s, 1H), 1.40 (d, *J* = 7.8 Hz, 2H), 1.29 (d, *J* = 9.4 Hz, 2H); ^{13}C NMR (100 MHz, DMSO-d_6): δ 193.9, 145.1, 141.0, 140.7, 136.5, 135.8, 135.7, 135.7, 134.2, 131.7, 130.8, 129.3, 127.8, 125.9, 113.7, 33.7, 33.3, 25.4, 25.3; Elemental analysis for $C_{19}H_{16}O_3$ calcd. C, 78.06; H, 5.52. Found C, 77.66; H, 5.31; HRMS (ESI) for $[C_{19}H_{16}O_3+H]^+$: calcd., 293.1177; Found: 293.1170.

6-(2-Methoxyphenyl)-1,4,4a,8a-tetrahydro-1,4-ethanonaphthalene-5,8-dione (50a).

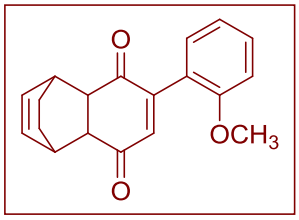

Starting from **38** (200 mg, 0.93 mmol), **50a** was isolated as an orange yellow solid (193 mg, 70%): mp 143 – 145 °C; FT-IR (ν_{max}, cm^{-1}): 2927, 2856, 1743, 1655, 1518, 1462, 1256, 1167, 1019; ^{1}H NMR (400 MHz, $CDCl_3$): δ 7.37 (ddd, *J* = 1.8, 7.3, 8.3 Hz, 1H), 7.08 (dd, *J* = 1.8, 7.4 Hz, 1H), 6.94 – 6.99 (m, 1H), 6.90 (d, *J* = 8.3 Hz, 1H), 6.65 (s, 1H), 6.16 – 6.39 (m, 2H), 3.76 (s, 3H), 3.13 – 3.26 (m, 3H), 3.07 (dd, *J* = 2.7, 9.2 Hz, 1H), 1.66 – 1.78 (m, 2H), 1.34 – 1. 46 (m, 2H); ^{13}C NMR (100 MHz, $CDCl_3$): δ 198.3, 196.8, 155.8, 151.5, 138.0, 133.1, 131.8, 130.2, 128.8, 122.9, 119.9, 110.2, 54.5, 49.4, 49.1, 34.1, 33.8, 24.1, 23.4; Elemental analysis for $C_{19}H_{18}O_3$ calcd. C, 77.53; H, 6.16. Found C, 77.19; H, 6.04; HRMS (ESI) for $[C_{19}H_{18}O_3+Na]^+$: calcd., 317.1153; Found: 317.1149.

2.2.4.2. General Procedure for the synthesis of 27 – 30:

To a 10 mL round bottom flask compound (0.2 mmol) was dissolved in tetrahydrofuran (THF, 5 mL) and potassium carbonate (0.5 mmol, 2.5 equiv) was added to the above solution. The reaction flask was stirred at room temperature overnight. Consumption of the starting material was confirmed by TLC analysis. The reaction mixture was washed with 5 mL of de-ionized water and extracted with ethyl acetate (4 × 5 mL). The combined organic layer was dried (anhydrous Na_2SO_4, 5 g), filtered and the filtrate was evaporated under reduced pressure to obtain crude product. The crude mixture was purified by a short silica gel column by washing with ethyl acetate: petroleum ether (3:4 ratio, v/v). The organic solvent was evaporated under reduced pressure to obtain pure material.

6-Phenyl-1,4-dihydro-1,4-ethanonaphthalene-5,8-dione (51).

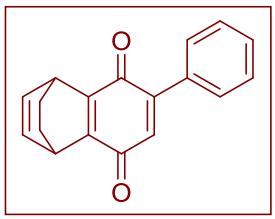

Starting from **39** (50 mg, 0.19 mmol), **51** was isolated as a yellow semi-solid (41 mg, 83%): FT-IR (ν_{max}, cm^{-1}): 2928, 2817, 1648, 1585, 1488, 1337, 1011; ^1H NMR (400 MHz, $CDCl_3$): δ 7.33 – 7.48 (m, 5H), 6.68 (s, 1H), 6.33 – 6.50 (m, 2H), 4.39 (dd, *J* = 1.7, 18.5 Hz, 2H), 1.50 (dd, *J* = 4.8, 6.0 Hz, 2H), 1.35 – 1.44 (m, 2H); ^{13}C NMR (100 MHz, $CDCl_3$): δ 183.7, 182.8, 148.6, 148.5, 144.4, 134.0, 133.2, 132.8, 132.1, 131.7, 130.9, 124.5, 34.2, 33.8, 24.8, 24.7; HRMS (ESI) for $[C_{18}H_{14}O_2+H]^+$: calcd., 263.1072; Found: 263.1063.

6-(4-Methoxyphenyl)-1,4-dihydro-1,4-ethanonaphthalene-5,8-dione (52).

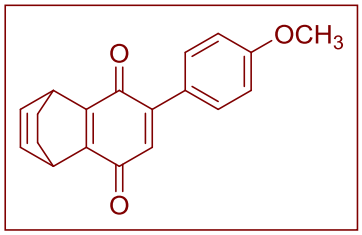

Starting from **41** (50 mg, 0.17 mmol), **52** was isolated as an orange semi-solid (19 mg, 38%): FT-IR (ν_{max}, cm^{-1}): 2924, 1649, 1563, 1511, 1460, 1340, 1240, 1181, 1028; ^1H NMR (400 MHz, $CDCl_3$): δ 7.32 – 7.54 (m, 2H), 6.84 – 7.02 (m, 2H), 6.64 (s, 1H), 6.31 – 6.50 (m, 2H), 4.27 – 4.47 (m, 2H), 3.83 (s, 3H), 1.42 – 1.53 (m, 2H), 1.31– 1.41 (m, 2H); ^{13}C NMR (100 MHz, $CDCl_3$): δ 184.1, 183.6, 161.1, 148.5, 148.3, 144.8, 134.0, 133.9, 131.0, 130.6, 125.7, 114.0, 55.4, 34.2, 33.7, 24.8, 24.7.; HRMS (ESI) for $[C_{19}H_{16}O_3+H]^+$: calcd., 293.1177; Found: 293.1174.

6-(4-Acetylphenyl)-1,4-dihydro-1,4-ethanonaphthalene-5,8-dione (53).

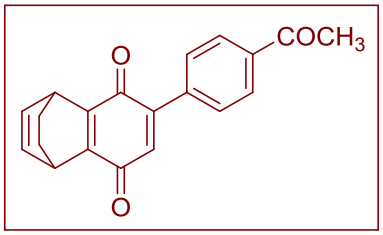

Starting from **45a+45b** (50 mg, 0.16 mmol), **53** was isolated as a yellow semi-solid (31 mg, 62%): FT-IR (ν_{max}, cm^{-1}): 2929, 2872, 1682, 1650, 1602, 1460, 1359, 1268, 1142, 1041; ^{1}H NMR (400 MHz, $CDCl_3$): δ 7.91 – 7.99 (m, 2H), 7.51 – 7.56 (m, 2H), 6.72 (s, 1H), 6.40 – 6.44 (m, 2H), 4.35 – 4.43 (m, 2H), 2.61 (s, 3H), 1.49 – 1.54 (m, 2H), 1.37 – 1.41 (m, 2H); ^{13}C NMR (100 MHz, $CDCl_3$): δ 197.7, 183.6, 182.6, 148.6, 144.5, 137.8, 137.6, 134.0, 133.8, 132.9, 129.7, 128.5, 128.4, 128.3, 34.2, 33.8, 26.8, 24.8, 24.7; HRMS (ESI) for $[C_{20}H_{16}O_3+H]^+$: calcd., 305.1177; Found: 305.1172.

2.2.4.3. ^{1}H NMR experiment for studying enolization potential. A stock solution of sodium deuteroxide (NaOD) in DMSO-*d*$_6$ was prepared by mixing 10 μL of 30 wt. % NaOD in D_2O with 490 μL of DMSO-*d*$_6$. ^{1}H NMR spectrum was recorded for **39** (10 mg) in DMSO–*d*$_6$ (0.6 mL) at 25 °C. To the solution of **39** in DMSO-*d*$_6$ (0.6 mL) 0.2 equiv of NaOD (10 μL from the above mentioned stock solution) was added at room temperature (25 °C) and after 15 min ^{1}H NMR spectra was recorded on a 400MHz NMR spectrometer. By following similar experimental conditions the ^{1}H NMR experiments for **41**, **42**, **45** and **47** were carried out.

2.2.4.4. Stability studies using HPLC. A stock solution of compound (10 mM) was diluted to 1 mM in pH 7.4 phosphate buffer (100 mM): acetonitrile ACN (1:1 ratio, v/v) and incubated at 37 ºC over a period of 2-8 h. The reaction mixture was filtered (0.22 μm) and injected (25 μL) in a high performance liquid chromatograph (HPLC) attached with a diode-array detector (detection wavelength was 254 nm) and a Zorbax SB C-18 reversed phase column (250 mm × 4.6 mm, 5 μm). A mobile phase of water: acetonitrile was used with a run time of 25 min: multistep gradient technology with a flow rate of 1 mL/min – starting with 50:50 % → 0 – 5 min, 40:60 → 5 – 10 min, 30:70 → 10 – 15 min, 20:80 → 15 – 20 min, 50:50 → 20 – 23 min, 50:50 → 23 – 25 min.

2.2.4.5. Superoxide detection by luminol assay: 5-Amino-2,3-dihydro-1,4-phthalazinedione solution (Luminol, 4 mM) was prepared in 30 mM aqueous sodium hydroxide and stored under ice. To a microwell plate, a stock solution of the compound (2 μL of 1 mM) was added to phosphate buffer (100 mM pH 8.0, 193 μL) followed by luminol (5 μL, final 100 μM in 200 μL) in 6 repeats. The resulting mixture was incubated at 37 ºC for 25 min and chemiluminescence was measured using a microtiter plate reader.

2.2.4.6. Estimation of hydrogen peroxide. A solution of the test compound (1 μL, 1 mM, 10 μM final concentration) was added to 25 mM phosphate buffer of pH 7.4 (45 μL) and incubated at 37 ºC for 60 min. To the incubated reaction mixture, 50 μL of a premixed solution of 10-acetyl-3,7- dihydroxyphenoxazine or Amplex Red® (prepared by following manufacturer's protocol from Invitrogen) was added and incubated at RT for 25 min before measuring the fluorescence using a microtiter plate reader (excitation 550 nm; emission 590 nm).

2.2.5 – Spectral Charts:

^{1}H NMR Spectrum (400 MHz, $CDCl_3$) of Compound **40**

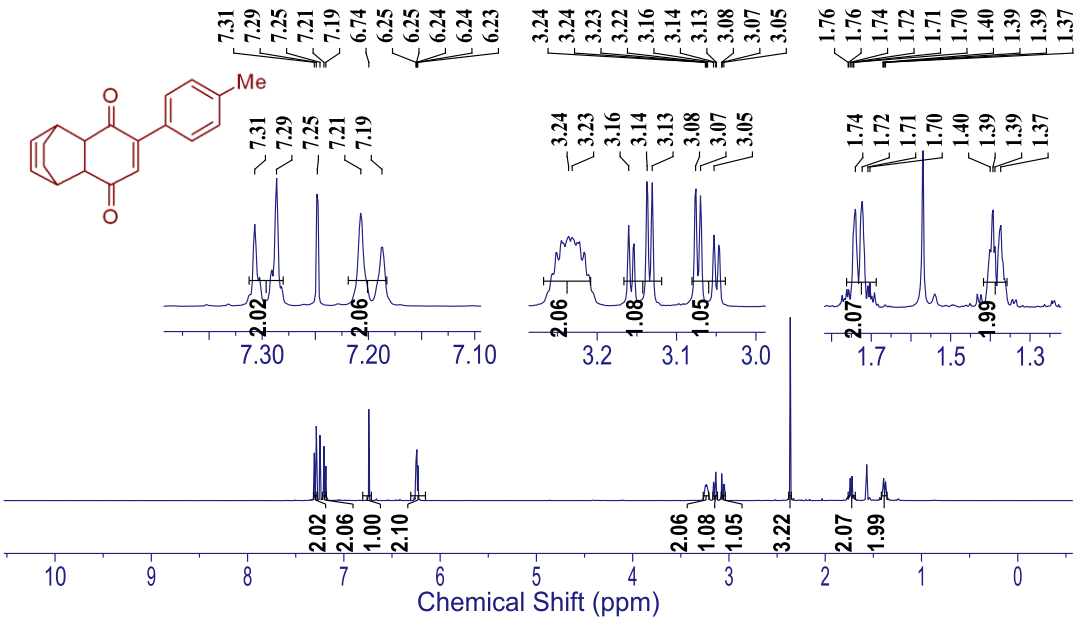

^{13}C NMR Spectrum (100 MHz, $CDCl_3$) of Compound **40**

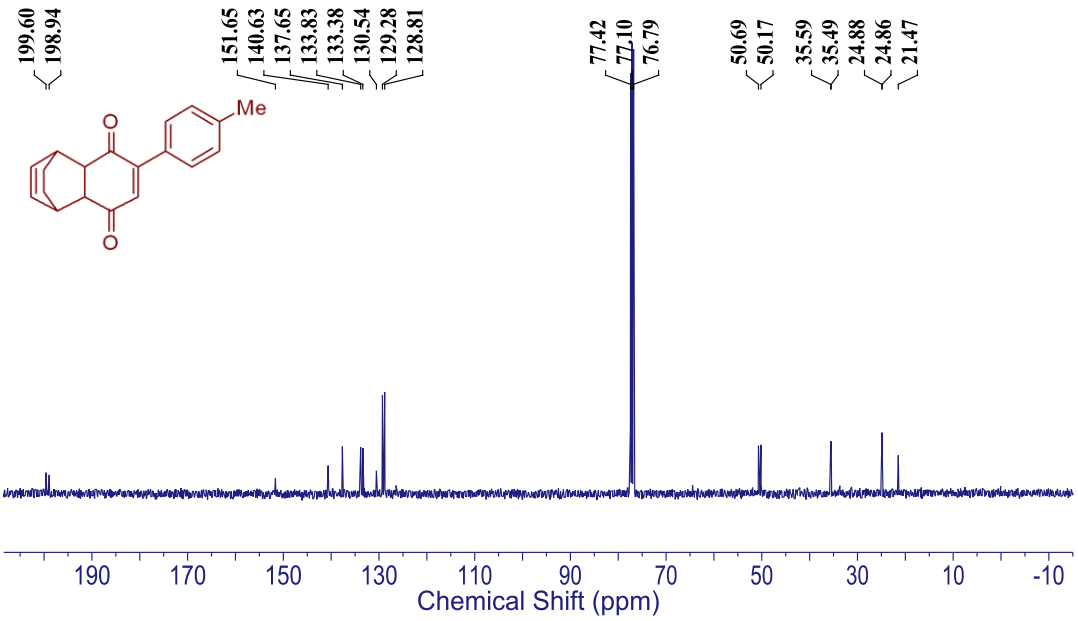

^{1}H NMR Spectrum (400 MHz, $CDCl_3$) of Compound **41**

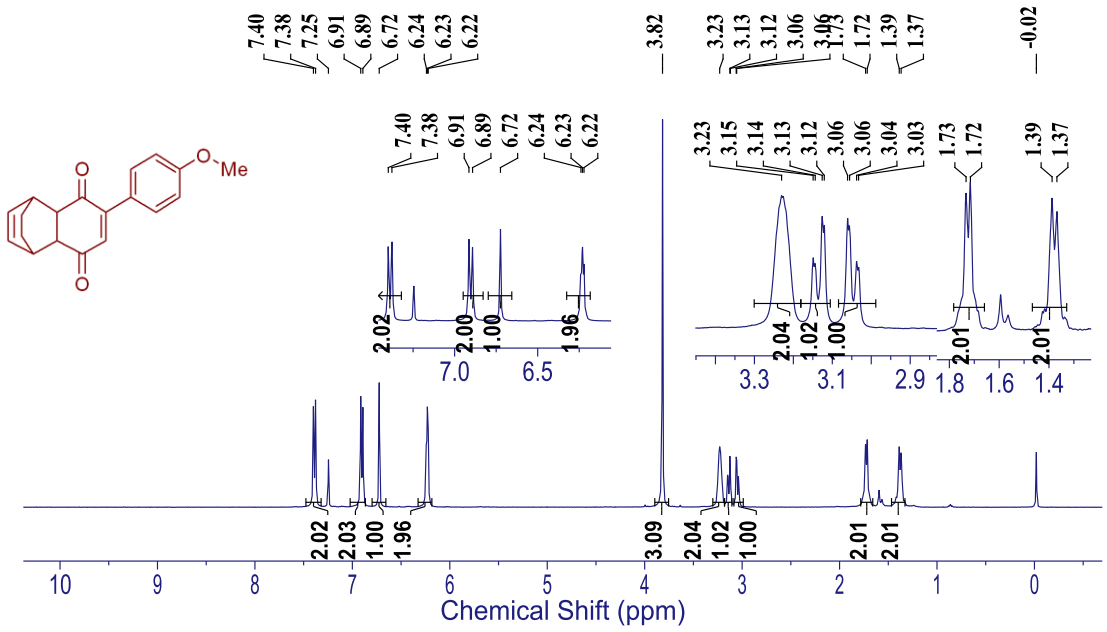

^{13}C NMR Spectrum (100 MHz, $CDCl_3$) of Compound **41**

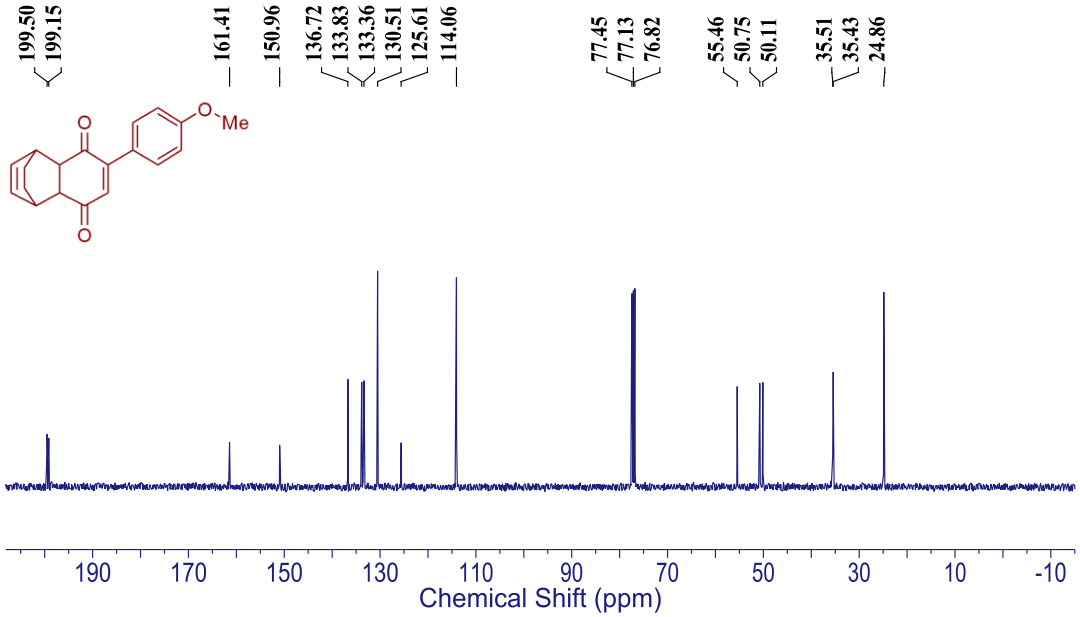

^{1}H NMR Spectrum (400 MHz, $CDCl_3$) of Compound **42**

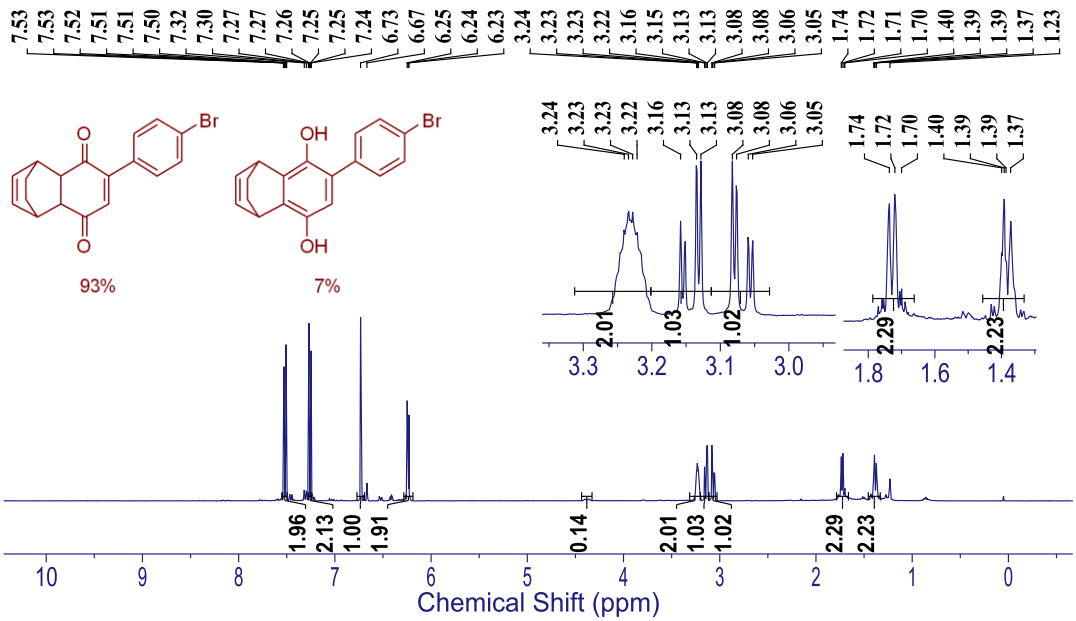

^{13}C NMR Spectrum (100 MHz, $CDCl_3$) of Compound **42**

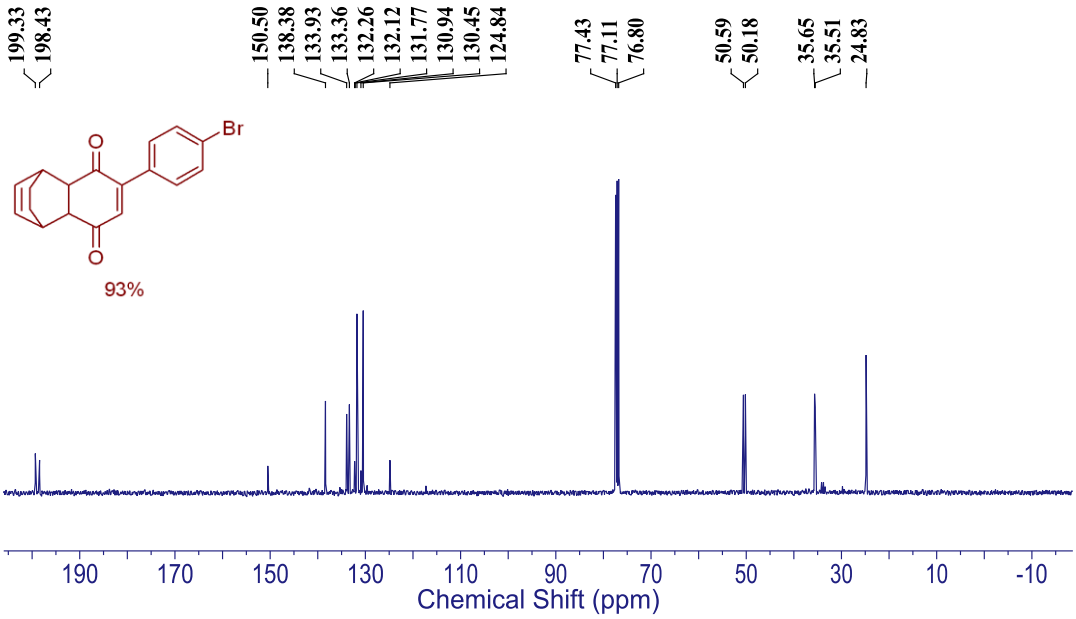

^{1}H NMR Spectrum (400 MHz, DMSO-d_6) of Compound **43**

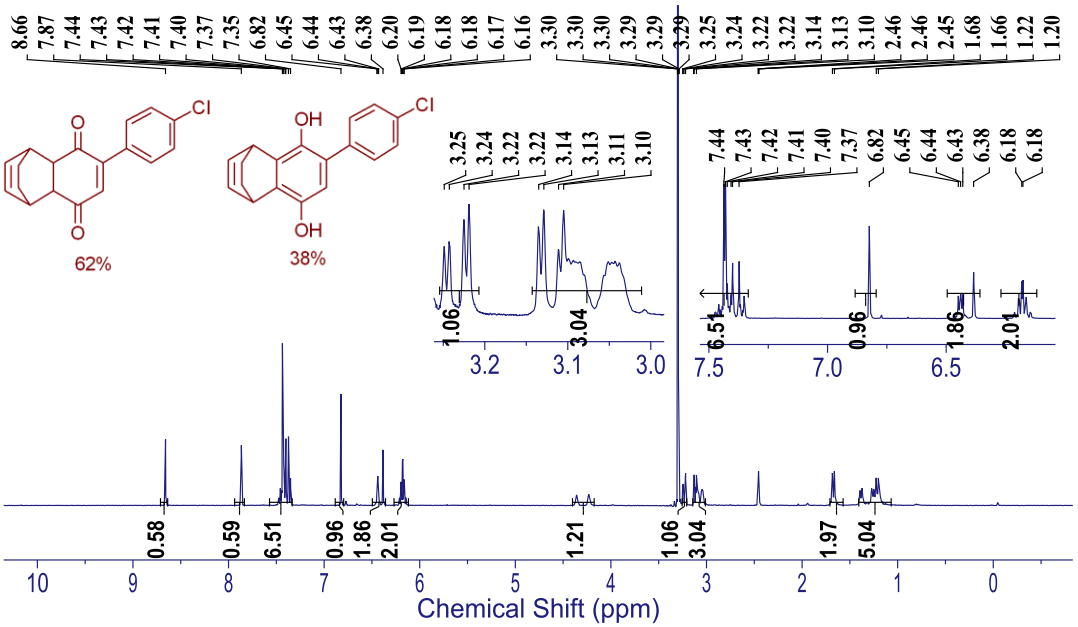

^{13}C NMR Spectrum (100 MHz, $CDCl_3$) of Compound **43**

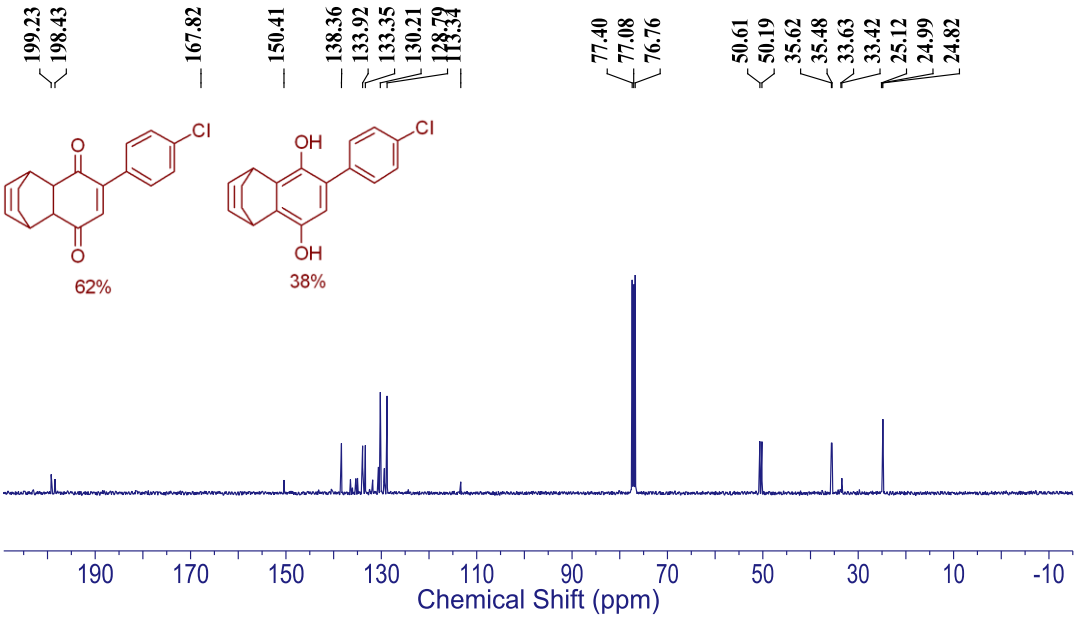

^{1}H NMR Spectrum (400 MHz, $CDCl_3$) of Compound **45**

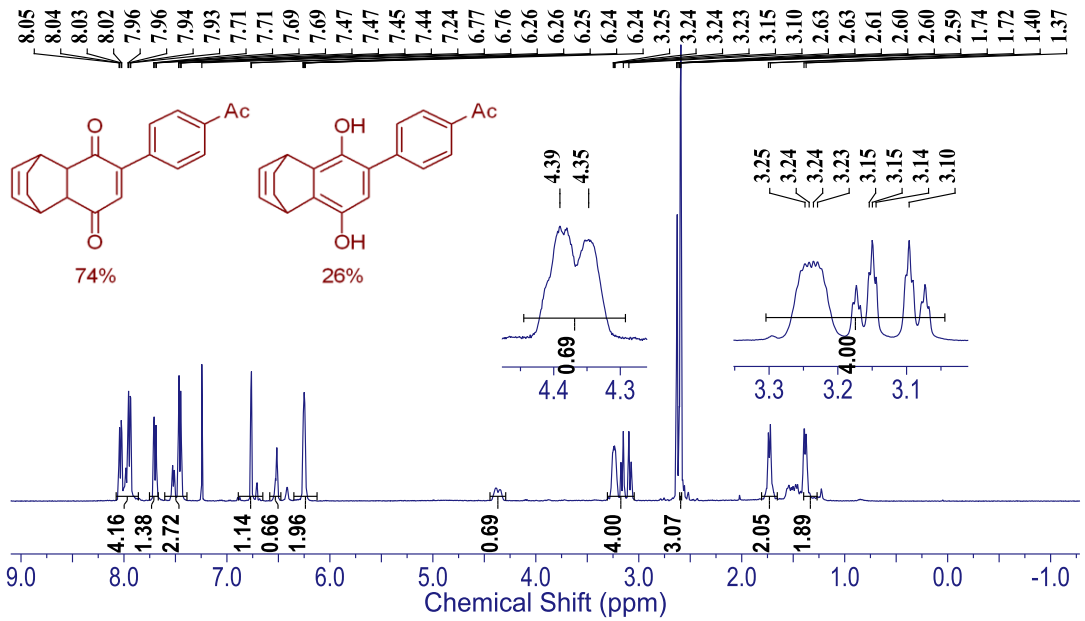

^{13}C NMR Spectrum (100 MHz, $CDCl_3$) of Compound **45**

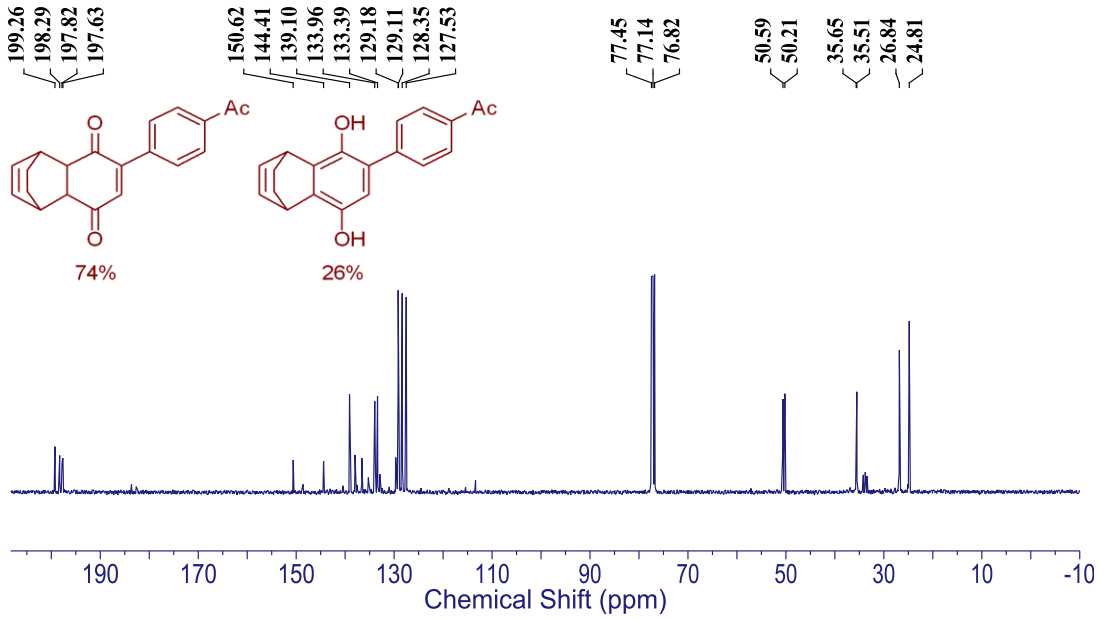

^{1}H NMR Spectrum (400 MHz, DMSO-d_6) of Compound **47**

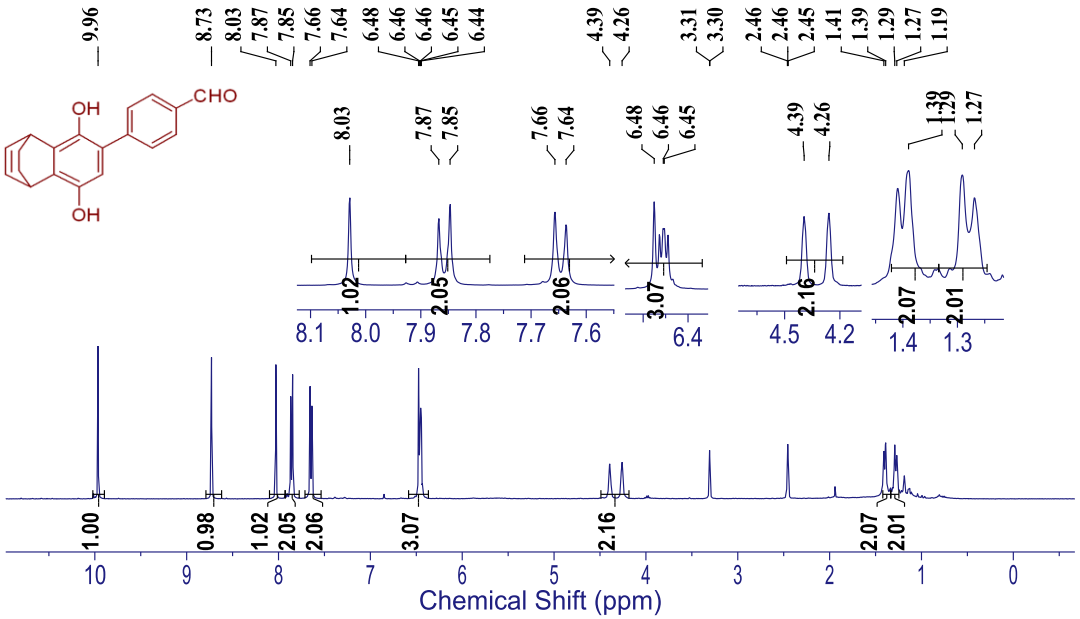

^{13}C NMR Spectrum (100 MHz, DMSO-d_6) of Compound **47**

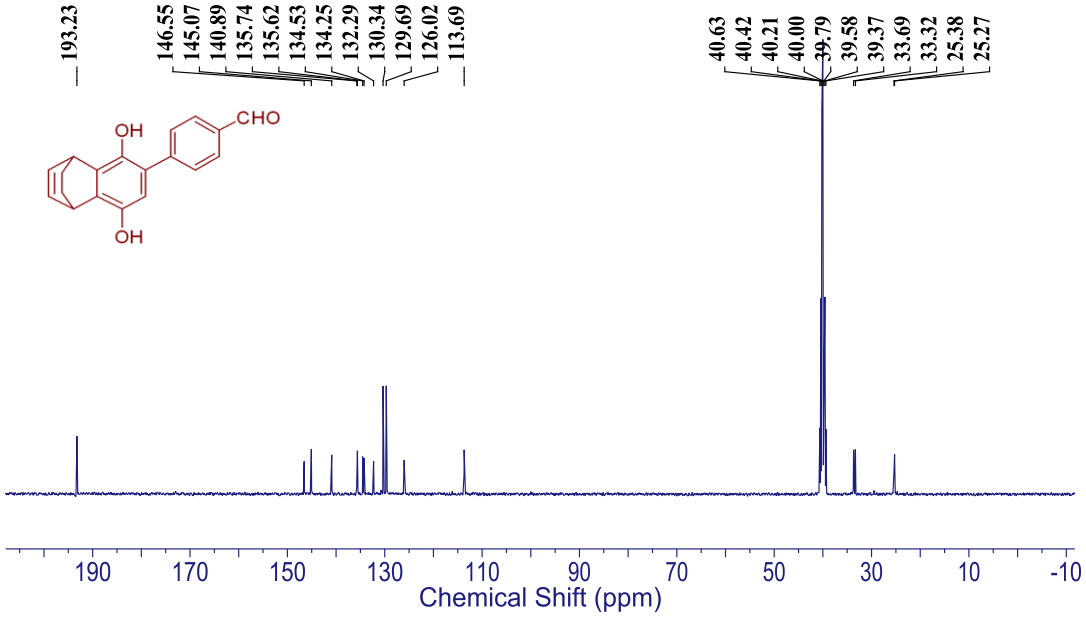

2.2.6. References:

1. Dharmaraja, A. T.; Alvala, M.; Sriram, D.; Yogeeswari, P.; Chakrapani, H. Design, synthesis and evaluation of small molecule reactive oxygen species generators as selective Mycobacterium tuberculosis inhibitors. *Chem. Commun.* **2012,** 48, 10325-10327.
2. Fujiwara, Y.; Domingo, V.; Seiple, I. B.; Gianatassio, R.; Del Bel, M.; Baran, P. S. Practical C-H Functionalization of Quinones with Boronic Acids. *J. Am. Chem. Soc.* **2011,** 133, 3292-3295.
3. Exner, O. *Correlation Analysis in Chemistry*. N.B Chapman and J. Shorter, Eds: 1978; Vol. Ch. 10.
4. Hansch, C.; Leo, A.; Taft, R. W. A survey of Hammett substituent constants and resonance and field parameters. *Chem. Rev.* **1991,** 91, 165-195.
5. Sardella, D. J.; Heinert, D. H.; Shapiro, B. L. Nuclear magnetic resonance studies of enol-enol and keto-enol equilibria in substituted benzoylacetones. *J. Org. Chem.* **1969,** 34, 2817-2821.
6. Campbell, R. D.; Harmer, W. L. B-Diketones. IV. Synthesis of Monosubstituted Benzoylcyclopentanones1. *J. Org. Chem.* **1963,** 28, 379-383.
7. Campbell, R. D.; Gilow, H. M. B-Diketones. II. Ultraviolet and Infrared Spectra of Some 2-Aroylcyclohexanones1,2. *J. Am. Chem. Soc.* **1960,** 82, 5426-5431.
8. Trung Pham, H.; Marquetty, C.; Pasquier, C.; Hakim, J. Luminol assay for microdetermination of superoxide dismutase activity: Its application to human fetal blood. *Anal. Biochem.* **1984,** 142, 467-472.
9. Zhou, M.; Diwu, Z.; Panchuk-Voloshina, N.; Haugland, R. P. A Stable Nonfluorescent Derivative of Resorufin for the Fluorometric Determination of Trace Hydrogen Peroxide: Applications in Detecting the Activity of Phagocyte NADPH Oxidase and Other Oxidases. *Anal. Biochem.,* **1997,** 253, 162-168.
10. Avshalumov, M. V.; Chen, B. T.; Rice, M. E. Mechanisms underlying H2O2-mediated inhibition of synaptic transmission in rat hippocampal slices. *Brain Res.* **2000,** 882, 86-94.
11. Marat V. Avshalumov , M. E. R. NMDA Receptor Activation Mediates Hydrogen Peroxide-Induced Pathophysiology in Rat Hippocampal Slices. *J. Neurophysiol.* **2002,** 87, 2896-2903.

12. Pellmar, T. C.; Hollinden, G. E.; Sarvey, J. M. Free radicals accelerate the decay of long-term potentiation in field CA1 of guinea-pig hippocampus. *Neuroscience* **1991,** 44, 353-359.
13. Kalghatgi, S.; Spina, C. S.; Costello, J. C.; Liesa, M.; Morones-Ramirez, J. R.; Slomovic, S.; Molina, A.; Shirihai, O. S.; Collins, J. J. Bactericidal Antibiotics Induce Mitochondrial Dysfunction and Oxidative Damage in Mammalian Cells. *Sci. Transl Med.* **2013,** 5, 192ra85.
14. Koubek, E.; Haggett, M. L.; Battaglia, C. J.; Ibne-Rasa, K. M.; Pyun, H. Y.; Edwards, J. O. Kinetics and Mechanism of the Spontaneous Decompositions of Some Peroxoacids, Hydrogen Peroxide and t-Butyl Hydroperoxide. *J. Am. Chem. Soc.* **1963,** 85, 2263-2268.
15. Bellomo, G.; Jewell, S. A.; Thor, H.; Orrenius, S. Regulation of intracellular calcium compartmentation: studies with isolated hepatocytes and t-butyl hydroperoxide. *Proc. Natl. Acad. Sci. USA* **1982,** 79, 6842-6846.
16. Latour, I.; Demoulin, J. B.; Buc-Calderon, P. Oxidative DNA damage by t-butyl hydroperoxide causes DNA single strand breaks which is not linked to cell lysis. A mechanistic study in freshly isolated rat hepatocytes. *FEBS Lett.* **1995,** 373, 299-302.
17. Eastgate, M. D.; Buono, F. G. Mechanistic insight into the palladium-catalyzed 1,4-oxidation of 1,3-dienes to 1,4-dicarboxy-alk-2-enes. *Angew. Chem. Int. Ed.* **2009,** 48, 5958-5961.
18. Porter, R. F.; Rees, W. W.; Frauenglass, E.; Wilgus, H. S.; Nawn, G. H.; Chiesa, P. P.; Gates, J. W. The Chemistry of Thioether-Substituted Hydroquinones and Quinones. I. The 1,4-Addition of a Heterocyclic Mercaptan to Quinones. *J. Org. Chem.* **1964,** 29, 588-594.
19. Deb, A.; Manna, S.; Maji, A.; Dutta, U.; Maiti, D. Iron-Catalyzed Direct C–H Arylation of Heterocycles and Quinones with Arylboronic Acids. *Eur. J. Org. Chem.* **2013,** 2013, 5251-5256.

CHAPTER 3: SMALL MOLECULE BASED ENZYME ACTIVATED REACTIVE OXYGEN SPECIES GENERATOR IN BACTERIA

3.1 Introduction:

In Chapter 2.1, we have identified a new small molecule scaffold for ROS generation in buffer as well as in cells. 2,3-dihydro-1,4-naphthoquines undergo a keto-enol tautomerism in buffer to form a 1,4-diol, which upon exposure to aerobic atmosphere reacts with molecular O_2 to generate ROS such as $O_2^{\bullet-}$ and hydrogen peroxide, H_2O_2. From the library of compounds evaluated, **4** was identified as an efficient ROS generator in extracellular as well as intracellular media. Although compound **4** could enhance the level of intracellular ROS in *E. coli* an extracellular decomposition of **4** to generate ROS is inevitable (Figure 3.1).

Figure 3.1. Graphical representation of ROS generation from **4** in extracellular as well as intracellular media

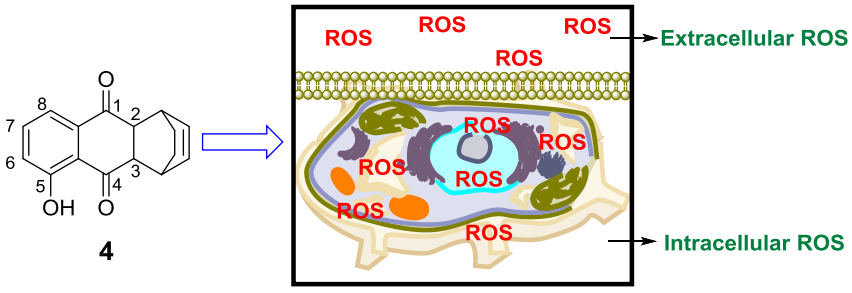

Due to its poor cell permeability and short life, $O_2^{\bullet-}$ must be produced *in situ* by reaction with oxygen for use in biochemical studies.[1] Hence, either small organic molecules that spontaneously generate $O_2^{\bullet-}$ or enzymatic methods that turnover a substrate to generate $O_2^{\bullet-}$ are frequently used. A combination of hypoxanthine and xanthine oxidase (X + XO), where hypoxanthine is metabolized by XO to produce $O_2^{\bullet-}$, is often used for biochemical studies and predominantly produces $O_2^{\bullet-}$ in the proximity of cells.[2] Any $O_2^{\bullet-}$ that is produced must diffuse across a lipid bilayer to exert its effects.[3] However, several studies indicate that $O_2^{\bullet-}$ is not highly permeable at neutral pH and hence, this method may not be useful for enhanced intracellular ROS generation.[4] The aromatic quaternary amine, paraquat[5] or menadione,[6] which require bioactivation for $O_2^{\bullet-}$ production, have often been used in biological studies but at elevated concentrations that

can potentially complicate mechanistic interpretations (Figure 3.2).[5,7] Although the azo compound, SOTS-1, generates $O_2^{\bullet-}$ in a temporally controlled manner after dissolution in buffer,[8,9] its selectivity for intracellular ROS production is not predicted (Figure 3.2). Thus, a cell permeable small molecule that can predictably increase intracellular $O_2^{\bullet-}$ is not available. Such a tool could be useful to study the vulnerability of *E. coli* to enhanced intracellular ROS. In this chapter, we design and synthesize a small molecule that is activated by a bacterial enzyme to generate ROS and is well suited to simulate enhanced ROS in bacteria.

Figure 3.2. Structures of organic small molecules based ROS generators

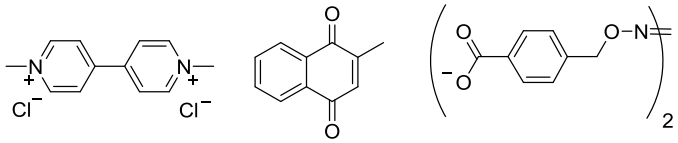

3.2. Results and Discussion:

3.2.1. Synthesis and Characterization:

From our previous studies, **4** was identified to generate $O_2^{\bullet-}$ in ambient aerobic buffer through a keto-enol tautomerism as the first step (Scheme 3.1).[10] Enolization of the carbonyls in **4** is promoted by a proximal H-bonding of the 5-OH and 4-C=O group. As a consequence, ROS generation by this compound was enhanced in comparison with an analogous benzylated derivative **8**, which was a poor generator of $O_2^{\bullet-}$ under similar conditions (Figure 3.3).[10]

Figure 3.3. Pro-ROS generator design: A generic design of enzyme triggered intracellular ROS generator derived from **4** and **8** based on hydrogen bonding for enolization and ROS generation.

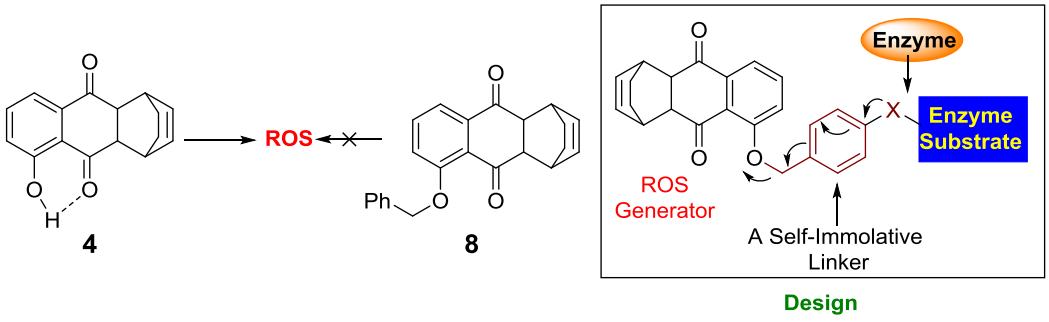

Thus, protection of 5-OH group in **4** with a self-immolative linker attached with a substrate for an enzyme that is expressed intracellularly was designed for selective enhancement of intrabacterial ROS (Figure 3.3).

Scheme 3.1. A scheme for activation of **54**, a cell permeable ROS generator: the 4-nitrobenzyl derivative **54** is a substrate for nitro reduction, which would convert **54** to the active ROS producing **4**. When this transformation is catalyzed by a bacterial enzyme *E. coli* nitroreductase (NTR), exclusive intracellular accumulation of ROS is predicted in bacteria.

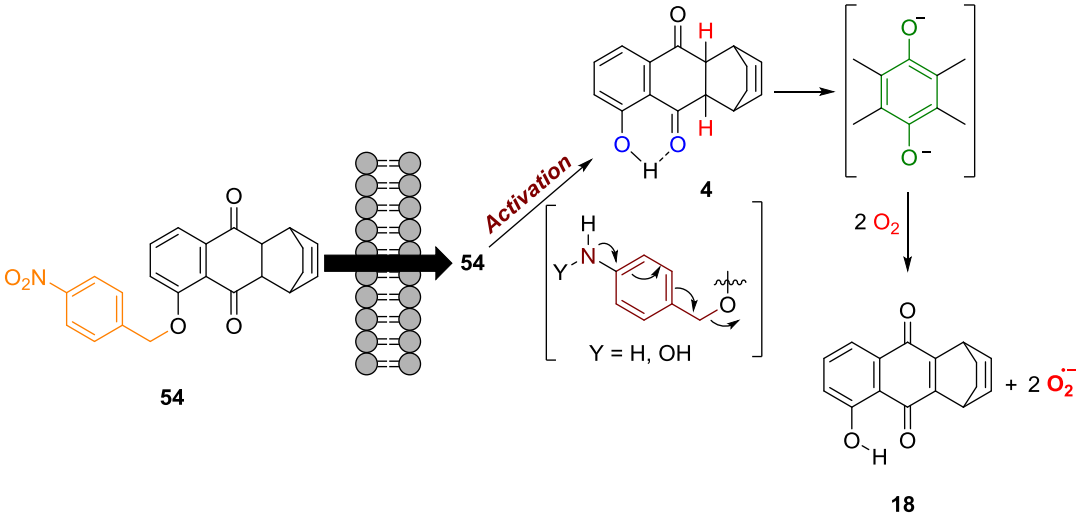

Scheme 3. 2. Synthesis of **54** from a reaction of **4** with 4-nitrobenzyl bromide

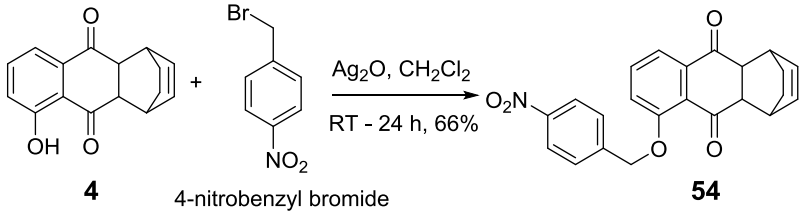

5-(4-Nitrobenzyloxy)-1,4,4a,9a-tetrahydro-1,4-ethanoanthracene-9,10-dione (**54**) was considered as a cell-permeable $O_2^{\bullet-}$ generator (Scheme 3.1). The 4-nitrobenzyl group is a known substrate for *E. coli* nitroreductase (NTR),[11] a commonly expressed oxygen-insensitive[12] bacterial enzyme, that reduces a broad range of aromatic nitro compounds to amines using nicotinamide adenine dinucleotide phosphate (NADPH) as a reducing co-factor.[13] Reduction of the nitro group might lead to a rearrangement leading to the departure of the active ROS generator **4**. Similarly in the case of **54**, where intramolecular

H-bonding is not possible, enolization is disfavoured and this compound is predicted to be a poor $O_2^{\bullet-}$ generator in buffer (Scheme 3.1). Compound **54** was synthesized from **4** by reaction with 4-nitrobenzylbromide in 66% yield (Scheme 3.2).

3.2.2. Chemoreductive activation of 54 and ROS generation studies in buffer:

Initially, suitability of the substrate **54** for reductive activation and release of **4** was examined by chemoreduction. Here, **54** was reduced by treatment with a reducing mixture Zinc and ammonium formate in 1:1 methanol and buffer medium (Scheme 3.3).[14] A complete conversion of **54** to **4** was observed after 60 min as followed by HPLC analysis.

Scheme 3.3. Chemoreduction of **54** using Zinc and ammonium formate for 60 min at 37 °C in pH 7.4 phosphate buffer and methanol (1:1, v/v)

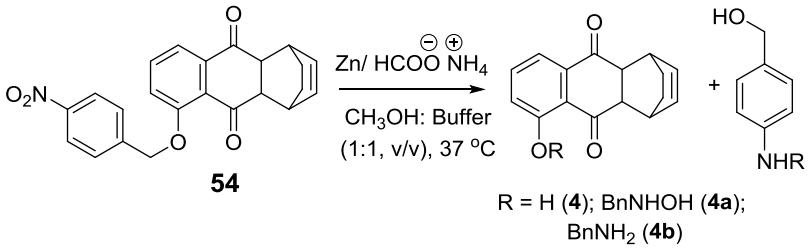

Figure 3.4. HPLC analysis of chemoreduction of **54**: HPLC traces of **54**, **4** and a reaction mixture of **54** (1 mM) with Zn/ ammonium formate in MeOH: phosphate buffer (1:1, v/v) after 1 h.

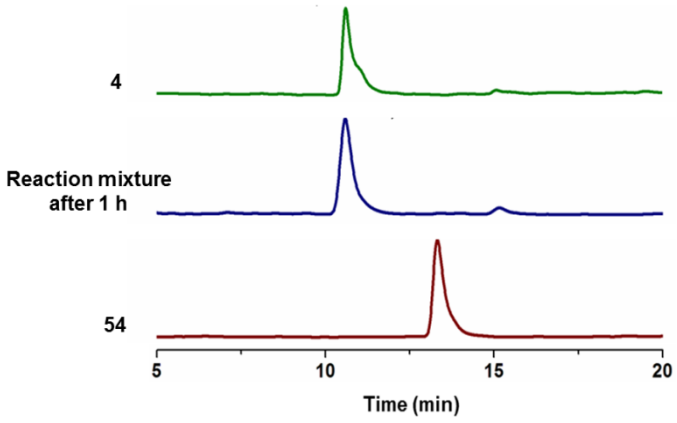

Under the HPLC experimental conditions we did not observe any peak for intermediate formation, however mass spectral analysis of the reaction mixture revealed the formation of 4-hydroxylamine (**4a**) and 4-aminobenzyl (**4b**) intermediates along with **4** (Figure 3.5)

This study suggests that the compound **54** is capable of undergoing reduction and decomposes to release the active ROS generator **4**, which is consistent with a reduction-rearrangement cascade (Figure 3.3).[13]

Figure 3.5. Mass spectra: Chemoreduction of **54** using Zn/ammonium formate in MeOH: pH 7.4 phosphate buffer (1 mL, 1:1 v/v) after 1 h.

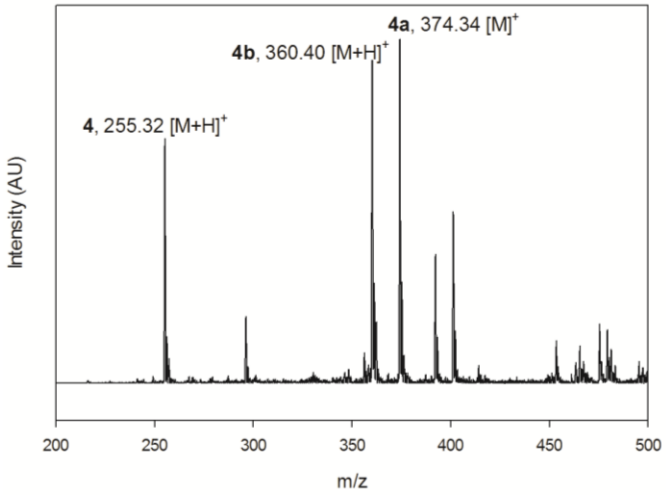

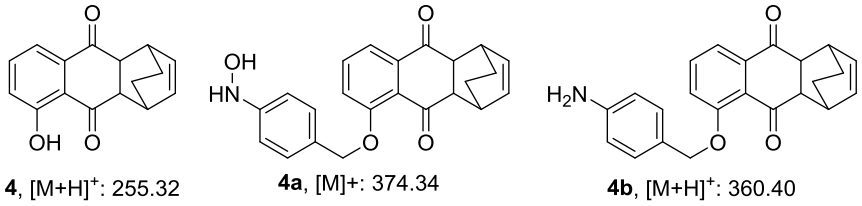

4, $[M+H]^+$: 255.32 **4a**, [M]+: 374.34 **4b**, $[M+H]^+$: 360.40

Next, luminol-based chemiluminescence assay was performed to determine $O_2^{\bullet-}$ generation from **54** in ambient aerobic buffer. When compound **54** alone was treated with luminol in buffer no chemiluminescence was observed. However, upon addition of NTR (a stock of NTR and NADPH (3 μL of 1 mM solution in buffer)) to **54** indicated an enhanced $O_2^{\bullet-}$ level suggesting that this compound is activated only in the presence of NTR to generate $O_2^{\bullet-}$ (Figures 3.6A & 3.6B).[15] An efficient $O_2^{\bullet-}$ generation was observed from **4** and addition of NTR to **4** did not have any effect on the $O_2^{\bullet-}$ generation profile implying NTR does not interfere with compound's ROS generation potential (Figures 3.6A & 3.6B). Under similar conditions, **8** (a benzyl-protected derivative of **4**) produced a

minimal level of $O_2^{\bullet-}$ reiterating the importance of nitro-group to trigger the release of **4** and subsequent $O_2^{\bullet-}$ generation. (Figures 3.6A & 3.6B).

Scheme 3.4. Decomposition products of **55**, a NTR enzyme substrate during a reaction with NTR

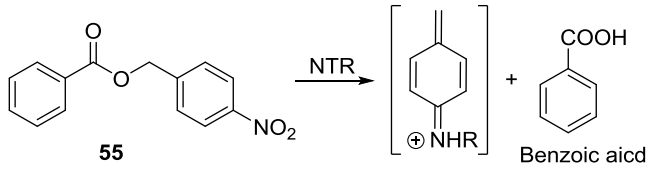

Figure 3.6. Estimation of $O_2^{\bullet-}$ in ambient aerobic aqueous buffer. (A) Chemiluminescence measurement upon reaction with luminol as a measure of $O_2^{\bullet-}$ production was carried out with various compounds (10 μM) and combinations in pH 8.0 buffer. (B) Results of the above assay conducted after 30 min. + NTR implies *E. coli* nitroreductase and NADPH; X + XO: hypoxanthine and xanthine oxidase were used; 10 equiv of **55** (1 mM) was wherever applicable.

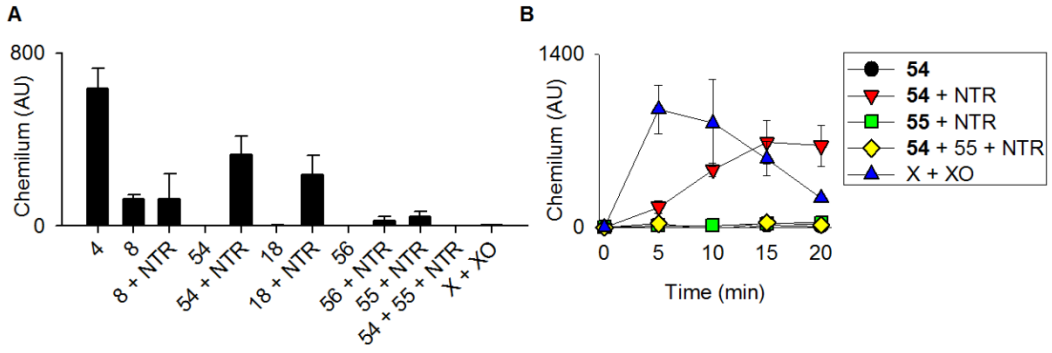

4-Nitrobenzyl benzoate **55**, which is a substrate for NTR, which should not produce ROS during its metabolism by this enzyme, was synthesized using a reported procedure.[16] Compound **55** (100 μM) was metabolized by NTR and as predicted no evidence for $O_2^{\bullet-}$ was found (Figure 3.6A & 3.6B) indicating that possible products of metabolism of the 4-nitrobenzyl group were incapable of generating ROS (Scheme 3.4).[16] When **54** and **55** (10 equiv) were co-incubated in the presence of NTR,[17] diminished $O_2^{\bullet-}$ was observed possibly due to inhibition in the turnover of **54** to **4** (Figure 3.2). Under similar experimental conditions, $O_2^{\bullet-}$ generated by **4** and **8** was consistent with previously reported data (Figures 3.6A & 3.6B).[10]

During a time course for superoxide generation from **54** with NTR, a gradual increase in the level of $O_2^{\bullet-}$ over a period of 20 min in aerobic buffer was observed. Whereas, a rapid generation of $O_2^{\bullet-}$ was observed with hypoxanthine and xanthine oxidase (X+XO), a routinely used method for $O_2^{\bullet-}$ generation (Figure 3.6B). A bacterial enzyme, NTR triggered ROS generation from **54,** offers advantages over X+XO by a temporally controlled generation of $O_2^{\bullet-}$ and better suited for biological studies (Figure 3.6B).

A HPLC-based dihydroethidium (DHE) assay was used to independently assess $O_2^{\bullet-}$ production from **54** (Figure 3.7). While oxidation of DHE to ethidium (E^+) is possible with numerous oxidants, 2-OH-$E^+$is produced exclusively by the reaction of $O_2^{\bullet-}$ with DHE (Figure 3.7).[18] In the DHE assay, **4** was found to generate 2-OH-E^+ confirming that this compound generates $O_2^{\bullet-}$ (Figure 3.7). During incubation of **54** in the presence of NTR, nearly complete disappearance of DHE with concomitant formation of 2-OH-E^+ was observed,[19] thus confirming the intermediacy of $O_2^{\bullet-}$ (Figure 3.7). A comparable $O_2^{\bullet-}$ generation profile for **54** was observed with X+XO in buffer by the means of DHE assay indicating a NTR mediated activation of **54** to generate $O_2^{\bullet-}$.

Figure 3.7. A HPLC-based dihydroethidium (DHE) assay: DHE assay was used to infer generation of $O_2^{\bullet-}$ from 100 μM of compounds after incubation in pH 8.0 buffer for 3 h. 2-OH-E^+, which is exclusively formed by the reaction of $O_2^{\bullet-}$ with DHE elutes at 30.9 min, and E^+, which is formed by non-specific oxidation of DHE elutes at 31.7 min.

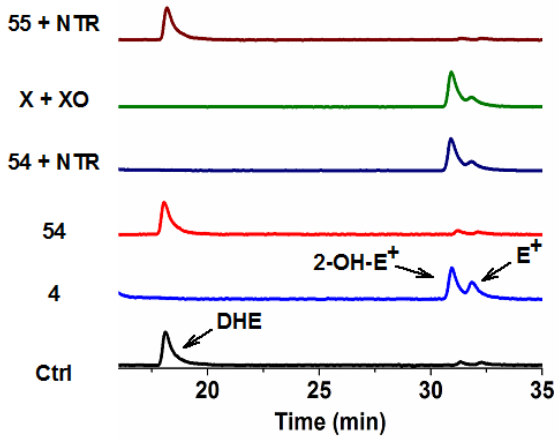

H_2O_2 is produced by $1e^-$ transfer to $O_2^{\bullet-}$ and we estimated H_2O_2 using an Amplex Red® fluorescence assay.[20] In the absence of NTR, negligible H_2O_2 was produced during incubation of **54** (10 μM). But in the presence of NTR, a yield of 3.65 μM H_2O_2 was recorded during 1 h (Figure 3.8). As expected, the non-ROS generating NTR substrate **55** alone did not generate any H_2O_2 during its incubation with NTR in buffer, while co-treatment of **55** with **54** and NTR has significantly suppressed the level of H_2O_2 produced. This result is consistent with $O_2^{\bullet-}$ data obtained from **54** with and without **55** (Figure 3.6). Taken together, our data supports **54** as a NTR-activated ROS generator under ambient aerobic conditions in aqueous buffer.

Figure 3.8. Estimation of hydrogen peroxide generated during incubation of 10 μM of each compound in pH 7.4 was estimated using an Amplex Red® fluorescence assay.

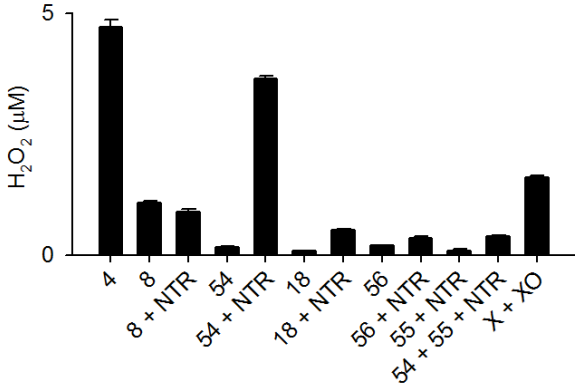

3.2.3. Stability studies on 54 and mechanism of ROS generation:

Two pathways by which compound **54** can generate ROS; one is a direct reaction of **54** with molecular O_2 in buffer and is expected to produce **56** as an organic product (Scheme 3.5). Further, a NTR mediated decomposition cascade can produce **18** from **56**. Other pathway is NTR mediated activation of **54** to release **4** and the mechanism of ROS generation from **4** is well established. In order to study this possibility, HPLC mediated decomposition study was conducted on **54** under physiological conditions. After 18 h of incubation of **54** in buffer at 37 °C <20% of decomposition of **54** to **56** was observed, thus eliminating the possibility of a direct electron transfer from **54** to O_2 for ROS generation (Figure 3.9B). Formation of **56** as an oxidized product of **54** was confirmed by comparing authentic HPLC trace of **56** (Figure 3.9B). Compound **56** was independently synthesized by a reaction of **54** with K_2CO_3 in THF (Scheme 3.6). During the same time

period (18 h) a nearly complete conversion of **4** to **18** was observed (Figure 3.9A). Thus data indicates that **54** need to be converted to **4** for any significant ROS generation (Scheme 3.5). This observation was further supported by $O_2^{\bullet-}$ and H_2O_2 generated from **54** only in the presence of NTR (Figure 3.6 & 3.8)

Scheme 3.5. Proposed mechanisms for ROS generation during incubation of **54** in buffer in the presence of NTR.

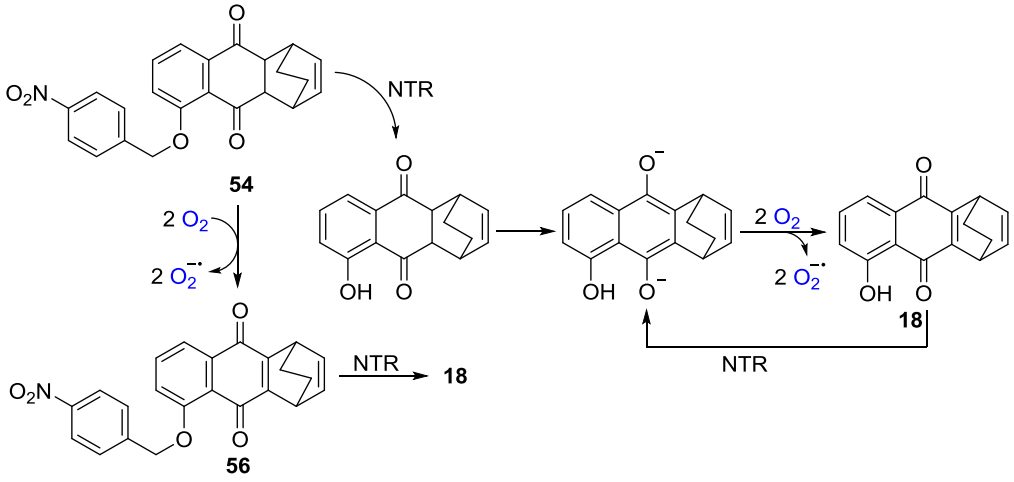

Figure 3.9. Stability studies on **54** and **4** in ambient aerobic buffer carried out using HPLC: Representative traces for: A) Conversion of compound **4** to **18** in phosphate buffer (pH 7.4, 100 mM). Nearly complete decomposition of **4** was observed at 18 h; B) decomposition of compound **54** to **56** in phosphate buffer (pH 7.4, 100 mM) during 18 h, where <20% decomposition of **54** was observed.

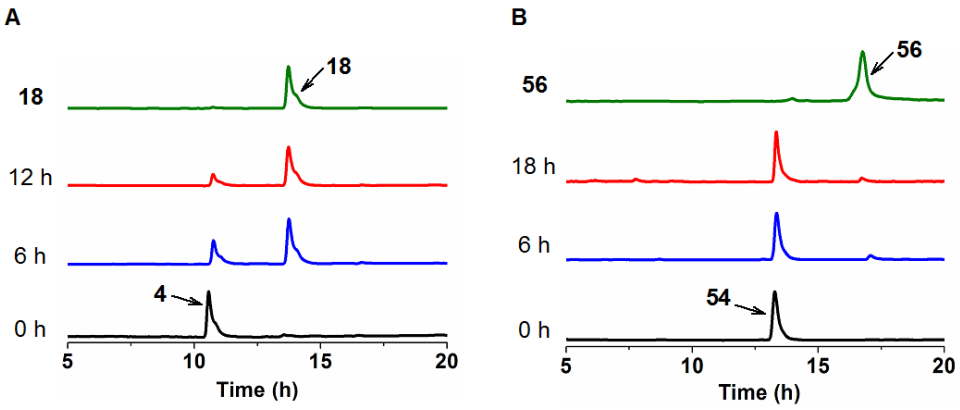

Scheme 3.6. Synthesis of **56** from **54**.

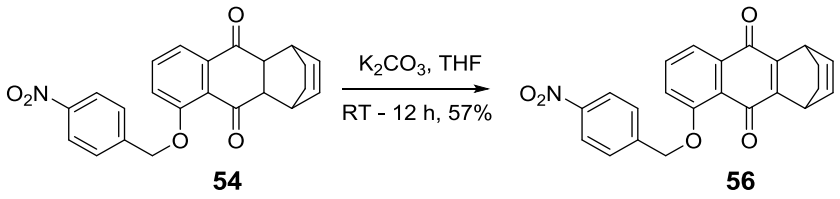

3.2.4. Extracellular and intracellular ROS generation studies:

DHE assay was used for the detection of intracellular $O_2^{\bullet-}$ generation from **54**, in order to determine the ability of **54** to enhance intracellular $O_2^{\bullet-}$ in bacteria. DHE assay is reported to be selective for intracellular $O_2^{\bullet-}$ detection.[21]

Figure 3.10. ROS generation during incubation with *E. coli*: (A) HPLC traces of assay for intracellular $O_2^{\bullet-}$ production using a dihydroethidium (DHE) assay. Incubation with **54** (250 μM) was for 30 min and DHE levels indicate unoxidized dye while 2-OH-E^+ formed is an indicator for $O_2^{\bullet-}$ production and E^+ is indicative of increase in oxidative species. (B) Extracellular H_2O_2 generated by compounds (100 μM) during incubation of *E. coli* during 1 h was estimated using an Amplex Red® fluorescence assay; 10 equiv of **55** (1 mM) was used. Ctrl: untreated bacteria.

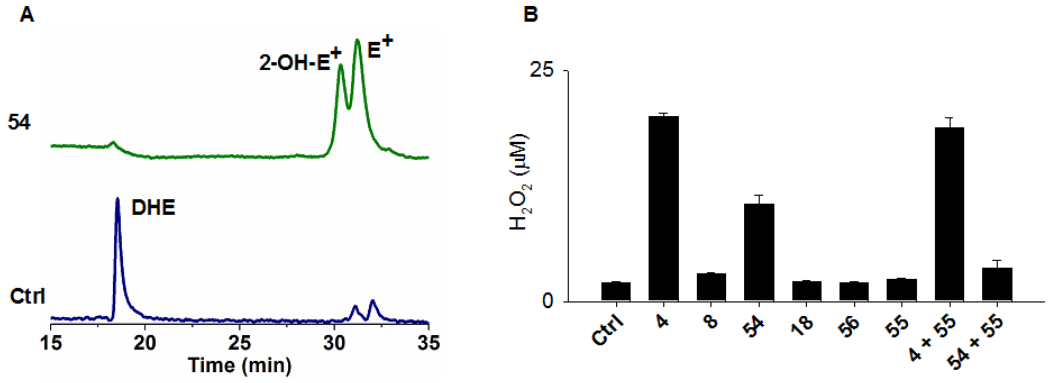

In this assay, *E. coli* was incubated with DHE with and without **54** for 30 min. Cell pellet was collected after centrifugation to remove any excess reagents. Using a probe sonicator the cells were lysed in buffer, the resulting lysate was analyzed to assess DHE, and 2-OH-E^+ using HPLC attached with a fluorescence detector.[19,21] A control experiment was carried out on *E. coli* bacterium by treating with DHE and the analysis showed unreacted DHE with negligible amount of oxidized DHE (Figure 3.10A). Under similar

experimental conditions, incubation of **54** and DHE with *E. coli* produced 2-OH-E^+ with concomitant loss of DHE, suggestive of intracellular $O_2^{\bullet-}$ production (Figure 3.10A). Thus, the experiment confirms that, **54** is a cell permeable organic small molecule and intracellular NTR is capable of activating **54** for ROS generation in bacteria.

An accurate quantification of $O_2^{\bullet-}$ using the DHE assay is difficult, hence a measurement of H_2O_2 was carried out as this provides a quantitative basis for assessing ROS production.[22] H_2O_2 is a freely diffusible ROS across bacterial cell walls and is typically estimated as extracellular H_2O_2.[23,24] Incubation of *E. coli* with **54** (100 μM) produced 10.5 μM H_2O_2 during 1 h (Figure 3.10B). Under similar conditions, **4** was found to significantly enhance the extracellular H_2O_2. In the treatment of *E. coli* with a competitive substrate for intracellular NTR, **55** alone did not increase the extracellular H_2O_2. While nearly complete abrogation of H_2O_2 was observed when **54** was co-treated with **55** (10 equiv).[17] However, no inhibition in ROS generation by **4** was observed during the treatment with **55** (Figure 3.10B) suggesting that **55** inhibited metabolism of **54** to **4**.

Figure 3.11. Extracellular and intracellular ROS generation from **54** in *E. coli*: (A) H_2O_2 generation during incubation of *E. coli* with **54** (100 μM) was recorded during 6 h as described above. A first order rate constant for ROS production was calculated as 0.96 h^{-1}. (B) *E. coli* treated with **54** (100 μM) for 1 h; centrifugation and removal of the supernatant followed by re-suspension of bacteria in fresh media. H_2O_2 generated after incubation of bacteria for 3 h was recorded as described above. (C) A 2,7-Dichlorodihydrofluorescein-diacetate ($DCFH_2$-DA)-based fluorescence assay was used to estimate oxidative species generated intracellularly in *E. coli*. Increase in relative fluorescence intensity (RFI) with respect to DMSO (0.5%); ROS generation during incubation with *E. coli*: (A) equiv of **55** (1 mM) was used. Ctrl: untreated bacteria. Student T-test performed on this data provided a P value of <0.001.

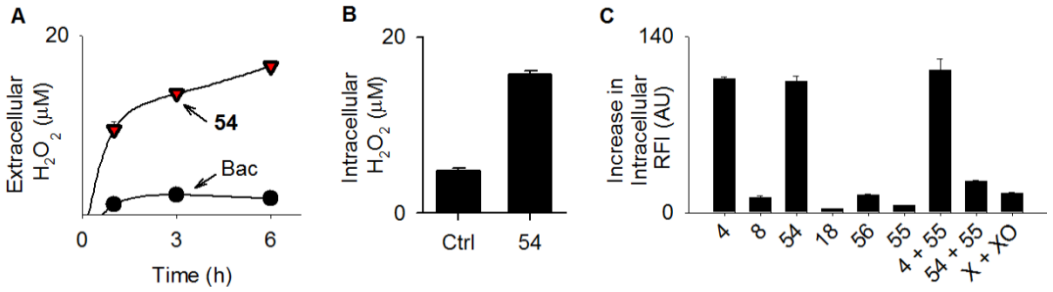

Further, a temporally controlled intracellular ROS generation profile from **54** was observed when a time course for ROS generation was carried out during incubation of *E. coli* with **54**, a yield of 17% of H_2O_2 was quantified during 6 h of incubation (Figure 3.11A). Next, to understand the metabolism of **54** in *E coli* by intracellular NTR enzyme, a series of experiments were designed. Firstly, *E. coli* was incubated with **54** for 1 h, centrifuged to aspirate the media containing any **54**, re-suspended with fresh media and measured the H_2O_2 generation over 6 h. During the process any **54** remaining in the extracellular media was discarded and detection of any H_2O_2 produced would be due to intracellular activation of **54** and we have recorded a H_2O_2 yield of 16.5%. A minimal difference in yields of H_2O_2 obtained during this experiment (Figure 3.11B) and during a bolus treatment of **54** (17%) (Figure 3.11A) supporting intracellular metabolism to produce ROS was the major pathway. Further, to investigate if any NTR is secreted in the extracellular medium during the bacterial culture, which could catalyze the activation of **54** for extracellular H_2O_2 generation, *E. coli* was grown overnight and the cell-free media was incubated with **54**. No significant increase in H_2O_2 was found even after 3 h suggesting that extracellular activation of **54** was not important.

Figure 3.12. Representative data for supercoiled pBR322 plasmid DNA damage assay: Reaction mixtures (20 μL) containing 100 ng of Form I DNA in pH 8.0 phosphate buffer (100 mM) and compound (50 μM) were incubated at 37 °C for 6 h. NTR refers to NTR + NADPH; equimolar Fe(II) was used where applicable. Nicked DNA is represented by II.

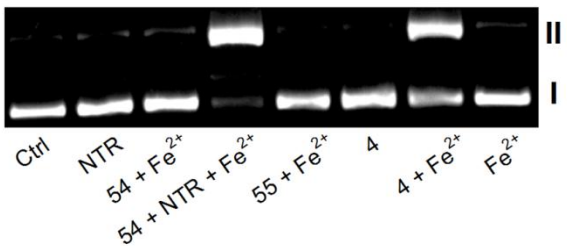

Generation of $^{\bullet}OH$ is inevitable when $O_2^{\bullet-}$ and H_2O_2 (Scheme 3.1) are produced in the intracellular environment. Exposure of *E. coli* to **54** could also produce $^{\bullet}OH$. Generation of $^{\bullet}OH$ radical from **54** with NTR in the presence of Fe^{2+} was assessed using a supercoiled plasmid DNA cleavage assay. Gel image of the compound treated DNA describes the capability of this compound to generate $^{\bullet}OH$ in the presence of metal ions (Figure 3.12).[10] A treatment of **54** alone or **54** and Fe^{2+} with DNA did not induce any nick in the supercoiled plasmid. Addition of NTR into the reaction mixture containing **54**, Fe^{2+} and DNA showed significant cleavage in the plasmid evident from DNA gel image supporting the use of **54** for the enhancement of ROS. Under similar conditions, control experiments carried out with **4** and **55** were consistent with the expected result (Figure 3.12).

Due to its extremely short half-life and indiscriminate reactivity, *in vivo* detection of hydroxyl radical is challenging and the specificity of previously used fluorescence assays for $^{\bullet}OH$ has been questioned.[25] Instead, using two independent methods, the ability of **54** to increase intracellular oxidative species was studied. *E. coli* was incubated with dichlorofluorescein-diacetate, $DCFH_2$-DA, a non-fluorescent dye and followed by treatment with **54** resulting in an increased intracellular fluorescence attributable to oxidative species (including $^{\bullet}OH$) (Figure 3.11C).[26] Further evidence obtained for an increased oxidative intracellular environment caused by **54** was through the formation of E^+ in DHE assay (Figure 3.10A).[21]

Compound **54** was next compared with some routinely used methods for ROS generation both in the test-tube as well as in cellular assays. As described in Section 3.2.2, the X + XO protocol produced both $O_2^{\bullet-}$ and H_2O_2 in buffer (Figures 3.6A, 3.6B & 3.7). The time course of X + XO showed a burst of $O_2^{\bullet-}$ production while **54** + NTR showed a gradual increase in ROS during this time period (Figure 3.6A). Thus, for biochemical studies, the distinct pattern for ROS production by **54** + NTR might simulate gradual ROS production. In cell-based assays, the increase in intracellular ROS by X + XO was much lower in comparison with **54**, an observation that is consistent with diminished permeability of X + XO (Figure 3.11C).[27] Identical to the observation in the test tube assays, intracellular ROS generation by **54** was nearly completely inhibited by **55** in

E.coli (Figure 3.11C). Similarly, in cellular assays at comparable concentrations with menadione, despite several attempts, non-specific decomposition of DHE without formation of 2-OH-E^+ or E^+ was observed. This result might help explain the need for elevated concentrations of this compound for intracellular $O_2^{\bullet-}$ generation in bacteria.[7] Hence, the use of **54** complements the existing repertoire of ROS generators while offering distinct advantages such as cell permeability and temporal control.

Bioreduction of quinone **56** by enzymes including NTR can also produce ROS.[13,17] However, we find significantly low levels of ROS generation from **56** in cellular assays (Figures 3.10B and 3.11C), a diminished rate for intracellular redox cycling of **56** might be possible. The precise rationale for this observation is unclear but steric hindrance might hamper the accessibility of the quinone ring to reductive enzymes. Menadione is often used for enhancement of intracellular ROS levels to induce oxidative stress in cells,[7,28,29] however, in addition to bioreduction this quinone also was found to react with intracellular thiols such as cysteine and glutathione. Unlike menadione, **56** was unreactive with thiols including cysteine suggesting that thiol addition may not be of relevance.[30] Although biocatalytic reduction of **54** by NTR requires NADPH as a cofactor,[13] our observation that the treatment of *E. coli* with **55** resulted in no significant increase of H_2O_2 (Figure 3.10B)[31] suggested that such perturbations of NADPH levels (estimated millimolar concentrations)[32] does not result in ROS generation.

3.2.5. Effect of enhanced intracellular ROS on bacterial growth:

A growth inhibition assay was performed on *E. coli* with **54** to assess the impact of intrabacterial ROS enhancement.[33] No evidence for inhibition of growth of four wild-type strains of *E. coli* was found even at 100 μM concentration of **54**. Under these assay conditions, major classes of clinical antibiotics such as kanamycin, ciprofloxacin, ampicillin, rifampicin and chloramphenicol were effective in bacterial growth inhibition with MICs in the previously reported ranges (0.06 – 8 μg/mL).[34] Compounds **4**, **18** and the nitroaryl derivatives, **55** and **56** were found to be poor inhibitors of *E. coli* growth suggesting that the possible products of metabolism[17] of the **54** were not toxic to *E. coli*.[22] Previously, it has been shown that due to its poor cell permeability, $O_2^{\bullet-}$ by itself exhibits

little toxicity towards bacteria.[4] In our study, we demonstrated that a gradual increase in intracellular $O_2^{\bullet-}$ produced upon treatment of *E. coli* with **54** is tolerated well by this bacterium. However, this does not preclude the possibility of other bacteria including *Mycobacterium tuberculosis* being sensitive to ROS. As discussed previously, Brynildsen and coworkers,[7] using a library of *E. coli* mutants that have been engineered to study effects of increasing ROS, have suggested the possible use of ROS as an adjuvant. Using **54**, we tested this hypothesis and found that the efficacy of aminoglycoside antibiotics have significantly enhanced in the presence of **54** (Table 3.1). For example, when co-treated with **54**, we found an 8-fold decrease in MIC of gentamycin suggesting that this antibiotic could be used at lower concentrations to achieve similar bactericidal effects in the presence of **54**. This result might thus help develop new ROS-based adjuvants to address the major side-effects of aminoglycosides including nephrotoxicity and ototoxicity.

Table 3. 1. Bacterial growth inhibition by antibiotics in the presence of additives determined against *E. coli*[a]

Entry	Compound	Additive[b]	MIC, μg/mL	Fold Change[c]
1	Kanamycin	-	8	-
2	Kanamycin	4	2	4
3	Kanamycin	54	2	4
4	Kanamycin	55	8	-
5	Kanamycin	56	8	-
6	Gentamycin	-	2	-
7	Gentamycin	54	0.25	8
8	Streptomycin	-	8	-
9	Streptomycin	54	2	4

[a]*E. coli* K12 MG1655 was used; [b]The additive was used in 50 μM; [c]Fold change is (MIC without any additive)/(MIC with additive at the specified concentration).

3. 3. Conclusion:

In summary, we developed a small molecule that is capable of predictably increasing intracellular levels of ROS in a model bacterium. A bacterial enzyme, *E. coli* nitroreductase was used as a trigger to activate **54** and showed that the compound was responding to the enzyme to generate ROS in buffer as well as in bacteria. A temporally controlled generation of ROS in bacteria was characterized from compound **54**. To our knowledge, this is the first report of a rationally designed cell permeable enzyme activated $O_2^{\bullet-}$ generator that is highly suited for spatio-temporally controlled ROS generation to study oxidative stress in bacteria. Under our experimental conditions, enhancement of intracellular ROS using **54** or **4** did not affect the bacterial growth. However, an enhanced sensitivity of the bacterium to aminoglycoside antibiotics was found when co-treated with **54** (8 fold), implying a potential application of intracellular ROS generator **54** as an adjuvant to aminoglycoside antibiotics.

3.4. Experimental and Characterization Data:

3.4.1. Experimental Section

3.4.1.1. Synthesis of 5-(4-nitrobenzyloxy)-1,4,4a,9a-tetrahydro-1,4-ethanoanthracene-9,10-dione (54).

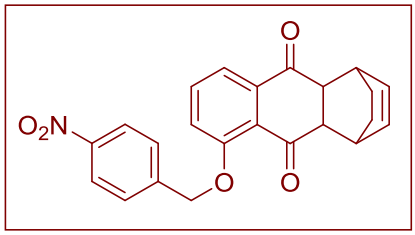

To a 50 mL round bottom flask containing 1,1-dichloromethane (DCM, 8 mL), **4** (200 mg, 0.79 mmol), 4-nitrobenzylbromide (510 mg, 2.36 mmol) were added followed by Ag_2O (729 mg, 3.15 mmol); the reaction flask was covered with aluminium foil, flushed with nitrogen gas and stirred for 24 h at room temperature. Upon complete consumption of starting material as determined by thin layer chromatography (TLC) analysis, the reaction mixture was filtered through a celite bed. The filtrate was evaporated to dryness under reduced pressure to obtain crude product. The crude material was purified by silica gel column chromatography using ethyl acetate (5→30 %) and petroleum ether solvent system to obtain a pale yellow solid (201 mg, 66%): mp 178 – 180 °C; FT-IR (ν_{max}, cm^{-1}): 2958, 2864, 1684, 1590, 1520, 1452, 1340, 1288; ^1H NMR (400 MHz, $CDCl_3$): δ 8.25 (d, *J* = 8.5 Hz, 2H), 7.74 (d, *J* = 8.4 Hz, 2H), 7.50 – 7.61 (m, 2H), 7.11 – 7.22 (m, 1H), 6.05 – 6.23 (m, 2H), 5.28 (d, *J* = 13.5 Hz, 1H), 5.23 (d, *J* = 13.6 Hz, 1H), 3.28 – 3.40 (m, 2H), 3.13 – 3.28 (m, 2H), 1.67 – 1.71 (m, 2H), 1.31 – 1.46 (m, 2H); ^{13}C NMR (100 MHz, $CDCl_3$): δ 197.9, 196.2, 156.7, 147.6, 143.7, 138.8, 134.4, 134.1, 133.6, 127.3, 126.2, 124.0, 119.6, 118.3, 69.7, 52.1, 51.0, 34.3, 33.7, 24.7, 24.6; HRMS (ESI) for $[C_{23}H_{19}NO_5+H]^+$: calcd., 390.1341; Found: 390.1346; Elemental analysis for $C_{23}H_{19}NO_5$ calcd. C, 70.94; H, 4.62; N, 3.60. Found. C 70.84; H, 4.46; N, 3.38.

3.4.1.2– Synthesis of 5-(4-nitrobenzyloxy)-1,4-dihydro-1,4-ethanoanthracene-9,10-dione (56):

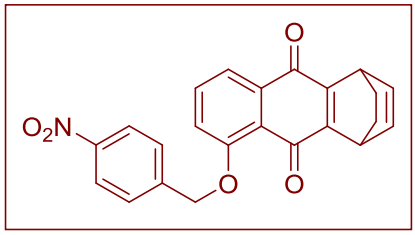

To a 10 mL round bottom flask compound **54** (30 mg, 0.08 mmol) was dissolved in tetrahydrofuran (THF, 5 mL) and potassium carbonate (21 mg, 0.16 mmol) was

added to the above solution. The reaction flask was stirred at room temperature overnight. Consumption of the starting material was confirmed by TLC analysis. The reaction mixture was washed with 5 mL of de-ionized water and extracted with ethyl acetate (4 × 5 mL). The combined organic layer was dried (anhydrous Na_2SO_4, 5 g), filtered and the filtrate was evaporated under reduced pressure to obtain crude product. The crude mixture was purified by a short silica gel column by washing with ethyl acetate: petroleum ether (3:4 ratio, v/v). The organic solvent was evaporated under reduced pressure to obtain a yellow solid (17 mg, 57%): mp 290 °C; FT-IR (ν_{max}, cm^{-1}): 2923, 1643, 1439, 1384, 1339, 1295; ^{1}H NMR (400 MHz, $CDCl_3$): δ 8.32 (d, *J* = 8.5 Hz, 2H), 7.88 (d, *J* = 8.5 Hz, 2H), 7.82 (d, *J* = 7.5 Hz, 1H), 7.65 (t, *J* = 8.0 Hz, 1H), 7.26-7.29 (m, 1H), 6.42 – 6.46 (m, 2H), 5.36 (d, *J* = 13.4 Hz, 1H), 5.32 (d, *J* = 13.4 Hz, 1H), 4.56 – 4.59 (m, 1H), 4.48 – 4.53 (m, 1H), 1.54 (d, *J* = 9.1 Hz, 2H), 1.42 (d, *J* = 7.8 Hz, 2H); ^{13}C NMR (100 MHz, $CDCl_3$): δ 134.5, 134.0, 133.9, 127.3, 124.0, 120.2, 69.7, 34.0, 29.7, 24.8; HRMS (ESI) for $[C_{23}H_{17}NO_5+H]^+$: calcd., 388.1185; Found: 388.1176.

3.4.2 Superoxide Estimation.

3.4.2.1 Luminol Assay:

5-Amino-2,3-dihydro-1,4-phthalazinedione solution (Luminol, 4 mM) was prepared in 30 mM aqueous sodium hydroxide and stored under ice. To a microwell plate, a stock solution of the compound (2 μL of 1 mM) was added to phosphate buffer (100 mM pH 8.0, 193 μL) followed by luminol (5 μL, final 100 μM in 200 μL). The resulting mixture was incubated at 37 ºC for 25 min during which the luminescence was measured using a microtiter plate reader. A stock solution of commercially available *E. coli* nitroreductase (NTR) was prepared using 1 mg of a lyophilized powder dissolved in phosphate buffer (150 μL). For experiments with nitroreductase, NADPH (3 μL, 1 mM), *E. coli* nitroreductase (NTR, 2 μL of stock) was added with total volume of the reaction mixture being 200 μL. Hypoxanthine (2 μL, 1 mM) and xanthine oxidase (2 μL of 0.02 U/mL) were used as a positive control. When the experiments with **4** or **55** + NTR were conducted in the presence of EDTA (10 equiv), no significant difference in luminescence

values suggesting that superoxide generation was not affected by metal ions such as Fe(II).

3.4.2.2 Dihydroethidium (DHE) assay:

A stock solution of dihydroethidine (DHE, 1.12 mg, 3.55 μmol) was prepared in DMSO (355 μL) and stored in the dark at −20 ºC until its use. A stock solution of the compound (10 μL, 10 mM) and DHE (10 μL of 10 mM) were reacted in acetonitrile: phosphate buffer of pH 7.4 (1:1, v/v, 100 mM, final volume 100 μL) for 3 h at 37 ºC. The reaction mixture was diluted to 100 μM using acetonitrile: phosphate buffer of pH 7.4 (1:1, v/v, to a final volume of 1 mL). In the experiments with NTR, NADPH (4 μL of 1 mM), nitroreductase (NTR, 2 μL stock as previously prepared) was used. The reaction mixture was filtered (0.22 μm) and injected (25 μL) in an Agilent high performance liquid chromatograph (HPLC) attached with a fluorescence detector (excitation at 356 nm; emission at 590 nm). The column used was Zorbax SB C-18 reversed phase column (250 mm × 4.6 mm, 5 μm), the mobile phase was water: acetonitrile containing 0.1% trifluoroacetic acid and a gradient starting with 10: 90 to 30: 70 → 0 – 45 min, 0: 100 → 45 – 50 min, 0: 100 → 50 – 55 min, 10: 90 → 55 – 60 min was used with a flow rate of 0.5 mL/min. Under these conditions literature report indicate that if superoxide is produced, a peak for 2-hydroxyethidium (2-OH-E^+), which elutes at 30.9 min, would be observed.[3-5] When other oxidative species are generated, ethidium (E^+) is formed. Again, according to literature reports E^+ elutes at 31.7 min.[3-5] We independently confirmed the formation of 2-OH-E^+ and E^+ by mass spectrometry. Hypoxanthine 10 μL, 1 mM) and xanthine oxidase (5 μL of 0.02 U/mL) were mixed in phosphate buffer (pH 7.4, 100 mM) along with DHE (10 μL of 10 mM, 100 μM final concentration) for 2 h and served as a positive control.

3.4.3 Estimation of hydrogen peroxide.

A solution of the test compound (1 μL, 1 mM, 10 μM final concentration) was added to 50 mM phosphate buffer of pH 7.4 (45 μL) and incubated at 37 ºC for 60 min. To the

incubated reaction mixture, 50 μL of a premixed solution of 10-acetyl-3,7-dihydroxyphenoxazine or Amplex Red® (prepared by following manufacturer's protocol from Invitrogen) was added and incubated at RT for 25 min before measuring the fluorescence using a microtiter plate reader (excitation 550 nm; emission 590 nm). For the enzymatic assay, NADPH (2 μL of 1 mM) and nitroreductase (NTR, 1 μL stock as previously prepared) was used. For the assay with X + XO, a mixture of hypoxanthine (1 μL, 1 mM) and xanthine oxidase (1 μL of 0.02 U/mL) were mixed in phosphate buffer (pH 7.4, 100 mM) was used.

3.4.4 Intracellular superoxide detection.

A similar procedure was followed from Section 2.1.4.13

3.4.5 Extracellular hydrogen peroxide estimation.

E. coli (EC2065) was cultured in 5 mL of Luria Bertani (LB) medium at 37 ºC for 16 h and centrifuged to aspirate out the medium and re-suspended to an O.D of 1.0 with fresh LB medium. A stock solution of the compound in DMSO (0.5%) was added so that the final concentration was 100 μM. In the experiments where **55** was co-treated with **4** or **56**, 10 eq., of **55** (1 mM) was used. After incubation for 1 h, the bacterial suspension was centrifuged and the extracellular media was separated. To the media (divided in several 50 μL portions in a 96-well microplate), 50 μL of a premixed solution of 10-acetyl-3,7-dihydroxyphenoxazine or Amplex Red® (prepared by following manufacturer's protocol from Invitrogen) was added and incubated at RT for 25 min before measuring the fluorescence using a microtiter plate reader (excitation 550 nm; emission 590 nm). A calibration curve with known concentrations of hydrogen peroxide was generated in LB medium and was used to quantify hydrogen peroxide produced during incubation of test analytes. Data presented are an average of three independent experiments.

3.4.6 Estimation of intracellular oxidative species - $DCFH_2$-DA assay.

A similar procedure was followed from Section 2.1.4.14

3.4.7 Supercoiled plasmid DNA damage assay.

DNA cleavage was analyzed by the conversion of pBR322 circular DNA to open circular and/or linear forms. Briefly, pBR322 DNA (100 ng) was incubated with the compound (50 μM) in the presence of 1 eq. of $FeCl_2$ in pH 8.0 phosphate buffer and the final volume was 20 μL. The solutions were incubated at 37 °C for 6 h. For the experiment of **54** with NTR, NADPH (2 μL of 1 mM), nitroreductase (NTR, 1 μL stock as previously prepared) were used. The solutions were mixed with bromophenol blue (0.25 wt.%, 4 μL) and loaded in a 1.0 % agarose gel (0.5 g in 50 mL of 1x TAE; 1.0 μg/mL Gel Red®), and immediately subjected to electrophoresis in a horizontal slab gel apparatus containing 1x TAE buffer as medium for 45 min under constant 90 V. After electrophoresis, the DNA was visualized under GBOX Syngene UV-transilluminator, photographed using Genesnap-7.04. Only NTR and NADPH did not induce significant DNA cleavage (see below lane marked NTR) and neither did Fe(II).

3.4.8 Chemoreduction of 1c with Zn and ammonium formate:

Compound **54** (5 mg, 12.8 mmol) was dissolved in 2 mL of a 1:1 solution of methanol and phosphate buffer (100 mM, pH 7.4). To this mixture, ammonium formate (2 mg, 2 eq.) and zinc dust (100 mg) were added and the reaction mixture was stirred at 37 ºC for 60 min. The reaction mixture was filtered (0.22 μm) and injected (25 μL) in an Agilent high performance liquid chromatograph (HPLC) attached with a diode-array detector (detection wavelength was 254 nm) and a Zorbax SB C-18 reversed phase column (250 mm × 4.6 mm, 5 μm). A mobile phase of water: acetonitrile was used with a run time of 25 min: multistep gradient technology with a flow rate of 1 mL/min – starting with 50:50 % → 0 – 5 min, 40:60 → 5 – 10 min, 30:70 → 10 – 15 min, 20:80 → 15 – 20 min, 50:50 → 20 – 23 min, 50:50 → 23 – 25 min. Authentic compounds **4** and **18** were injected to identify the peak position of the reaction products. Mass Spectrometry (LC-MS, Waters LC/MS) of the ensuing mixture after 1 h was carried out to identify the products and intermediates formed during the reaction. Two independent experiments were conducted, each carried out in duplicate and representative data is presented below.

3.4.9 HPLC decomposition data.

Compounds **4** and **54** (1 mM) were reacted independently in pH 7.4 phosphate buffer (100 mM): acetonitrile ACN (1:1 v/v) with a concentration of 1 mM at 37 ºC over a period of 18 h, in duplicate. The reaction mixture was filtered (0.22 μm) and injected (25 μL) in an Agilent high performance liquid chromatograph (HPLC) following method as described above. Authentic compounds **18** and **56** were injected to verify the peak position of the reaction products. Two independent experiments were conducted, each carried out in duplicate and representative data is presented below.

3.4.10 Determination of minimum inhibitory concentration.

A similar protocol was followed from section 2.1.4.18.

3.4.11. Adjuvant Studies.

A similar protocol was followed from section 2.1.4.22.

3.5. Spectral Charts:

^{1}H NMR Spectrum (400 MHz, $CDCl_3$) of Compound **54**

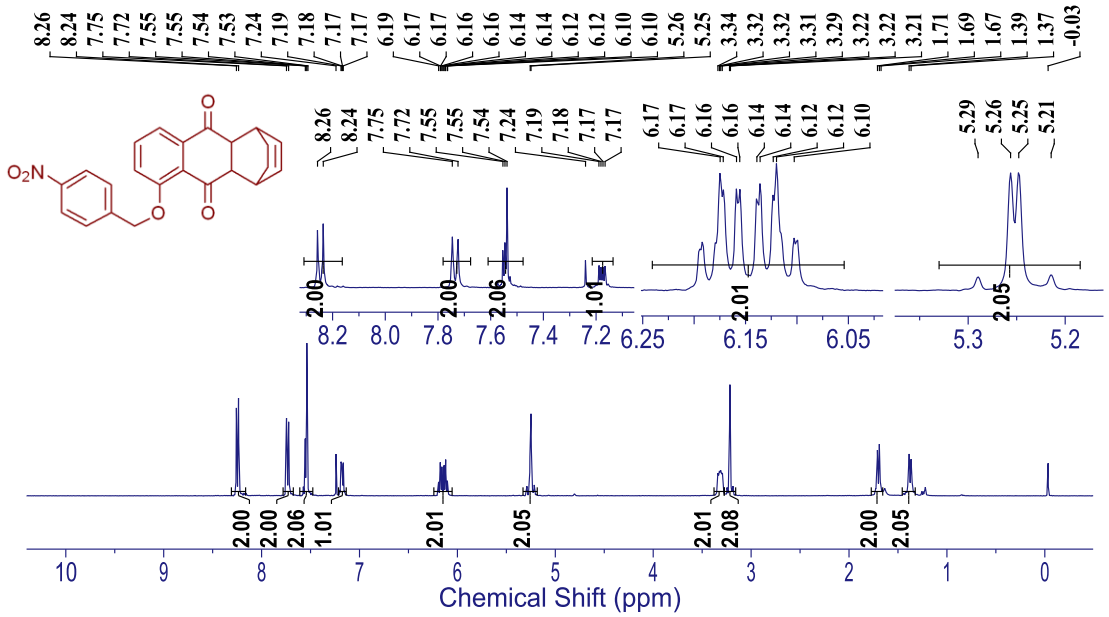

^{13}C NMR Spectrum (100 MHz, $CDCl_3$) of Compound **54**

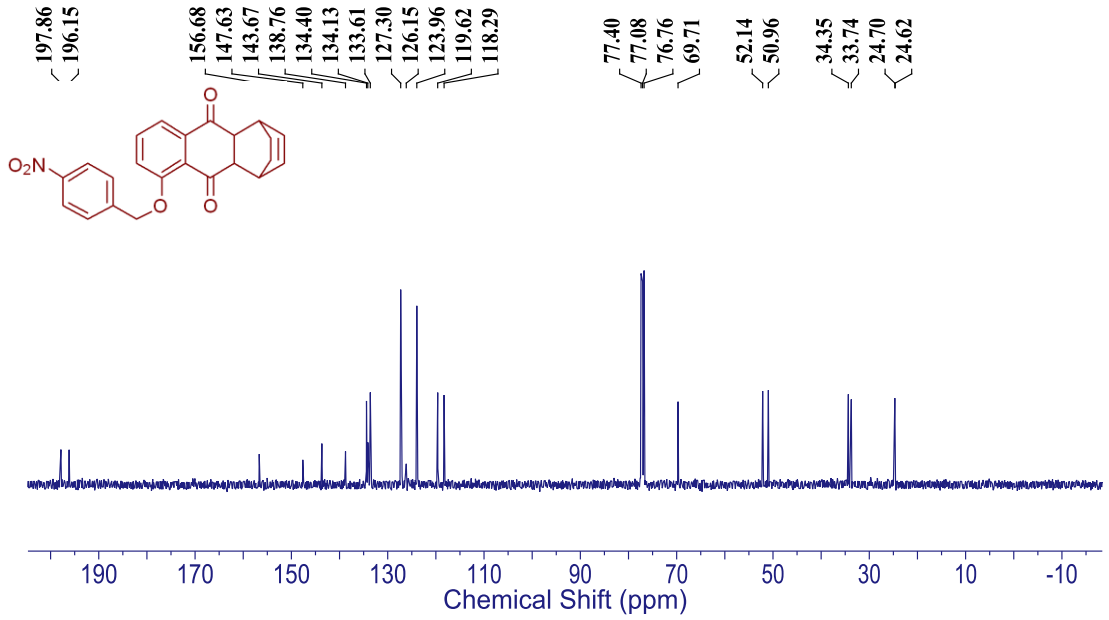

^{1}H NMR Spectrum (400 MHz, $CDCl_3$) of Compound **56**

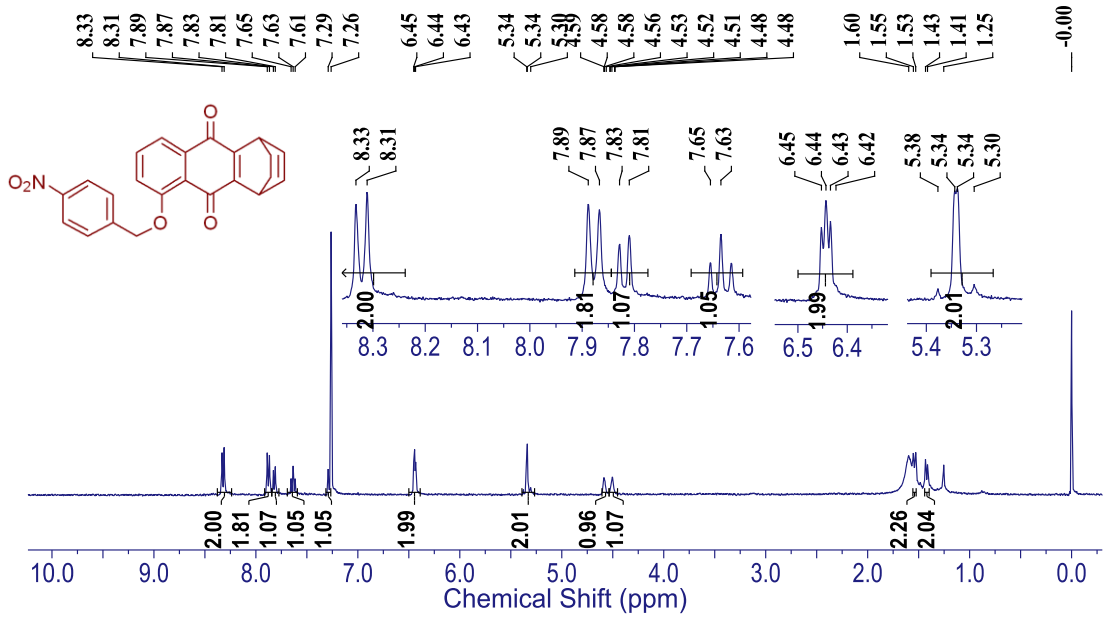

3.6. References:

1. Fang, F. C. Antimicrobial reactive oxygen and nitrogen species: Concepts and controversies. *Nat. Rev. Microbiol.,* **2004,** 2, 820-832.
2. McCord, J. M.; Fridovich, I. The reduction of cytochrome c by milk xanthine oxidase. *J. Biol. Chem.,* **1968,** 243, 5753-5760.
3. Lynch, R. E.; Fridovich, I. Permeation of the erythrocyte stroma by superoxide radical. *J. Biol. Chem.* **1978,** 253, 4697-4699.
4. Korshunov, S. S.; Imlay, J. A. A potential role for periplasmic superoxide dismutase in blocking the penetration of external superoxide into the cytosol of Gram-negative bacteria. *Mol. Microbiol.* **2002,** 43, 95-106.
5. Hassan, H. M.; Fridovich, I. Paraquat and Escherichia coli. Mechanism of production of extracellular superoxide radical. *J. Biol. Chem.* **1979,** 254, 10846-10852.
6. Imlay, J. A.; Fridovich, I. Assay of metabolic superoxide production in Escherichia coli. *J. Biol. Chem.,* **1991,** 266, 6957-6965.
7. Brynildsen, M. P.; Winkler, J. A.; Spina, C. S.; MacDonald, I. C.; Collins, J. J. Potentiating antibacterial activity by predictably enhancing endogenous microbial ROS production. *Nat. Biotechnol.,* **2013,** 31, 160-165.
8. Ingold, K. U.; Paul, T.; Young, M. J.; Doiron, L. Invention of the First Azo Compound To Serve as a Superoxide Thermal Source under Physiological Conditions: Concept, Synthesis, and Chemical Properties1. *J. Am. Chem. Soc.,* **1997,** 119, 12364-12365.
9. Bedard, L.; Young, M. J.; Hall, D.; Paul, T.; Ingold, K. U. Quantitative Studies on the Peroxidation of Human Low-Density Lipoprotein Initiated by Superoxide and by Charged and Neutral Alkylperoxyl Radicals. *J. Am. Chem. Soc.* **2001,** 123, 12439-12448.
10. Dharmaraja, A. T.; Alvala, M.; Sriram, D.; Yogeeswari, P.; Chakrapani, H. Design, synthesis and evaluation of small molecule reactive oxygen species generators as selective Mycobacterium tuberculosis inhibitors. *Chem. Commun.,* **2012,** 48, 10325-10327.
11. Anlezark, G. M.; Melton, R. G.; Sherwood, R. F.; Coles, B.; Friedlos, F.; Knox, R. J. The bioactivation of 5-(aziridin-1-yl)-2,4-dinitrobenzamide (CB1954)-I. Purification and properties of a nitroreductase enzyme from Escherichia coli - A

potential enzyme for antibody-directed enzyme prodrug therapy (ADEPT). *Biochem. Pharmacol.,* **1992,** 44, 2289-2295.

12. Zenno, S.; Koike, H.; Tanokura, M.; Saigo, K. Gene cloning, purification, and characterization of NfsB, a minor oxygen-insensitive nitroreductase from Escherichia coli, similar in biochemical properties to FRase I, the major flavin reductase in Vibrio fischeri. *J. Biochem.,* **1996,** 120, 736-744.
13. Race, P. R.; Lovering, A. L.; Green, R. M.; Ossor, A.; White, S. A.; Searle, P. F.; Wrighton, C. J.; Hyde, E. I. Structural and mechanistic studies of Escherichia coli nitroreductase with the antibiotic nitrofurazone: Reversed binding orientations in different redox states of the enzyme. *J. Biol. Chem.,* **2005,** 280, 13256-13264.
14. Channe Gowda, D.; Mahesh, B.; Gowda, S. Zinc-catalyzed ammonium formate reductions: Rapid and selective reduction of aliphatic and aromatic nitro compounds. *Indian J. Chem. Sec B.,* **2001,** 40, 75-77.
15. Trung Pham, H.; Marquetty, C.; Pasquier, C.; Hakim, J. Luminol assay for microdetermination of superoxide dismutase activity: Its application to human fetal blood. *Anal. Biochem.* **1984,** 142, 467-472.
16. Sharma, K.; Sengupta, K.; Chakrapani, H. Nitroreductase-Activated Nitric Oxide (NO) Prodrugs. *Bioorg. Med. Chem. Lett.,* **2013**, 23, 5964-5967.
17. Roldan, M. D.; Perez-Reinado, E.; Castillo, F.; Moreno-Vivian, C. Reduction of polynitroaromatic compounds: the bacterial nitroreductases. *FEMS Microbiol. Rev.* **2008,** 32, 474-500.
18. Zhao, H.; Joseph, J.; Fales, H. M.; Sokoloski, E. A.; Levine, R. L.; Vasquez-Vivar, J.; Kalyanaraman, B. Detection and characterization of the product of hydroethidine and intracellular superoxide by HPLC and limitations of fluorescence. *Proc. Natl. Acad. Sci.,* **2005,** 102, 5727-5732.
19. Zielonka, J.; Vasquez-Vivar, J.; Kalyanaraman, B. Detection of 2-hydroxyethidium in cellular systems: A unique marker product of superoxide and hydroethidine. *Nat. Protoc.,* **2008,** 3, 8-21.
20. Zhou, M.; Diwu, Z.; Panchuk-Voloshina, N.; Haugland, R. P. A Stable Nonfluorescent Derivative of Resorufin for the Fluorometric Determination of Trace Hydrogen Peroxide: Applications in Detecting the Activity of Phagocyte NADPH Oxidase and Other Oxidases. *Anal. Biochem.,* **1997,** 253, 162-168.

21. Georgiou, C. D.; Papapostolou, I.; Grintzalis, K. Superoxide radical detection in cells, tissues, organisms (animals, plants, insects, microorganisms) and soils. *Nat. Protoc.,* **2008,** 3, 1679-1692.
22. Liu, Y.; Imlay, J. A. Cell death from antibiotics without the involvement of reactive oxygen species. *Science* **2013,** 339, 1210-1213.
23. Kamsler, A.; Segal, M. Hydrogen peroxide as a diffusible signal molecule in synaptic plasticity. *Mol. Neurobiol.,* **2004,** 29, 167-178.
24. Waghray, M.; Cui, Z.; Horowitz, J. C.; Subramanian, I. M.; Martinez, F. J.; Toews, G. B.; Thannickal, V. J. Hydrogen peroxide is a diffusible paracrine signal for the induction of epithelial cell death by activated myofibroblasts. *FASEB J.,* **2005,** 19, 854-856.
25. Menter, J. M.; Filipescu, N. Photochemical detection of intramolecular energy transfer between nonconjugated chromophores in rigid model compounds. *J. Chem. Soc. (B)* **1970**, 464-468.
26. Wardman, P. Fluorescent and luminescent probes for measurement of oxidative and nitrosative species in cells and tissues: Progress, pitfalls, and prospects. *Free Radical Biol. Med.,* **2007,** 43, 995-1022.
27. Hassan, H. M.; Fridovich, I. Paraquat and Escherichia coli. Mechanism of production of extracellular superoxide radical. *J. Biol. Chem.,* **1979,** 254, 10846-10852.
28. Keyes, S. R.; Rockwell, S.; Sartorelli, A. C. Modification of the metabolism and cytotoxicity of bioreductive alkylating agents by dicoumarol in aerobic and hypoxic murine tumor cells. *Cancer Res.* **1989,** 49, 3310-3.
29. Beck, R.; Verrax, J.; Dejeans, N.; Taper, H.; Calderon, P. B. Menadione reduction by pharmacological doses of ascorbate induces an oxidative stress that kills breast cancer cells. *Int. J. Toxicol.* **2009,** 28, 33-42.
30. Allen, L.-A. H.; McCaffrey, R. L. To activate or not to activate: distinct strategies used by Helicobacter pylori and Francisella tularensis to modulate the NADPH oxidase and survive in human neutrophils. *Immunol. Rev.* **2007,** 219, 103-117.
31. Brumaghim, J. L.; Li, Y.; Henle, E.; Linn, S. Effects of Hydrogen Peroxide upon Nicotinamide Nucleotide Metabolism in *Escherichia Coli*. *J. Biol. Chem.* **2003,** 278, 42495-42504.
32. Kumar, S. R.; Imlay, J. A. How Escherichia coli tolerates profuse hydrogen peroxide formation by a catabolic pathway. *J. Bacteriol.,* **2013,** 2, 4659-4679.

33. CLSI. Performance standards for antimicrobial suceptibility testing; twenty second supplement,. *National Committee for Clinical Laboratory Standards (NCCLS), M100-22* **2012,** 32.

34. Fang, F. C. Antibiotic and ROS linkage questioned. *Nat. Biotechnol.*, **2013,** 31, 415-416.

CHAPTER 4: SYNTHESIS AND CHARACTERIZATION OF THIOL-TRIGGERED REACTIVE OXYGEN SPECIES (ROS) GENERATORS AND ANTIBACTRERIAL STUDIES

4.1. Introduction:

In Chapter 2, we developed small molecule based ROS generators for enhancement of intracellular ROS and antibacterial applications. These ROS generators were found to inhibit the growth of *Mycobacterium tuberculosis* with a minimum inhibitory concentration of <1 μg/mL, whereas other Gram positive and Gram negative bacteria were resistant to the enhanced ROS environment. One of the highly efficient ROS generators, **4** (Chapter 2.1) was treated with *E. coli*, a Gram negative bacterium, and *Staphylococcus aureus*, a Gram positive bacterium, where no significant effect on the bacterial growth was observed even at 100 μM concentrations of **4**. The possibility of **4** to decompose in extracellular medium to generate ROS is a concern. Hence, an intracellular ROS generator selectively activated inside bacteria to generate ROS could be better suited for antibacterial applications.

In Chapter 3, a bacterial nitroreductase activated ROS generator **54** was shown to permeate bacterial cells and triggered only inside bacteria to enhance intracellular ROS. However, an enhancement of intrabacterial ROS using **54** (100μM) in *E. coli* was appeared ineffective in inhibiting bacterial growth. Thus, enhancing intracellular ROS alone does not significantly inhibit bacterial growth. Bacteria have developed a strong antioxidant system to tolerate enhanced intracellular ROS production. Reduced thiols (RSH) such as cysteine (Cys) and glutathione (GSH) are the main small molecule based antioxidants ubiquitous in cells (Figure 4.1). They maintain the intracellular redox homeostasis and during enhanced ROS conditions these RSH react with ROS to suppress the oxidative stress induced and generate oxidized thiol dimers, RS-SR (Cys-Cys or GS-SG). The glutathione dimer, GS-SG is found in low concentrations in comparison to its reduced counterpart (GSH) in cells, where GSH: GS-SG acts as redox buffer and the ratio is found in the range of 1:1 to 3:1.[1,2] Enhanced production of ROS in cells could elevate the levels of GS-SG and induce stress inside cells. Hence, the excess GS-SG is reduced by enzymes such as

thioredoxin reductase or glutathione reductase to restore the levels of GSH:GS-SG in cells.[2] Thus, maintaining the ratio of RSH: RS-SR is vital for cellular functions and depleting the reduced thiol levels inside bacteria could disturb the redox homeostasis. This process would result in increased cellular stress that could lead to cell death.

Figure 4.1. Low molecular weight reduced thiols found in cells

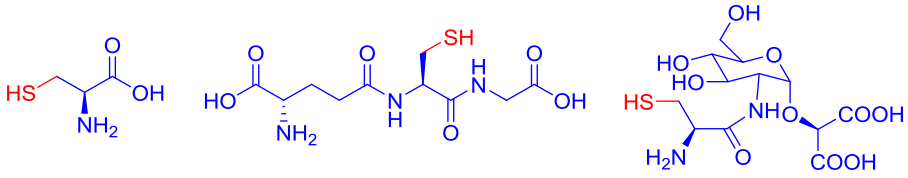

Cysteine Glutathione Bacillithiol

Fosfomycin is an epoxide containing polar small molecule and a broad spectrum antibiotic that has been used to treat a number of bacterial infections (Figure 4.2).[3] Its mechanism of action involves inhibition of a cell wall biosynthetic enzyme UDP-*N*-acetylglycosamine-1-carboxyvinyltransferase (*MurA*) through a covalent modification. Another epoxide based small molecule, terreic acid is a 2-methyl-3-hydroxy-5,6-dihydroepoxybenzoquinone (Figure 4.2). Terreic acid is a fungal metabolite, with antibiotic properties, is also found to modify the same target, *MurA* for its bacterial inhibitory action. In addition to its targets, fosfomycin is also reported to deplete intracellular bacterial thiols such as bacillithiol (BSH) (Figure 4.1). BSH is a low molecular weight thiol found in *Bacillus* and *Staphylococcus* bacteria.[4,5] A covalent modification of BSH by fosfomycin might lead to depleted intracellular thiol levels which in turn could induce oxidative stress.

Figure 4.2. Structure of thiol alkylating epoxides

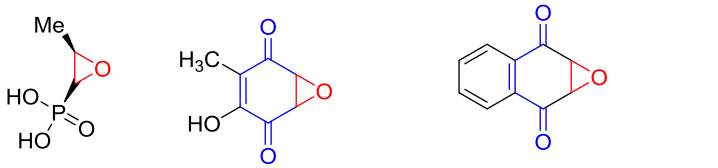

Fosfomycin Terreic acid 2,3-epoxy-1,4-naphthoquinone (**74**)

Since ROS generation alone does not appear be sufficient to inhibit the bacterial growth as inferred from our earlier studies (Chapter 2 and 3), we hypothesized that a design for depleting intracellular thiol and concomitantly enhancing intracellular ROS could be useful for targeting bacteria. Thus, 2,3-epoxy-1,4-naphthoquinone could be a

model scaffold, which would get activated by a thiol to generate ROS. 1,4-Naphthoquinone-based epoxides (NQE) are constituents of a number of natural products with medicinal properties.[6,7] For example, 2,3-epoxysesamone[8,9] and frenolicin[10-17] have shown anti-bacterial, anti-fungal and/or anti-proliferative activities (Figure 4.3).

Figure 4.3. Some naturally occurring 1,4-naphthoquinone-based epoxides

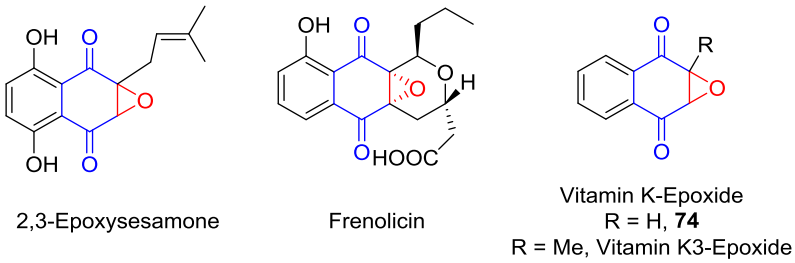

A reaction of 2,3-epoxy-1,4-naphthoquinones with biologically relevant nucleophiles including GSH might contribute to their medicinal properties.[18] For example, 2,3-epoxy-2,3-dihydro-1,4-naphthoquinone (**74**) is a target for reaction with nucleophiles such as thiols.[19] Furthermore, under aerobic conditions, addition of GSH to **74** has been shown to generate ROS.[19] Recently, Vitamin K3-epoxide (Figure 4.3) was shown to generate ROS intracellularly to induce oxidative stress in human glioma cells.[20]

In our study, we proposed to synthesize a series of 2,3-epoxy-1,4-naphthoquinones and evaluate their reactivity with biologically relevant nucleophiles, their ROS generation profiles, and their ability to inhibit bacterial growth. We hypothesized that the propensity of epoxides to react with nucleophiles for ROS generation could be modulated by systematic variation of substituents around the epoxide as well as aryl ring of 2,3-epoxy-1,4-naphthoquinone (Figure 4.4). An enhanced reactivity of the epoxide with nucleophiles is expected for compounds with an electron withdrawing group in proximity to the epoxide functionality of 2,3-epoxy-1,4-naphthoquinone and perhaps affect ROS generation; conversely, a diminished reactivity is possible with an electron-donating group. A series of compounds with a range of H_2O_2 generation profiles would allow us to study the effects of modulating rates of ROS generation and their antibacterial efficiency.

Figure 4.4. Proposed scaffold for systematically modulating epoxide reactivity of quinone epoxides. R = Electron withdrawing or donating groups.

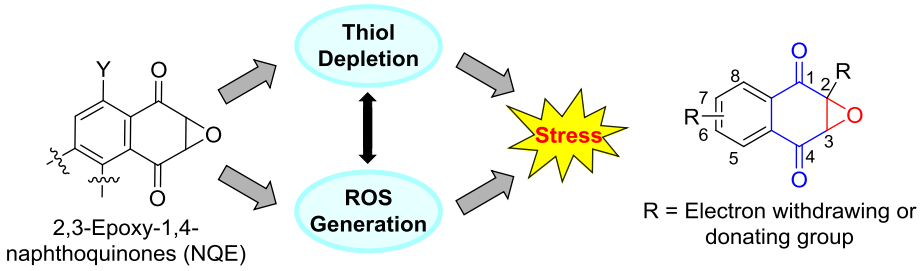

4.2. Results and Discussion:

4.2.1. Synthesis and characterization:

Epoxidation of substituted 1,4-naphthoquinones produced corresponding 2,3-epoxy-1,4-naphthoquinones.[21] Nitration of 1,4-naphthoquinone (**20**) gave 5-nitro-1,4-naphthoquinone (**57**) and 6-nitro-1,4-naphthoquinone (**58**) in 78% and 9% yields, respectively (Scheme 4.1).[22,23] An electron donating amino group on the aryl ring could be obtained by reduction of **57** with Sn/HCl to afford **59** in a nearly quantitative yield (Scheme 4.1).[24]

Scheme 4.1. Synthesis of **57** – **59**.

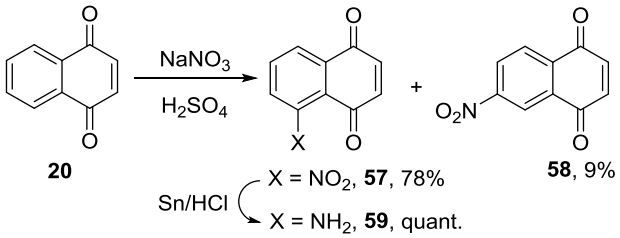

5-Hydroxy-1,4-naphthoquinone (Juglone, **21**), which was synthesized using a reported reaction and subjected to a silver oxide (Ag_2O) mediated alkylation with bromoethane produced **60** in 87% yield (Table 4.1, entry 1).[25] Under similar conditions, a reaction of **21** with benzyl bromides produced **23** and **61** in 98% and 96% yields, respectively (Table 4.1, entries 2-3). Menadione or Vitamin K3 (**62**) and plumbagin (**63**) were obtained from commercial sources. Benzylation of **63** produced **64** in 99% yield (Table 4.1, entry 4).

Table 4.1. Synthesis of derivatives of Juglone (**21**) and Plumbagin (**63**)

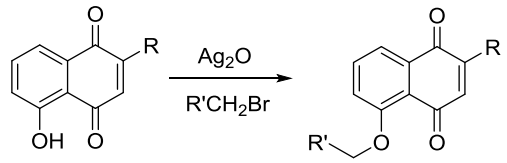

R = H, 21
R = Me, 63

23, 60, 61, 64

Entry	Quinone	R	R′	Product	Yield
1	**21**	H	Me	**60**	87
2	**21**	H	Ph	**23**	98
3	**21**	H	4-CF_3Ph	**61**	96
4	**63**	Me	Ph	**64**	99

Table 4.2. Synthesis of 2-aryl-1,4-naphtoquinones **66** - **73**

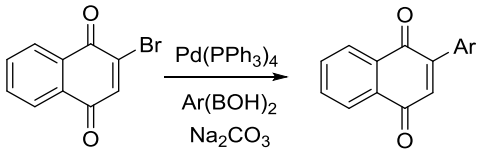

66-73

Entry	Ar	Product	Time (h)	Yield (%)
1	Ph	**66**	1.5	90
2	3-NO_2Ph	**67**	12	28
3	4-AcPh	**68**	10	43
4	4-FPh	**69**	5	52
5	4-MePh	**70**	10	78
6	2-OMePh	**71**	24	82
7	3-OMePh	**72**	7	93
8	4-OMePh	**73**	7	81

Next, a Pd-catalyzed Suzuki coupling of 2-bromo-1,4-naphthoquinone with phenylboronic acid was carried out to afford 2-phenyl-1,4-naphthoquinone (**66**) in 90% yield (Table 4.2, entry 1).[26] Under similar reaction conditions, arylboronic acids

containing electron withdrawing groups with 2-bromo-1,4-naphthoquinone produced the desired products **67**-**69** in diminished yields in comparison with **66** (28-52%, Table 4.2, entries 2-4).[26-28] Compounds **70**-**73** with electron donating substituents on the aryl ring were isolated in yields ranging from 78-93% (Table 4.2, entries 5-8), which were comparable or better than the yield of **66** under similar reaction conditions.[26-28]

A sodium hypochlorite mediated epoxidation of **20** produced the corresponding epoxide **74** in 88% yield (Table 4.3, entry 1).[29] Compounds **21**, **57**-**61** reacted completely in 30 min upon treatment with hypochlorite to produce the epoxides **75**-**81** in moderate to good yields (Table 4.3, entries 2-8).[30,31] X-ray diffraction analysis of **78** revealed the presence of intramolecular H-bonding between 5-hydroxyl group and 4-carbonyl group (Figure 4.5A).

Figure 4.5. X-ray diffraction analysis of **78** (A) and **92** (B)

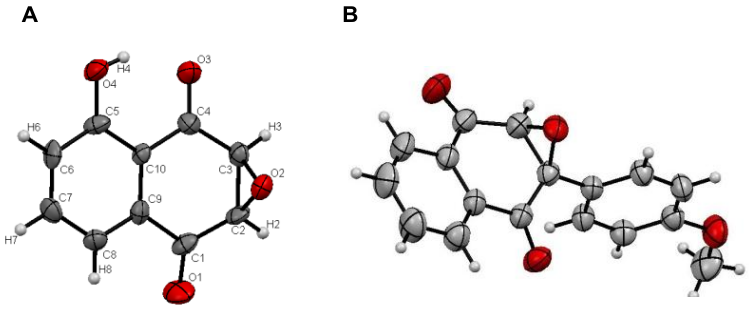

Epoxidation of quinones **62**-**64** with hypochlorite afforded the corresponding products **82**-**84** in yields ranging from 45-89% (Table 4.3, entries 9-11). A slow reaction of 2-phenyl-1,4-naphthoquinone with sodium hypochlorite (120 min) was observed in comparison with all other compounds prepared in this study (Table 4.3, entry 12). Other 2-aryl epoxides were synthesized in yields ranging from 52-93% (Table 4.3, entries 12-19). Additional evidence for the structure of **92** was obtained by X-ray crystallographic analysis of this compound (Figure 4.5B).

4.2.2. Stability studies of 74 with biologically relevant nucleophiles in buffer:

The ability of compound **74** to react with various biologically relevant nucleophiles in pH 7.4 buffer was examined following its synthesis. Initially a reaction of **74** with thiols such as cysteine (Cys) and glutathione (GSH) showed nearly 70% of

decomposition within 5 min (Figure 4.6). The reactivity of **74** with GSH was consistent with previous reports.[19] Compound **74** was stable and unreactive towards other amino acids (10 equiv) tested such as glycine, alanine, serine, methionine, arginine and tyrosine with >90% of **74** remaining after 7 h. No significant decomposition was observed in the presence of 10 equiv of nucleobases and the epoxide was nearly completely recovered after 24 h. Taken together, these results suggested that **74** was highly selective towards reaction with thiols.

4.2.3. Stability studies of compounds with glutathione in buffer:

Further, we examined the reactivity of other epoxides prepared in this study with GSH (1 equiv) under similar conditions used for **74**. A range of reactivities for the 2,3-epoxy-2,3-dihydro-1,4-naphthoquinones **75-81** with GSH was recorded under these conditions (Figure 4.6). An electron withdrawing nitro group has enhanced the reaction rate with GSH (Figure 4.6) as predicted while electron donating groups reduced the reaction rate. In the case of **75**, 12% remained after 5 min while 6% of **76** remained during the same time period (Table 4.3, entries 2-3).

A diminished reactivity for compounds with electron donating group is expected. For example, 5-amino derivative **77**, after 5 min of reaction 68% still remained, which was slower than **74** (Table 4.3, entry 4). Reactivity of Juglone derivative **78** (26% remained after 5 min) was similar to **74** suggesting that the hydroxyl group had no major effect on modulating the rate of epoxide opening (Table 4.3, entry 5). On the other hand, O-alkylated juglone derivatives with ethyl or benzyl groups (**79**, **80** or **81**) showed a diminished reactivity with GSH in comparison to **78** or **74**. Intramolecular H-bonding in **74** might have accelerated epoxide opening by GSH (Table 4.3, entries 6-8). Thus, these results suggested that although remote, substitution on the aryl ring appeared to have a significant effect on the rate of reactivity of the epoxide with thiols.

Table 4.3. Synthesis of 2,3-epoxy-1,4-naphthoquinones **74-92**

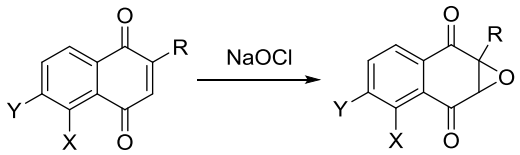

74-92

Entry	Quinone	Time (min)	Epoxide	X	Y	R	Yield (%)
1	**20**	5	**74**	H	H	H	88
2	**57**	20	**75**	NO_2	H	H	67
3	**58**	15	**76**	H	NO_2	H	88
4	**59**	30	**77**	NH_2	H	H	43
5	**21**	5	**78**	OH	H	H	68
6	**60**	25	**79**	OEt	H	H	68
7	**23**	15	**80**	OBn	H	H	81
8	**61**	35	**81**	$OCH_2(4\text{-}CF_3Ph)$	H	H	82
9	**62**	15	**82**	H	H	Me	89
10	**63**	30	**83**	OH	H	Me	65
11	**64**	60	**84**	OBn	H	Me	45
12	**66**	120	**85**	H	H	Ph	97
13	**67**	25	**86**	H	H	$3\text{-}NO_2Ph$	81
14	**68**	30	**87**	H	H	4-AcPh	74
15	**69**	20	**88**	H	H	4-FPh	52
16	**70**	15	**89**	H	H	4-Me	78
17	**71**	40	**90**	H	H	2-OMe	82
18	**72**	25	**91**	H	H	3-OMe	93
19	**73**	45	**92**	H	H	4-OMe	81

A decreased reactivity with GSH was observed with an introduction of a methyl group at the 2-position of 2,3-epoxy-1,4-naphthoquinone (as in **82**) (Table 4.3, entry 9; Figure 4.6). This result was consistent with previous reports where the rate of reaction of **82** with GSH was found to be diminished in comparison with **74**. No major effect was observed with an addition of a 5-hydroxyl (**83**) group to Vitamin

K3-epoxide on reactivity with thiols (Table 4.3, entry 10). However, the presence of a 5-benzyloxy group (**84**) resulted in a diminution in reactivity with GSH and 94% of **84** remaining after 5 min (Table 4.3, entry11). The reactivity of 2-aryl-2,3-epoxy-1,4-naphthoquinone with GSH was also studied under similar conditions. Reaction of **85** with GSH in 5 min was comparable with that of **82** under similar reaction conditions (Table 4, entry 12). An increased reactivity was seen in the case of electron withdrawing substituents on the aryl ring (**86-88**, Table 4.3, entries 13-15). Electron donating groups did not have a major effect on the reactivity of 2-aryl epoxides with thiols (**89-92**, Table 4.3, entries 16-19).

Figure 4.6. Reactivity of 2,3-epoxy-1,4-naphthoquinones **74-84** towards thiols as measured by % compound remaining after 5 min of reaction with GSH (1 equiv) in pH 7.4 buffer.

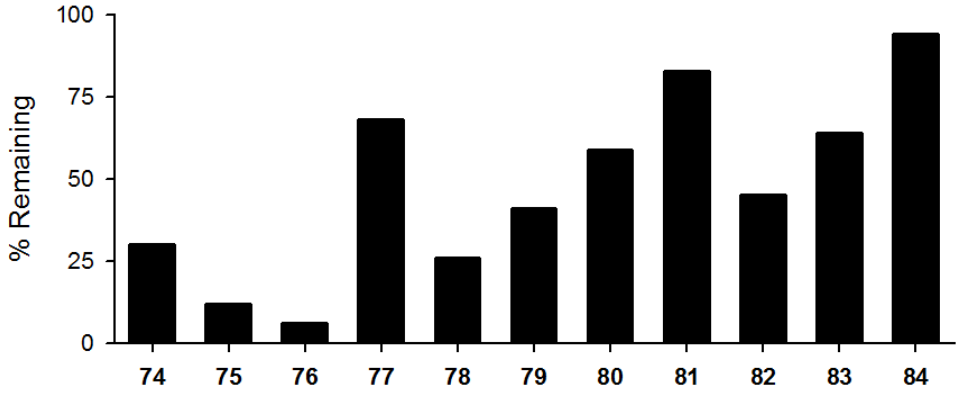

4.2.4. Studies of ROS generation from epoxides 74-92:

Epoxide ring opening of **74** with glutathione leads to formation of **74b**, which then undergoes a keto-enol tautomerism to form the 1,4-diol **74c**. Subsequent reaction of **74c** with molecular oxygen generates ROS and **74d** as a major organic product. (Scheme 4.2).[19] Xylenol orange based colorimetric assay was used to estimate the amount of H_2O_2 generated from the epoxides **74-92**. Compound **74** (100 μM) in the presence of 5 equiv GSH in aerobic pH 7.4 buffer produced 4.4 μM of H_2O_2 during 30 min (Table 4.4, entry 1).[32] An enhanced yield of H_2O_2 (5.2 μM) was observed with introduction of an electron withdrawing nitro substituent **75** (Table 4.4, entry 2). Under similar conditions, the 6-nitro derivative **76** had produced 8.34 μM of H_2O_2,

which was also the fastest in reacting with GSH amongst the analogues tested (Table 4.4, entry 3). A diminished level of H_2O_2 generation was observed with **77** containing an electron-donating amino group in comparison with **74** (Table 4.4, entry 4).

Scheme 4.2. 2,3-Epoxy-2,3-dihydro-1,4-naphthoquinone reacts with thiols in the presence of oxygen to generate peroxide.

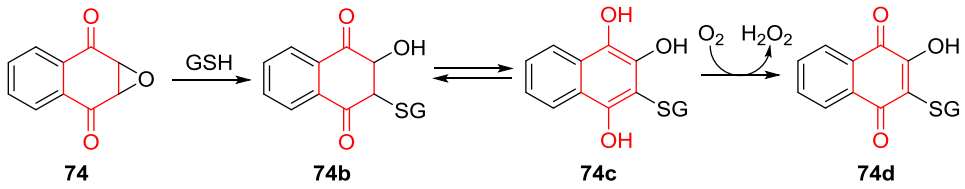

The juglone derivative **78** formed 5.64 μM of peroxide in the same time period, which was comparable with peroxide generated from **74** under similar conditions (Table 4.4, entry 5). Derivatives **79-81** with electron donating ether substituents produced negligible amounts of peroxide (Table 4.4, entries 6-8). Taken together, these results suggested that thiol-mediated peroxide generation profiles from 2,3-epoxy-2,3-dihydro-1,4-naphthoquinones can be modulated by changing substituents on the aryl ring. Rationalizing the differences in amounts of peroxide generated require further characterization and study. However, a possible contributor to differences in peroxide levels would be the reactivity of intermediate **74c** with oxygen, which might be affected by steric and electronic effects of the aryl ring (Scheme 4.2) Electron withdrawing groups on 2,3-epoxy-1,4-naphthoquinone were found to enhance the reactivity with thiol consequently increased ROS generation, conversely, electron releasing groups were found to diminish reactivity with thiol and ROS generation.

Addition of GSH to **82** would produce the thiolated adduct **82b** and elimination of water from **82b** produces **82c** as a major organic product (Scheme 4.3).[19,33] For a keto tautomer to undergo enolization to give the enol tautomer α-hydrogen is necessary. Due to the absence of α-hydrogen in **82b**, a buffer mediated enolization in **82b** is disfavoured, hence no ROS generation is expected from **82**. Under similar conditions only negligible amount of H_2O_2 generation was observed with **82** in comparison with **74**.[19] Similar results were observed with **83** and **84** in pH 7.4 phosphate buffer after 30 min of incubation with GSH. (Table 4.4, entry 9).

Table 4.4. Glutathione-mediated decomposition of 2,3-epoxy-1,4-naphthoquinones (**74**-**92**) and H_2O_2 yield upon reaction with GSH.

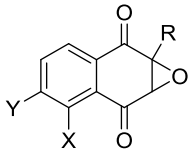

74 - 92

Entry	Compd	X	Y	R	% Rem.[a]	H_2O_2 (μM)[b]
1	**74**	H	H	H	30	4.40
2	**75**	NO_2	H	H	12	5.20
3	**76**	H	NO_2	H	6	8.34
4	**77**	NH_2	H	H	68	1.68
5	**78**	OH	H	H	26	5.64
6	**79**	OEt	H	H	41	1.68
7	**80**	OBn	H	H	59	1.60
8	**81**	OCH_2(4-CF_3Ph)	H	H	83	1.68
9	**82**	H	H	Me	45	1.52
10	**83**	OH	H	Me	64	1.60
11	**84**	OBn	H	Me	94	1.58
12	**85**	H	H	Ph	44	1.44
13	**86**	H	H	3-NO_2Ph	29	1.40
14	**87**	H	H	4-AcPh	16	1.36
15	**88**	H	H	4-FPh	32	1.36
16	**89**	H	H	4-Me	66	1.48
17	**90**	H	H	2-OMe	54	1.28
18	**91**	H	H	3-OMe	43	1.46
19	**92**	H	H	4-OMe	37	1.40

[a]Reaction of the various compounds with 1 equiv GSH were conducted in pH 7.4 and % compound remaining after 5 min was estimated using HPLC analysis. Values represented are an average of two independent runs. [b]compounds (100 μM) were reacted with 5 equiv GSH in the presence of oxygen and H_2O_2 formed after 30 min. of reaction was estimated using a xylenol orange-based colorimetric assay.

Scheme 4.3. 2-Methyl-2,3-epoxy-1,4-naphthoquinone (**82**) reacts with thiols to produce 2-methyl-3-glutathionyl-1,4-naphthoquinone (**82c**).

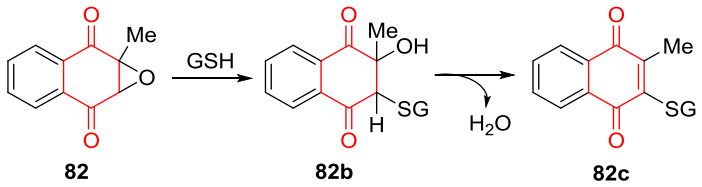

Furthermore, in all the cases tested, only a negligible amount of H_2O_2 was produced for compounds with a substituent on the epoxide ring, irrespective of nature of the substituent (Table 4.4, entries 10-19). Thus, unlike compound **74-81** where a thiol alkylation and subsequent ROS generation is possible, for compounds **82-92** (2-substituted 2,3-epoxy-1,4-naphthoquinones) any biological effects might be primarily due to reactions with thiols.

4.2.5. Antibacterial studies:

Staphylococcus aureus (*S. aureus*) is among the most prevalent Gram-positive pathogens predominantly causing invasive skin infections.[34] This pathogen has acquired resistance to most frontline antibiotics including those belonging to the methicillin class.[35,36] Globally, infections caused by methicillin-resistant strains of *S. aureus* (MRSA) is on the rise but only a limited number of antibiotics are in development.[37] Hence, new strategies to target MRSA are in urgent need. Intracellular reducing environment inside cells is maintained using BSH in *S. aureus.* Attenuating anti-oxidant systems such as BSH enhances the stress inside cells and has been shown to sensitize *S. aureus*.[5] The clinical use of Fosfomycin is wide spread due to its excellent bactericidal effects against multi-drug resistant strains.[3,38] A recent study shows that of >400 clinical isolates of *S. aureus* including MRSA, 99.3% were found to be susceptible to Fosfomycin.[39] Hence, covalent modification of thiols could be a possible strategy to develop new MRSA inhibitors.

Having synthesized a series of thiol activated ROS generators, we tested the ability of these ROS generators to inhibit methicillin sensitive (MSSA) and resistant strains of *S. aureus* (MRSA). Antibacterial testing was performed on MSSA and MRSA with only selective compounds, such as **74-76** and **78**. These were the fastest in reacting with thiols and also the best ROS generators among the analogues tested. We found a

minimum inhibitory concentration of 16 μg/mL for **74**-**76** and **78** against MSSA and MRSA (Table 4.5).

Table 4.5. Antibacterial activity of **74**-**76** and **78** against MSSA and MRSA

Entry	Compd	% MIC μg/mL[a]	
		MSSA	MRSA
1	**74**	16	16
2	**75**	16	16
3	**76**	16	16
4	**78**	16	16

[a]Minimum inhibitory concentration (MIC) is the lowest concentration required to inhibit 99% of bacterial growth MSSA = *Staphylococcus aureus* ATCC 29213, MRSA = *Staphylococcus aureus* ATCC 33591; MICs were provided by Vitas Pharma.

The difference in the reactivity of these compounds with thiol as well as ROS generation did not have an effect on their inhibitory potential against *S. aureus*. Although these compounds could completely inhibit *S. aureus* only at 16 μg/mL concentration, this is a significant improvement, since enhancement of intracellular ROS alone did not have an impact on the bacterial growth as learned from Chapters 2 and 3.

4.3 Revised design of Indole based thiol activated ROS generators:

4.3.1. Revised design of Indole-epoxide scaffold (IND-NQE):

Preliminary results have shown that thiol depletion in conjunction with proposed ROS generation was an effective strategy to inhibit drug resistant Gram positive bacterium *S. aureus*. We have revised the design in order to improve the antibacterial efficiency. An indole based scaffold was preferred to introduce a structural handle for fine tuning thiol reactivity and ROS generation of the compounds. The ability of 2,3-epoxy-1,4-naphthoquinones to react with thiols to generate ROS is well documented.[40,41] Fusing this scaffold with an indole, which is considered as a "privileged" scaffold, might lead to improved pharmacological properties (Scheme 4.4).[42] Furthermore, reactivity of thiols to the epoxide is predicted in part to affect antimicrobial activity and hence, the presence of three structural handles (R, X and Y) might be useful in modulating thiol reactivity and as a consequence MRSA inhibitory potency (Scheme 4.4).

Scheme 4.4. Proposed indole-based 2,3-epoxy-1,4-naphthoquinone scaffolds

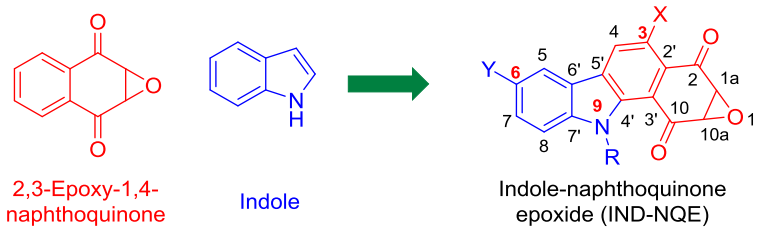

The proposed IND-NQE analogues were synthesized in three steps starting from substituted indole-3-carboxaldehydes.

4.3.2. Synthesis and characterization:

Initially, 3-vinyl-indole was synthesized by Wittig olefination of indole-3-carboxaldehyde with methyltriphenylphosphonium bromide, which was not isolated but subjected to Diels-Alder cycloaddition reaction with 1,4-benzoquinone followed by aerobic oxidation in ethanol gave **121** in 64% yield (Table 4.6, entry 1).

Table 4.6. Synthesis of **121-130**

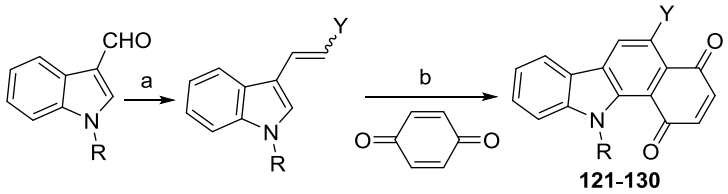

Entry	R	Y	Product	% Yield[c]
1	H	H	**121**	64
2	Et	H	**122**	18
3	^{i}Pr	H	**123**	23
4	Allyl	H	**124**	10
5	Bn	H	**125**	14
6	H	Me	**126**	14
7	Et	Me	**127**	13
8	^{i}Pr	Me	**128**	11[d]
9	Allyl	Me	**129**	21
10	Bn	Me	**130**	25

[a]Conditions: YCH_2PPh_3Br, ^{n}BuLi, THF; [b]Conditions: EtOH, RT, overnight; [c]isolated yield; [d]Crude yield (>80% purity by ^{1}H NMR analysis)

Next, a sodium hypochlorite mediated epoxidation of **121** produced the desired epoxide **135** (Table 4.7, entry 1) in 94% yield. Following similar synthetic strategy: Wittig followed by Diels-Alder methodology, indole-quinones with various *N*-alkyl substituents (**122-125**) were synthesized (Table 4.6, entries 2-5).

Epoxidation of these quinones gave the corresponding epoxides in yield ranging from 94-96% (Table 4.7, entries 2-5). Next, substituent Y was changed during the Wittig reaction by the use of ethyltriphenylphosphonium bromide and **126-130** where Y = Me were isolated in 11-25% yields (Table 4.6, entries 6-10). Subsequent epoxidation of these compounds gave the corresponding epoxides **140-144** in 71-95% yields (Table 4.7, entries 6-10).

Table 4.7. Synthesis of epoxides **135-144**

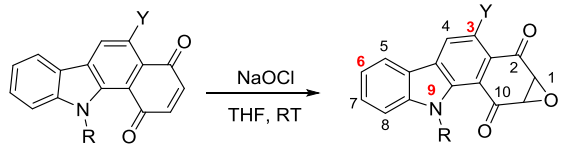

121-130 **135-144**

Entry	R	Y	Product	% Yield
1	H	H	**135**	94
2	Et	H	**136**	96
3	^{i}Pr	H	**137**	96
4	Allyl	H	**138**	94
5	Bn	H	**139**	96
6	H	Me	**140**	85
7	Et	Me	**141**	71
8	^{i}Pr	Me	**142**	84
9	Allyl	Me	**143**	95
10	Bn	Me	**144**	88

X-ray diffraction analysis of crystalline **138** and **143** showed that the quinone ring assumed a boat-like conformation with the remaining aromatic rings being nearly planar (Figure 4.8). The approach of the nucleophile must occur from the side

opposite to the epoxide ring where it might encounter a steric barrier due to the carbonyls at the C-2 and C-10 positions.

Figure 4.7. X-Ray diffraction analysis of (A) **138** and (B) **143**

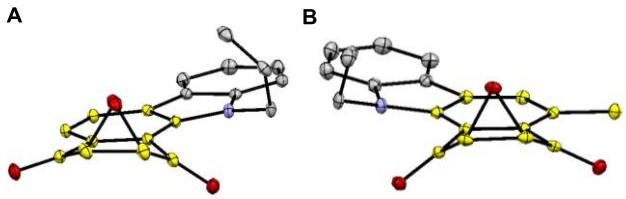

4.3.3. Stability studies on 135 – 144 with cysteine in pH 7.4 buffer:

Reactivity of the compounds with thiol was examined by reacting compounds **135-144** with cysteine (10 equiv) at 37 ºC in pH 7.4 phosphate buffer. The reaction mixture was analyzed by HPLC after 60 min of incubation to estimate amount of epoxide remaining (%) was determined.

Figure 4.8. Comparison of data obtained for analogues **135-139** and their respective homologues **140-144**: (A) % remaining upon reaction with cysteine (10 equiv) determined by HPLC analysis of the reaction mixture after 1 h; (B) Extracellular hydrogen peroxide estimated after incubation of the compound at 50 μM with *S. aureus* for 1 h.

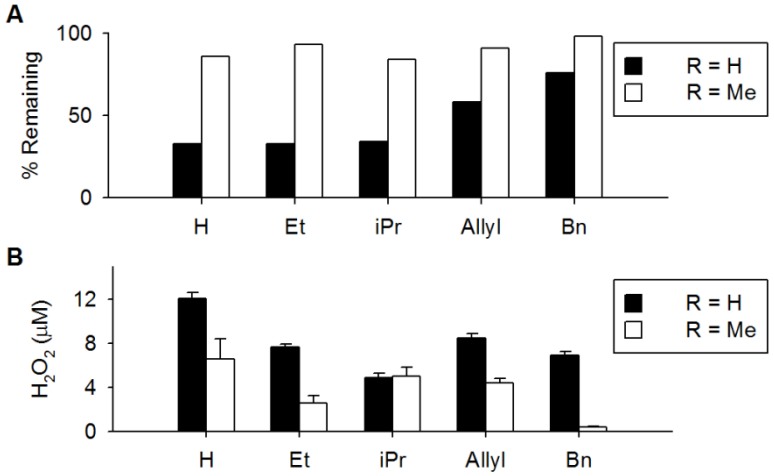

For **135** in buffer mediated reaction with cysteine, 33% remaining after 60 min was quantified. A nearly comparable level of decomposition for **136** and **137** (33 and 34% respectively) was observed. Reactivity of *N*-allyl derivative **138** was slightly on the lower side with 58% remaining in comparison with **135**. Under similar conditions the introduction of benzyl substituent (**139**) resulted in decreased reactivity with 76% of

compound remaining. Our data showed that the analogues with Y = H have a range of reactivity with cysteine (33-76% remaining; Table 4.8, entries 1-5).

It appears that a larger substituent on the nitrogen of indole led to decreased reactivity of the epoxide ring. However, the effect of introducing a methyl substituent at the C-3 position resulted in diminished reactivity with >80% remaining in all cases tested (Table 4.8, entries 6-10). The trend in reactivity was apparent during comparison of the two groups with the same "R" at the *N*-position was identical (Figure 4.9A). Thus, our data suggests that increasing sterics on the C-3 diminishes reactivity of the epoxide towards nucleophilic attack. Although the precise structural basis for the hindrance remains to be completely determined, it appears that a structural tool for controlling the reactivity with thiols is possible.[43,44]

4.3.4. Extracellular ROS generation from 135 – 144 in S. aureus:

The ability of compounds **135-144** to permeate cells and react with intracellular thiols to generate ROS was assessed by measurement of extracellular hydrogen peroxide. We have incubated compounds with *S. aureus* for 60 min and quantified extracellular H_2O_2[45-47] using an Amplex Red-based fluorescence assay.[48] There was no particular trend in H_2O_2 production observed with **135** – **139** and majority of compounds when treated at 25 μM were found to generate in excess of 5 μM of H_2O_2 (Table 4.8, entries 1-5). Similar to thiol reactivity, it was found that compounds with Y = H (**135**-**139**) had enhanced ROS generating capability in comparison with the Y = Me (**140**-**144**) (Table 4.8, entries 6-10, Figure 4.9B) suggesting that increased reactivity with a thiol in a test-tube correlated well with enhanced ROS production in bacteria.

4.3.5. Antibacterial studies:

The inhibitory potential of these compounds against methicillin-sensitive *S. aureus* (MSSA) was next tested. The minimum inhibitory concentrations (MICs) for **135-139** were in the range of 0.5-4 μg/mL (Table 4.8, entries 1-5). Compound **137** was identified as highly efficient inhibitor with an MIC of 0.5 μg/mL with MSSA. An MIC of 4 μg/mL was obtained for **135** and three compounds (**136**, **138** and **139**) were effective at 2 μg/mL in inhibiting MSSA. Analogues with methyl substitution at the 3-position (Y = Me), which had diminished reactivity with thiols and poor ROS generating capability, were also found to be poor inhibitors of MSSA at the highest

concentrations of 32 μg/mL tested (Table 4.8, entries 6-10). Thus, it appears that both thiol reactivity and ROS generation are important for the compound to be a good inhibitor of MSSA (Table 4.8, entries 1-5).

Table 4.8. Results of thiol-mediated decomposition and antibacterial activity against MSSA and MRSA

Entry	Compd	% Remaining[a]	H_2O_2 (μM)[b]	% MIC μg/m[c]	
				MSSA	MRSA
1	**135**	33	12.1	4	8
2	**136**	33	7.1	2	1
3	**137**	34	4.9	0.5	0.25
4	**138**	58	8.5	2	2
5	**139**	76	6.7	2	2
6	**140**	86	6.6	>32	>32
7	**141**	93	2.6	>32	4
8	**142**	84	5.0	>32	16
9	**143**	91	4.4	>32	>32
10	**144**	98	0.4	>32	>32
11	**145**	29	4.0	>32	>32
12	**146**	27	4.0	>32	>32
13	**147**	43	2.4	>32	>32
14	**148**	38	5.2	2	2
15		Vancomycin		0.5	1.0

[a]Reaction of the epoxide with 10 equiv cys was conducted in pH 7.4 and % compound remaining after 60 min was estimated using HPLC analysis. [b]Extracellular H_2O_2 measured using Amplex Red® assay after 60 min incubation with *S. aureus*. [c]Minimum inhibitory concentration (MIC) is the lowest concentration required to inhibit 99% of bacterial growth MSSA = *Staphylococcus aureus* ATCC 29213, MRSA = *Staphylococcus aureus* ATCC 33591; MICs were obtained from Vitas Pharma.

When this library (**135**-**144**) was tested against methicillin resistant strain of *S. aureus*, MRSA 33591 (Table 4.8, entries 1-5) four compounds (**136**-**139**) were found

to have excellent MICs ≤ 2 μg/mL (Table 4.8, entries 2-5) and the best inhibitor was found to be **137** with MIC of 0.25 μg/mL (Table 4.8, entry 3), which was better than one of the commercially used antibiotics for the treatment of MRSA infections, Vancomycin (Table 4.8, entry 15). Similar to MSSA, for compounds Y = Me (**140** – **144**) observed MICs were greater than 8 μg/mL, further insisting that reactivity of compounds with thiol and ROS generation together plays an important role in inhibiting bacterial growth (Table 4.8, entries 6-10).

4.3.6. Analogues of 137 and their antibacterial studies:

Among the compounds tested in this study, highly potent inhibitor of MRSA was *N*-isopropyl derivative of IND-NQE (**137**). To study the effect of varying substitutions at the 6-position of **137**, compounds **145**-**148** were synthesized. Starting from indole-3-carboxaldehyde (**103**-**106**), a Wittig olefination was carried out with methyltriphenylphosphonium bromide to obtain 3-vinylindoles followed by a [4+2] cycloaddition reaction with 1,4-benzoquinone produced the quinones **131**-**134** (Table 4.9, entries 1-4). The crude quinones were epoxidized to obtain **145**-**148** with two step overall yields ranging from 36 – 88%. (Table 4.10, entries 1-4). The 6-position is located "*para*" to the nitrogen of indole and hence, may have an effect on changing availability of the lone pair, which is conjugated to the carbonyl of the quinone.

Table 4.9. Synthesis of **131**-**134**

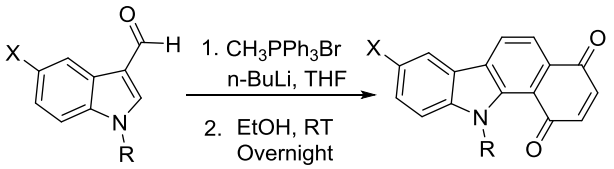

103-106 **131-134**

Entry	R	X	Reactant	Product	Yield[a]
1	^{i}Pr	Br	**103**	**131**	30
2	^{i}Pr	CN	**104**	**132**	13[b]
3	^{i}Pr	F	**105**	**133**	22
4	^{i}Pr	OMe	**106**	**134**	60

[a]Crude yield (>80% purity determined by ^{1}H NMR analysis); [b]Isolated yield.

The analogues **145-148** were found to react with thiols and also generated H_2O_2 when incubated with *S. aureus* (Table 4.8, entries 11-14). There was no clear effect of changing substituents on the 6-position suggesting that the lone-pair on the nitrogen did not significantly affect epoxide reactivity or ROS generating ability. When tested for bacterial growth inhibitory activity, among the *N*-isopropyl derivatives (Table 4.8, entries 11-14) only **148** was found to be a good MRSA inhibitor (Table 4.8, entry 14), and remaining compounds **145-147** were found to be inactive (Table 4.8, entries 11-13), reason for which is not clear and needs further investigation. Thus, our structure-activity relationship study shows that substitution at the 3-position resulted in diminished thiol reactivity, lower ROS generation and poor inhibitory activity while no clear trend could be found by changing substitution at the 6-position. Nevertheless, our data reveal **137** as the best MRSA inhibitor among analogues tested and this compound was identified as the lead for further studies.

Table 4.10. Synthesis of **145-148**

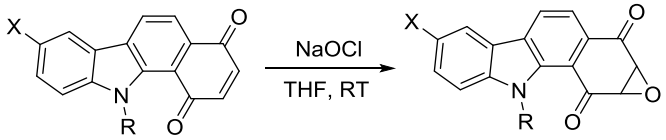

131-134 **145-148**

Entry	R	X	Reactant	Product	Yield[a]
1	^{i}Pr	Br	**131**	**145**	65
2	^{i}Pr	CN	**132**	**146**	53[b]
3	^{i}Pr	F	**133**	**147**	36
4	^{i}Pr	OMe	**134**	**148**	88

[a]Yield was for epoxidation of crude quinone; [b]Isolated yield

4.3.7. Mechanistic studies on 137:

ROS generation by **137** involves reaction with free thiols to form thiolated adduct (**I**, Scheme 4.5), which then subsequently undergoes a keto-enol tautomerism to produce a diol(ate) **II**. The intermediate **II** transfers an electron to oxygen to produce $O_2^{\bullet-}$ and in the process this intermediate is oxidized to **III** (Scheme 4.5). Mass spectrometry of the reaction mixture of **137** glutathione in pH 7.4 buffer revealed the formation of **III** supporting the proposed mechanism as shown in Scheme 4.5. In addition, under these

reaction conditions, we also observed the formation of GS–SG (expected $[M+K]^+$ = 651.1157; obtained $[M+K]^+$ = 651.0668), which is indicative of thiol oxidation, again, symptomatic of ROS generation.

Scheme 4.5. Proposed mechanism for glutathione-mediated decomposition of **137** to generate ROS.

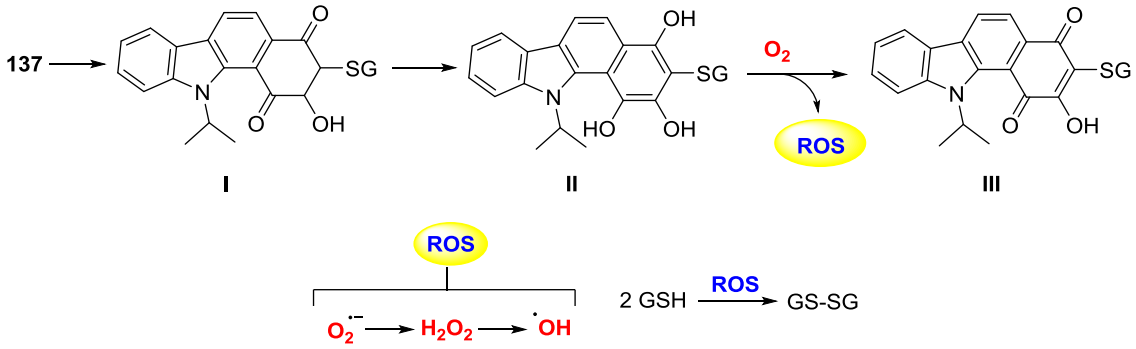

The cell permeability of the compounds and their capability to deplete intracellular thiols was tested using a *mono*-bromobimane (mBBr) fluorescence assay.[4,49,50] In this study, a reaction of thiol with weakly fluorescent mBBr produces a highly fluorescent thiolated adduct (Scheme 4.6). Hence, increased fluorescence is an indicator of greater free thiol levels inside cells and vice versa. The results of this assay were consistent with depletion of intracellular thiols in *S. aureus* upon exposure to **137** in comparison with untreated control (Figure 4.10A).

Scheme 4.6. Reaction of *mono*-bromobimane (mBBr) with thiol

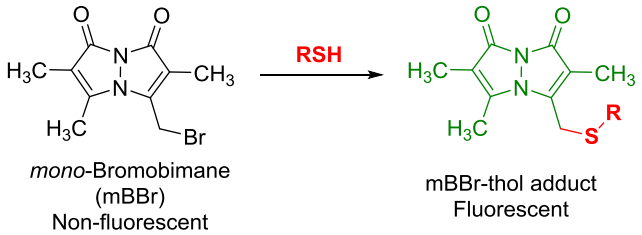

When compared with Fosfomycin and *N*-phenylmaleimide (NPM), we find that **137** was better at depleting thiols intracellularly (Figure 4.10A). In order to understand whether thiol depletion and ROS generation were integral to the mechanism of action of this series of compounds, selected analogues were compared with **137** in the aforementioned assay. We chose **135** (MIC = 4 μg/mL) and **140** (MIC = 16 μg/mL).

Among these derivatives we found that the MICs roughly correlated with thiol depleting ability. For example, **140**, did not appear to deplete thiols in comparison with untreated control and was a poor MRSA inhibitor (Figure 4.10A).

Further, intracellular ROS generation by **137** in *S. aureus* was examined using dihydroethidine (DHE) assay.[46,51,52] DHE specifically reacts with $O_2^{\bullet -}$ to produce 2-hydroxyethidium (2-OH-E^+) and the presence of ethidium (E^+) is an indicator for global enhancement of oxidative species including hydroxyl radical. After 60 min of incubation of **137** and DHE with *S. aureus*, cells were lysed, and extracted with acetonitrile: buffer (1:1, 100 µL, v/v) and the supernatant was analyzed by HPLC connected with a fluorescence detector. When MSSA cells were incubated with **137** for 1 h, we find nearly complete disappearance of DHE as well as increased levels of 2-OH-E^+ and E^+ suggestive of increased intracellular ROS (Figure 4.10B). Under similar conditions, when fosfomycin was tested, we find increased oxidative species including $O_2^{\bullet -}$ suggesting that depletion of intracellular antioxidant thiols resulted in increased oxidative stress.

Figure 4.9. Intracellular thiol depletion and ROS generations studies: (A) Intracellular thiol depletion in *S. aureus* measured after 60 min of incubation at 37 °C using *mono*-bromobimane (mBBr) based fluorimetric assay: Fos: Fosfomycin; NPM: N-phenylmaleimide. (B) Representative traces of a dihydroethidium (DHE) assay for study of increased intracellular ROS in *S. aureus* during independent incubation of **137** and Fosfomycin (Fos). Superoxide specifically react with DHE to produce 2-hydroxyethidium (2-OH-E^+); Ethidium (E^+) is formed by non-specific oxidation of DHE and is indicative of a general increase in oxidative species.

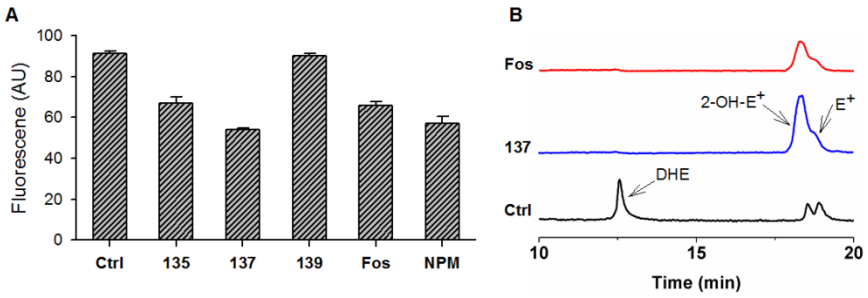

Table 4.11. Minimum inhibitory concentrations (MIC) against MRSA clinical isolates.[a]

Entry	MRSA Isolate	MIC of **137**		MIC of Vancomycin	
		μg/mL	μM	μg/mL	μM
1	7419	0.25	0.8	1	0.7
2	B19506	0.25	0.8	0.5-2	0.35-1.4
3	K-1	0.25	0.8	1	0.7
4	7425	0.25	0.8	0.5-2	0.35-1.4
5	7386	0.25	0.8	0.5-1	0.35-0.7
6	9902	1	3.2	0.5	0.35
7	288	0.5	1.6	0.5	0.35
8	21838	0.25	0.8	0.5	0.35
9	853	0.5	1.6	0.5	0.35
10	7419	0.5	1.6	0.5	0.35
11	151	0.5	1.6	0.5	0.35

[a]MICs were provided by Vitas Pharma.

Finally, the lead **137** was tested for its toxicity towards mammalian cells using a standard cell viability assay against human lung carcinoma cell line A549. The growth inhibitory potency 50% (GI_{50}) was found to be >30 μM, suggesting **137** is not toxic to human cells at concentrations where it is effective against MRSA (0.8-3.2 μM). Next, in order to test if **137** unique mechanisms would allow it to overcome resistance in MRSA, we tested the efficacy of **137** to inhibit patient-derived stains of drug resistant MRSA. In this assay, MICs of 0.25-0.5 μg/mL were recorded suggesting that **137**'s activity against patient-derived strains were conserved (Table 4.11). The *in vitro* activity of **137** against MRSA appears to be comparable or better than the commercially used antibiotic Vancomycin (MIC = 0.5 – 2 μg/mL, Table 4.11).

4.4. Conclusion:

We have developed a 2,3-epoxy-1,4-naphthoquinone based thiol activated scaffold for ROS generation in buffer as well as inside cells. A series of 2,3-epoxy-1,4-

naphthoquinones were found to be efficient in reacting with thiols to generate ROS and moderately active against MSSA and MRSA. Our revised design of indole based scaffold offered structural handle to modulate the reactivity with thiols for ROS generation. From our study, we have shown that the compound permeates inside to react with thiols and to enhance intracellular ROS in *S. aureus*. Introduction of a substituent at 6-position found to decrease the reactivity with thiols, consequently slowing down the ROS generation. We have identified highly potent inhibitor of MRSA **137** with an MIC of 0.25 μg/mL, which is better than commercially used antibiotic Vancomycin (1.0 μg/mL). In addition, **137** was found to retain its activity against many of the hospital isolates of drug resistant strains of *S. aureus*. From the mechanistic studies, it appears that a combination of covalent modification of biological thiols and enhancement of ROS in bacteria is an integral mechanism of action of the lead compound.

4.5. Experimental and Characterization Data:

Experimental Section:

Compounds **58**, **59**, **60**, **21**, **61**, **23**, **66**, **67**, **70**, **71**, **72**, **73**, **74**, **78**, **89**, **81** and **82** are previously[22-30] reported and spectral data that we obtained was consistent with literature values.

4.5.1. General procedure for benzylation of 5-hydroxy-1,4-naphthoquinones.

To a 50 mL round bottom flask containing 1,1-dichloromethane (DCM, 8 mL),compound (1 mmol), benzylbromide (2.0 mmol) were added followed by Ag_2O (3.0 mmol); the reaction flask was covered with aluminium foil, flushed with nitrogen gas and stirred for 24 h at room temperature. Upon complete consumption of starting material as determined by thin layer chromatography (TLC) analysis, the reaction mixture was filtered through a celite bed. The filtrate was evaporated to dryness under reduced pressure to obtain crude product. The crude material was purified by silica gel column chromatography using ethyl acetate (5→30 %) and petroleum ether solvent system to obtain pure material.

5-(4-Trifluoromethylbenzyloxy)-1,4-naphthoquinone (61).

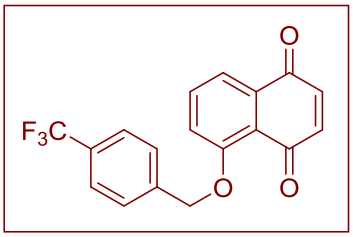

Starting from **21** (200 mg, 1.15 mmol), the naphthoquinone **61** was isolated as a bright yellow crystalline solid (366 mg, 96%): mp 136 – 138 °C; FT-IR (ν_{max}, cm^{-1}): 3075, 1658, 1614, 1583, 1451, 1386, 1305, 1250, 1170, 1106, 1058, 1026, 955; ^1H NMR (400 MHz, $CDCl_3$): δ 8.32 (d, *J* = 6.0 Hz,1H), 7.77 (d, *J* = 5.2 Hz,1H), 7.69 (d, *J* = 5.6 Hz, 3H), 7.44 (t, *J* = 5.8 Hz, 1H), 7.35 (d, *J* = 6.2 Hz, 1H), 6.90 (s, 2H), 5.45 (s, 2H); ^{13}C NMR (100 MHz, $CDCl_3$): δ 196.2, 184.4, 158.1, 141.0, 136.5, 135.3, 128.4, 127.9, 112.0, 119.3, 77.5, 77.2, 77.0, 67.1; HRMS (ESI): calcd. for $[C_{18}H_{11}F_3O_3+Na]^+$: 355.0558; Found: 355.0558.

5-Benzyloxy-2-methyl-1,4-naphthoquinone (64).

Starting from **63** (200 mg, 1.06 mmol), the naphthoquinone **64** was isolated as a bright yellow solid (298 mg, 98%): mp 150 – 152 °C; FT-IR (ν_{max}, cm^{-1}): 3043, 2854, 2346, 1747, 1653, 1575, 1446, 1363, 1251, 1054, 965, 903, 831, 768, 729; ^1H NMR (400 MHz,

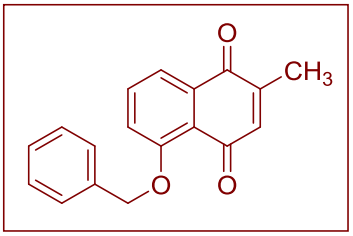

$CDCl_3$): δ 7.75 (dd, *J* = 1.0, 7.6 Hz, 1H), 7.55-7.62 (m, 3H), 7.40 (t, *J* = 7.5 Hz, 2H), 7.28-7.33 (m, 2H), 6.72 (q, *J* = 1.5 Hz, 1H), 5.27 (s, 2H), 2.10 (d, *J* = 1.6 Hz, 3H); ^{13}C NMR (100 MHz, $CDCl_3$): δ 185.9, 184.4, 158.4, 145.5, 138.0, 136.2, 134.6, 128.8, 128.0, 126.8, 120.6, 119.8, 119.6, 71.0, 16.0; HRMS (ESI): calcd., for $[C_{18}H_{14}O_3+Na]^+$: 301.0841; Found: 301.0844.

4.5.2. General procedure for coupling of arylboronic acids with 2-bromo-1,4-naphthoquinone

To a mixture of THF: H_2O (9:1 v/v, 100 mL) under nitrogen atmosphere, 2-bromo-1,4-naphthoquinone (1equiv), sodium carbonate (2 equiv), arylboronic acid (1.5 equiv) and $Pd(PPh_3)_4$ (3 mol%) were added. The reaction mixture was stirred at room temperature until TLC analysis showed complete disappearance of starting material. Work up involved separation of the aqueous layer from the organic layer, washing of the aqueous layer with ethyl acetate (3 × 10 mL). The combined organic layers were dried (sodium sulphate) and filtered; removal of solvent under reduced pressure from the filtrate produced the crude product, which was purified by silica gel column chromatography (5→15 % ethyl acetate in petroleum ether) to obtain the desired product.

2-(4-Acetylphenyl)-1,4-naphthoquinone (68).

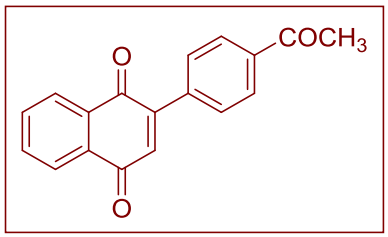

Starting from 2-bromo-1,4-naphthoquinone **64** (300 mg, 1.27 mmol), the naphthoquinone **68** was isolated as a yellow solid (159 mg, 43%): mp 170 – 172 °C; FT-IR (ν_{max}, cm^{-1}): 3068, 1744, 1657, 1591, 1548, 1402, 1357, 1302, 1258, 1171, 1109, 1018, 958; ^{1}H NMR (400 MHz, $CDCl_3$): δ 8.18-8.19 (m, 1H), 8.12-8.13 (m, 1H), 8.04 (d, *J* = 6.3 Hz, 2H), 7.80 (d, *J* = 3.4 Hz, 2H), 7.66 (d, *J* = 6.4 Hz, 2H), 7.10 (s, 1H), 2.65 (s, 3H); ^{13}C NMR (100 MHz, $CDCl_3$): d 197.6, 184.9, 184.0, 147.2, 137.9, 136.0, 134.2, 134.17, 129.8, 129.1, 128.4, 127.5, 127.2, 126.2, 26.9; HRMS (ESI): calcd. for $[C_{18}H_{12}O_3+Na]^+$: 299.0684; Found: 299.0684.

2-(4-Fluorophenyl)-1,4-naphthoquinone (69).

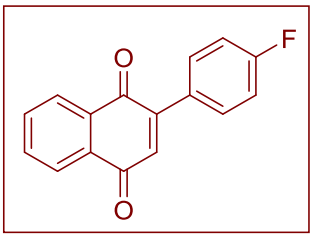

Starting from 2-bromo-1,4-naphthoquinone **64** (154 mg, 1.10 mmol), the naphthoquinone **69** was isolated as a yellow solid (142 mg, 66%): mp 142 – 144 °C; FT-IR (ν_{max}, cm^{-1}): 3068, 2961, 1742, 1685, 1593, 1507, 1301, 1259, 1160, 1102, 1009; ^{1}H NMR (400 MHz, $CDCl_3$): δ 8.16-8.18 (m, 1H), 8.10-8.12 (m, 1H), 7.76-7.78 (m, 2H), 7.55-7.59 (m, 2H), 7.16 (t, *J* = 8.6 Hz, 2H), 7.05 (s, 1H); ^{13}C NMR (100, MHz, $CDCl_3$): δ 185.1, 184.4, 165.3, 162.8, 147.1, 135.1, 134.0, 132.4, 132.1, 131.6, 131.5, 129.4, 127.2, 126.1, 115.9, 115.7; HRMS (ESI): calcd. for $[C_{16}H_9FO_2+Na]^+$: 275.0484; Found: 275.0484.

4.5.3. General Procedure for Epoxidation

To a stirred solution of the naphthoquinone (1 mmol) in THF (2 mL), sodium hypochlorite (1 mmol, 1.5 mL of 5 wt % solution) was added and the resulting reaction mixture was stirred at room temperature (25 °C). The reaction mixture was diluted with water (15 mL), and extracted using ethyl acetate (3 × 10 mL). The organic layers were combined and then washed with brine (10 mL), and dried (Na_2SO_4). The crude obtained by removal of sodium sulfate by filtration was then purified by silica gel column chromatography (1 → 5 % ethyl acetate in petroleum ether).

2,3-Epoxy-2,3-dihydro-5-nitro-1,4-naphthoquinone (75).

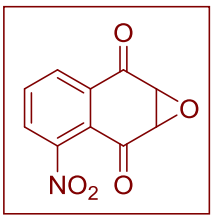

Starting from **57** (100 mg, 0.49 mmol), the epoxide **75** was isolated as a white solid (72 mg, 67%): mp 141 – 142 °C; FT-IR (ν_{max}, cm^{-1}): 3051, 2922, 2852, 1703, 1595, 1542, 1373, 1323, 1294; ^{1}H NMR (400 MHz, $CDCl_3$): δ 8.15 (dd, *J* = 0.9, 7.8 Hz, 1H), 7.97 (dd, *J* = 8.0, 1.2 Hz, 1H), 7.86 (t, *J* = 7.8 Hz, 1H), 4.15 (d, *J* = 4.1 Hz, 1H), 4.12 (d, *J* = 4.1 Hz, 1H); ^{13}C NMR (100 MHz, $CDCl_3$): δ 188.8, 188.2, 148.7, 134.4, 132.6, 130.5, 129.2, 126.3, 55.6, 55.1; Elem. Anal. Calcd., for $C_{10}H_5NO_5 \cdot 0.05\ H_2O$: C, 54.81; H, 2.30; N, 6.39. Found: C, 54.69; H, 2.77; N, 6.49.

2,3-Epoxy-2,3-dihydro-6-nitro-1,4-naphthoquinone (76).

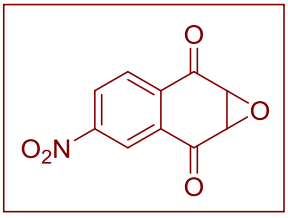

Starting from **58** (100 mg, 0.49 mmol), the epoxide **76** was isolated as a white solid (94 mg, 88%): mp 140 – 141 °C; FT-IR (ν_{max}, cm^{-1}): 3076, 3040, 2372, 1705, 1603, 1573, 1344, 1290, 994; ^{1}H NMR (400, MHz, $CDCl_3$): δ 8.82 (d, *J* = 2.2 Hz, 1H), 8.58 (dd, *J* = 2.3, 8.3 Hz, 1H), 8.20 (d, *J* = 8.6 Hz, 1H), 4.15 (dd, *J* = 3.7, 6.4 Hz, 2H); ^{13}C NMR (100 MHz, $CDCl_3$): δ 189.2, 188.6, 144.9, 135.5, 129.3, 128.8, 122.7, 55.7, 55.6; HRMS (MALDI): calcd. for $[C_{10}H_5NO_5+K]^+$: 258.2487; Found: 258.2380.

2,3-Epoxy-2,3-dihydro-5-amino-1,4-naphthoquinone (77).

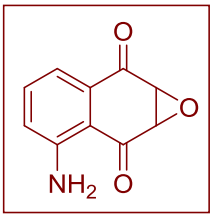

Starting from **59** (173 mg, 1.00 mmol), epoxide **77** was isolated as a pale yellow solid (81 mg, 43%): mp 131 – 132 °C; FT-IR (ν_{max}, cm^{-1}): 3746, 3403, 2926, 1704, 1646, 1601, 1540, 1327, 1287, 1002, 993; ^{1}H NMR (400 MHz, $CDCl_3$): δ 7.41 (dd, *J* = 7.4, 8.2 Hz, 1H), 7.28 (dd, *J* = 1.2, 7.3 Hz, 1H), 6.92 (dd, *J* = 0.9, 8.7 Hz, 1H), 6.33 (br, 2H), 3.94 (d, *J* = 3.7 Hz, 1H), 3.90 (d, *J* = 3.7 Hz, 1H); ^{13}C NMR (100 MHz, $CDCl_3$): δ 192.4, 191.6, 150.4, 135.3, 133.0, 123.1, 116.9, 111.4, 56.0, 55.2; HRMS (MALDI) calcd., for $[C_{10}H_7NO_3+K]^+$: 228.0063; Found: 228.0014.

2,3-Epoxy-2,3-dihydro-5-ethyloxy-1,4-naphthoquinone (79).

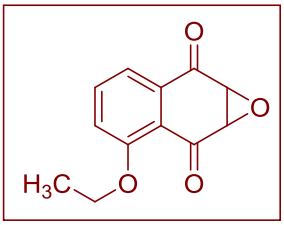

Starting from **60** (150 mg, 0.74 mmol), the epoxide **79** was isolated as a grayish white solid (109 mg, 68%): mp 110 – 112 °C; FT-IR (ν_{max}, cm^{-1}): 3079, 2982, 2940, 1697, 1584, 1457, 1396, 1325, 1285, 1156, 1115, 1048, 995; ^{1}H NMR (400 MHz, $CDCl_3$): δ 7.61 (t, *J* = 8.0 Hz, 1H), 7.47 (dd, *J* = 0.9, 7.8 Hz, 1H), 7.25 (d, *J* = 8.7 Hz, 1H), 4.16-4.22 (m, 1H), 3.96-4.14 (m, 3H), 1.47 (t, *J* = 6.9 Hz, 3H); ^{13}C NMR (100 MHz, $CDCl_3$): δ 191.9, 190.2, 158.7, 135.1, 133.9, 120.4, 119.1, 65.3, 55.5, 55.3, 14.6; HRMS (ESI): calcd., for $[C_{12}H_{10}O_4+Na]^+$: 241.0477; Found: 241.0478.

2,3-Epoxy-2,3-dihydro-5-(4trifluoromethylbenzyloxy)-1,4-naphthoquinone (81).

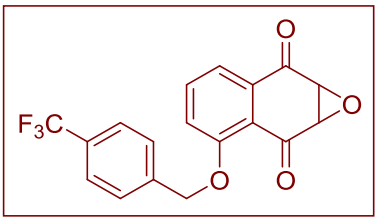

Starting from **61** (150 mg, 0.45 mmol), the epoxide **81** was isolated as a white solid (129 mg, 82%): mp 144 – 146 °C; FT-IR (ν_{max}, cm^{-1}): 3080, 1698, 1585, 1450, 1395, 1317, 1284, 1261, 1173, 1109, 1064, 985; ^{1}H NMR (400 MHz, $CDCl_3$): δ 8.05 (d, *J* = 7.8 Hz, 1H), 7.62-7.68 (m, 3H), 7.56 (d, *J* = 7.8 Hz, 1H), 7.42 (t, *J* = 7.8 Hz, 1H), 7.30 (d, *J* = 8.7 Hz, 1H), 5.40 (d, *J* = 13.7 Hz, 1H), 5.34 (d, *J* = 13.7 Hz, 1H), 3.99-4.01 (m, 2H); ^{13}C NMR (100 MHz, $CDCl_3$): δ 191.6, 190.1, 157.6, 135.4, 134.5, 134.0, 132.7, 128.1, 127.9, 125.9, 125.8, 120.6, 119.9, 119.3, 66.92, 66.89, 55.6, 55.3; HRMS (ESI): calcd. for $[C_{18}H_{11}F_3O_4+Na]^+$: 371.0507; Found: 371.0506. [Note: Multiple and weak signals were seen in the aromatic region of ^{13}C NMR due to the coupling of fluorine atoms (–CF_3)with the adjacent phenyl ring carbons].

2,3-Epoxy-2-methyl-5-benzyloxy-1,4-naphthoquinone (84).

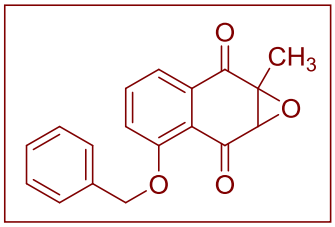

Starting from **64** (150 mg, 0.57 mmol), the epoxide **84** was isolated as a pale yellow solid (72 mg, 45%): mp 115 – 117 °C. FT-IR (ν_{max}, cm^{-1}): 3080, 1699, 1583, 1447, 1387, 1327, 1286, 1251, 1075, 1032, 965; ^{1}H NMR (400 MHz, $CDCl_3$): δ 7.55-7.59 (m, 2H), 7.49 (d, *J* = 7.3 Hz, 2H), 7.39 (t, *J* = 7.3 Hz, 2H), 7.27-7.32 (m, 2H), 5.25 (d, *J* = 12.4 Hz,1H), 5.17 (d, *J* = 12.4 Hz, 1H), 3.83 (s, 1H), 1.71 (s, 3H); ^{13}C NMR (100 MHz, $CDCl_3$): δ 193.0, 191.1, 157.9, 135.9, 135.0, 134.4, 128.8,128.2 126.9, 121.1, 119.9, 119.4, 71.0, 61.7, 61.65, 14.6; HRMS (ESI): calcd for $[C_{18}H_{14}O_4+Na]^+$: 317.0790; Found: 317.0790.

2,3-Epoxy-2-(3-nitrophenyl)-1,4-naphthoquinone (86).

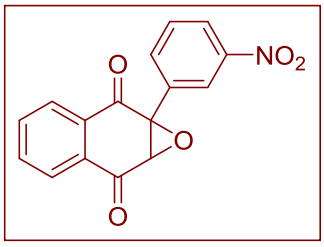

Starting from **67** (100 mg, 0.36 mmol), the epoxide **86** was isolated as a white solid (84 mg, 81%): mp 129 – 131 °C; FT-IR (ν_{max}, cm^{-1}): 3089, 2924, 1695, 1590, 1530, 1345, 1296, 1200, 1123, 1028; ^{1}H NMR (400 MHz, $CDCl_3$): δ 8.35 (s, 1H), 8.28 (d, *J* = 8.2 Hz, 1H), 8.06-8.09 (m, 1H), 7.99-8.02 (m, 1H), 7.79-7.83 (m,

3H), 7.63 (td, *J*= 2.8, 8.0 Hz, 1H), 3.96 (d, *J* = 3.0 Hz, 1H); ^{13}C NMR (100 MHz, $CDCl_3$): δ 189.9, 189.4, 148.3, 135.1, 135.06, 133.8, 133.1, 132.1, 131.8, 129.7, 128.1, 127.2, 124.4, 122.9, 63.5, 63.0; HRMS (MALDI): calcd., for $[C_{16}H_9NO_5+K]^+$: 334.0118; Found: 334.0220.

2,3-Epoxy 2-(4-acetylphenyl)-1,4-naphthoquinone (87).

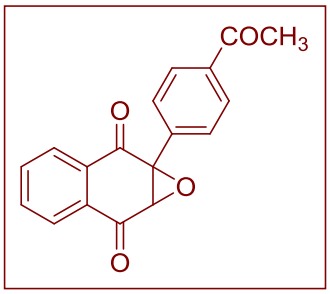

Starting from **68** (100 mg, 0.36 mmol), the epoxide **87** was isolated as a pale yellow solid (78 mg, 74%): mp 147 – 149 °C; FT-IR (ν_{max}, cm^{-1}): 3068, 2319, 1744, 1657, 1592, 1548, 1462, 1402, 1357, 1302, 1258, 1171, 1109, 1018; ^{1}H NMR (500 MHz, $CDCl_3$): δ 8.08-8.10 (m, 1H), 8.02 (d, *J* = 8.4 Hz, 3H), 7.79-7.81 (m, 2H), 7.57 (d, *J* = 8.4 Hz, 2H,), 3.94 (s, 1H), 2.63 (s, 3H); ^{13}C NMR (125 MHz, $CDCl_3$): δ 197.7, 190.4, 189.8, 137.7, 135.9, 135.0, 134.9, 132.3, 131.8, 129.1, 128.5, 128.0, 127.9, 127.5, 127.1, 64.1, 63.0, 26.9; HRMS (MALDI): calcd., for $[C_{18}H_{12}O_4 +H]^+$: 293.0814; Found: 293.0990.

2,3-Epoxy-2-(4-fluorophenyl)-1,4-naphthoquinone (88).

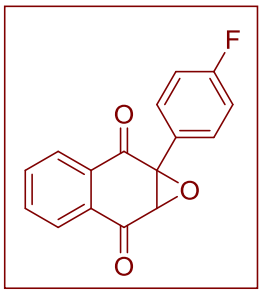

Starting from **69** (70 mg, 0.28 mmol), the epoxide **88** was isolated as a white solid (39 mg, 52%): mp 143 – 145 °C; FT-IR (ν_{max}, cm^{-1}): 2923, 1690, 1597, 1515, 1333, 1298, 1233, 1160, 1023; ^{1}H NMR (400 MHz, $CDCl_3$): δ 8.07-8.09 (m, 1H), 8.00-8.02 (m, 1H), 7.79 (dd, *J* = 3.5, 5.7 Hz, 2H), 7.44-7.48 (m, 2H), 7.13 (t, *J* = 8.7 Hz, 2H), 3.94 (s, 1H); ^{13}C NMR (100 MHz, $CDCl_3$): δ 190.8, 190.2, 134.9, 134.8, 132.4, 131.9, 129.7, 128.0, 127.0, 126.7, 115.9, 115.6, 64.1, 63.1; HRMS (MALDI): calcd., for $[C_{16}H_9FO_3+Na]^+$: 291.0433; Found: 291.0443.

2,3-Epoxy-2-(4-methylphenyl)-1,4-naphthoquinone (89).

Starting from **70** (100 mg, 0.40 mmol), the epoxide **89** was isolated as a white solid (81 mg, 78%): mp 146 – 148 °C; FT-IR (ν_{max}, cm^{-1}): 2919, 1701, 1585, 1516, 1457, 1381, 1324, 1282, 1260, 1152, 1115, 1028; ^{1}H NMR (400 MHz, $CDCl_3$): δ 7.97 (dd, *J* = 3.2, 5.5 Hz, 1H), 7.89 (dd, *J* = 3.2, 6.0 Hz, 1H), 7.66 (dd, *J* = 3.4, 5.9 Hz, 2H), 7.26 (d, *J* = 7.8

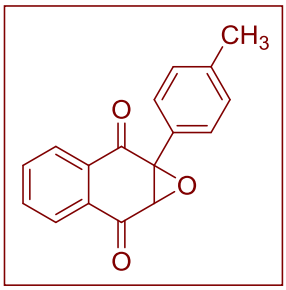

Hz, 2H), 7.15 (d, *J* = 7.8 Hz, 2H), 3.84 (s, 1H), 2.29 (s, 3H); ^{13}C NMR (100 MHz, $CDCl_3$): δ 191.2, 190.5, 139.4, 134.8, 134.6, 132.6, 131.9, 129.3, 128.0, 127.8, 127.6, 127.0, 64.7, 63.1, 21.4; HRMS (MALDI): calcd., for $[C_{17}H_{12}O_3+Na]^+$: 287.0684; Found: 287.0773.

2,3-Epoxy-2-(2-methoxyphenyl)-1,4-naphthoquinone (90).

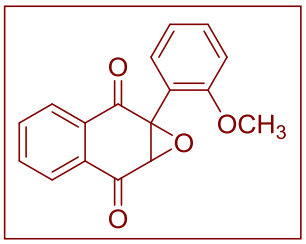

Starting from **71** (110 mg, 0.42 mmol), the epoxide **90** was isolated as a white solid (96 mg, 82%): mp 122 – 124 °C; FT-IR (ν_{max}, cm^{-1}): 2934, 2842, 1694, 1594, 1498, 1463, 1398, 1284, 1193, 1105, 1019; ^{1}H NMR (400 MHz, $CDCl_3$): δ 8.06-8.08 (m, 1H), 8.02-8.04 (m, 1H), 7.75-7.77 (m, 2H), 7.37-7.43 (m, 2H), 7.02 (t, *J* = 7.5 Hz, 1H), 6.94 (d, *J* = 8.3 Hz, 1H), 3.89 (s, 1H), 3.75 (s, 3H); ^{13}C NMR (100 MHz, $CDCl_3$): δ 191.6, 189.4, 157.9, 134.7, 134.5, 132.4, 132.1, 130.9, 128.1, 128.0, 127.0, 120.7, 110.5, 63.4, 62.0, 55.7; HRMS (ESI): calcd., for $[C_{17}H_{12}O_4+Na]^+$: 303.0663; Found: 303.0634.

2,3-Epoxy-2-(3-methoxyphenyl)-1,4-naphthoquinone (91).

Starting from **72** (100 mg, 0.34 mmol), the epoxide **91** was isolated as a pale yellow semi-solid (89 mg, 93%): FT-IR (ν_{max}, cm^{-1}): 2926, 2844, 1697, 1594, 1460, 1279, 1234, 1179, 1114, 1045; ^{1}H NMR (400 MHz, $CDCl_3$): δ 8.03 (dd, *J* = 2.6, 4.6 Hz, 1H), 7.95 (dd, *J* = 2.7, 4.4 Hz, 1H), 7.72 (dd, *J* = 2.6, 4.6 Hz, 2H), 7.29 (t, *J* = 6.4 Hz, 1H,), 6.99 (d, *J* = 6.1 Hz, 1H), 6.93 (d, *J* = 1.1 Hz, 1H), 6.90 (dd, *J* = 1.4, 6.6 Hz, 1H), 3.89 (s, 1H), 3.76 (s, 3H); ^{13}C NMR (100 MHz, $CDCl_3$): δ 191.0, 190.2, 159.7, 134.8, 134.7, 132.6, 132.3, 131.9, 129.7, 128.0, 127.0, 120.0, 115.3, 113.0, 64.6, 63.0, 58.4; HRMS (MALDI): calcd. for $[C_{17}H_{12}O_4+H]^+$: 281.0814; Found: 281.0966.

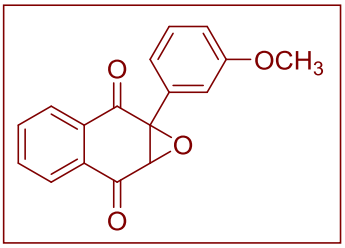

2,3-Epoxy-2-(4-methoxyphenyl)-1,4-naphthoquinone (92).

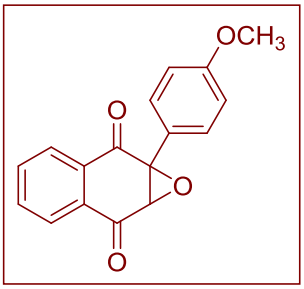

Starting from **73** (70 mg, 0.27 mmol), the epoxide **92** was isolated as a white solid (60 mg, 81%): mp 126 – 128 °C; FT-IR (ν_{max}, cm^{-1}): 2988, 2924, 2826, 1696, 1601, 1515, 1463, 1392, 1301, 1246, 1180, 1111, 1034; ^{1}H NMR (400 MHz, $CDCl_3$): δ 8.08 (dd, *J* = 3.0, 6.0 Hz,1H), 8.00 (dd, *J* = 3.3, 6.4 Hz, 1H), 7.77 (dd, *J* = 3.4, 5.5 Hz, 2H), 7.40 (d, *J* = 8.7 Hz, 2H), 6.96 (d, *J* = 8.7 Hz, 2H), 3.95 (s, 1H), 3.83 (s, 3H); ^{13}C NMR (100 MHz, $CDCl_3$): δ 191.3, 190.7, 160.4, 134.8, 134.6, 132.6, 131.9, 129.2, 128.0, 126.9, 122.7, 114.1, 64.6, 63.1, 55.5; HRMS (ESI): calcd., for $[C_{17}H_{12}O_4+Na]^+$: 303.0633; Found: 303.0632.

4.5.4. General procedure for Vilsmeier–Haack formylation:

To a cold solution (0 ºC) of indole (1 eq.) in dry *N*,*N*-dimethylformamide (DMF, 10 mL), drop wise addition of the Vilsmeier adduct (generated by mixing phosphoryl chloride ($POCl_3$, (4 equiv) and DMF (4equiv) at 0 ºC under nitrogen atmosphere) in a 50 mL RB flask was carried out. The reaction mixture was stirred for 90 min at room temperature. Then, the reaction was quenched with aqueous sodium hydroxide (5 M, 50 mL) and the stirring was continued for 60 min at 100 ºC. After bringing the reaction mixture to RT, it was diluted with cold water (0 - 4 ºC, 50 mL) and the compound was extracted with multiple fractions of ethyl acetate (5×10 mL). The combined organic phase was washed with brine (20 mL), dried over anhydrous Na_2SO_4 (5 g), filtered. The filtrate was evaporated to dryness under reduced pressure to obtain crude product. This crude product was purified using silica gel (60-120 mesh) column chromatography with a mixture of ethyl acetate and hexane (1:1 ratio, v/v) as the eluant.

4.5.5. General procedure for synthesis of *N*-substituted indole-3-carboxaldehydes:

To an ice-cold solution of indole-3-carboxaldehyde in dry DMF (25 mL) NaH (60% in mineral oil, 2 eq.) was added in portions and stirring was continued in melting ice bath for 2h. Upon complete consumption of the starting material (TLC analysis), the reaction mixture was diluted with ice-cold water (50 mL). The aqueous layer was extracted with multiple fractions of chloroform (5 × 10 mL), the combined organic phase was washed

with brine (10 mL), dried over anhydrous Na_2SO_4 (5 g), filtered and the filtrated was evaporated under reduced pressure to obtain the crude product. This was purified by silica gel (100-200 mesh) chromatography using ethyl acetate and hexane mixture (1:2, v/v) as an eluant.

4.5.6. General procedure for Wittig olefination:

A turbid solution of Wittig salt, alkyltriphenylphosphonium bromide (1.5 eq.) in anhydrous THF was cooled to -50 ºC, to this *n*-BuLi (2.5 M in hexane, 1.1 eq.) was added drop wise, and stirred for 60 min at -50 ºC. A solution of indole-3-carboxaldehyde (1 equiv) in dry THF was added drop wise to the above solution and stirred at -50 ºC for 2 h. Then the reaction mixture was quenched with cold water (0 – 4 ºC, 20 mL), and extracted using ethyl acetate (5 × 10 mL). The combined organic layer was washed with brine (10 mL), dried over anhydrous Na_2SO_4 (5 g), filtered and the filtrate evaporated to dryness under reduced pressure. The crude material was purified by silica gel column chromatography eluting with ethyl acetate and hexane mixture (1:4, v/v). Note: During purification compound decomposes in silica column, needs to be eluted out within 15-20 min form the silica column. These olefins are unstable and are either used for the next reaction immediately or stored at -20 ºC but used within 2-3 days.

4.5.7. General procedure for synthesis of 121-134.

To a solution of the 3-alkenylindole (1 eq.) in ethanol (5 mL), a solution of *p*-benzoquinone (2.5 equiv) in ethanol (5 mL) was added at room temperature by slow addition, and stirring was continued at RT until complete consumption of the starting material was observed (TLC analysis). The volatiles were removed under reduced pressure to obtain the crude product and this was purified by silica gel column chromatography using ethyl acetate and hexane mixture (1:6, v/v) as an eluant.

11H-Benzo[a]carbazole-1,4-dione (121).

Starting from 3-vinyl-1H-indole, **107** (510 mg, 3.56 mmol), **121** was isolated as a brownish red solid (560 mg, 64%): mp 251 – 253 °C; FT-IR (ν_{max}): 1646, 1566, 1414, 1303, 1216, 1114, 1019; ^{1}H NMR (400 MHz, $CDCl_3$): δ 10.40 (s (br), 1H), 8.33 (d, *J*=

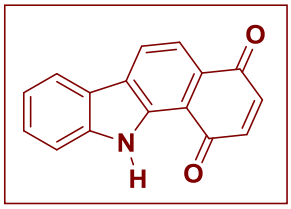

8.1 Hz, 1H), 8.19 (d, *J* = 7.8 Hz, 1H), 7.92 (d, *J* = 7.9 Hz, 1H), 7.52 – 7.54 (m, 2H), 7.28 – 7.32 (m, 1H), 6.93 (s, 2H); ^{13}C NMR (100 MHz, DMSO-d_6): δ 187.0, 185.8, 143.4, 139.4, 139.0, 137.0, 130.1, 129.3, 128.6, 126.5, 121.8, 121.3, 121.0, 119.9, 117.1, 113.4; HRMS (ESI) for $[C_{16}H_9NO_2+H]^+$: calcd., 248.0712; Found: 248.0711.

11-Ethyl-1H-benzo[a]carbazole-1,4(11H)-dione (122).

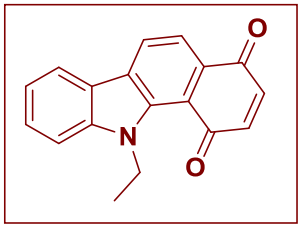

Starting from *N*-ethyl-3-vinylindole, **108** (1 g, 5.83 mmol), **122** was isolated as a brownish red-solid (285 mg, 18%): mp 138 – 140 °C; FT-IR (ν_{max}): 1740, 1643, 1512, 1443, 1375, 1221, 1038; ^{1}H NMR (400 MHz, $CDCl_3$): δ 8.32 (d, *J* = 7.9 Hz, 1H), 8.07 (d, *J* = 7.7 Hz, 1H), 8.00 (d, *J* = 8.0 Hz, 1H), 7.51-7.58 (m, 2H), 7.28-7.32 (m, 1H), 6.92 (q, *J* = 14.0 Hz, 2H), 4.63 (q, *J* = 10.6 Hz, 2H), 1.40 (t, *J* = 7.0 Hz, 3H); ^{13}C NMR (100 MHz, $CDCl_3$): δ 186.0, 185.6, 144.3, 140.2, 137.0, 131.6, 131.3, 128.4, 125.1, 122.2, 121.0, 120.8, 118.6, 118.2, 110.8, 42.5, 14.4; HRMS (ESI) for $[C_{18}H_{13}NO_2+H]^+$: calcd., 276.1025; Found: 276.1033.

11-Isopropyl-1H-benzo[a]carbazole-1,4(11H)-dione (123).

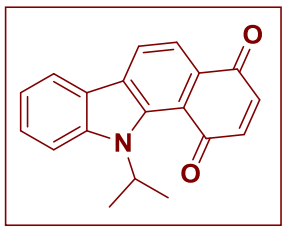

Starting from *N*-isopropyl-3-vinylindole, **109** (765 mg, 4.13 mmol), **123** was isolated as a brownish red solid (280 mg, 23%): mp 138 – 140 °C; FT-IR (ν_{max}): 1740, 1643, 1512, 1443, 1375, 1038; ^{1}H NMR (400 MHz, $CDCl_3$): δ 8.25 (d, *J* = 7.8 Hz, 1H), 8.05 (d, *J* = 7.7 Hz, 1H), 7.96 (d, *J* = 7.8 Hz, 1H), 7.71 (d, *J* = 8.4 Hz, 1H), 7.44-7.48 (m, 1H), 7.25 (t, *J* = 7.4 Hz, 1H), 6.88 (d, *J* = 5.5 Hz, 1H), 6.72 (s, 1H), 4.85-4.96 (m, 1H), 1.65 (d, *J* = 6.9 Hz, 6H); ^{13}C NMR (100 MHz, $CDCl_3$): δ 186.2, 185.8, 143.0, 140.0, 139.6, 136.8, 136.6, 131.5, 131.4, 127.6, 124.8, 123.7, 121.1, 120.8, 118.8, 118.4, 114.3, 52.3, 21.2; HRMS (ESI) for $[C_{19}H_{15}NO_2+H]^+$: calcd., 290.1181; Found: 290.1184.

11-Allyl-Benzo[a]carbazole-1,4-dione (124).

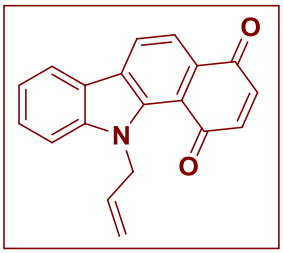

Starting from *N*-allyl-3-vinylindole, **110** (500 mg, 2.72 mmol), **124** was isolated as a brownish red solid (80 mg, 10%): mp 138 – 140 °C; FT-IR (ν_{max}): 1741, 1649, 1588, 1462, 1413, 1118, 1024, 923; ^{1}H NMR (400 MHz, DMSO- d_6): δ 8.58 (dt, *J* = 1.3, 7.8 Hz, 1H), 8.26 (d, *J* = 7.8 Hz, 1H), 7.86 – 7.88 (m, 1H), 7.70 (d, *J* = 8.4 Hz, 1H), 7.55 (t, *J* = 7.8 Hz, 1H), 7.30 (t, *J* = 7.4 Hz, 1H), 7.06 (dd, *J* = 1.4, 10.1 Hz, 1H), 6.97 (dd, *J* = 1.1, 10.3 Hz, 1H), 5.82 (ddd, *J* = 5.2, 10.4, 22.0 Hz, 1H), 5.20 (d, *J* = 4.8 Hz, 2H), 5.02 (d, *J* = 10.4 Hz, 1H), 4.80 (d, *J* = 17.2 Hz, 1H); ^{13}C NMR (100 MHz, DMSO- d_6): δ 186.2, 185.5, 144.8, 140.9, 137.8, 137.2, 134.3, 131.2, 131.1, 129.0, 126.0, 122.1, 121.7, 119.1, 118.5, 117.3, 112.0, 49.7; HRMS (ESI) for $[C_{19}H_{13}NO_2+H]^+$: calcd., 288.1025; Found: 288.1026.

11-Benzyl-1H-benzo[a]carbazole-1,4(11H)-dione (125).

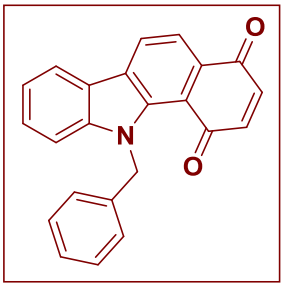

Starting from *N*-allyl-3-vinylindole, **111** (1 g, 4.28 mmol), **125** was isolated as a brownish red solid (190 mg, 14%): mp 139 – 141 °C; FT-IR (ν_{max}): 1655, 1611, 1463, 1412, 1289; ^{1}H NMR (400 MHz, $CDCl_3$): δ 8.38 (d, *J* = 8.3 Hz, 1H), 8.13 (d, *J* = 7.8 Hz, 1H), 8.02-8.04 (m, 1H), 7.49-7.53 (m, 1H), 7.43 (d, *J* = 8.2 Hz, 1H), 7.31 -7.35 (m, 1H), 7.15 -7.20 (m, 3H), 6.90 (ABq, *J* = 10.1, 18.6 Hz, 2H), 6.83 (s, 2H), 5.79 (s, 2H); ^{13}C NMR (100 MHz, DMSO- d_6): δ 186.3, 185.4, 150.0, 140.6, 138.2, 138.0, 137.2, 131.4, 131.2, 129.1, 128.9, 127.4, 126.8, 126.2, 122.1, 121.8, 119.1, 118.7, 112.1, 50.3; HRMS (ESI) for $[C_{23}H_{15}NO_2+H]^+$: calcd., 338.1181; Found: 338.1178.

5-Methyl-2,3-dihydro-1H-benzo[a]carbazole-1,4(11H)-dione (126).

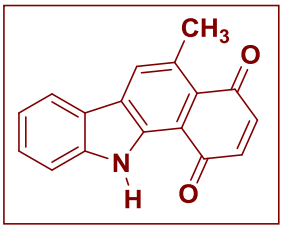

Starting from 3-(1-propenyl) –indole, **112** (1 g, 6.36 mmol), **126** was isolated as a brownish red-solid (235 mg, 14%): mp 224 – 226 °C; FT-IR (ν_{max}): 1739, 1646, 1367, 1224; ^{1}H NMR (400 MHz, $CDCl_3$): δ 10.46 (s, 1H), 8.05 (s, 1H), 8.01 (d, *J* = 8.5 Hz,

1H), 7.48 (dd, *J* = 1.2, 6.2 Hz, 2H), 7.23-7.27 (m, 1H), 6.82 (d, *J* = 1.9 Hz, 2H), 2.80 (s, 3H); ^{13}C NMR (100 MHz, $CDCl_3$): δ 188.1, 187.0, 142.5, 140.5, 137.5, 136.8, 132.6, 129.5, 128.5, 126.3, 121.5, 121.2, 120.8, 115.2, 111.7, 23.4; HRMS (ESI) for $[C_{17}H_{11}NO_2+H]^+$: calcd., 262.0868; Found: 262.0863.

11-Ethyl-5-methyl-1H-benzo[a]carbazole-1,4(11H)-dione (127).

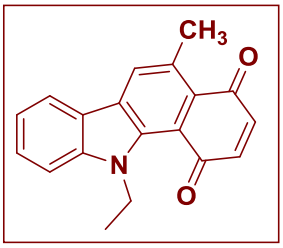

Starting from *N*-ethyl-3-(1-propenyl) –indole, **113** (350 mg, 1.88 mmol), **127** was isolated as a red-solid (70 mg, 13%): mp 132 – 134 °C; FT-IR (ν_{max}): 1740, 1645, 1512, 1443, 1375, 1221, 1038; ^{1}H NMR (400 MHz, $CDCl_3$): δ 8.13 (d, *J* = 3.3 Hz, 1H), 8.05 (d, *J* = 7.7 Hz, 1H), 7.50-7.57 (m, 2H), 7.26-7.30 (m, 1H), 6.91 (dd, *J* = 1.3, 10.1 Hz, 1H), 6.84 (dd, *J* = 1.3, 10.1 Hz, 1H), 4.51 (dq, *J* = 1.7, 7.1 Hz, 2H), 2.83 (s, 3H), 1.29 (t, *J* = 7.1 Hz, 3H); ^{13}C NMR (100 MHz, $CDCl_3$): δ 187.7, 186.6, 145.1, 138.7, 138.0, 132.7, 131.1, 129.0, 128.4, 121.0, 120.8, 110.8, 100.0, 42.1, 23.8, 13.7; HRMS (ESI) for $[C_{19}H_{15}NO_2+H]^+$: calcd., 290.1181; Found: 290.1176.

11-Allyl-5-methyl-1H-benzo[a]carbazole-1,4(11H)-dione (129).

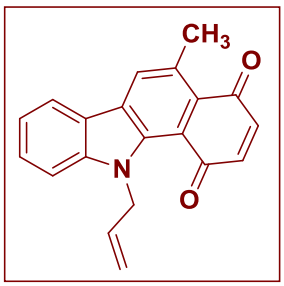

Starting from *N*-allyl-3-(1-propenyl) –indole, **115** (1 g, 5.07 mmol),**129** was isolated as a red-solid (310 mg, 21%): mp 140 – 142 °C; FT-IR (ν_{max}): 1646, 1616, 1466, 1265, 1253, 1191, 1100; ^{1}H NMR (400 MHz, $CDCl_3$): δ 8.13 (s, 1H), 8.06 (dd, *J* = 0.6, 7.8 Hz, 1H), 7.50-7.56 (m, 2H), 7.28-7.32 (m, 1H), 6.86 (dd, *J* = 10.1, 23.3 Hz, 2H), 5.77-5.87 (m, 1H), 5.06-5.13 (m, 3H), 4.92-4.97 (m, 1H), 2.84 (s, 3H); ^{13}C NMR (100 MHz, $CDCl_3$): δ 187.6, 186.5, 145.6, 138.7, 138.0, 133.4, 133.0, 129.0, 128.5, 122.0, 121.0, 120.8, 117.2, 111.1, 49.8, 23.7; HRMS (ESI) for $[C_{20}H_{15}NO_2+H]^+$: calcd., 302.1181; Found: 302.1191.

11-Benzyl-5-methyl-1H-benzo[a]carbazole-1,4(11H)-dione (130).

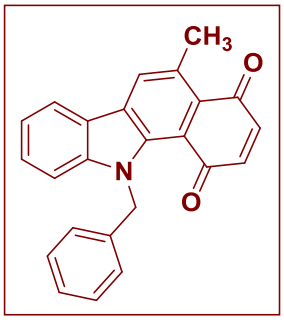

Starting from *N*-benzyl-3-(1-propenyl) –indole, **116** (1 g, 4.04 mmol), **130** was isolated as a red-solid (360 mg, 25%): mp 145 – 147 °C; FT-IR (ν_{max}): 1740, 1644, 1512, 1443, 1375, 1038; ^{1}H NMR (400 MHz, $CDCl_3$): δ 8.15 (s, 1H), 8.08 (t, *J* = 7.3 Hz, 1H), 7.48-7.52 (m, 1H), 7.43 (d, *J* = 8.2 Hz, 1H), 7.30 (t, *J* = 7.8 Hz, 1H), 7.12-7.15 (m, 3H), 6.82-6.85 (m, 2H), 6.75 (q, *J* = 13.3 Hz, 2H), 5.72 (s, 2H), 2.82 (s, 3H); ^{13}C NMR (100 MHz, $CDCl_3$): δ 187.5, 186.6, 146.0, 138.6, 138.0, 137.7, 137.2, 133.1, 131.1, 129.0, 128.6, 128.5, 127.2, 126.7, 122.0, 121.1, 121.0, 120.5, 111.2, 50.5, 23.7; HRMS (ESI) for $[C_{24}H_{17}NO_2+H]^+$: calcd., 352.1338; Found: 352.1337.

11-Isopropyl-1,4-dioxo-4,11-dihydro-1H-benzo[a]carbazole-8-carbonitrile (132).

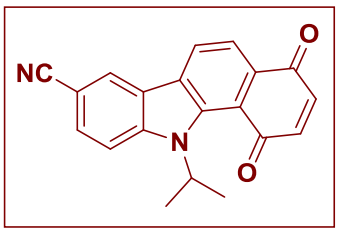

Starting from *N*-isopropyl-5-cyano-3-vinylindole,**118** (338 mg, 1.60 mmol), **132** was isolated as a red-solid (67 mg, 13%): mp 252 – 254 °C; FT-IR (ν_{max}): 2221, 1658, 1607, 1477, 1288, 1206, 1119; ^{1}H NMR (400 MHz, $CDCl_3$): δ 8.43 (d, *J* = 1.1 Hz, 1H), 8.35 (d, *J* = 8.1 Hz, 1H), 8.11 (d, *J* = 8.1 Hz, 1H), 7.84 (d, *J* = 8.7 Hz, 1H), 7.66 (dd, *J* = 8.7, 1.7 Hz, 1H), 6.95-7.04 (m, 2H), 5.01 (septet, *J* = 7.0 Hz, 1H), 1.72 (d, *J* = 7.1 Hz, 6H);^{13}C NMR (100 MHz, $CDCl_3$): δ 186.0, 185.2, 144.4, 140.0, 137.0, 132.5, 130.2, 129.7, 126.0, 125.3, 123.8, 119.8, 119.3, 114.8, 103.8, 52.7, 21.2; HRMS (ESI) for $[C_{20}H_{14}N_2O_2+H]^+$: calcd., 315.1134; Found: 315.1141.

4.5.8. General procedure for epoxidation. To a solution of the quinone in THF, sodium hypochlorite (9-12 wt. % in water, 10 eq.) was added and the reaction mixture was stirred at RT in an open container. Upon complete consumption of the starting material (TLC analysis), the reaction mixture was diluted with water (10 mL), and extracted with multiple portions of ethyl acetate (5 × 5 mL). The combined organic phase was washed with brine (10 mL), dried over anhydrous Na_2SO_4 (5 g), filtered and the filtrate was

evaporated to dryness to get the crude product. Silica gel chromatography of the crude using a mixture ethyl acetate and hexane (1:5, v/v) as an eluant gave pure material.

1aH-oxireno[2',3':4,5]benzo[1,2-a]carbazole-2,10(9H,10aH)-dione (135).

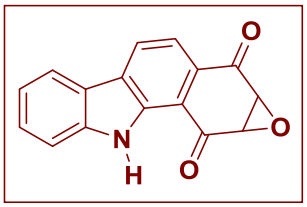

Starting from **121** (70 mg, 0.28 mmol), **135** (70 mg, 94%) was isolated as an orange yellow crystalline solid: mp 226 – 228 °C; FT-IR (ν_{max}): 3397, 2921, 1681, 1587, 1114; ^{1}H NMR (400 MHz, DMSO- d_6): δ 11.97 (s, 1H), 8.58 (dd, *J* = 1.6, 7.9 Hz, 1H), 8.23 (d, *J* = 7.9 Hz, 1H), 7.74 (dd, *J* = 8.2, 16.6 Hz, 2H), 7.50 (t, *J* = 7.6 Hz, 1H), 7.25 (t, *J* = 7.5 Hz, 1H), 4.17 (dd, *J* = 3.9, 10.4 Hz, 2H); ^{13}C NMR (100 MHz, DMSO-d_6): δ 192.3, 191.6, 143.1, 137.1, 130.0, 129.1, 128.6, 127.2, 121.8, 121.2, 121.0, 117.3, 114.5, 113.4, 55.8, 55.7; HRMS (ESI) for $[C_{16}H_9NO_3+H]^+$: calcd., 264.0655; Found: 264.0660.

9-Ethyl-1aH-oxireno[2',3':4,5]benzo[1,2-a]carbazole-2,10(9H,10aH)-dione (136).

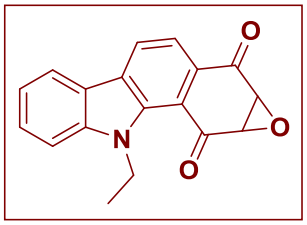

Starting from **122** (50 mg, 0.18 mmol), **136** (51 mg, 96%) was isolated as a bright yellow crystalline solid: mp 145 – 147 °C; FT-IR (ν_{max}): 3042, 2964, 1682, 1626, 1432, 1202, 1131, 1026; ^{1}H NMR (400 MHz, $CDCl_3$): δ 8.29-8.32 (m, 1H), 8.07 (d, *J* = 7.7 Hz, 1H), 7.83 (dd, *J* = 2.5, 9.1 Hz, 1H), 7.49-7.58 (m, 2H), 7.30 (t, *J* = 7.4 Hz, 1H), 4.36-4.51 (m, 2H), 4.10-4.14 (m, 2H), 1.28 (t, *J* = 7.1 Hz, 3H); ^{13}C NMR (100 MHz, $CDCl_3$): δ 192.5, 191.4, 143.6, 136.8, 131.3, 130.0, 128.5, 125.3, 121.9, 121.0, 120.9, 118.1, 117.6, 110.3, 56.1, 54.7, 40.6, 13.1; Elemental analysis for $C_{18}H_{13}NO_3$calcd. C, 74.22; H, 4.50; N, 4.81. Found C 74.18; H, 4.33; N, 4.74; HRMS (ESI) for $[C_{18}H_{13}NO_2+H]^+$: calcd., 292.0968; Found: 292.0983.

9-Isopropyl-1aH-oxireno[2',3':4,5]benzo[1,2-a]carbazole-2,10(9H,10aH)-dione (137).

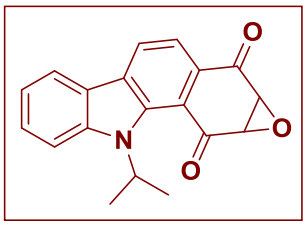

Starting from **123** (70 mg, 0.242 mmol), **137** (74 mg, 96%) was isolated as a bright yellow crystalline solid: mp 204 – 206 °C; FT-IR (ν_{max}): 2968, 1683, 1622, 1569, 1416, 1373, 1200, 1116, 1026; ^{1}H NMR (400 MHz, $CDCl_3$): δ 8.24 (d, *J* = 8.0 Hz, 1H), 8.06 (d, *J* = 7.8 Hz, 1H), 7.83 (d, *J* = 7.8 Hz, 1H), 7.72 (d, *J* = 8.5 Hz, 1H), 7.50 (dt, *J* = 1.0, 8.2 Hz, 1H), 7.26 (dd, *J* = 7.6, 14.1 Hz, 1H), 4.64-4.74 (m, 1H), 4.10 (s, 2H), 1.96 (d, *J* = 6.8 Hz, 3H), 1.39 (d, *J* = 6.9 Hz, 3H); ^{13}C NMR (100 MHz, $CDCl_3$): δ 193.3, 191.0, 142.1, 138.6, 130.9, 130.0, 127.7, 125.0, 123.3, 121.2, 120.6, 118.3, 117.4, 113.9, 56.5, 54.6, 51.3, 20.7, 20.4; HRMS (ESI) for $[C_{19}H_{15}NO_2+H]^+$: calcd., 306.1125; Found: 306.1126.

9-Allyl-1aH-oxireno[2',3':4,5]benzo[1,2-a]carbazole-2,10(9H,10aH)-dione (138).

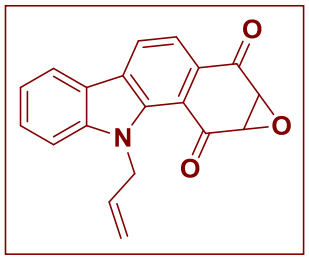

Starting from **124** (50 mg, 0.174 mmol), **138** (50 mg, 94%) was isolated as a greenish yellow crystalline solid: mp 152 – 154 °C; FT-IR (ν_{max}): 3004, 2923, 2252, 1740, 1443, 1375, 1039; ^{1}H NMR (400 MHz, $CDCl_3$): δ 8.37 (d, *J* = 8.1 Hz, 1H), 8.12 (dd, *J* = 0.8, 7.8 Hz, 1H), 7.89 (d, *J* = 8.0 Hz, 1H), 7.51-7.60 (m, 2H), 7.34 (dt, *J* = 1.2, 7.9 Hz, 1H), 5.70 (tdd, *J* = 3.6, 6.8, 13.8 Hz, 1H), 5.20-5.17 (m, 1H), 5.08-5.10 (m, 1H), 4.96-5.03 (m, 1H), 4.87-4.92 (m, 1H), 4.09 (s, 2H); ^{13}C NMR (100 MHz, $CDCl_3$): 192.4, 191.4, 143.9, 136.9, 131.8, 131.2, 129.8, 128.5, 125.2, 121.9, 121.2, 121.0, 118.4, 118.2, 118.1, 110.4, 56.1, 54.6, 48.0; Elemental analysis for $C_{19}H_{13}NO_3$ calcd. C, 75.24; H, 4.32; N, 4.62. Found, C 74.83; H, 4.57; N, 4.244; HRMS (ESI) for $[C_{19}H_{13}NO_3+H]^+$: calcd., 304.0968; Found: 304.0971.

9-Benzyl-1aH-oxireno[2',3':4,5]benzo[1,2-a]carbazole-2,10(9H,10aH)-dione (139).

Starting from **125** (50 mg, 0.148 mmol), **139** (50 mg, 96%) was isolated as a greenish yellow crystalline solid: mp 134 – 136 °C; FT-IR (ν_{max}): 2922, 2853, 1680, 1587, 1117; ^{1}H NMR (400 MHz, $CDCl_3$): δ 8.39 (d, *J* = 8.0 Hz, 1H), 8.16 (d, *J* = 7.8 Hz, 1H), 7.85 (d,

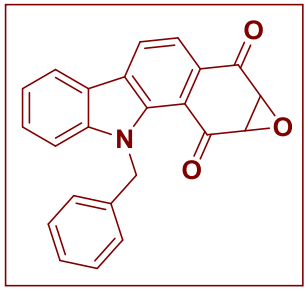

J = 7.9 Hz, 1H), 7.57-7.61 (m, 2H), 7.34-7.38 (m, 1H), 7.21-7.18 (m, 3H), 6.78-6.80 (m, 2H), 5.79 (d, *J* = 16.6 Hz, 1H), 5.55 (d, *J* = 16.6 Hz, 1H), 3.94 (d, *J* = 4.3 Hz, 1H), 3.87 (d, *J* = 4.3 Hz, 1H); ^{13}C NMR (100 MHz, $CDCl_3$): δ 192.5, 191.3, 144.5, 136.8, 136.0, 131.3, 129.7, 128.7, 128.6, 127.6, 127.0, 125.1, 121.9, 121.3, 121.1, 118.6, 118.4, 110.5, 55.8, 54.3, 49.1; Elemental analysis for $C_{23}H_{15}NO_3$ calcd. C, 78.17; H, 4.28; N, 3.96. Found, C 77.87; H, 4.095; N, 3.95; HRMS (ESI) for $[C_{23}H_{15}NO_3+H]^+$: calcd., 354.1125; Found: 354.1128.

3-Methyl-1aH-oxireno[2',3':4,5]benzo[1,2-a]carbazole-2,10(9H,10aH)-dione (140).

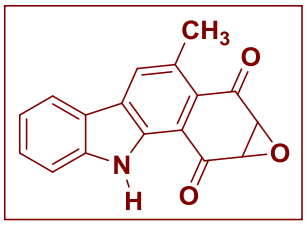

Starting from **126** (50 mg, 0.19 mmol), **140** (45 mg, 85%) was isolated as an orange red crystalline solid: mp 224 – 226 °C; FT-IR (ν_{max}): 2252, 1740, 1643, 1512, 1443, 1375, 1038; ^{1}H NMR (400 MHz, $CDCl_3$): δ 10.13 (s, 1H), 8.13 (s, 1H), 8.03 (d, *J* = 7.8 Hz, 1H), 7.47 – 7.52 (m, 2H), 7.27 (td, *J* = 5.8 Hz, 2.2 Hz, 1H), 4.00 (q, *J* = 9.5 Hz, 2H), 2.71 (s, 3H); ^{13}C NMR (100 MHz, $CDCl_3$): δ 193.3, 193.1, 142.0, 137.2, 131.4, 130.1, 129.1, 128.5, 126.9, 121.3, 121.1, 120.9, 114.3, 111.7, 55.5, 55.4, 21.8; HRMS (ESI) for $[C_{17}H_{11}NO_3+H]^+$: calcd., 278.0817; Found: 278.0813.

9-Ethyl-3-methyl-1aH-oxireno[2',3':4,5]benzo[1,2-a]carbazole-2,10(9H,10aH)-dione (141).

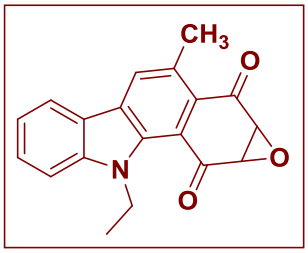

Starting from **127** (45 mg, 0.15 mmol), **141** (37 mg, 71%) was isolated as a yellow solid: mp 159 – 161 °C; FT-IR (ν_{max}): 1680, 1427, 1258, 1199, 1124; ^{1}H NMR (400 MHz, $CDCl_3$): δ 8.14 (s, 1H), 8.05 (d, *J* = 7.8 Hz, 1H), 7.55 (t, *J* = 7.6 Hz, 1H), 7.47 (d, *J* = 8.3 Hz, 1H), 7.27 (t, *J* = 7.4 Hz, 1H), 4.38 (q, *J* = 14.2 Hz, 2H), 4.14 (d, *J* = 4.6 Hz, 1H), 4.12 (d, *J* = 4.5 Hz, 1H), 2.71 (s, 3H), 1.21 (t, *J* = 7.1 Hz,

3H); ^{13}C NMR (100 MHz, $CDCl_3$): δ 193.7, 193.4, 143.9, 135.4, 130.4, 130.2, 128.3, 127.8, 121.6, 121.0, 120.6, 118.4, 110.1, 56.2, 54.5, 40.1, 21.8, 12.8; Elemental analysis for $C_{19}H_{15}NO_3$calcd. C, 74.74; H, 4.95; N, 4.59. Found C 75.01; H, 4.61; N, 4.14; HRMS (ESI) for $[C_{19}H_{15}NO_3+H]^+$: calcd., 306.1125; Found: 306.1133.

9-Isopropyl-3-methyl-1aH-oxireno[2',3':4,5]benzo[1,2-a]carbazole-2,10(9H,10aH)-dione (142).

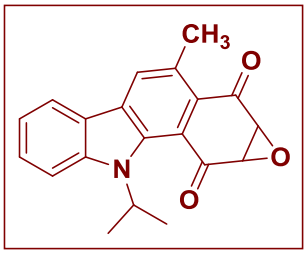

Starting from **128** (55 mg, 0.18 mmol), **142** (48 mg, 84%) was isolated as a yellow solid: mp 177 – 179 °C; FT-IR (ν_{max}): 1680, 1264, 1202, 1192, 1031; ^{1}H NMR (400 MHz, $CDCl_3$): δ 8.10 (s, 1H), 8.06 (d, *J* = 7.8 Hz, 1H), 7.69 (d, *J* = 8.5 Hz, 1H), 7.49 (dt, *J* = 0.9, 6.8 Hz, 1H), 7.27 (d, *J* = 7.4 Hz, 1H), 4.55 – 4.66 (m, 1H), 4.12 (q_{AB}, *J* = 9.5 Hz, 2H), 2.72 (s, 3H), 1.92 (d, *J* = 6.8 Hz, 3H), 1.38 (d, *J* = 7.0 Hz, 3H); ^{13}C NMR (100 MHz, $CDCl_3$): δ 194.9, 193.0, 142.5, 137.6, 130.9, 129.8, 128.0, 127.6, 123.0, 121.1, 120.3, 118.6, 113.7, 56.6, 54.5, 51.1, 22.0, 20.6, 20.3; Elemental analysis for $C_{20}H_{17}NO_3$ calcd. C, 75.22; H, 5.37; N, 4.39. Found, C 75.55; H, 5.16; N, 4.03; HRMS (ESI) for $[C_{20}H_{17}NO_3+H]^+$: calcd., 320.1281; Found: 320.1286.

9-Allyl-3-methyl-1aH-oxireno[2',3':4,5]benzo[1,2-a]carbazole-2,10(9H,10aH)-dione 143).

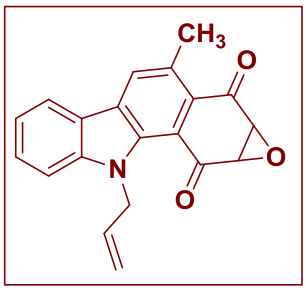

Starting from **129** (70 mg, 0.23 mmol), **143** (70 mg, 95%) was isolated as a yellow crystalline solid: mp 148 – 150 °C; FT-IR (ν_{max}): 2921, 1690, 1455, 1258, 1194, 1002; ^{1}H NMR (400 MHz, $CDCl_3$): δ 8.11 (s, 1H), 8.05 (d, *J* = 7.7 Hz, 1H), 7.53 (t, *J* = 8.7 Hz, 1H), 7.46 (d, *J* = 8.3 Hz, 1H), 7.28 (t, *J* = 7.3 Hz, 1H), 5.57 – 5.63 (m, 1H), 5.15 (d, *J* = 19.1 Hz, 1H), 5.04 (d, *J* = 19.1 Hz, 1H), 4.79 – 4.90 (m, 2H), 4.07 (d, *J* = 1.7 Hz, 2H), 2.69 (s, 3H); ^{13}C NMR (100 MHz, $CDCl_3$): δ 193.4, 193.3, 144.2, 135.5, 131.8, 130.7, 130.1, 128.4, 128.1,

127.5, 121.5, 121.0, 120.8, 119.1, 118.0, 110.1, 56.3, 54.5, 47.4, 21.8; Elemental analysis for $C_{20}H_{15}NO_3$ calcd. C, 72.06; H, 4.56; N, 4.20. Found, C 72.22; H, 4.50; N, 4.22; HRMS (ESI) for $[C_{20}H_{15}NO_3+H]^+$: calcd., 318.1125; Found: 318.1134.

9-Benzyl-3-methyl-1aH-oxireno[2',3':4,5]benzo[1,2-a]carbazole-2,10(9H,10aH)-dione (144).

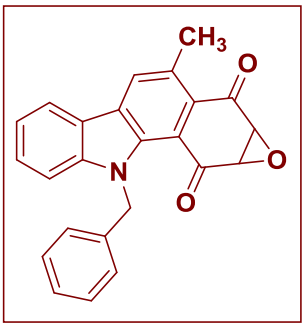

Starting from **130** (50 mg, 0.20 mmol), **144** (65 mg, 88%) was isolated as a yellow crystalline solid: mp 161 – 163 °C; FT-IR (ν_{max}): 3024, 2920, 1735, 1684, 1454, 1259, 1194; ^{1}H NMR (400 MHz, $CDCl_3$): δ 8.17 (s, 1H), 8.14 (d, *J* = 7.8 Hz, 1H), 7.53 – 7.57 (m, 2H), 7.33 (dt, *J* = 1.6, 7.8 Hz, 1H), 7.15 – 7.19 (m, 3H), 6.73 – 6.75 (m, 2H), 5.76 (d, *J* = 16.6 Hz, 1H), 5.42 (d, *J* = 16.6 Hz, 1H), 3.90 (d, *J* = 4.6 Hz, 1H), 3.78 (d, *J* = 4.6 Hz, 1H), 2.68 (s, 3H); ^{13}C NMR (100 MHz, $CDCl_3$): δ 193.5, 193.2, 144.8, 136.0, 135.3, 130.8, 130.2, 128.6, 128.5, 128.0, 127.5, 127.3, 127.1, 121.4, 121.0, 120.8, 110.1, 55.8, 54.2, 48.6, 21.7; Elemental analysis for $C_{24}H_{17}NO_3$ calcd. C, 78.46; H, 4.66; N, 3.81. Found, C 78.82; H, 4.61; N, 3.53; HRMS (ESI) for $[C_{24}H_{17}NO_3+H]^+$: calcd., 368.1281; Found: 368.1293.

6-Bromo-9-isopropyl-1aH-oxireno[2',3':4,5]benzo[1,2-a]carbazole-2,10(9H,10aH)-dione (145).

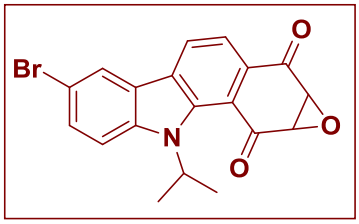

Starting from **131** (30 mg, 0.08 mmol), **145** (20 mg, 65%) was isolated as a yellow crystalline solid: mp 194 – 196 °C; FT-IR (ν_{max}): 2967, 1680, 1447, 1276, 1202, 731; ^{1}H NMR (400 MHz, $CDCl_3$): δ 8.22 (d, *J* = 8.1 Hz, 1H), 8.19 (d, *J* = 1.1 Hz, 1H), 7.85 (d, *J* = 8.0 Hz, 1H), 7.59 (d, *J* = 1.3 Hz, 2H), 4.63 – 4.73 (m, 1H), 4.12 (s, 2H), 1.94 (d, *J* = 7.0 Hz, 3H), 1.37 (d, *J* = 7.0 Hz, 3H); ^{13}C NMR (100 MHz, $CDCl_3$): δ 193.1, 190.8, 140.6, 138.8, 130.6, 130.4, 129.6, 125.2,

125.1, 123.8, 118.6, 118.1, 115.2, 113.7, 56.4, 54.5, 51.4, 20.7, 20.4; HRMS (ESI) for $[C_{19}H_{14}BrNO_3+H]^+$: calcd., 384.0230; Found: 384.0222.

6-Cyano-9-isopropyl-1aH-oxireno[2',3':4,5]benzo[1,2-a]carbazole-2,10(9H,10aH)-dione (146).

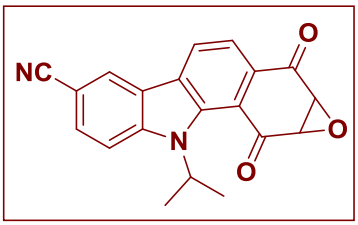

Starting from **132** (55 mg, 0.17 mmol), **146** (30 mg, 53%) was isolated as a yellow solid: mp 247 – 249 °C; FT-IR (ν_{max}): 2222, 1683, 1475, 1286, 1211; ^{1}H NMR (400 MHz, $CDCl_3$): δ 8.39 (d, *J* = 1.0 Hz, 1H), 8.30 (d, *J* = 8.1 Hz, 1H), 7.92 (d, *J* = 7.9 Hz, 1H), 7.85 (d, *J* = 8.7 Hz, 1H), 7.73 (dd, *J* = 1.6, 8.7 Hz, 1H), 4.68 – 4.78 (m, 1H), 4.15 (s, 2H), 1.98 (d, *J* = 6.9 Hz, 3H), 1.42 (d, *J* = 7.0 Hz, 3H); ^{13}C NMR (100 MHz, $CDCl_3$): δ 193.0, 190.5, 143.6, 139.1, 131.2, 130.3, 129.3, 126.1, 125.4, 123.4, 119.6, 119.5, 118.8, 114.4, 103.8, 56.4, 54.6, 51.8, 20.9, 20.4; HRMS (ESI) for $[C_{20}H_{14}N_2O_3+H]^+$: calcd., 331.1077; Found: 331.1095.

6-Fluoro-9-isopropyl-1aH-oxireno[2',3':4,5]benzo[1,2-a]carbazole-2,10(9H,10aH)-dione (147).

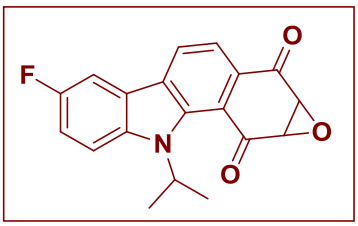

Starting from **133** (40 mg, 0.13 mmol), **147** (15 mg, 36%) was isolated as a yellow solid: mp 210 – 212 °C; FT-IR (ν_{max}): 2921, 2851, 1672, 1468, 1450, 1276, 1130, 854; ^{1}H NMR (400 MHz, $CDCl_3$): δ 8.23 (d, *J* = 7.9 Hz, 1H), 7.85 (d, *J* = 7.9 Hz, 1H), 7.73 (dd, *J* = 2.5, 8.3 Hz, 1H), 7.66 (dd, *J* = 4.1, 9.1 Hz, 1H), 7.27 (dd, *J* = 2.6, 8.9 Hz, 1H), 4.65 – 4.72 (m, 1H), 4.12 (s, 2H), 1.95 (d, *J* = 6.9 Hz, 3H), 1.37 (d, *J* = 7.0 Hz, 3H); ^{13}C NMR (100 MHz, $CDCl_3$): δ 193.1, 191.0, 159.1, 156.6, 139.4, 138.3, 130.5, 130.2, 125.3, 124.0, 118.2, 116.0, 115.7, 114.6, 114.5, 106.7, 106.5, 56.4, 54.5, 51.4, 20.8, 20.5; HRMS (ESI) for $[C_{19}H_{14}FNO_3+H]^+$: calcd., 324.1030; Found: 324.1033.

9-Isopropyl-6-methoxy-1aH-oxireno[2',3':4,5]benzo[1,2-a]carbazole-2,10(9H,10aH)-dione (148).

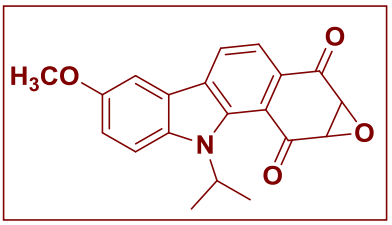

Starting from **134** (50 mg, 0.16 mmol), **148** (46 mg, 88%) was isolated as a orange crystalline solid: mp 179 – 181 °C; FT-IR (ν_{max}): 2968, 2937, 1672, 1480, 1279, 1195, 1031; ^{1}H NMR (400 MHz, $CDCl_3$): δ 8.24 (d, *J* = 8.0 Hz, 1H), 7.82 (d, *J* = 7.9 Hz, 1H), 7.62 (d, *J* = 8.8 Hz, 1H), 7.52 (d, *J* = 2.5 Hz, 1H), 7.15 (dd, *J* = 2.6, 9.0 Hz, 1H), 4.62 – 4.72 (m, 1H), 4.11 (s, 2H), 3.91 (s, 3H), 1.94 (d, *J* = 6.8 Hz, 3H), 1.36 (d, *J* = 7.0 Hz, 3H); ^{13}C NMR (100 MHz, $CDCl_3$): δ 193.2, 191.1, 154.6, 137.0, 130.8, 130.0, 125.0, 124.0, 117.8, 117.5, 114.7, 103.1, 56.4, 56.0, 54.5, 51.2, 20.8, 20.6; HRMS (ESI) for $[C_{20}H_{17}NO_4+H]^+$: calcd., 336.1230; Found: 336.1244.

4.5.9 Nucleophile-mediated decomposition of epoxides 74-92:

4.5.9.1 Reaction of 74 with nucleophiles:

To a solution of the naphthoquinone epoxide (10 mM) in CH_3CN: H_2O (1:1, v/v, 10 μL), 10 equiv of nucleophile (10 mM, 100 μL) in pH 7.4 phosphate buffer (25 mM) was added. This solution was diluted to 1 mL by adding 890 μL CH_3CN: H_2O (1:1, v/v). The reaction mixture was maintained at RT before the measurement of amount of epoxide remaining by using high performance liquid chromatography (HPLC).

4.5.9.2 Reaction of epoxides 74-92 with GSH:

To a solution of 10 mM naphthoquinone epoxide in DMSO (10 μL), 1 eq. of GSH (10 mM, 10 μL) in water, and pH 7.4 phosphate buffer (180 μL, 25 mM) were added and the solution was diluted to 1ml by adding 800 μL CH_3CN: H_2O (1:1, v/v). The reaction mixture was kept at RT for 30 min before the measurement of amount of epoxide remaining by using high performance liquid chromatography (HPLC). Mass spectrometric analysis of the products of reaction of **75** and **77** with GSH provided evidence for the formation of **75a** and **77a** respectively.

4.5.10. Hydrogen peroxide Estimation 74-92:

Xylenol orange (1.25 mM) stock solution was prepared by dissolving 9.5 mg (12.5 μmol) in 10 mL of de-ionised water. This solution was diluted 10-fold using de-ionised water to get 125 μM stock solution. A 1 M solution of sorbitol (1.82 g, 1 mol in 10 mL dI water) was also prepared and diluted to produce 100 mM stock solution. A 250 mM ferrous ammonium sulphate (FAS) solution was prepared by dissolving 980.3 mg of FAS in 10 mL of 2.5 M sulphuric acid. This solution was further diluted 10-fold by using 2.5 M sulphuric acid for the final stock solution of FAS (25 mM). Xylenol orange and sorbitol stock solutions were mixed together in a ratio of 1:1 (v/v) and to this 100:1 (v/v) FAS stock solution was added to obtain the final FOX stock solution, which is used for the hydrogen peroxide estimation. A calibration curve was generated with hydrogen peroxide. Estimation of hydrogen peroxide generated during the reaction of epoxides with GSH: To a solution of 10 mM epoxide in DMSO (5 μL) 5 equiv of GSH (10 mM, 25 μL) in water and 70 μL pH 7.4 phosphate buffer (25 mM) were added and the reaction mixture was exposed to 1 mL of oxygen gas and kept at RT for 30 min and 900 μL of FOX solution. The final solution was kept at RT for 25 min and the absorption at 586 nm was measured using a spectrophotometer.

4.5.11. Thiol mediated decomposition studies of 135-148 by HPLC.

Compound (1 mM) was reacted with cysteine (10 mM) in pH 7.4 phosphate buffer (100 mM): acetonitrile ACN (1:1 v/v) at 37 ºC for 1 h. The reaction mixture was filtered (0.22 μm filter) and injected (25 μL) in an Agilent high performance liquid chromatograph (HPLC) attached with a diode-array detector (detection wavelength was 254 nm) and a Zorbax SB C-18 reversed phase column (250 mm × 4.6 mm, 5μm). The following method with a mobile phase of water: acetonitrile was used with a run time of 25 min: multistep gradient with a flow rate of 1 mL/min – starting with 50:50 % → 0 – 5 min, 40:60 → 5 – 10 min, 30:70 → 10 – 15 min, 20:80 → 15 – 20 min, 50:50 → 20 – 23 min, 50:50 → 23 – 25 min. Each assay was conducted in duplicate and an average is reported.

4.5.13. Extracellular hydrogen peroxide estimation 135-148.

S. aureus (MSSA 29213) was cultured in 5 mL of Miller Hinton Broth (CA-MHB) medium at 37 ºC for 2 h. The cultured bacteria were centrifuged to aspirate out the medium and re-suspended in LB medium to an optical density (O.D) of 0.1. A stock solution of the compound in DMSO was added so that the final concentration was 50 μM. After incubation for 1 h the cells were plated in a 96-microwell plate (divided in several 50 μL portions in a 96-well microplate), 50 μL of a premixed solution of 10-acetyl-3,7- dihydroxyphenoxazine or Amplex Red® (prepared by following manufacturer's protocol from Invitrogen) was added and incubated at RT for 25 min before measuring the fluorescence using a microtiter plate reader (excitation 550 nm; emission 590 nm). A calibration curve with known concentrations of hydrogen peroxide was generated in LB medium and was used to quantify hydrogen peroxide produced during incubation of test analytes.

4.5.14. Intracellular superoxide detection by DHE assay from 137.

S. aureus (MSSA 29213) was cultured in 5 mL of Miller Hinton Broth (CA-MHB) medium at 37 ºC for 2 h. The cultured bacteria were centrifuged to aspirate out the medium and re-suspended in LB medium of O.D adjusted to 0.1 and incubated with 25 μM of compound and 50 μM of dihydroethidine (DHE) for 30 min in dark by covering the falcon tube in an aluminum foil. The suspension was centrifuged to aspirate out any excess compound and/or DHE in the medium. Collected bacterial pellet was lysed by mixing with acetonitrile and vortexing it for 3 min (60s × 3). The cell lysate was then removed by centrifugation and the supernatant acetonitrile was separated and stored at –20 ºC before injecting in HPLC. Agilent high performance liquid chromatograph (HPLC) attached with a fluorescence detector (excitation at 356 nm; emission at 590 nm) and a Zorbax SB C-18 reversed phase column (250 mm × 4.6 mm, 5 μm) was used. The mobile phase was water: acetonitrile containing 0.1% trifluoroacetic acid and a gradient starting with 10: 90 % → 0 min, 10: 90 to 30: 70 → 0 – 45 min, 0: 100 → 45 – 50 min, 0: 100 → 50 – 55 min, 10: 90 → 55 – 60 min was used with a flow rate of 0.5 mL/min.

Under these conditions, if superoxide is produced, a peak for 2-hydroxyethidium (2-OH-E^+), which elutes at 30.9 min, would be observed.

4.5.15. Intracellular thiol depletion (mBBr assay).

Methicillin resistant *Staphylococcus aureus* (MRSA - ATCC 33591) was cultured in 5 mL of cation adjusted Miller Hinton broth (CA-MHB) at 37 ºC for 3 h and re-suspended with fresh medium to an O.D of 1.0. Compounds (50 μM of **135**, **137**, **139**, *N*-phenylmaleimide (NPM) in DMSO and fosfomycin (Fos in water) (0.5%) were added to the bacterial suspension and incubated for 60 min at 37 ºC. Next, centrifugation of the bacterial suspension followed by removal of extracellular media to remove any excess compound was carried out. The collected bacterial pellet was re-suspended with pH 7.4 phosphate buffer and 100 μL aliquots were placed in 4 repeats in wells of sterile flat bottom 96-well microtiter plates. A solution of *mono*-Bromobimane (mBBr 50 μM in DMSO (0.5%)) was added wells and incubated for 30 min before measuring fluorescence (excitation at 390nm; emission at 490 nm) using a Varioskan microplate reader.

4.5.16 Bacterial Growth inhibition studies.

The Minimum Inhibitory Concentration (MIC) assay is used to determine the inhibitory potential of a compound against bacterial pathogens. To determine the MIC, the microbroth dilution technique is commonly used as recommended by National Committee for Clinical Laboratory Standards.[6] For this, a fixed bacterial inoculum (5×10^5 cfu/mL) is added into a series of test wells in a microtitre plate that contain various concentrations of compound under test. Following a period of incubation (37 ºC, 18-20 h), the wells are examined for growth. The lowest concentration of antibiotic that inhibits growth of the organism, as detected visually is designated as the MIC.

4.5.17 Cytotoxicity Assay

To test the effect of **137** on the growth of mammalian cells, a cytotoxicity assay was performed as per published protocols.[7] In brief, 10,000 A549 (lung cell carcinoma) cells were seeded in a 96-well plate and grown for 24 hours at 37°C in a humidified atmosphere of 5% CO_2 and 95% air in F12K medium supplemented with 10% heat-inactivated fetal bovine serum, 1.5 g Sodium bicarbonate/L, 100 µg/mL of Penicillin and 10 µg/mL of Streptomycin. The next day, cells were washed with PBS and different concentrations of **137** were added in serum free media in triplicate. Following 72 h of incubation, MTT (3-(4, 5-Dimethyl-2-thiazolyl)-2, 5-diphenyl-2H-tetrazolium bromide) was added to a final concentration of 1 mg/mL for 5 hours. At the end of the incubation period, the media were removed by gently inverting the plate. DMSO was added to the wells to solubilize the formazan crystals and absorbance was read at 595 nm in a plate reader.

4.6. Spectral Charts:

^{1}H NMR Spectrum (400 MHz, $CDCl_3$) of Compound **65**

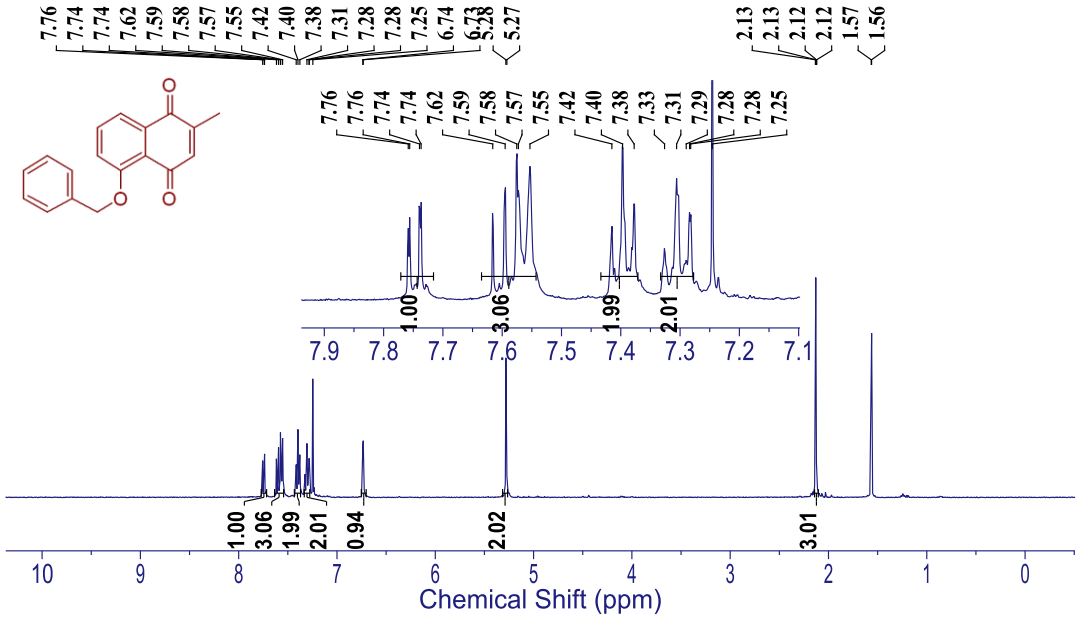

^{13}C NMR Spectrum (100 MHz, $CDCl_3$) of Compound **65**

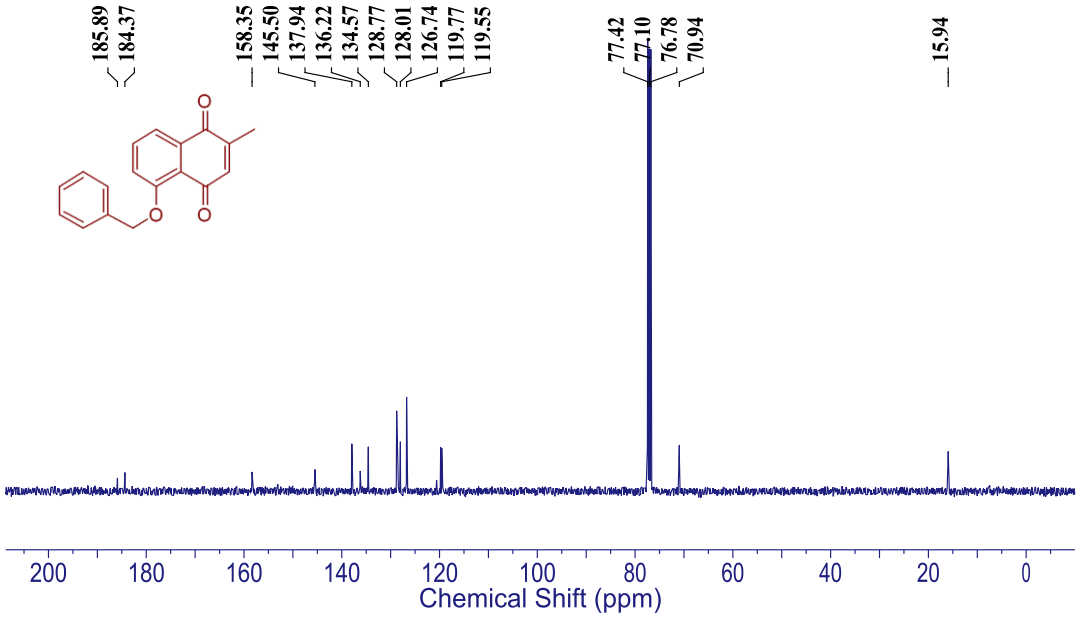

^{1}H NMR Spectrum (400 MHz, $CDCl_3$) of Compound **70**

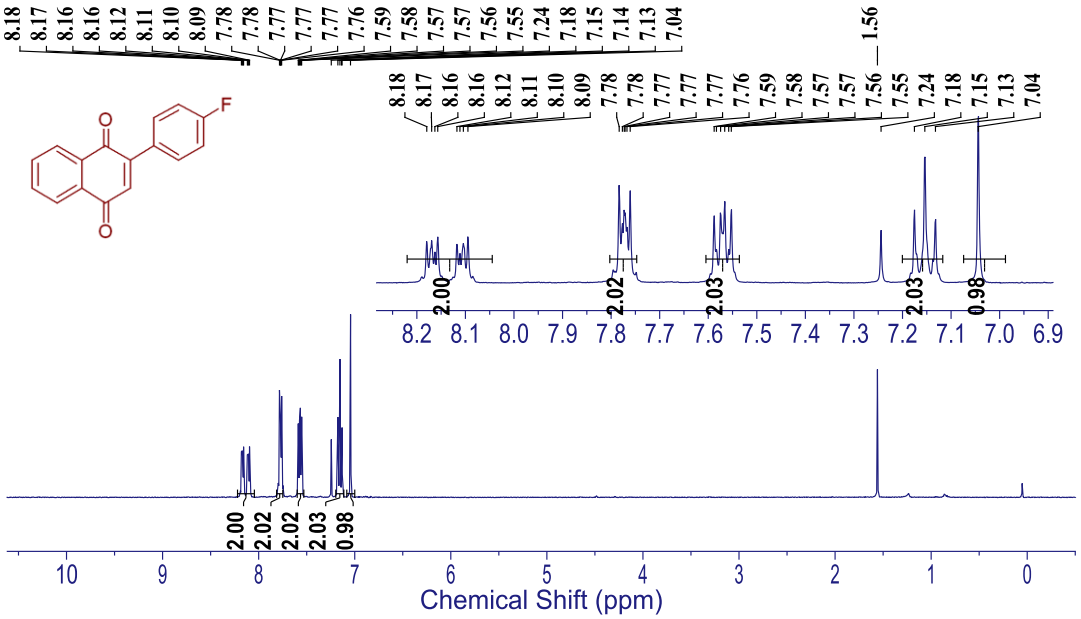

^{13}C NMR Spectrum (100 MHz, $CDCl_3$) of Compound **70**

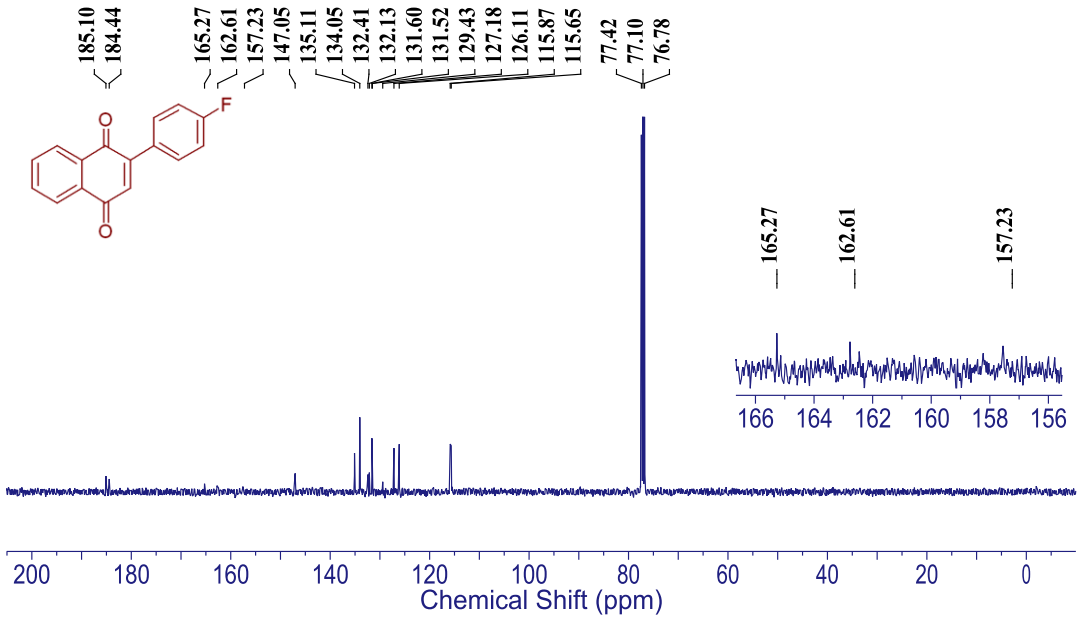

^{1}H NMR Spectrum (400 MHz, $CDCl_3$) of Compound **75**

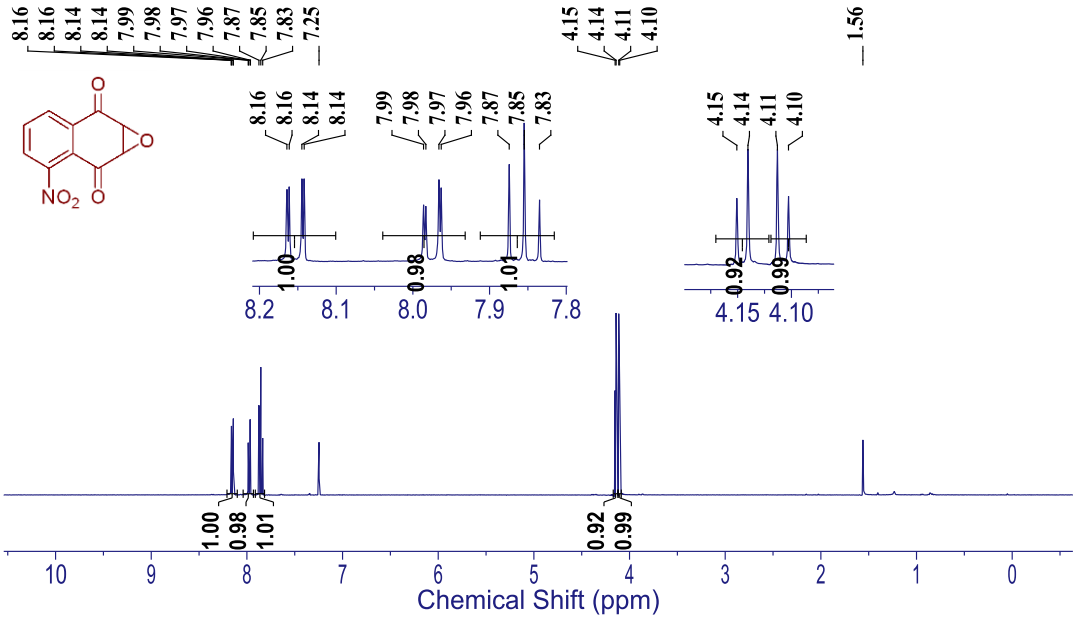

^{13}C NMR Spectrum (100 MHz, $CDCl_3$) of Compound **75**

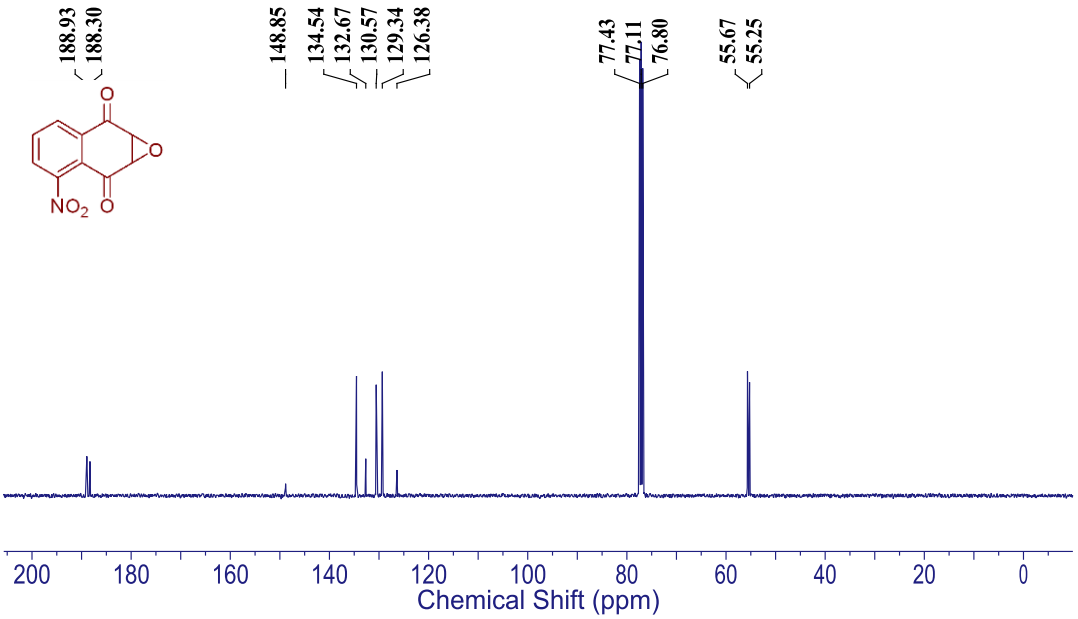

^{1}H NMR Spectrum (400 MHz, $CDCl_3$) of Compound **76**

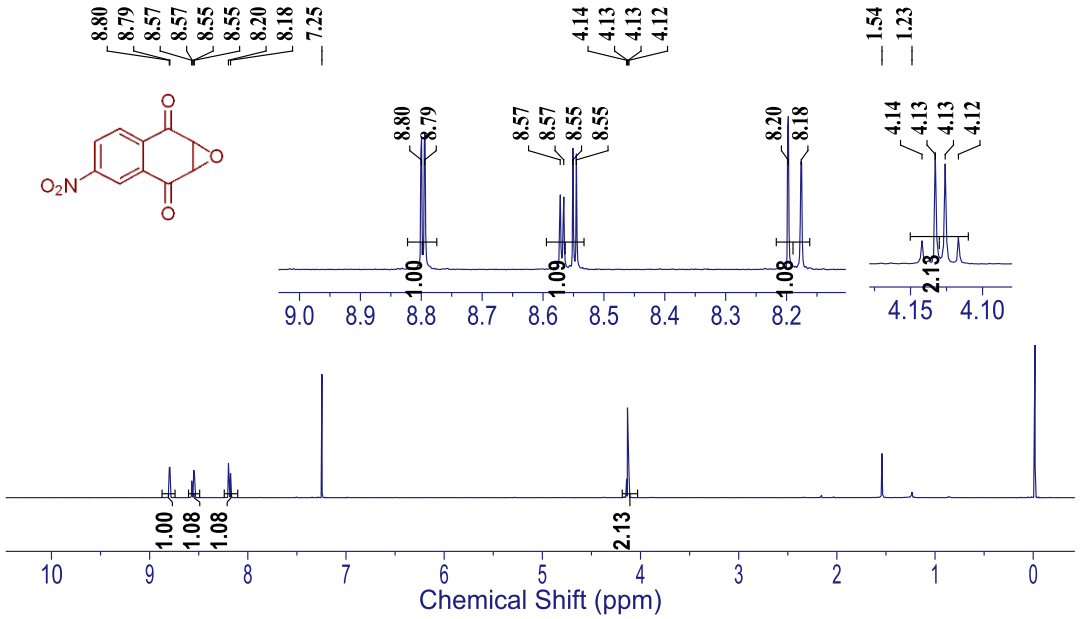

^{13}C NMR Spectrum (100 MHz, $CDCl_3$) of Compound **76**

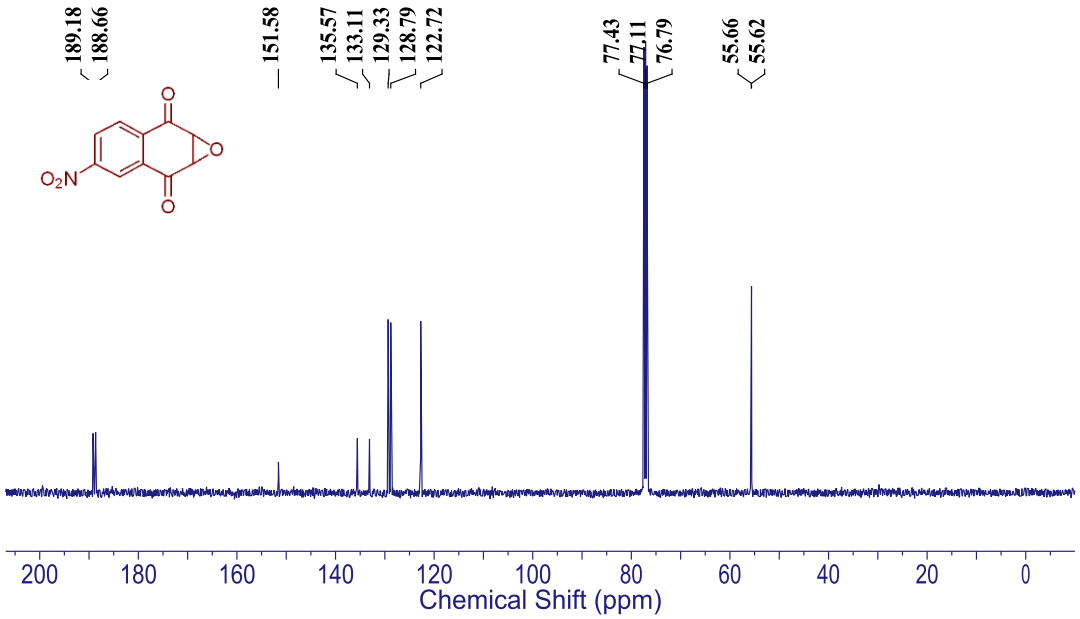

^{1}H NMR Spectrum (400 MHz, $CDCl_3$) of Compound **79**

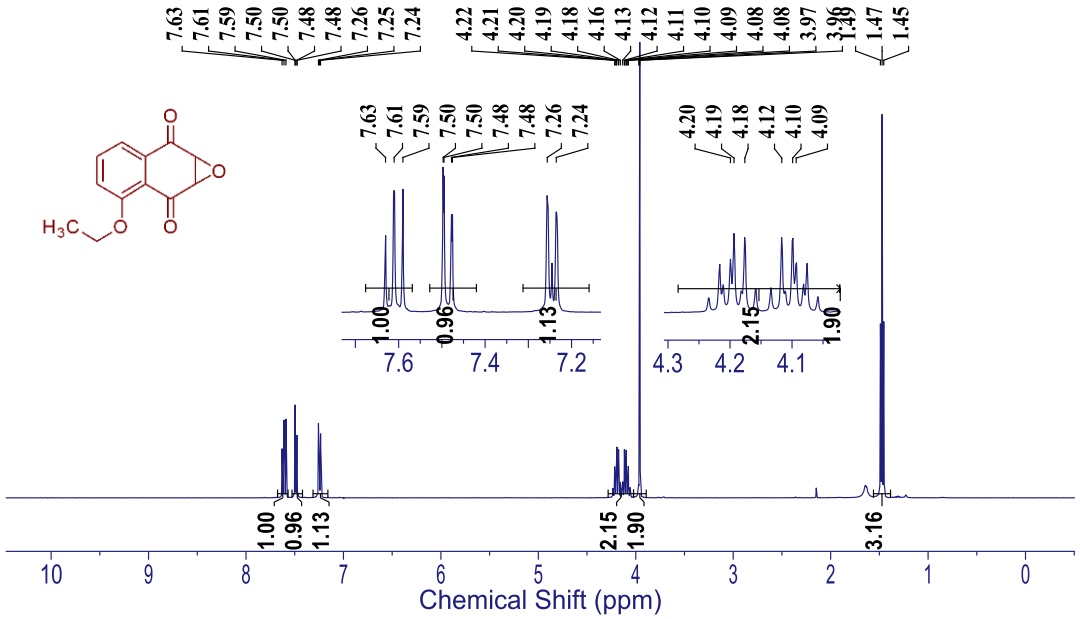

^{13}C NMR Spectrum (100 MHz, $CDCl_3$) of Compound **79**

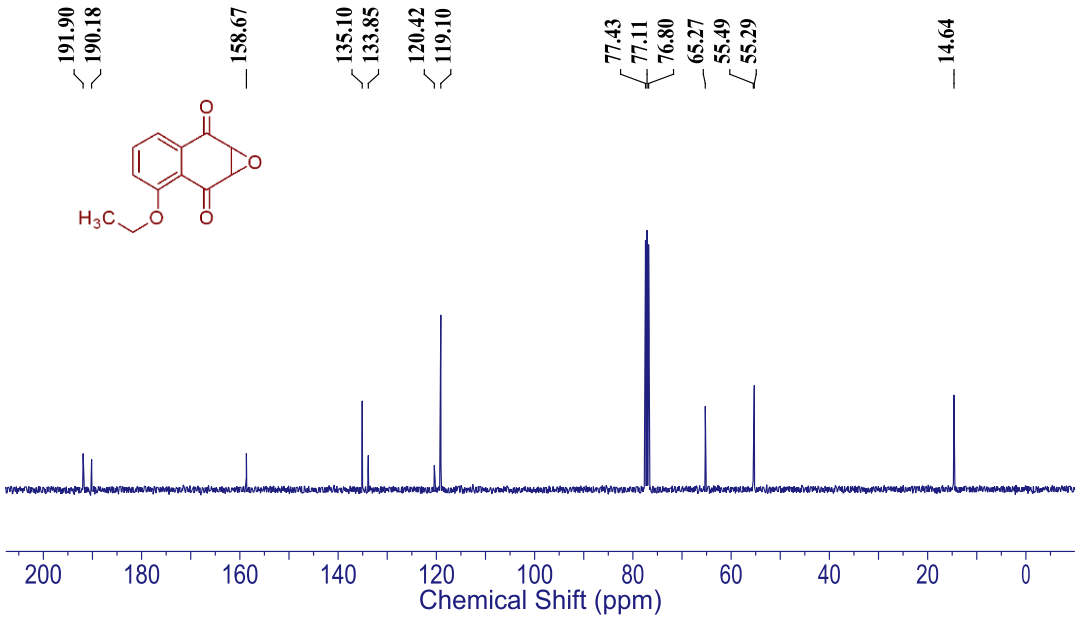

^{1}H NMR Spectrum (400 MHz, $CDCl_3$) of Compound **92**

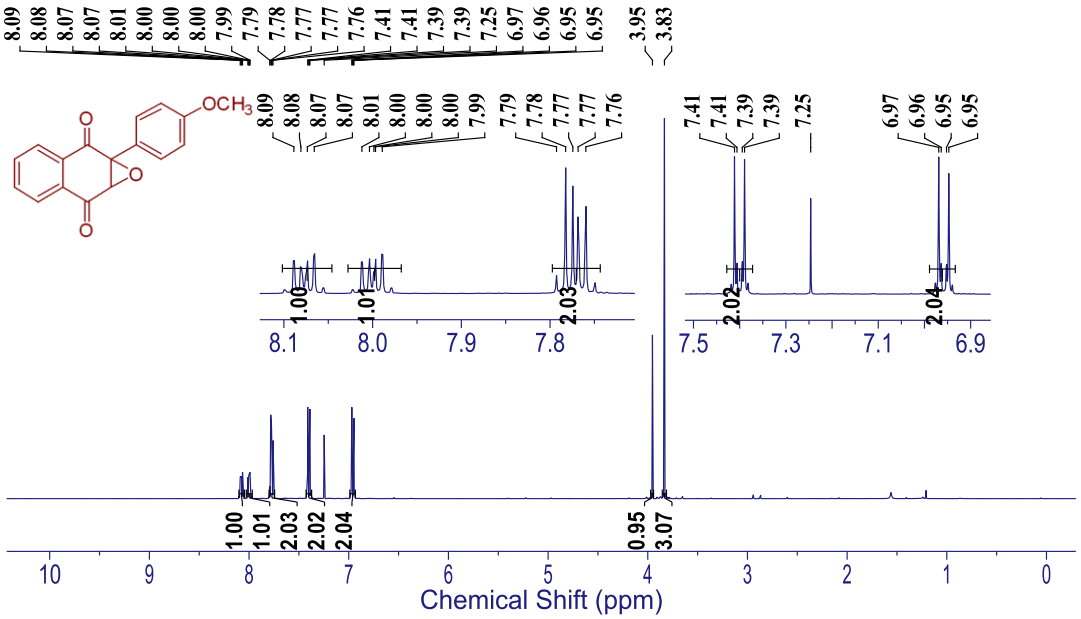

^{13}C NMR Spectrum (100 MHz, $CDCl_3$) of Compound **92**

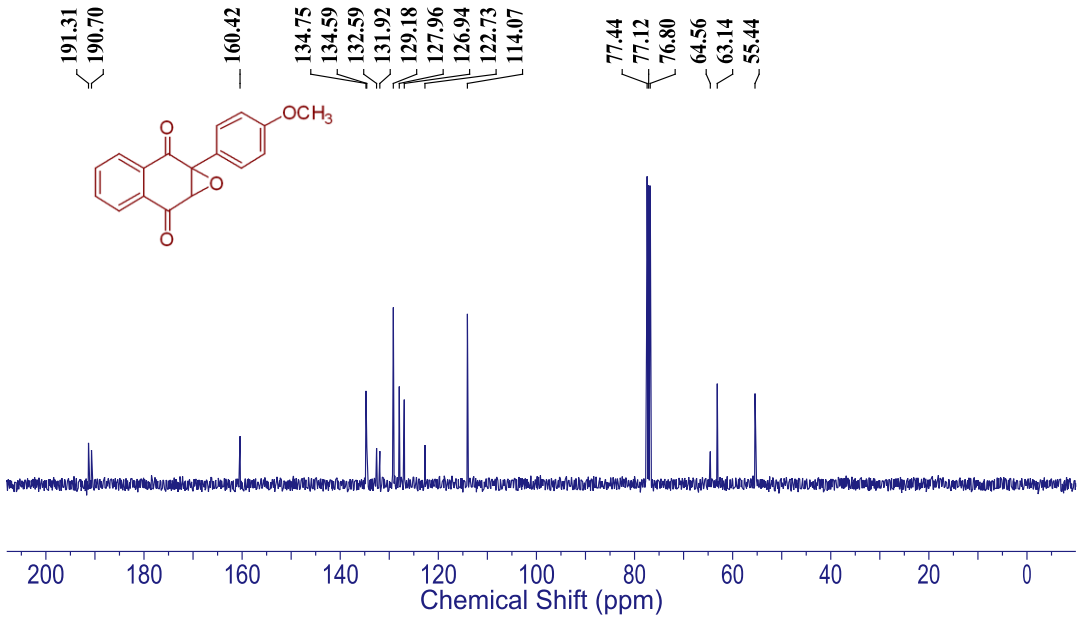

^{1}H NMR Spectrum (400 MHz, $CDCl_3$) of Compound **122**

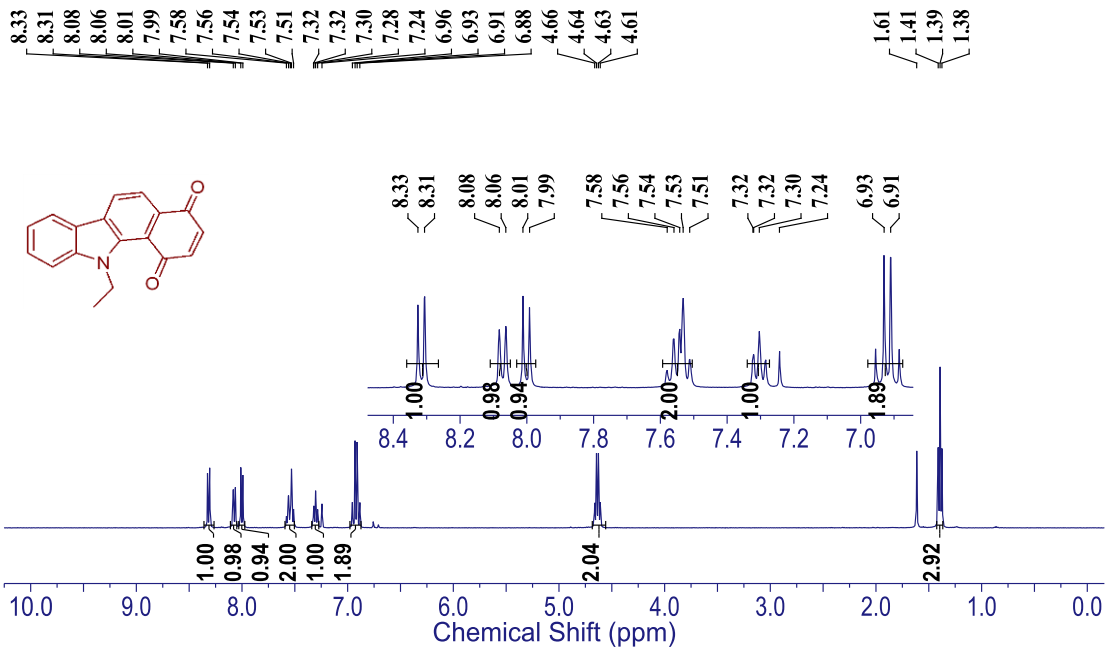

^{13}C NMR Spectrum (100 MHz, $CDCl_3$) of Compound **122**

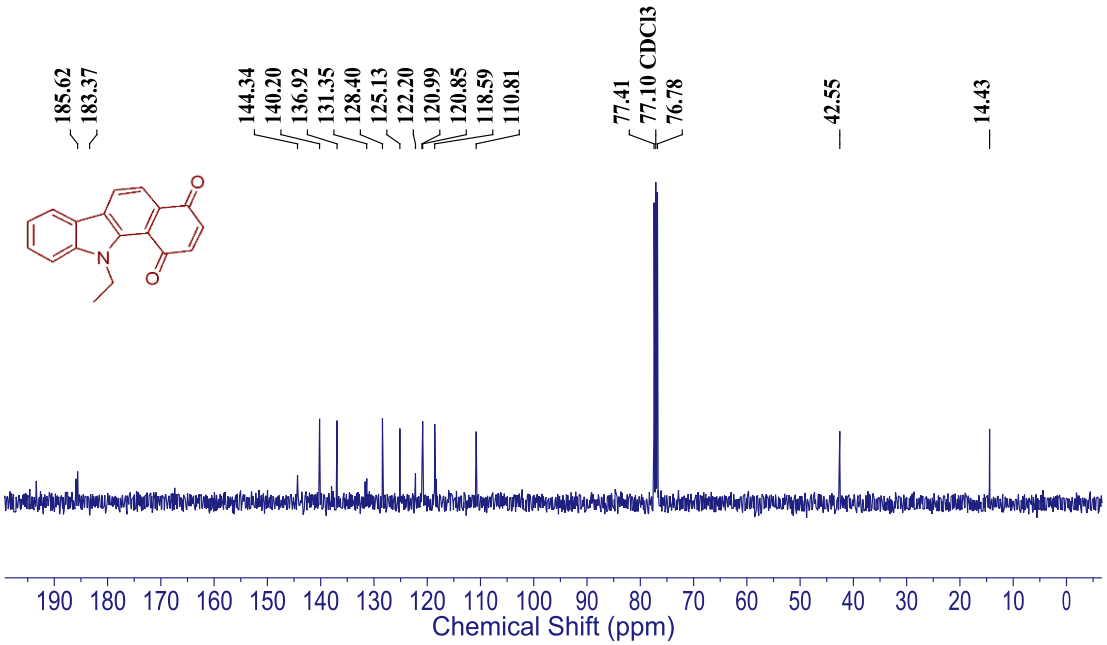

^{1}H NMR Spectrum (400 MHz, $CDCl_3$) of Compound **123**

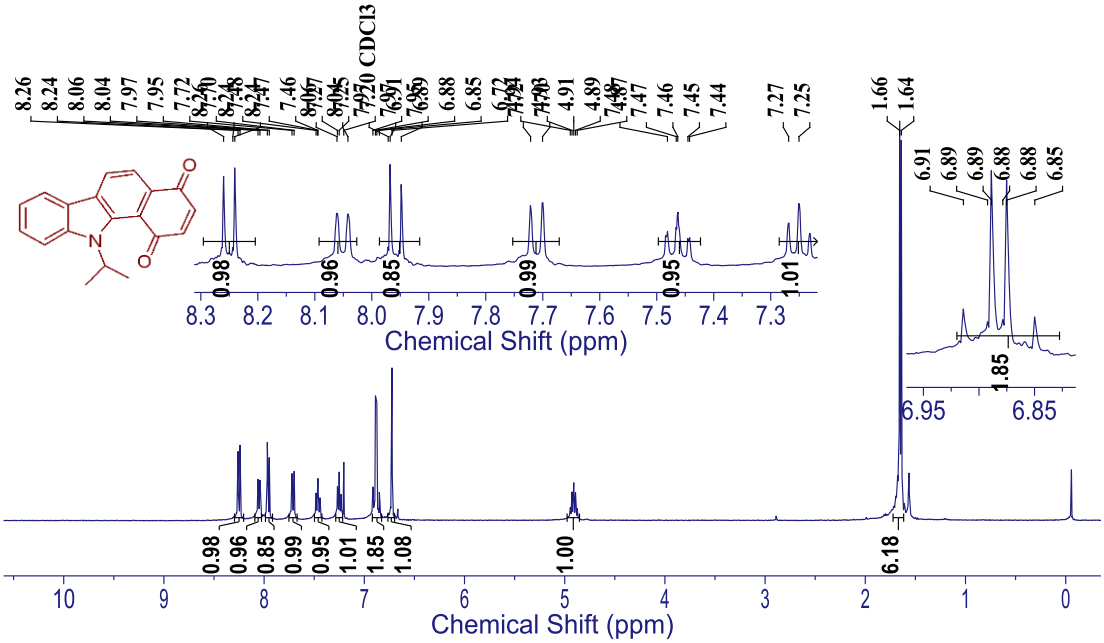

^{13}C NMR Spectrum (100 MHz, $CDCl_3$) of Compound **123**

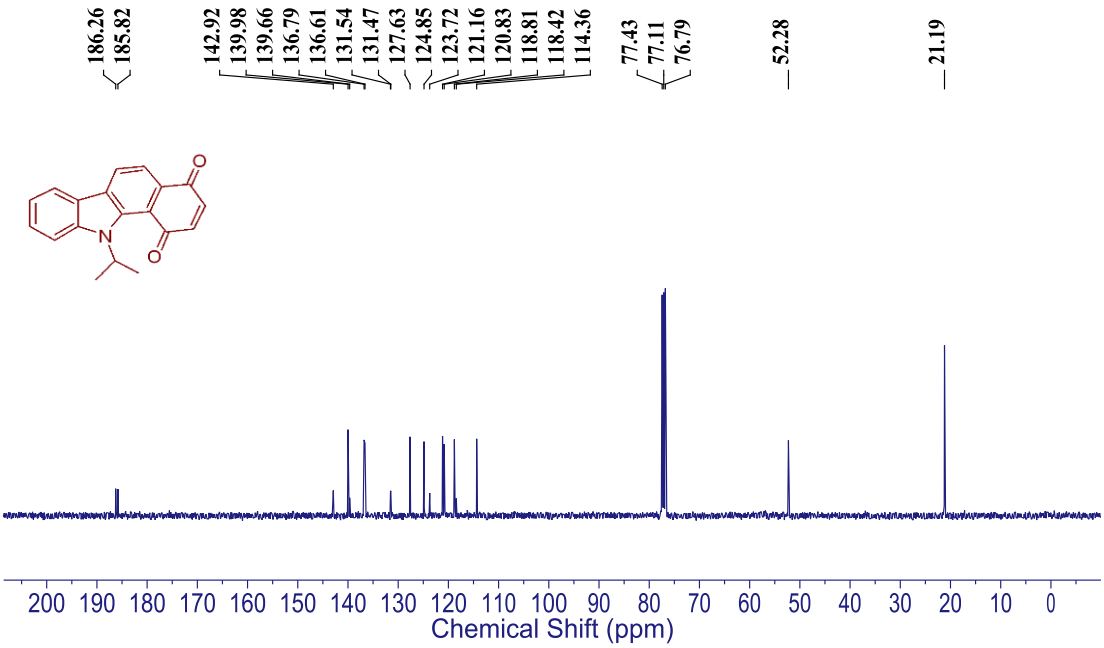

^{1}H NMR Spectrum (400 MHz, DMSO-d_6) of Compound **124**

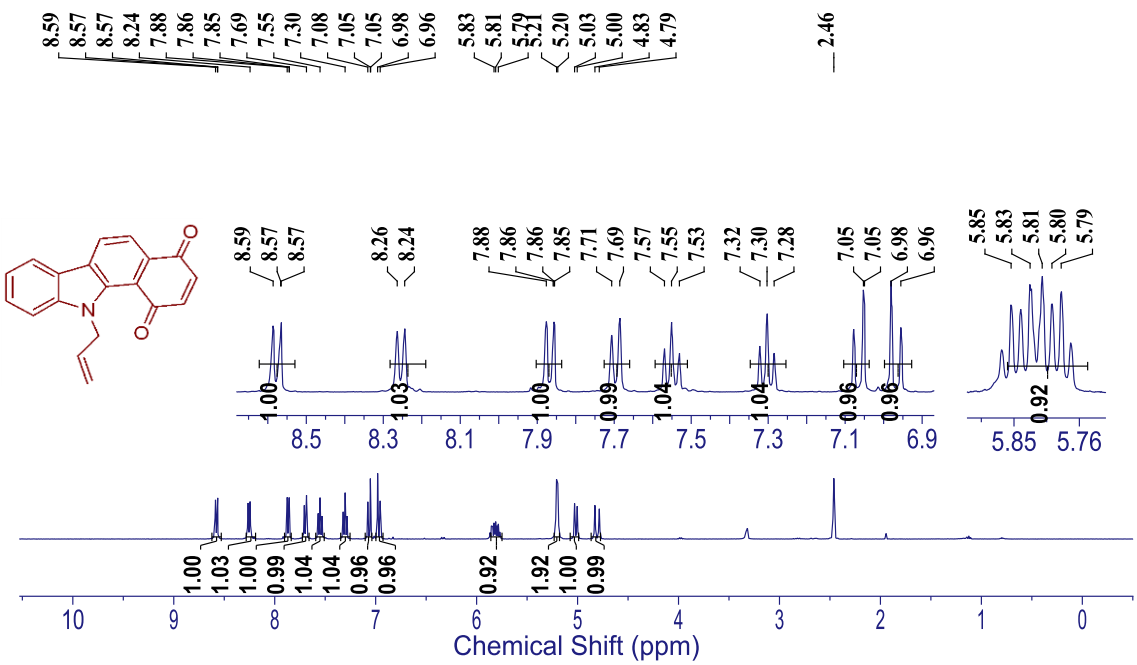

^{13}C NMR Spectrum (100 MHz, DMSO-d_6) of Compound **124**

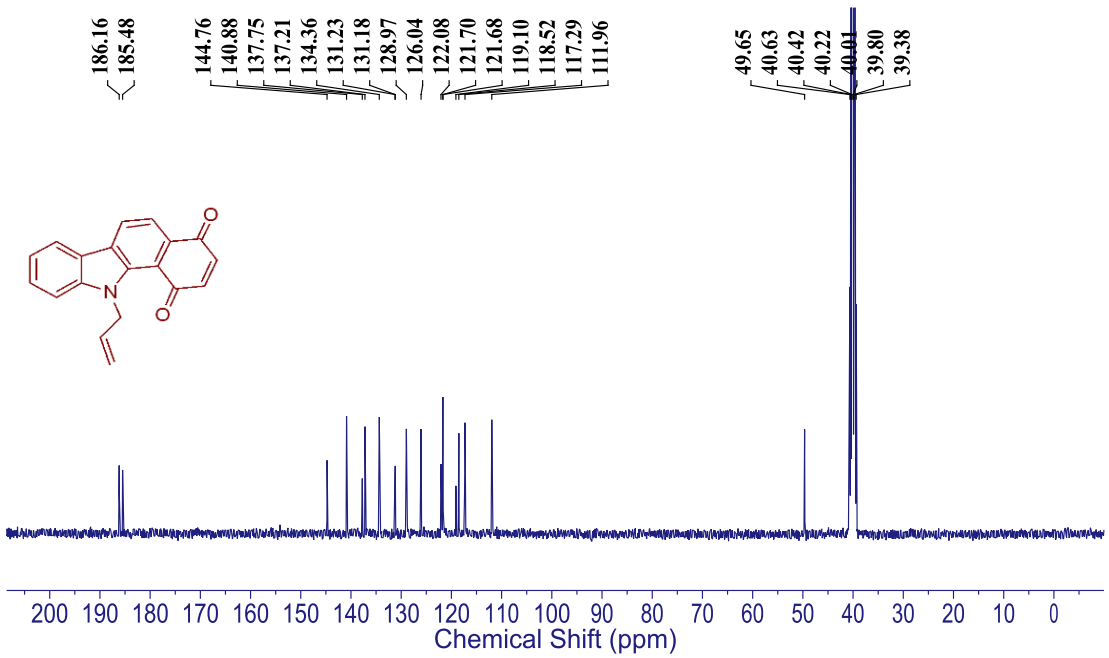

^{1}H NMR Spectrum (400 MHz, $CDCl_3$) of Compound **126**

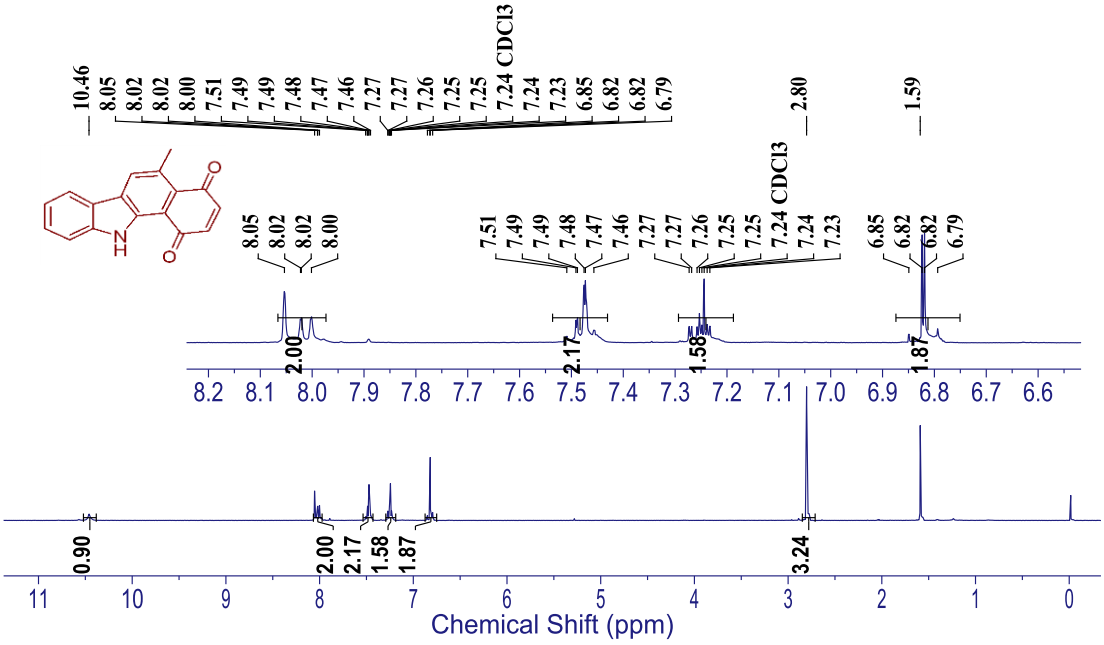

^{13}C NMR Spectrum (100 MHz, $CDCl_3$) of Compound **126**

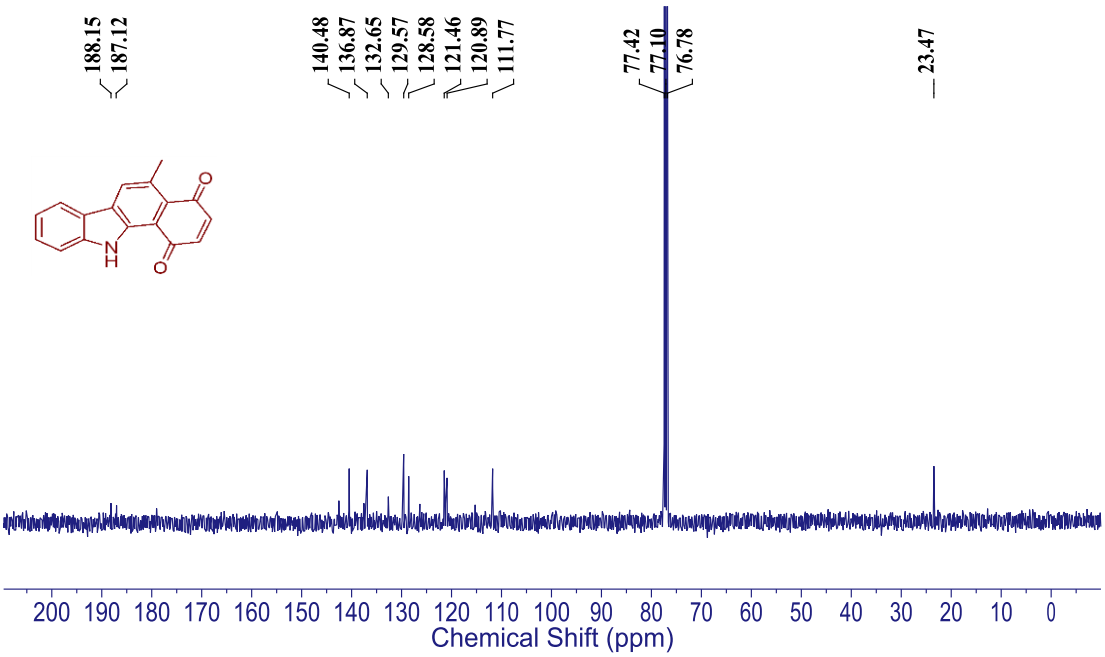

^{1}H NMR Spectrum (400 MHz, $CDCl_3$) of Compound **129**

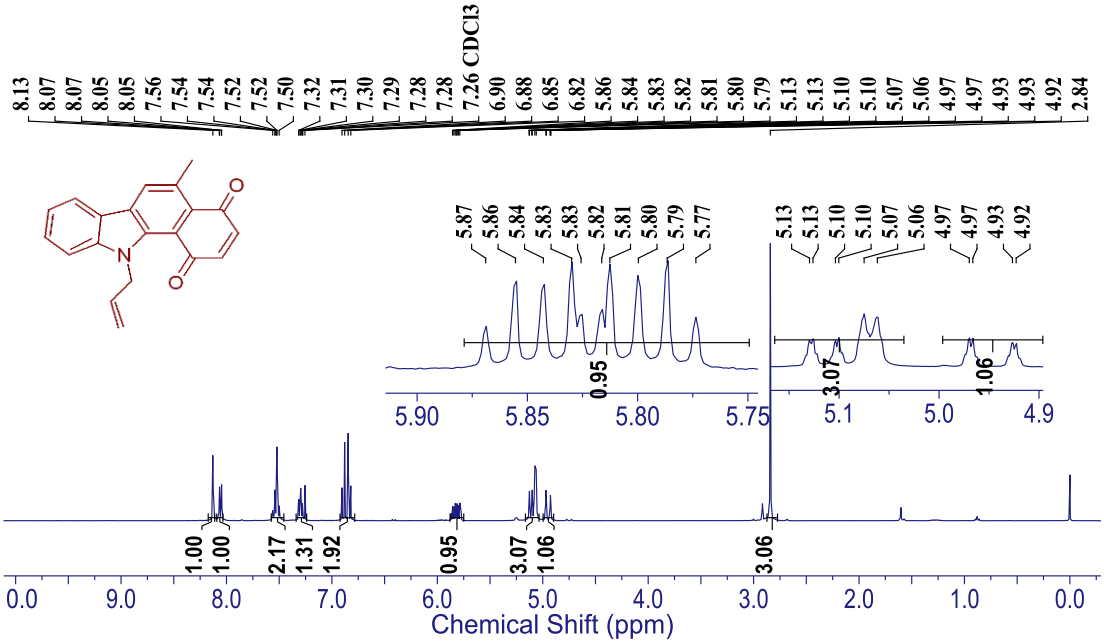

^{13}C NMR Spectrum (100 MHz, $CDCl_3$) of Compound **129**

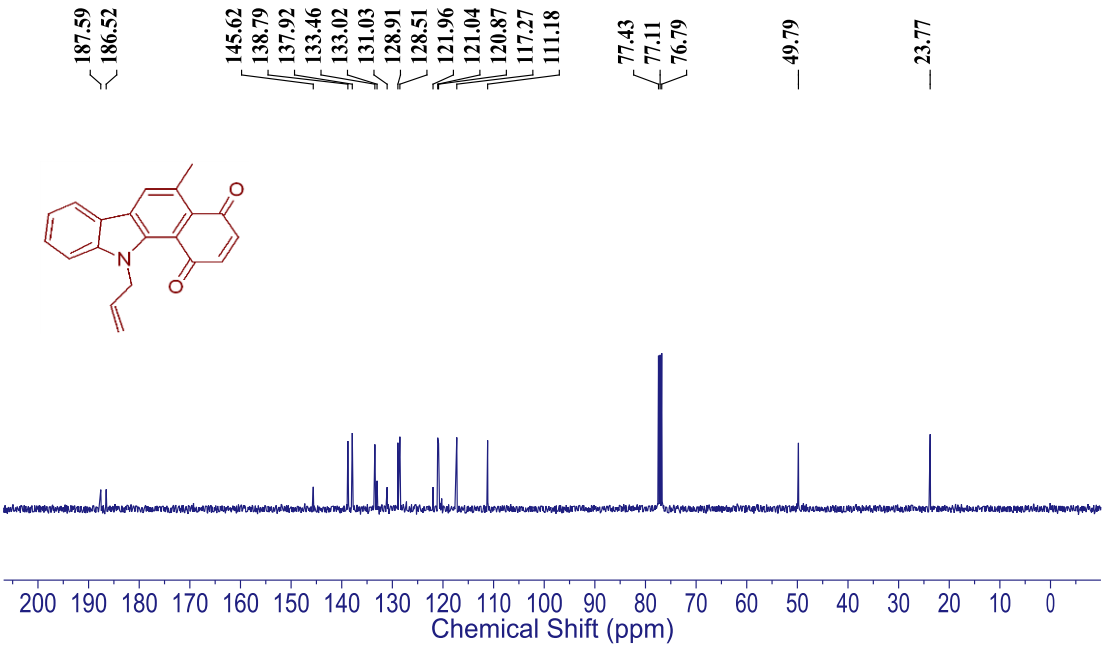

^{1}H NMR Spectrum (400 MHz, $CDCl_3$) of Compound **132**

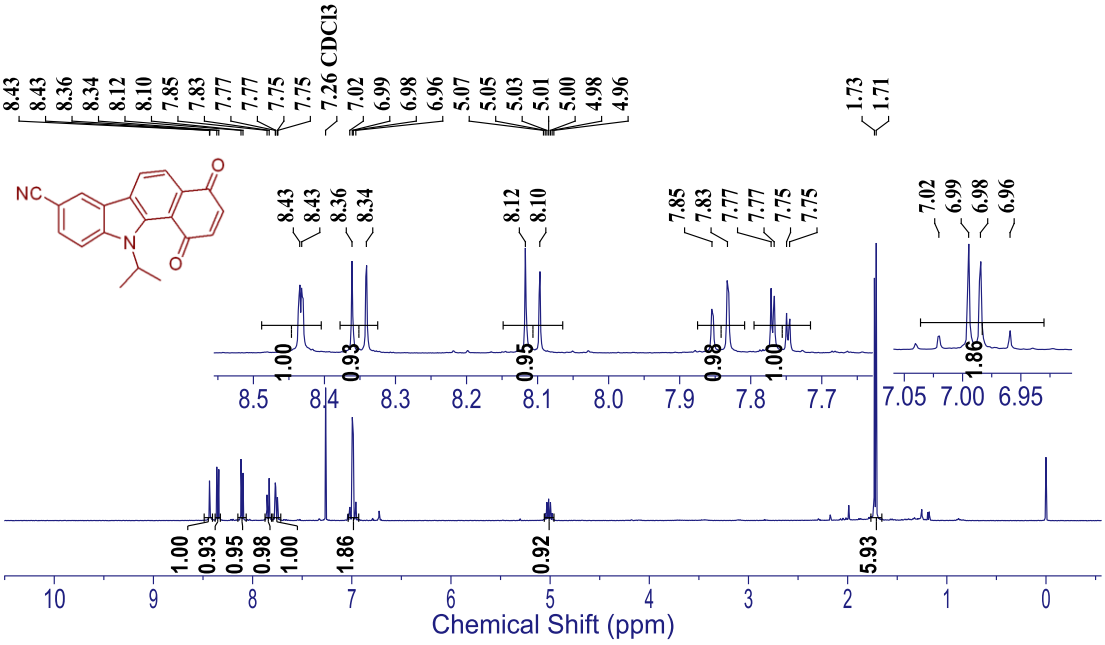

^{13}C NMR Spectrum (100 MHz, $CDCl_3$) of Compound **132**

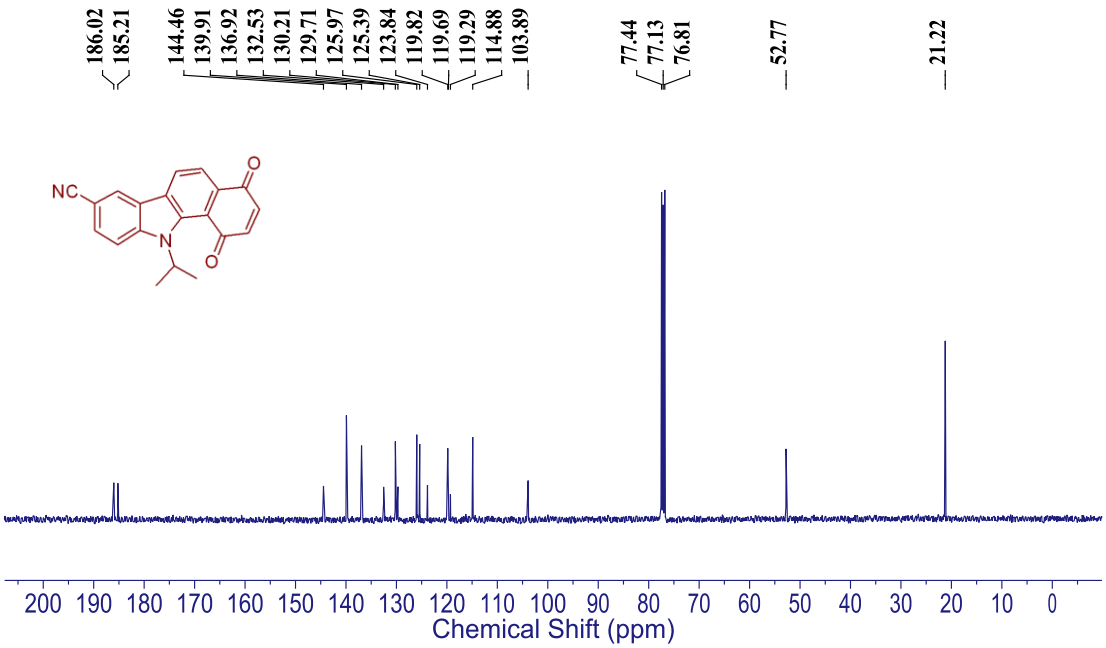

^{1}H NMR Spectrum (400 MHz, $CDCl_3$) of Compound **136**

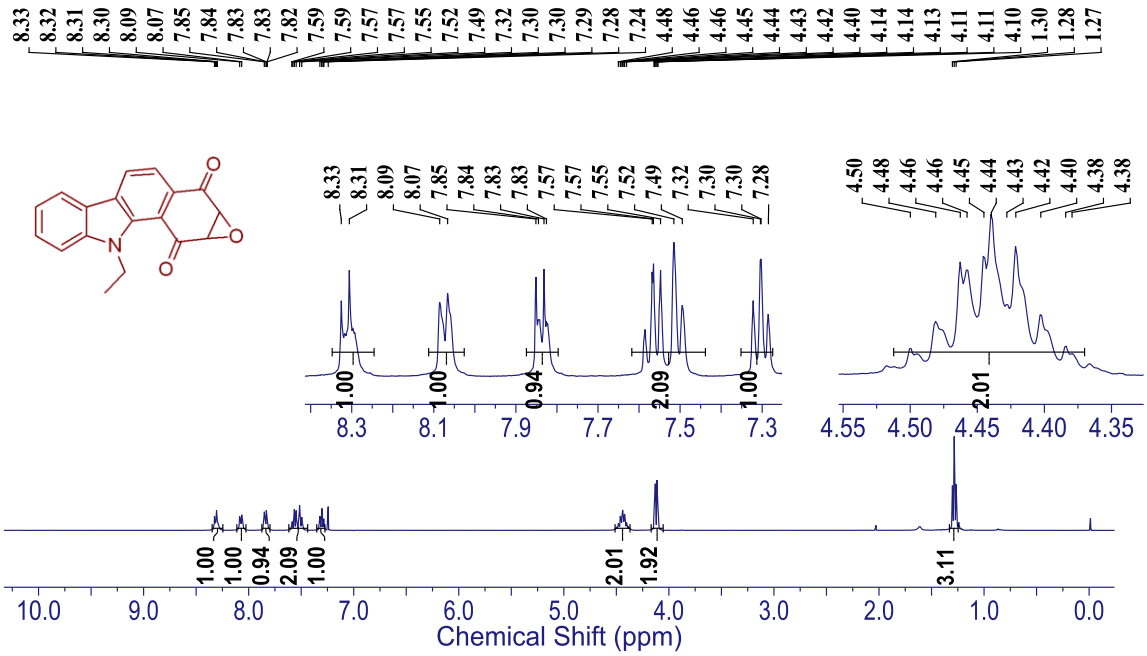

^{13}C NMR Spectrum (100 MHz, $CDCl_3$) of Compound **136**

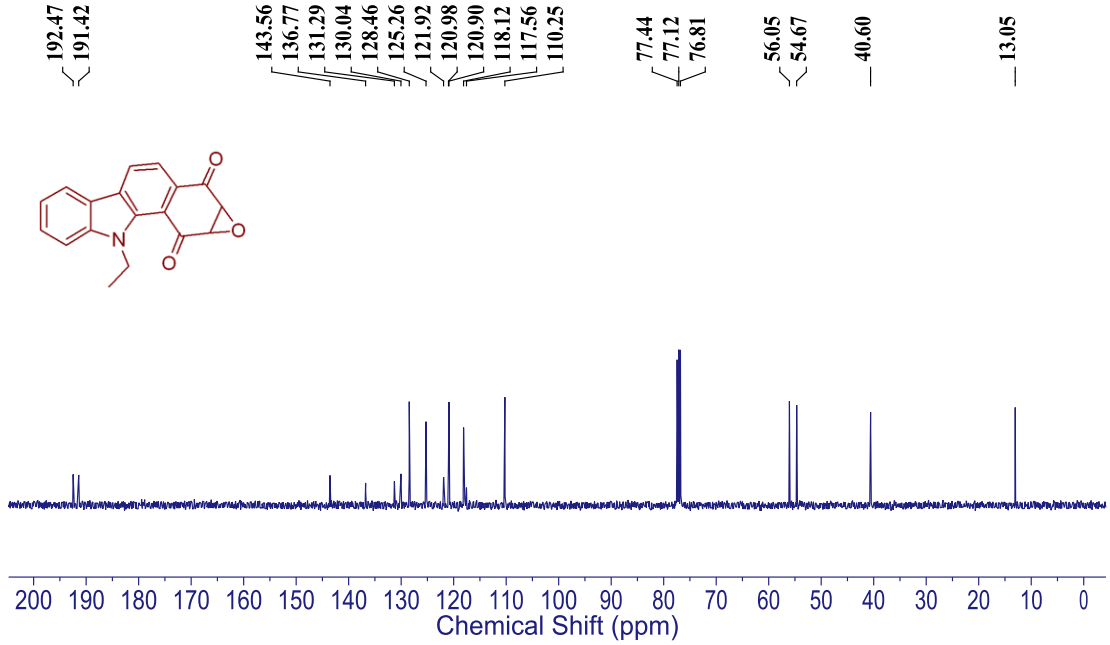

^{1}H NMR Spectrum (400 MHz, $CDCl_3$) of Compound **137**

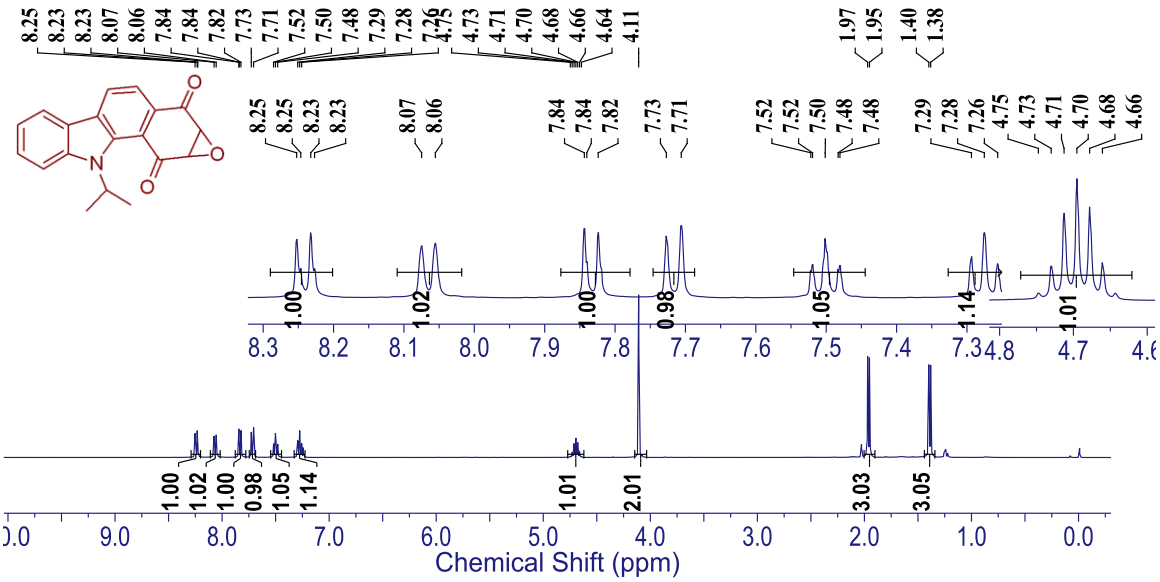

^{13}C NMR Spectrum (100 MHz, $CDCl_3$) of Compound **137**

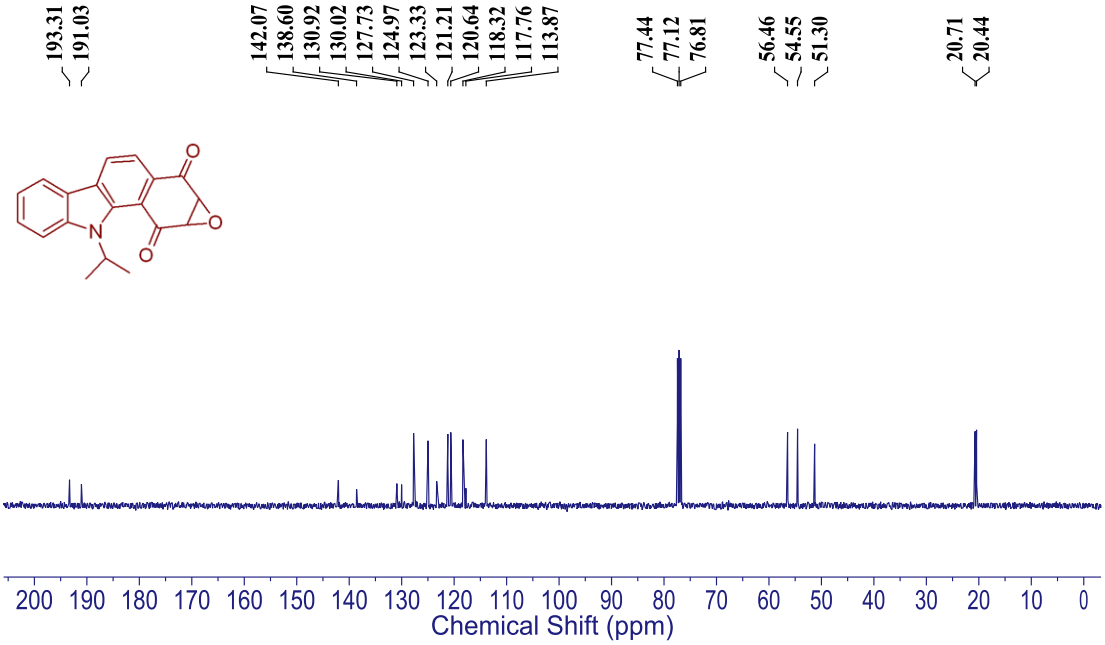

^{1}H NMR Spectrum (400 MHz, $CDCl_3$) of Compound **138**

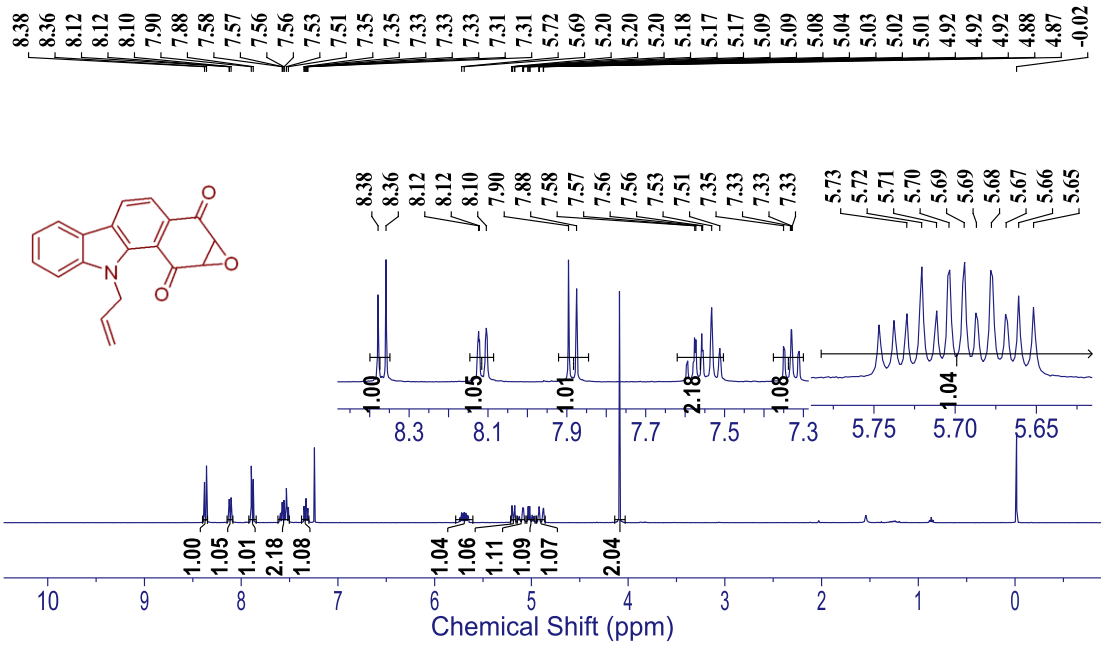

^{13}C NMR Spectrum (100 MHz, $CDCl_3$) of Compound **138**

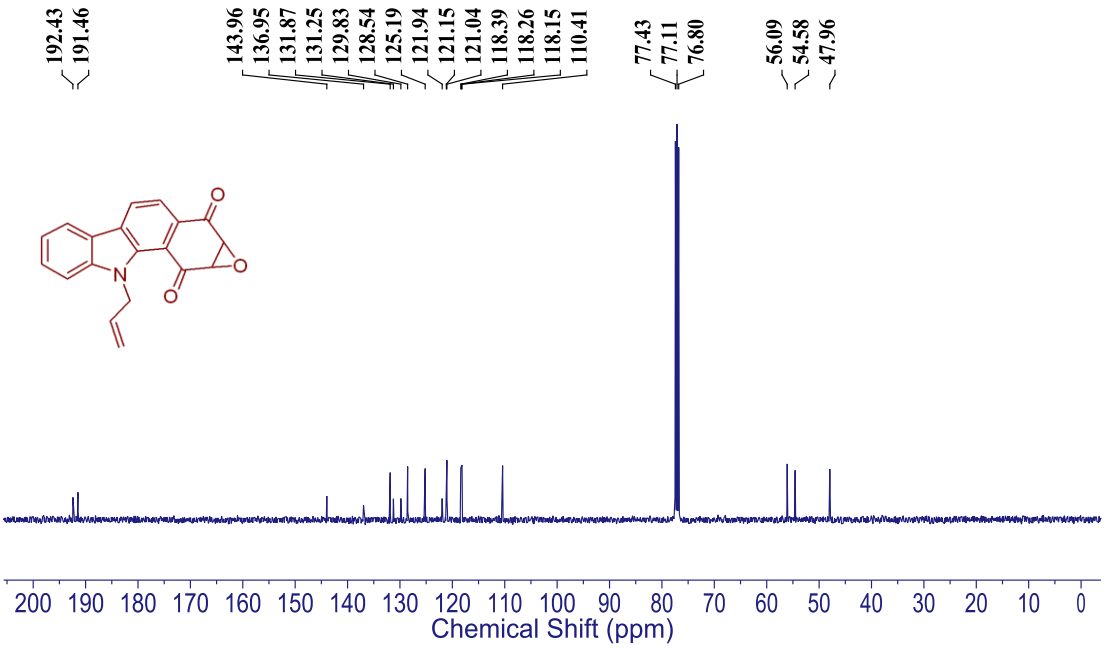

^{1}H NMR Spectrum (400 MHz, $CDCl_3$) of Compound **143**

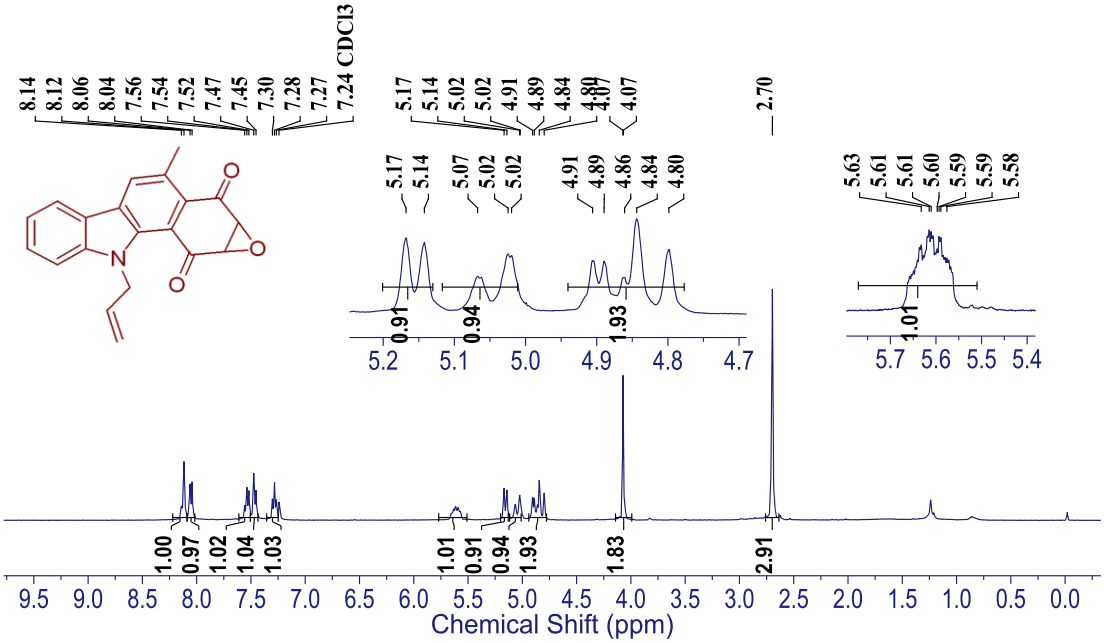

^{13}C NMR Spectrum (100 MHz, $CDCl_3$) of Compound **143**

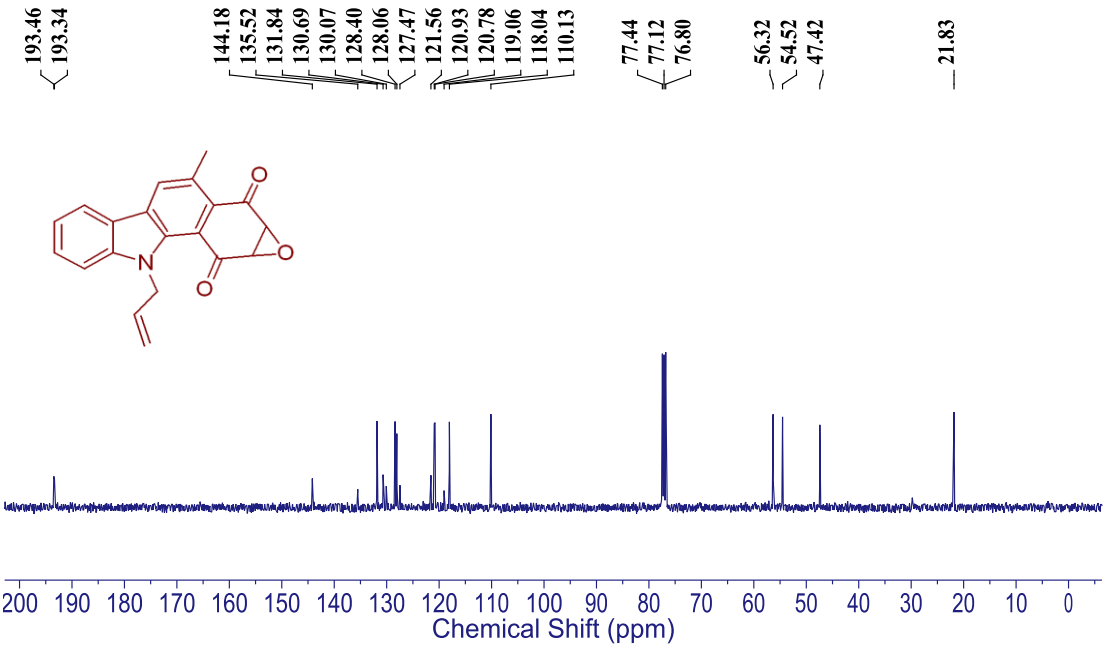

^{1}H NMR Spectrum (400 MHz, $CDCl_3$) of Compound **146**

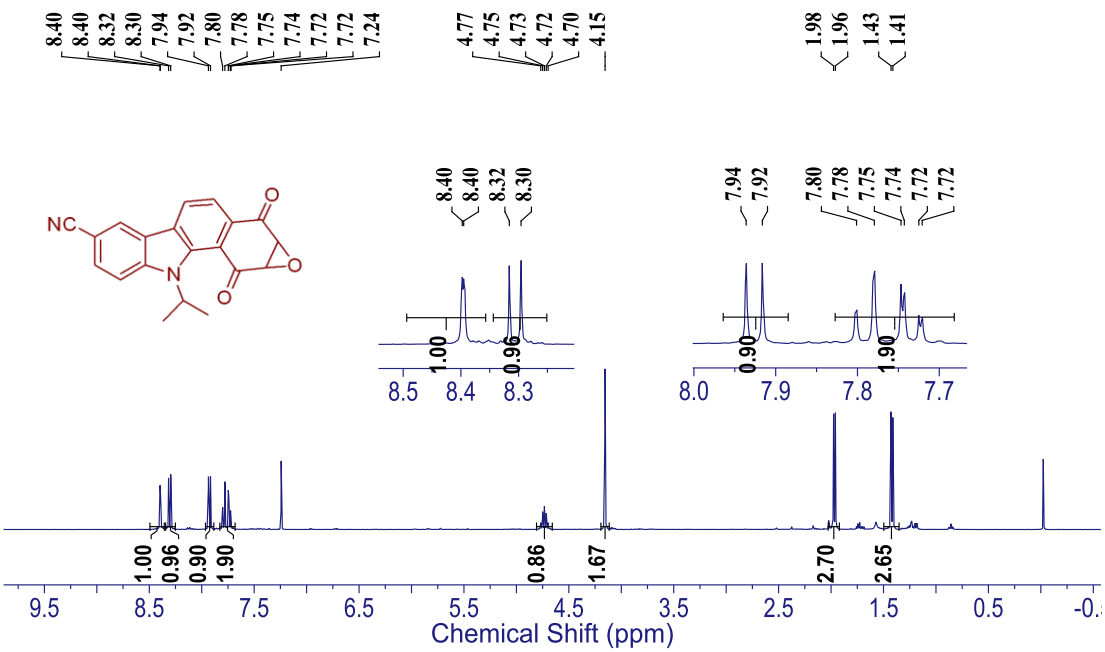

^{13}C NMR Spectrum (100 MHz, $CDCl_3$) of Compound **146**

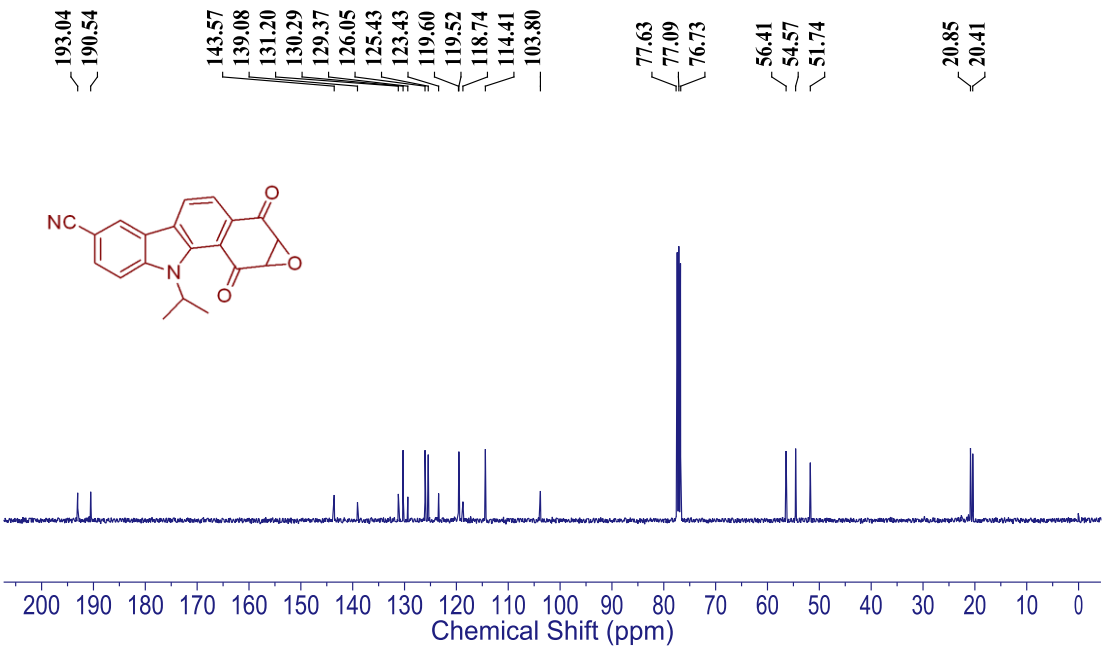

^{19}F NMR Spectrum (400 MHz, $CDCl_3$) of Compound **147**

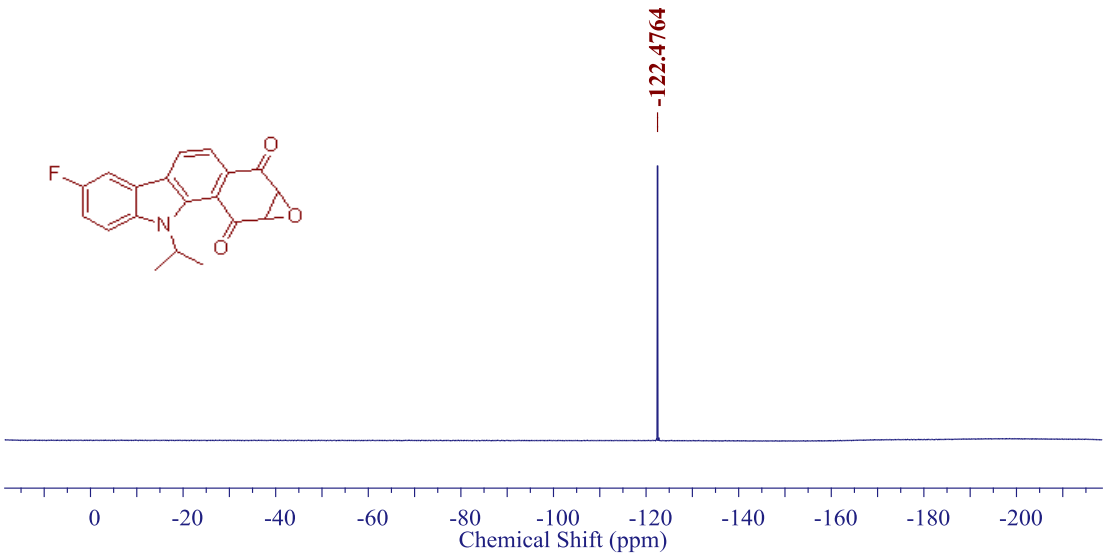

4.7. References:

1. Lohman, J. R.; Remington, S. J. Development of a family of redox-sensitive green fluorescent protein indicators for use in relatively oxidizing subcellular environments. *Biochemistry* **2008,** 47, 8678-88.
2. Foyer, C. H.; Noctor, G. Redox Homeostasis and Antioxidant Signaling: A Metabolic Interface between Stress Perception and Physiological Responses. *Plant Cell* **2005,** 17, 1866-1875.
3. Michalopoulos, A. S.; Livaditis, I. G.; Gougoutas, V. The revival of fosfomycin. *Intl. J. Infect. Dis.* **2011,** 15, e732-e739.
4. Newton, G. L.; Fahey, R. C.; Rawat, M. Detoxification of toxins by bacillithiol in *Staphylococcus aureus*. *Microbiol.* **2012,** 158, 1117-1126.
5. Newton, G. L.; Rawat, M.; La Clair, J. J.; Jothivasan, V. K.; Budiarto, T.; Hamilton, C. J.; Claiborne, A.; Helmann, J. D.; Fahey, R. C. Bacillithiol is an antioxidant thiol produced in Bacilli. *Nat. Chem. Biol.*, **2009,** 5, 625-627.
6. Adeniyi, B. A.; Robert, M. F.; Chai, H.; Fong, H. H. In vitro cytotoxicity activity of Diosquinone, a naphthoquinone epoxide. *Phytother. Res.* **2003,** 17, 282-4.
7. Alake, L. B. Antibacterial activity of diosquinone isolated from Diospyros tricolor. *Planta Med.* **1994,** 60, 477.
8. Furumoto, T. Biosynthetic origin of 2,3-epoxysesamone in a Sesamum indicum hairy root culture. *Biosci Biotechnol Biochem* **2009,** 73, 2535-7.
9. Hasan, A. F.; Furumoto, T.; Begum, S.; Fukui, H. Hydroxysesamone and 2,3-epoxysesamone from roots of Sesamum indicum. *Phytochem.* **2001,** 58, 1225-8.
10. Li, Q.; Khosla, C.; Puglisi, J. D.; Liu, C. W. Solution structure and backbone dynamics of the holo form of the frenolicin acyl carrier protein. *Biochem.* **2003,** 42, 4648-57.
11. Kossor, D. C.; Han, S.; Kemp, F. W.; Slauter, R. W.; Serota, D.; Rajaskarian, D.; Milner, N.; Davidovich, A.; Bogden, J. D. Administration of the oral antibiotic frenolicin-B selectively alters copper nutriture in male rats. *J. Nutr.* **2001,** 131, 3247-50.

12. Armer, R. E.; Dutton, C. J.; Fenner, B. R.; Greenwood, S. D.; Hall, K. T.; Rudge, A. J. Carbocyclic frenolicin analogues: novel anticoccidial agents. *Bioorg. Med. Chem. Lett.* **1998,** 8, 139-42.
13. Bibb, M. J.; Sherman, D. H.; Omura, S.; Hopwood, D. A. Cloning, sequencing and deduced functions of a cluster of Streptomyces genes probably encoding biosynthesis of the polyketide antibiotic frenolicin. *Gene* **1994,** 142, 31-9.
14. Tsuzuki, K.; Iwai, Y.; Omura, S.; Shimizu, H.; Kitajima, N. Nanaomycins production by a frenolicin B producing strain. *J. Antibiot.* **1986,** 39, 1343-5.
15. Omura, S.; Tsuzuki, K.; Iwai, Y.; Kishi, M.; Watanabe, S.; Shimizu, H. Anticoccidial activity of frenolicin B and its derivatives. *J. Antibiot.* **1985,** 38, 1447-8.
16. Iwai, Y.; Kora, A.; Takahashi, Y.; Hayashi, T.; Awaya, J.; Masuma, R.; Oiwa, R.; Omura, S. Production of deoxyfrenolicin and a new antibiotic, frenolicin B by Streptomyces roseofulvus strain AM-3867. *J. Antibiot.* **1978,** 31, 959-65.
17. Ellestad, G. A.; Kunstmann, M. P.; Whaley, H. A.; Patterson, E. L. The structure of frenolicin. *J. Am. Chem. Soc.* **1968,** 90, 1325-32.
18. Potashman, M. H.; Duggan, M. E. Covalent modifiers: An orthogonal approach to drug. *J. Med. Chem.* **2009,** 52, 1231-1246.
19. Brunmark, A.; Cadenas, E. 1,4-Reductive Addition of Glutathione to Quione Epoxides. *Free Radical Biol. Med.* **1989,** 6, 149-165.
20. Wu, J.; Chien, C.-C.; Yang, L.-Y.; Huang, G.-C.; Cheng, M.-C.; Lin, C.-T.; Shen, S.-C.; Chen, Y.-C. Vitamin K3-2,3-epoxide induction of apoptosis with activation of ROS-dependent ERK and JNK protein phosphorylation in human glioma cells. *Chemico-Biological Interactions* **2011,** 193, 3-11.
21. Rashid, A.; Read, G. Quinone epoxides. Part II. Synthesis of (±)-terreic acid and some related epoxides. *J. Chem. Soc. C* **1967**, 1323-25.
22. Cameron, D. W.; Feutrill, G. I.; Patti, A. F. Nucleophilic alkenes. VII. 1:1-Addition of 1,1-dimethoxyethane to 1,4-naphtoquinones substituted in the benzenoid ring. *Aust. J. Chem.* **1980,** 33, 1805-16.

23. Maugel, N.; Snider, B. B. Efficient Synthesis of the Tetracyclic Aminoquinone Moiety of Marmycin A. *Org. Lett.* **2009,** 11, 4926-29.
24. Betts, R. L.; Murphy, S. T.; Johnson, C. R. Enzymatic desymmetrization/resolution of epoxydiols derived from 1,4-naphthoquinone, 5-hydroxy-1,4-naphthoquinone and 5,8-dihydroxy-1,4-naphthoquinone. *Tetrahedron Asymm.* **2004,** 15, 2853-2860.
25. Yoshizawa, M.; Takeyama, Y.; Okano, T.; Fujita, M. Cavity-Directed Synthesis within a Self-Assembled Coordination Cage: Highly Selective [2 + 2] Cross-Photodimerization of Olefins. *J. Am. Chem. Soc.* **2003,** 125, 3243-3247.
26. Molina, M. T.; Navarro, C.; Moreno, A.; Csaky, A. G. Arylation of Benzo-Fused 1,4-Quinones by the Addition of Boronic Acids under Dicationic Pd(II)-Catalysis. *Org. Lett.* **2009,** 11, 4938-41.
27. Demchuk, O. M.; Pietrusiewicz, K. M. New and efficient protocol for arylation of quinones. *Synlett* **2009,** 7, 1149-53.
28. Shand, A. J.; Thomson, R. H. Diquinones. II. Formation of dibenzofuran derivatives by rearrangement of diquinones. *Tetrahedron* **1963,** 19, 1919-37.
29. Valderrama, J. A.; Gónzalez, M. F.; Torres, C. *Heterocycles* **2003,** 60, 2343-48.
30. Colona, S.; Gaggero, N.; Manfredil, A.; Spadoni, M.; Casella, L.; Carrea, G.; Pasta, P. Asymmetric weitz - scheffer epoxidation promoted by bovine serum albumin: Part III. Highly stereoselective synthesis of optically active epoxynaphthoquimones. *Tetrahedron* **1988,** 44, 5169-5178.
31. Valderrama, J. A. G., M. Florencia; Torres, Cristián. Epoxidation of Quinones with Urea Hydrogen Peroxide. *Heterocycles* **2003,** 60, 2343-2348.
32. Cho, Y. S.; Kim, H. S.; Kim, C. H.; Cheon, H. G. Application of the ferrous oxidation–xylenol orange assay for the screening of 5-lipoxygenase inhibitors. *Anal. Biochem.* **2006,** 351, 62-68.
33. Wilson, I.; Wardman, P.; Lin, T.-S.; Sartorelli, A. C. One-Electron Reduction of 2- and 6-Methyl-1,4-naphthoquinone Bioreductive Alkylating Agents. *J. Med. Chem.* **1986,** 29, 1381-1384.

34. Chambers, H. F.; DeLeo, F. R. Waves of resistance: *Staphylococcus aureus* in the antibiotic era. *Nat. Rev. Microbiol.,* **2009,** 7, 629-641.

35. Kobayashi, S. D.; Musser, J. M.; Deleoa, F. R. Genomic analysis of the emergence of vancomycin-resistant Staphylococcus aureus. *mBio* **2012,** 3.

36. Sass, P.; Berscheid, A.; Jansen, A.; Oedenkoven, M.; Szekat, C.; Strittmatter, A.; Gottschalk, G.; Bierbaum, G. Genome sequence of Staphylococcus aureus VC40, a vancomycin- and daptomycin-resistant strain, to study the genetics of development of resistance to currently applied last-resort antibiotics. *J. Bacteriol.,* **2012,** 194, 2107-2108.

37. Coates, A. R.; Halls, G.; Hu, Y. Novel classes of antibiotics or more of the same? *Br. J. Pharmacol.* **2011,** 163, 184-194.

38. Samonis, G.; Maraki, S.; Rafailidis, P. I.; Kapaskelis, A.; Kastoris, A. C.; Falagas, M. E. Antimicrobial susceptibility of Gram-negative nonurinary bacteria to fosfomycin and other antimicrobials. *Future Microbiol.* **2010,** 5, 961-970.

39. Falagas, M. E.; Maraki, S.; Karageorgopoulos, D. E.; Kastoris, A. C.; Kapaskelis, A.; Samonis, G. Antimicrobial susceptibility of Gram-positive non-urinary isolates to fosfomycin. *Intl. J. Antimicrob. Agents* **2010,** 35, 497-499.

40. Brunmark, A.; Cadenas, E. 1,4-reductive addition of glutathione to quinone epoxides: Mechanistic studies with h.p.l.c. with electrochemical detection under anaerobic and aerobic conditions and evaluation of chemical reactivity in terms of autoxidation reactions. *Free Radic. Biol. Med.* **1989,** 6, 149-165.

41. Dharmaraja, A. T.; Dash, T. K.; Konkimalla, V. B.; Chakrapani, H. Synthesis, thiol-mediated reactive oxygen species generation profiles and anti-proliferative activities of 2,3-epoxy-1,4-naphthoquinones. *Med. Chem. Comm.,* **2012,** 3.

42. Welsch, M. E.; Snyder, S. A.; Stockwell, B. R. Privileged scaffolds for library design and drug discovery. *Curr. Opin. Chem. Biol.* **2010,** 14, 347-361.

43. Malwal, S. R.; Sriram, D.; Yogeeswari, P.; Konkimalla, V. B.; Chakrapani, H. Design, Synthesis, and Evaluation of Thiol-Activated Sources of Sulfur

Dioxide (SO_2) as Antimycobacterial Agents. *J. Med. Chem.* **2012,** 55, 553-7.

44. Malwal, S. R.; Sriram, D.; Yogeeswari, P.; Chakrapani, H. Synthesis and antimycobacterial activity of prodrugs of sulfur dioxide (SO_2). *Bioorg. Med. Chem. Lett.* **2012,** 22, 3603-3606.
45. Khodade, V. S.; Dharmaraja, A. T.; Chakrapani, H. Synthesis, reactive oxygen species generation and copper-mediated nuclease activity profiles of 2-aryl-3-amino-1,4-naphthoquinones. *Bioorg. Med. Chem. Lett.* **2012,** 22, 3766-3769.
46. Dharmaraja, A. T.; Chakrapani, H. A Small Molecule for Controlled Generation of Reactive Oxygen Species (ROS). *Org. Lett.* **2014,** 16, 398-401.
47. Dharmaraja, A. T.; Dash, T. K.; Konkimalla, V. B.; Chakrapani, H. Synthesis, thiol-mediated reactive oxygen species generation profiles and anti-proliferative activities of 2,3-epoxy-1,4-naphthoquinones. *MedChemComm* **2012,** 3, 219 - 224.
48. Zhou, M.; Diwu, Z.; Panchuk-Voloshina, N.; Haugland, R. P. A Stable Nonfluorescent Derivative of Resorufin for the Fluorometric Determination of Trace Hydrogen Peroxide: Applications in Detecting the Activity of Phagocyte NADPH Oxidase and Other Oxidases. *Anal. Biochem.*, **1997,** 253, 162-168.
49. Lithgow, J. K.; Hayhurst, E. J.; Cohen, G.; Aharonowitz, Y.; Foster, S. J. Role of a Cysteine Synthase in Staphylococcus aureus. *J. Bacteriol.* **2004,** 186, 1579-1590.
50. Anderberg, S. J.; Newton, G. L.; Fahey, R. C. Mycothiol biosynthesis and metabolism: Cellular levels of potential intermediates in the biosynthesis and degradation of mycothiol in Mycobacterium smegmatis. *J. Biol. Chem.*, **1998,** 273, 30391-30397.
51. Georgiou, C. D.; Papapostolou, I.; Grintzalis, K. Superoxide radical detection in cells, tissues, organisms (animals, plants, insects, microorganisms) and soils. *Nat. Protoc.* **2008,** 3, 1679-1692.
52. Zhao, H.; Joseph, J.; Fales, H. M.; Sokoloski, E. A.; Levine, R. L.; Vasquez-Vivar, J.; Kalyanaraman, B. Detection and characterization of the

product of hydroethidine and intracellular superoxide by HPLC and limitations of fluorescence. *Proc. Natl. Acad. Sci. USA* **2005,** 102, 5727-5732.

Synopsis

Synthesis and Evaluation of Small Molecule Based Reactive Oxygen Species (ROS) Generators

Aerobic organisms are continuously exposed to oxygenated atmosphere and as a consequence, they are associated with elevated levels of intracellular reactive oxygen species (ROS) such as superoxide radical, $O_2^{\bullet-}$, hydrogen peroxide, H_2O_2, and hydroxyl radical, $^{\bullet}OH$ (Scheme 3.1).[1,2] In cells, $O_2^{\bullet-}$is produced by enzyme NADPH oxidases NOX2 and dismutation of $O_2^{\bullet-}$produces H_2O_2. Myeloperoxidase (MPO) is a cellular enzyme which mediates the transformation of H_2O_2 into hypochlorous acid (HOCl) (Scheme 1A).[1] These species are known to damage iron-sulfur (Fe-S) cluster proteins and in the process, release Fe^{2+} into the extracellular matrix.[3] A reaction of Fe^{2+} with H_2O_2 (Fenton reaction) generates hydroxyl radical ($^{\bullet}OH$), which is well known for causing oxidative damage in DNA, proteins and lipids (Scheme 1B).

Scheme 1. (A) Reactive oxygen species generation and control by antioxidants in biological settings; (B) Damaging effects of ROS to biomacromolecules such as DNA, proteins and lipids.

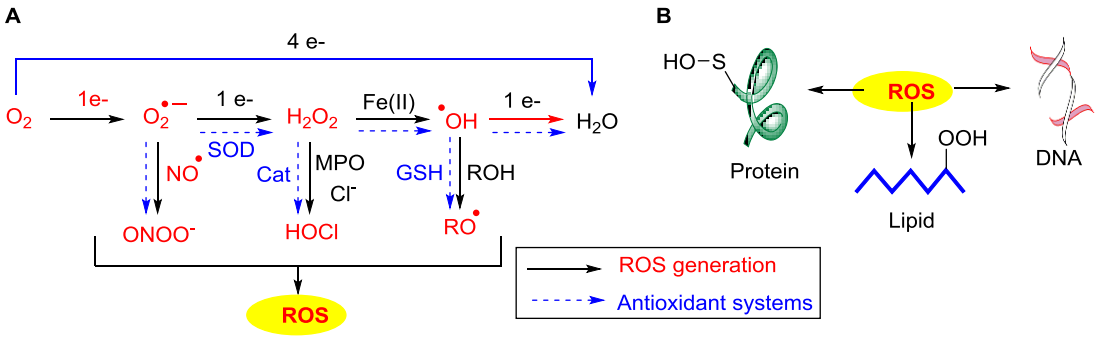

Together, these reactive oxygen species (ROS) can damage vital cellular components and are hence deployed by the immune system to counter infectious pathogens.[1,4] During immune response, ROS is mainly produced in phagocytes by NOX2. Strong phagosomal ROS production is essential for an efficient host defense against bacterial and fungal infections. However, oxidative damage is held in check by microorganisms which have sophisticated antioxidant and repair systems.[5,6] Thus ROS is an integral component of host response and during situations where oxidative stress can be overcome, infection results. In order to overcome these infections, three major classes of antibiotics are used: quinolones (DNA gyrase inhibitor),

aminoglycosides (amino acid biosynthesis inhibitor) and β-lactams (cell wall biosynthesis inhibitors). Their targets and binding mechanisms are well established in the literature.[6] However, recently it was proposed that along with these established molecular targets, antibiotics affects tricarboxylic acid cycle (TCA cycle) resulting in perturbations of NADPH homeostasis. All these events lead to an enhancement of intracellular free Fe^{2+} and ROS levels. This accumulation of ROS was reasoned out as a common mechanism for bacterial inhibition by clinical antibiotics.[7] Due to the paradigmatic shift in our understanding of antibiotic action, these findings have generated a lot of interest in the scientific community. A systems biology approach for predictably enhancing intrabacterial ROS was reported to sensitize bacteria to clinical antibiotics. In addition, the efficacy of clinical antibiotics was significantly improved in the presence of oxidative species suggesting a possible use for ROS as adjuvants.[11] Furthermore, reducing the ROS levels in *Staphylococcus aureus* by staphyloxanthine, a carbenoid antioxidant was reported to promote drug resistance in bacteria.[12] Thus, enhancement of intracellular ROS could be used to overcome drug resistance in bacteria. Due to the overuse of antibiotics, bacteria have acquired resistance to a majority of frontline drugs and hence any strategy that can help solve this global problem assumes importance.[6] Recently, three independent and contrarian reports have questioned the aforementioned hypothesis and show that ROS may not have a significant role to play in the mechanism of bacterial inhibition by clinical antibiotics.[8-10] Therefore, the precise roles of ROS in bacterial responses to antibiotics and its role in resistance remain to be completely elucidated and new studies are necessary.

We hypothesized that due to the capacity of ROS to severely damage cellular components at elevated levels, exposing bacteria to ROS using reliableROS sources might be effective against certain bacteria. In order to test this hypothesis, reliable organic sources of cell permeable ROS generators are necessary. This thesis comprises of four chapters. Chapter 1 presents an overview of ROS and the techniques used to enhance ROS in biochemical as well as cellular settings. In Chapter 2.1, we present the design, synthesis and evaluation of 2,3-dihydroquinones as ROS generators. Chapter 2.2 describes our efforts towards developing tunable ROS generators by varying substituent electronic effects on 2,3-dihydroquinones. In Chapter 3, a strategy for site directed ROS generation selectively inside bacteria and

its effects on bacterial growth are described. Finally, using a two-fold approach of thiol depletion and enhancement of ROS, we test the inhibitory effects of enhanced ROS against drug resistant bacteria. Together, scaffolds developed in this study for reliably enhancing intracellular ROS could be used for studying the precise role of ROS in biochemical events and certain compounds presented here might have applications as therapeutic agents.

Chapter 2.1: Design, Synthesis and Evaluation of Dihydroquinones as Reactive Oxygen Species (ROS) Generators:

Industrially H_2O_2 is produced from reduced anthraquinone upon exposure to atmospheric O_2. Based on this observation, a new design of surrogates of hydroquinone was considered (Scheme 2). These hydroquinones were synthesized by a [4+2] cycloaddition reaction of substituted 1,4-naphthoquinoes with cyclic-1,3-dienes. These 2,3-dihydroquinones were found to undergo a keto-enol tautomerism to form the 1,4-hydroquinone in aerobic buffer (Scheme 2), which can react with molecular O_2 to generate $O_2^{\bullet-}$, H_2O_2, and $^{\bullet}OH$ (in the presence of trace metal ions).

Scheme 2. Compound **4** tautomerize to enol, which can react with oxygen to generate superoxide and H_2O_2 as the inorganic products with concomitant formation of **18**. Bioreduction of quinone **18** and further redox cycling might also produce ROS.

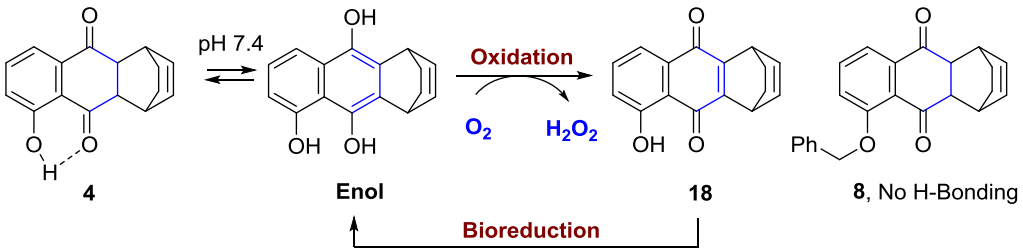

The compound's potential to generate $O_2^{\bullet-}$ was estimated using two independent assays. Luminol based chemiluminescence assay was used to infer $O_2^{\bullet-}$ generation in buffer from the compounds prepared in this study (Figure 1A).[13] A high performance liquid chromatography (HPLC) based dihydroethidium (DHE) assay was performed to independently confirm the $O_2^{\bullet-}$generation (Figure 1B).[14-16] Dismutation of $O_2^{\bullet-}$ leads to the formation of H_2O_2, which was confirmed by an Amplex Red fluorescence assay.[17] A DNA damage assay was performed on compounds to confirm

the production of $^{\bullet}OH$ in the presence of ferrous ions (Fe^{2+}).[18] From the aforementioned studies compound **4** (Scheme 2) was found to be an efficient ROS generator (65% yield of H_2O_2 generated after 3h in pH 7.4 buffer) among the compounds evaluated. A mechanism of buffer mediated keto-enol tautomerism followed by reaction with molecular O_2 to generate ROS was proposed. The participation of OH- group, possibly through intramolecular hydrogen bonding, was implicated in enhanced ROS generation by **4**. Removal of H-bonding capability by derivatization with a benzyl (Bn) group **8** was found to diminish the ROS generation, indicating the importance of free OH-group and its H-bonding for ROS generation (Scheme 2).

Figure 1. (A) Measurement of superoxide generation from **4** and **8** in pH 8.0 phosphate buffer at 37 °C using luminol based chemiluminescence assay; (B) ROS generation from **4** determined using a HPLC based dihydroethidium (DHE) assay. These data were compared with routinely used superoxide source xanthine and xanthine oxidase (X+XO).

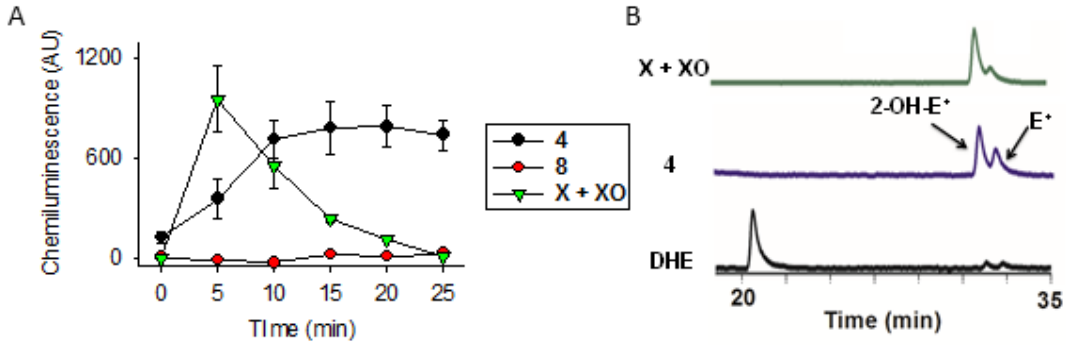

Next, the ability of compound **4** to permeate bacterial cells and generate ROS was established by DHE, Amplex Red and dichloro-dihydrofluorescein diacetate ($DCFH_2$-DA) assays.[18] Only in the presence of **4** an enhanced intracellular ROS was observed. ROS generated by **8** and untreated bacterial control were significantly lower in comparison with **4**. Having established a cell permeable efficient ROS generator, we tested the effect of enhancement of intracellular ROS in inhibiting bacteria. When a Gram negative bacterium, *E. coli* was exposed to ROS generator **4**, no substantial effect on the bacterial growth was detected. Next, the potential use of ROS as an adjuvant to commercial antibiotics was tested with aminoglycoside antibiotics such as kanamycin and gentamycin. We observed a significant enhancement in sensitivity of

E. coli to aminoglycoside antibiotics when co-treated with 50 μM of **4** (minimum inhibitory concentrations (MIC) enhancement of 4 fold with kanamycin and 8 fold with gentamycin). Under similar conditions with kanamycin, H_2O_2 (250 μM) showed a 2 fold enhancement in MIC and no effect was observed with menadione (250 μM), a routinely used ROS generator for enhancing intracellular ROS. A small library of closely related analogues was synthesized by reducing the external double bond and their ROS generation profiles were documented. All these compounds were tested for their ability to inhibit *Mycobacterium tuberculosis* (*Mtb*), one of the highly infective pathogens, that kills a million each year. A majority of the compounds were found to inhibit *Mtb* at less than 1 μg/mL MIC and further studies on mechanisms of these ROS generators to inhibit *Mtb* are currently underway. Thus, Chapter 2.1 describes the results of our design, synthesis and characterization of ROS generation from 2,-dihydro-1,4-napthoquinones. Their suitability for intracellular enhancement of ROS has been demonstrated.

Chapter 2.2: Substituent Effects on Reactive Oxygen Species (ROS) Generation by Hydroquinones

A reaction of 2,3-dihydro-1,4-benzoquinones with molecular O_2 for ROS generation was mediated by the intermediacy of an enol(ate), which was produced by tautomerization. Here, we studied effects of systematically changing substituents on the propensity of hydroquinones to enolize and the enol's ability to react with oxygen to generate ROS. We hypothesized that enhancing the electron density on the quinone ring might stabilize compound in keto form; conversely, introduction of electron withdrawing group would decrease the electron density on the quinone ring and expected to induce enolization to produce a stable enol. In order to achieve the goal, a series of 2-aryl-1,4-benzoquinones were synthesized following a two-step synthetic protocol: Firstly, a silver nitrate catalyzed reaction of arylboronic acids with 1,4-benzoquinone produced 2-aryl-1,4-benzoquinones and these were subjected to a [4+2] cycloaddition reaction with 1,3-cyclohexadiene to obtain desired 6-aryl-2,3-dihydro-1,4-benzoquinones.

Figure 2. (A) Portions of ^{1}H NMR of **39**-**42** and **45**-**47** depicting ratio of keto-enol tautomers (Hydrogens highlighted in red – keto isomer; gray – enol isomer; R =

H, **39**; R = Me, **40**; R = OMe, **41**; R = Br, **42**; R = Ac, **45**; R = NO_2, **46**; R = CHO, **47**); (B) Plot of log(K_X/K_H) for keto–enol equilibria of 2,3-dihydrobenzoquinones versus the Hammett substitution constant σ^+ (overall reaction constant ρ = 2.37; R^2 = 0.7420). (C) Time course of decomposition of **39** (1 mM, k_{39} = 0.28 h^{-1}, R^2 = 0.9875) and **47** (1 mM, k_{47} = 1.48 h^{-1}, R^2= 0.9546) in acetonitrile (pH 7.4 phosphate buffer (1/1, v/v)) based on HPLC analysis. (D) Time course of H_2O_2 generated from **39** (10 μM) and **47** (10 μM) over 6 h in pH 7.4 phosphate buffer measured using Amplex Red based fluorescence assay.

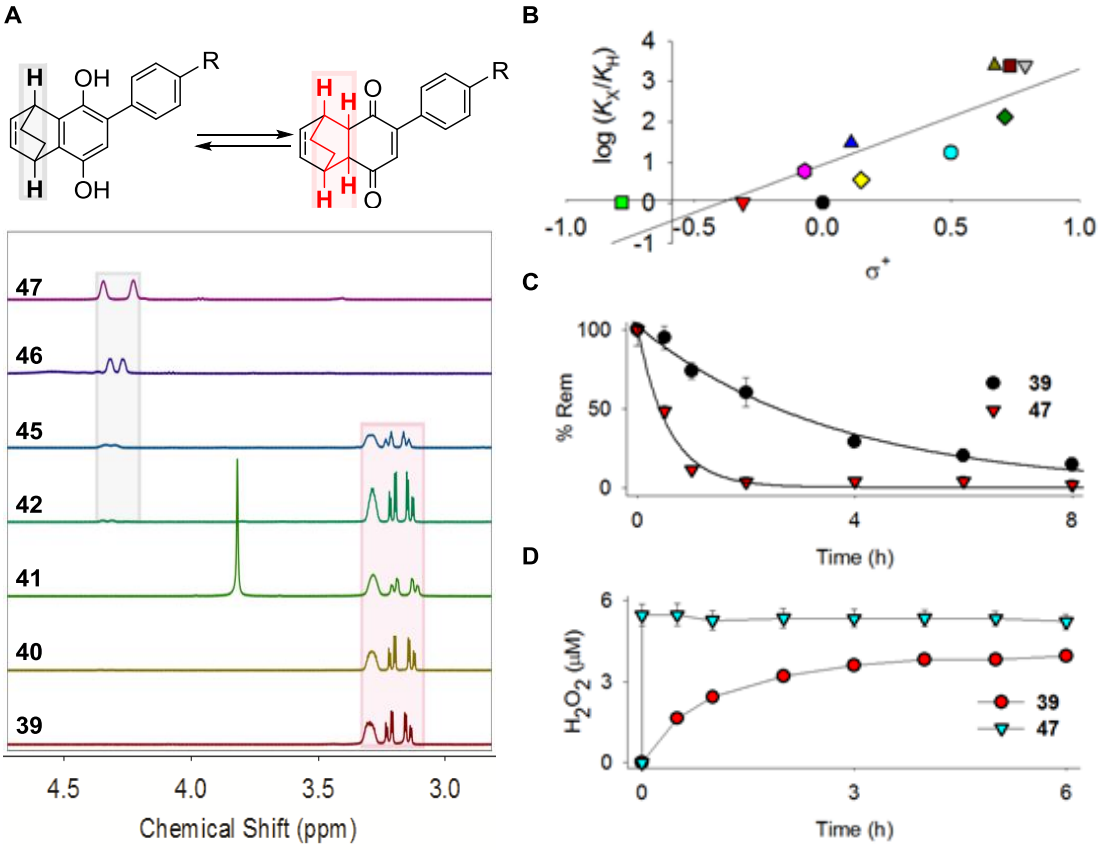

Next, stability of the keto and enol forms of 6-aryl-2,3-diydrobenzoquiones was studied using a proton-nuclear magnetic resonance (^{1}H-NMR). As predicted compounds with electron releasing groups (Me (**40**), and MeO (**41**)) were found to be stable predominantly in its keto form. In the ^{1}H NMR, signals for protons of α and β to the carbonyl (highlighted in red, Figure 2A) for the keto isomer appeared at 3.0-3.14 ppm.

Increasing electron withdrawing ability of the substituents on the aryl ring was found to promote enolization. This was evidenced by a new set of peaks that appeared

at 4.2-4.5 ppm for the bridgehead protons of enol tautomer (highlighted in gray, Figure 2A). A mixture of keto and enol tautomers were observed for compounds with Br (**42**), Cl (**43**), F (**44**) and acetyl substitutions and the calculated keto: enol ratio were ranging from 94:6 to 62:38. Further, with electron withdrawing substituents such as -NO_2 (**46**) and -CHO (**47**), only enol tautomer could be detected from ^{1}H NMR (Figure 2A). A linear free energy relationship (LFER) analysis of the equilibrium constant calculated based on the keto-enol ratio obtained from ^{1}H NMR studies and the Hammett substituents constant, σ^+ showed a nearly linear correlation and produced an overall reaction constant, ρ of +2.37, supporting the importance of electronic effects in controlling the position of the keto-enol equilibrium (Figure 2B). Next, we tested our hypothesis that propensity of the compounds to enolize determines reactivity with O_2 to generate ROS in buffer. Initially, we tested the stability of the compounds in buffer, where a slow decomposition was observed for **39** (keto form, $t_{1/2}$ = 2.5 h), on the other hand enol tautomer **47** ($t_{1/2}$ = 0.47 h) decomposed rapidly under similar conditions (Figure 2C). Thus, using a single scaffold, slow as well as rapid ROS generation was possible. Due to comparable physicochemical properties offered by a single scaffold, it is anticipated that this scaffold with diverse ROS generation profiles would be useful for biological studies.

Chapter 3: Small Molecule Based Enzyme Activated Reactive Oxygen Species (ROS) Generator in Bacteria

The hydroquinones synthesized and studied thus far are found to react with molecular O_2 to generate ROS in bacteria. However, decomposition of these hydroquinones in extracellular medium to generate ROS as well as within cells is possible. Selectively enhancing only intracellular ROS levels in bacteria is desirable but no reliable methods are available. Here, we proposed to develop a tool that only enhances ROS within cells. In order to achieve this goal, the presence of an intracellular bacterial enzyme trigger for ROS generation is necessary. As previously described, H-bonding through 5-OH group is crucial for efficient ROS generation by **4**, removal of the H-bonding by substitution of the -OH group in **4** with benzyl group (**8**) was found to significantly diminish the ROS generation (Scheme 3). Taking advantage of this observation, a scaffold for spatio-temporally controlled delivery of ROS in a model

bacterium *E. coli* was designed by protecting 5-hydroxy-2,3-dihydro-1,4-naphthoquinone (**4**) with an enzyme triggered self-immolative linker (Scheme 3).

Scheme 3. A design of enzyme triggered release of active ROS generator **4** for intracellular ROS generation

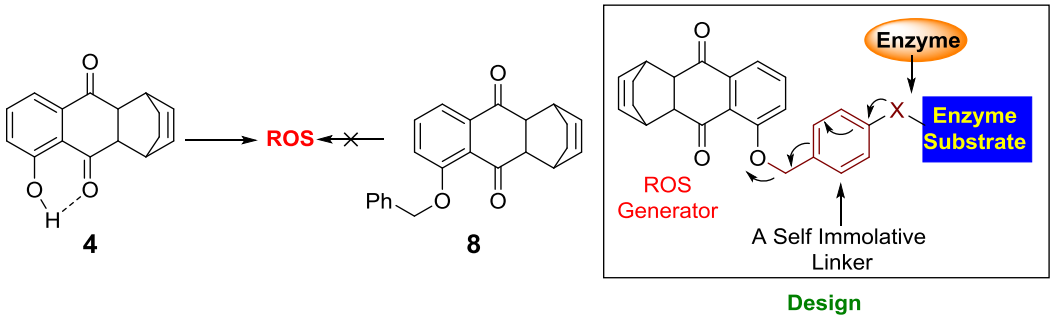

Nitroreductase (NTR) is a bacterial enzyme over expressed in *E.coli* and the 4-nitrobenzyl moiety is a reported substrate for NTR. We considered **54**, a *O*-4-nitrobenzyl derivative of **4**, as a potential Pro-ROS generator. A silver oxide (Ag_2O) mediated benzylation of **4** with 4-nitrobenzyl bromide, afforded the Pro-ROS generator (**54**). We studied the release of **4** from the reduced 4-nitrobenzyl derivatives **4a** and/or **4b**(Figure 3A). HPLC based analysis revealed the formation of **4** during a chemoreduction of **54** using Zinc and ammonium formate in methanol: buffer (1:1, v/v) at 37 °C. Further evidence for the formation of intermediates **4a**, **4b** and **4** was obtained by a mass spectral analysis of the reaction mixture. Next, the compound's ability to generate ROS such as $O_2^{\bullet -}$, H_2O_2 and $^{\bullet}OH$ in buffer with and without NTR was studied using established assays described in Chapter 2 (Figure 3B and 3C). As predicted, in the absence of NTR, no significant ROS generation was observed from **54** and an addition of NTR produced nearly comparable levels of $O_2^{\bullet -}$and H_2O_2 to the ROS generated by **4** in buffer. Thus, bacterial NTR enzyme triggered ROS generation in buffer has been achieved using **54**. Next, we tested the compound's permeability in bacteria to enhance the level of intracellular ROS. Carefully designed control experiments revealed a selective activation of **54** only inside bacteria to enhance intracellular ROS. When we tested the possibility of sensitizing bacteria to elevated ROS levels using **54**, *E. coli* was found to tolerate an enhanced intracellular ROS and no significant effect on the growth of this bacterium was observed under our experimental conditions. Nevertheless, the compound's utility as an adjuvant for potentiating the efficacy of aminoglycoside antibiotics against *E. coli* was

demonstrated. In summary, Chapter 3 describes an enzyme triggered scaffold for selectively increasing intracellular ROS in bacteria and their potential as an adjuvant to sensitize *E. coli* to aminoglycoside antibiotics.

Figure3. (A) Bacterial nitroreductase (NTR) activated release of **4** for spatio-temporally controlled ROS generation; (B) Superoxide generation from only **54** and in the presence of NTR in buffer measured using luminol based chemiluminescence assay; (C) Intracellular ROS generation determined using a HPLC based dihydroethidium (DHE) assay

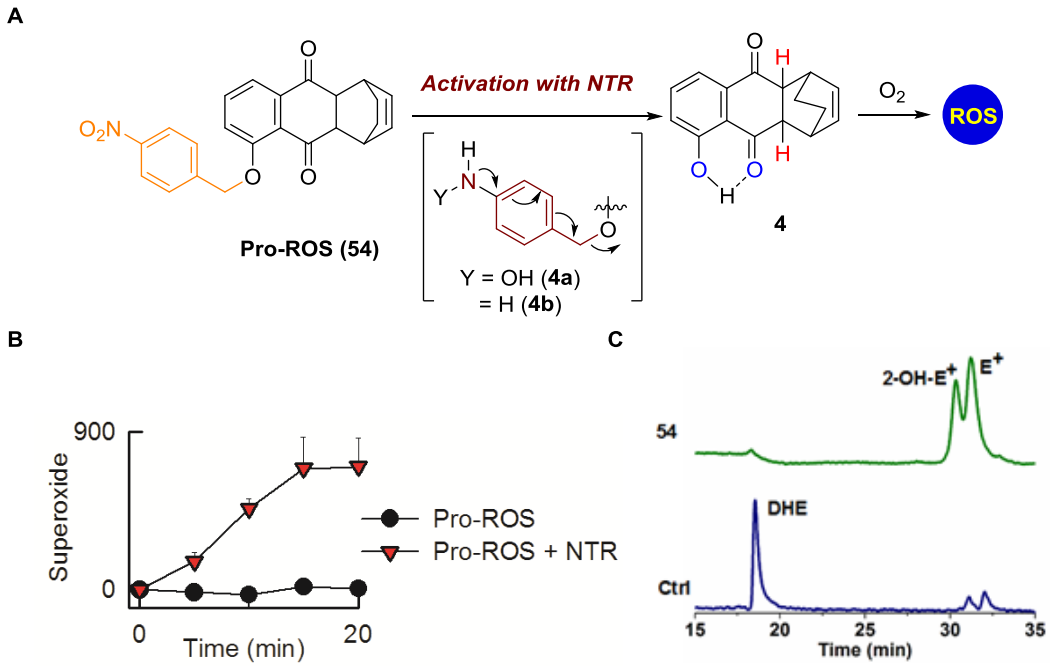

Chapter 4: Synthesis and Characterization of Thiol–Triggered Reactive Oxygen Species (ROS) Generators and Antibacterial Studies

We developed a small molecule based scaffold for ROS generation in extracellular medium and a scaffold triggered by an intracellular bacterial enzyme, nitroreductase to enhance ROS levels selectively inside bacteria. Although these compounds were found to permeate bacteria to enhance intracellular ROS levels, bacteria do not appear to be sensitive to elevated ROS levels. Thus, enhancing intracellular ROS alone appears insufficient to inhibit *E. coli* growth (Chapter 2.1). In this Chapter, a scaffold

that is induced by cellular thiols to generate ROS was considered (Scheme 4). Here, an amplification effect of ROS induced oxidative stress might occur: (a) due to depletion of intracellular antioxidant thiols and (b) by an enhancement of intracellular ROS levels.

Scheme 4. A design for increasing oxidative stress using thiol inducible ROS generators

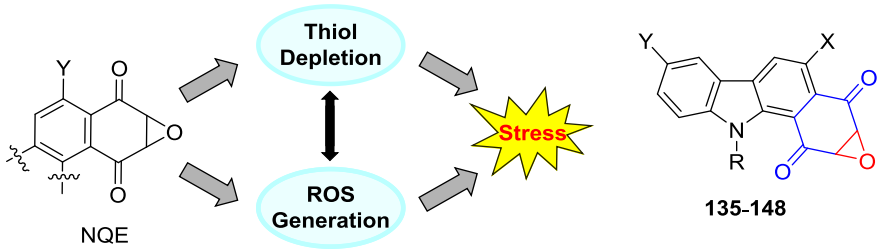

We synthesized a series of 2,3-epoxy1,4-naphthoquinones with electron releasing and withdrawing functional groups. Upon reaction with glutathione (GSH) we found a range of reactivities from 6-94% compound remaining after 30 min of reaction in buffer. In part, compounds ability to react with thiol was appeared to determine the level of ROS produced. Next, best ROS generators (**74**-**76**, **78**) among the compounds were tested for their inhibitory potential against methicillin resistant *Staphylococcus aureus* (MRSA). *S. aureus* is a Gram positive pathogen that affects a million each year and mainly causes skin infection in infants. All the compounds tested were found to inhibit MRSA but at elevated concentrations. Based on this result, our revised design was focused on an indole core which is found in many natural products and therapeutics. We synthesized a library of indole-2,3-epoxy-1,4-naphthoquinones (IND-NQE). Next, the reactivity of the compounds with cysteine was performed in buffer and a majority of the compounds were highly reactive with cysteine. Increasing the sterics on the indole nitrogen was found to slightly decrease the reactivity with cysteine. The ROS generating ability of the compounds in the presence of *S. aureus* was determined using Amplex Red based fluorescence assay after 60 min of compound treatment with *S. aureus* and compounds were found to generate above 5 μM of H_2O_2.

Scheme 5. Proposed mechanism for glutathione-mediated decomposition of **137** to generate ROS.

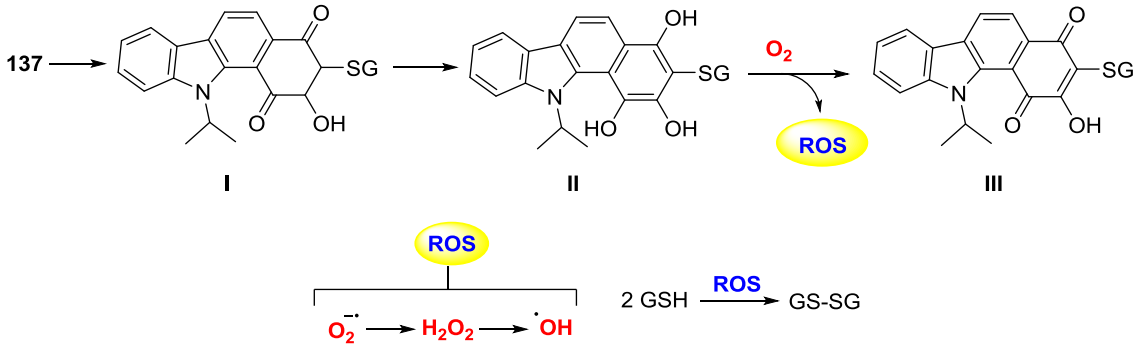

Next, the compounds inhibitory potential against MRSA was tested and a majority of the compounds were found be active at MIC ranging from 0.25 – 2 μg/mL. We have identified a lead compound *N*-isopropylindole derivate **137** with an MIC of 0.25 μg/mL. The *in vitro* inhibitory potential of the lead compound was better than commercially used antibiotic vancomycin (1 μg/mL). Further mechanistic studies were focused on **137**. The ROS generated by the reaction of **137** with GSH can react with excess glutathione (GSH) to produce the oxidized dimer GS-SG (Scheme 5). We find evidence for reaction of the formation of the adduct III and GS-SG thus suggesting multiple pathways for depletion of thiols. Accordingly, cellular assays with **137** showed intracellular thiol depletion and enhanced intracellular ROS. Furthermore, inhibitory potency of **137** against clinical isolates of MRSA (11 bacterial strains) was tested by our collaborators. The lead compound **137** was found to be a potent inhibitor with MICs that were comparable or better than vancomycin. In this Chapter, we presented the design and development of ROS-based efficient MRSA inhibitors including patient derived strains. Our data suggests that the enhancement of oxidative stress by thiol depletion and ROS generation could be used as a new strategy to overcome drug resistance in bacteria.

Taken togerther, enhancement of ROS within cells is challenging and among the methodologies available, 2,3-dihydro-1,4-naphthoquinones that we have developed are unique. They can spontaneously react with oxygen to produce superoxide radical anion in buffer and do not require bioreduction for ROS production. We have also developed scaffolds triggered by a bacterial enzyme or by intracellular thiols for site selective deliver of ROS in bacteria. Our preliminary investigation revealed that compounds capable of generating ROS and were good inhibitors of *Mtb* and MRSA

We have synthesized several new and improved analogues and conducted detailed investigations that support *Mtb* and MRSA are sensitive to enhanced intracellular ROS.

References:

1. Fang, F.C. Antimicrobial reactive oxygen and nitrogen species: Concepts and controversies. *Nat. Rev. Microbiol.,***2**, 820-832 (2004).
2. Fridovich, I. Superoxide radical: an endogenous toxicant. *Annu. Rev. Pharmacol. Toxicol.***23**, 239-257 (1983).
3. Imlay, J.A. Iron-sulphur clusters and the problem with oxygen. *Mol. Microbiol.,***59**, 1073-1082 (2006).
4. Nathan, C. & Cunningham-Bussel, A. Beyond oxidative stress: an immunologist's guide to reactive oxygen species. *Nat. Rev. Immunol.***13**, 349-361 (2013).
5. Allen, L.-A.H. & McCaffrey, R.L. To activate or not to activate: distinct strategies used by Helicobacter pylori and Francisella tularensis to modulate the NADPH oxidase and survive in human neutrophils. *Immunol. Rev.***219**, 103-117 (2007).
6. Walsh, C. Molecular mechanisms that confer antibacterial drug resistance. *Nature***406**, 775-781 (2000).
7. Kohanski, M.A., Dwyer, D.J., Hayete, B., Lawrence, C.A. & Collins, J.J. A Common Mechanism of Cellular Death Induced by Bactericidal Antibiotics. *Cell***130**, 797-810 (2007).
8. Brynildsen, M.P., Winkler, J.A., Spina, C.S., MacDonald, I.C. & Collins, J.J. Potentiating antibacterial activity by predictably enhancing endogenous microbial ROS production. *Nat. Biotech.***31**, 160-165 (2013).
9. Liu, C.I., *et al.* A cholesterol biosynthesis inhibitor blocks Staphylococcus aureus virulence. *Science***319**, 1391-1394 (2008).
10. Foti, J.J., Devadoss, B., Winkler, J.A., Collins, J.J. & Walker, G.C. Oxidation of the guanine nucleotide pool underlies cell death by bactericidal antibiotics. *Science***336**, 315-319 (2012).
11. Keren, I., Wu, Y., Inocencio, J., Mulcahy, L.R. & Lewis, K. Killing by bactericidal antibiotics does not depend on reactive oxygen species. *Science***339**, 1213-1216 (2013).
12. Liu, Y. & Imlay, J.A. Cell death from antibiotics without the involvement of reactive oxygen species. *Science***339**, 1210-1213 (2013).

13. Trung Pham, H., Marquetty, C., Pasquier, C. & Hakim, J. Luminol assay for microdetermination of superoxide dismutase activity: Its application to human fetal blood. *Anal. Biochem.,***142**, 467-472 (1984).
14. Zielonka, J., Vasquez-Vivar, J. & Kalyanaraman, B. Detection of 2-hydroxyethidium in cellular systems: A unique marker product of superoxide and hydroethidine. *Nat. Protoc.,***3**, 8-21 (2008).
15. Zhao, H., *et al.* Detection and characterization of the product of hydroethidine and intracellular superoxide by HPLC and limitations of fluorescence. *Proc. Natl. Acad. Sci.,***102**, 5727-5732 (2005).
16. Georgiou, C.D., Papapostolou, I. & Grintzalis, K. Superoxide radical detection in cells, tissues, organisms (animals, plants, insects, microorganisms) and soils. *Nat. Protoc.,***3**, 1679-1692 (2008).
17. Zhou, M., Diwu, Z., Panchuk-Voloshina, N. & Haugland, R.P. A Stable Nonfluorescent Derivative of Resorufin for the Fluorometric Determination of Trace Hydrogen Peroxide: Applications in Detecting the Activity of Phagocyte NADPH Oxidase and Other Oxidases. *Anal. Biochem.,***253**, 162-168 (1997).
18. Wardman, P. Fluorescent and luminescent probes for measurement of oxidative and nitrosative species in cells and tissues: Progress, pitfalls, and prospects. *Free Rad. Biol. Med.,***43**, 995-1022 (2007).

List of Figures

List of Tables

List of Schemes

List of Publications:

1. **Dharmaraja, A. T.,** Jain, C., and Chakrapani, H., "Substituents effects on reactive oxygen species (ROS) generation by hydrobenzoquinones" *J. Org. Chem.,* **2014**, *79*, 9413-9417.
2. **Dharmaraja**, **A. T**., and Chakrapani, H., "A Small Molecule for Controlled Generation of Reactive Oxygen Species (ROS)" *Org. Lett.,* **2014**, *16*, 398 – 401.
3. **Dharmaraja**, **A. T**., Alvala, M., Yogeeswari, P., Sriram, D., and Chakrapani, H., "Design, synthesis and evaluation of small molecule reactive oxygen species generators as selective *Mycobacterium tuberculosis* inhibitors" *Chem. Commun.,* **2012**, *48*, 10325 – 10327.
4. **Dharmaraja**, **A. T**., Dash, T., Konkimalla, B., and Chakrapani, H., "Synthesis, Thiol-Mediated Reactive Oxygen Species Generation Profiles and Anti-Proliferative Activities of 2,3-Epoxy-1,4-Naphthoquinones" *Med. Chem. Commun.,* **2012**, *3*, 212 – 216.

Manuscripts in Preparation

1. Priyanka, T.,[†] **Dharmaraja, A. T.**,[†] Chakrapani, H., and Singh, A., "Altering redox homeostasis in drug resistant *Mycobacterium tuberculosis* using small molecule reactive oxygen species generators" [†]Equal authorship
2. **Dharmaraja**, **A. T**., Sankar, R. K., Banerjee, A., Rangarajan, R., and Chakrapani, H., "Design, synthesis and evaluation of indole-Based 2,3-epoxy-1,4-naphthoquinones as methicillin-resistant *Staphylococcus aureus* (MRSA) inhibitors"

****

ChemComm

Cite this: *Chem. Commun.*, 2012, **48**, 10325–10327

www.rsc.org/chemcomm

COMMUNICATION

Design, synthesis and evaluation of small molecule reactive oxygen species generators as selective *Mycobacterium tuberculosis* inhibitors†

Allimuthu T. Dharmaraja,[a] Mallika Alvala,[b] Dharmarajan Sriram,[b] Perumal Yogeeswari[b] and Harinath Chakrapani*[a]

Received 24th July 2012, Accepted 20th August 2012
DOI: 10.1039/c2cc35343a

Here, we report 5-hydroxy-1,2,3,4,4*a*,9*a*-hexahydro-1,4-ethano-9,10-anthraquinone (13), a small molecule generating reactive oxygen species (ROS) in pH 7.4 buffer under ambient aerobic conditions that has selective and potent *Mycobacterium tuberculosis* growth inhibitory activity.

Tuberculosis (TB) remains a leading cause of morbidity and mortality in much of the world. *Mycobacterium tuberculosis* (*Mtb*), the etiological agent of this infectious disease, is a highly adaptive pathogen and an extremely difficult pathogen to kill. The alarming rise in co-infection with HIV as well as extensively drug resistant (XDR) and multi-drug resistant (MDR) strains[1] necessitates new chemotherapeutic strategies.[2] Maintenance of redox homeostasis is integral to the sustenance of metabolic processes and mycobacterial persistence. Any significant alterations in oxidative or reductive species might cause breakdown of this balance and lead to cell death.[3] For example, elevated levels of reactive oxygen species (ROS) such as superoxide $O_2^{-\bullet}$, hydrogen peroxide H_2O_2 and hydroxyl radical $^{\bullet}OH$ can cause irreparable damage to biomacromolecules including DNA leading to oxidative stress and might severely affect *Mtb* survival (Scheme 1).[4] A growing body of evidence points to normal human cells' ability to better tolerate alterations in redox homeostasis in comparison with cancer cells[5,6] and forms the basis of an emerging paradigm for new redox-directed cancer chemotherapeutics.[7] Thus, small molecules capable of perturbing mycobacterial redox homeostasis through generation of ROS might have selective *Mtb* growth inhibitory potential.[4]

2,3-Dihydro-1,4-benzoquinones (**A**) were considered as potential ROS generators (Scheme 2). Conversion of **A** to its tautomer 1,4-dihydroxyarene (**B**) might occur at physiological pH; the diol **B** can undergo aerobic oxidation to give **C** with concomitant production of $O_2^{-\bullet}$ and H_2O_2.[8] Variation of ring size "*n*" and functional groups X and Y could perturb keto–enol equilibria and as a consequence, ROS yields, allowing us to study the effects of varying ROS levels on *Mtb* growth inhibitory activity. Finally, 1,4-quinones such as **C** are candidates for bioreduction to regenerate **B**, which is capable of generating ROS.

In order to test our hypothesis, 2,3-dihydro-1,4-benzoquinones **1–12** were synthesized (ESI†) from commercially available starting materials by a [4 + 2] cycloaddition between a quinone and appropriate equivalents of a 1,3-diene (Fig. 1).

The ability of **1–12** to generate $O_2^{-\bullet}$ (Fig. 2a) and H_2O_2 (Fig. 2b) under ambient aerobic conditions in pH 7.4 buffer was estimated using reported assays.[9,10] The juglone derivative **4** generated the highest levels of ROS amongst **1–12**. Based on this result, we prepared a closely related analogue **13** by hydrogenation of **4** (Fig. 1). This compound was found to be superior to **4** in ROS generation for 30 min (Fig. 2a and b).

Anti-microbial effects of ROS are primarily mediated through induction of DNA damage.[4] Fe(II)-mediated nuclease activity of **1–13** was estimated using a pBR322 supercoiled plasmid cleavage assay and nick induction was observed in nearly all compounds tested (Fig. 2c). The compound's nuclease activity correlated well with its ROS generating ability, indicating that the observed DNA damaging effects were ROS-mediated (Pearson's correlation coefficient $R = 0.9475$, P-value < 0.0001, Fig. S2, ESI†).

In order to test our hypothesis that ROS generators can inhibit *Mtb* growth, a reported assay was used to determine minimum inhibitory concentrations (MICs) for **1–13** against *Mycobacterium tuberculosis* $H_{37}R_v$ (Table 1, entries 1–13).[11] Amongst these, four compounds: **3**, **4**, **6** and **13** were found to be good *Mtb* growth inhibitors with MICs < 10 μg mL^{-1}. Compounds **5** and **12** did not show any detectable inhibitory activity at 100 μg mL^{-1} (Table 1, entries 5 and 12). MIC of the best ROS generator **13** was superior to those of clinically used first-line TB drugs ethambutol and pyrazinamide (Table 1, entries 16–17) and presents opportunities for further development as a TB drug candidate.

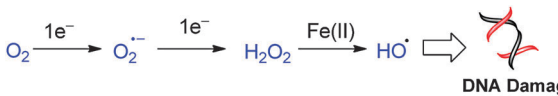

Scheme 1 Reactive oxygen species (ROS) generated through reduction of oxygen can damage biomacromolecules including DNA.

[a] *Department of Chemistry, Indian Institute of Science Education and Research (IISER) Pune, Pune 411 008, Maharashtra, India. E-mail: harinath@iiserpune.ac.in; Fax: +91-20-2589-9790; Tel: +91-20-2590-8090*
[b] *Department of Pharmacy, Birla Institute of Technology & Science Pilani, Hyderabad Campus, Jawahar Nagar, Hyderabad 500 078, India*

† Electronic supplementary information (ESI) available: Compound characterization data and assay procedures with relevant plots. CCDC 893408. For ESI and crystallographic data in CIF or other electronic format see DOI: 10.1039/c2cc35343a

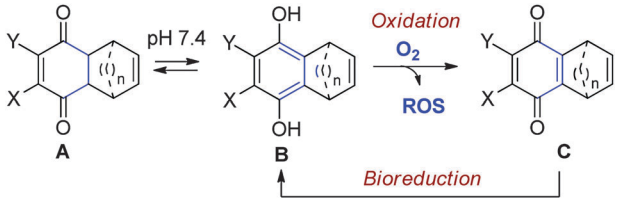

Scheme 2 Design of compounds that can perturb redox homeostasis by generating ROS.

Upon incubation of **13** at pH 7.4, HPLC analysis showed complete disappearance of **13** with concomitant formation of **14** at comparable rates in a nearly quantitative HPLC yield (Fig. 3a and b).[12] A first order increase of H_2O_2 for 12 h was observed with a maximal H_2O_2 yield of 72% (Fig. 3c). These results are consistent with a tentative mechanism based on enolization of 2,3-dihydro-1,4-naphthoquinones to produce a 1,4-diolate followed by reaction with oxygen to sequentially produce $O_2^{-\bullet}$ and H_2O_2 (Scheme S1, ESI†).[13,14] The presence of a proximal hydroxyl group appeared to diminish carbonyl π-character (IR spectroscopy, Fig. S6, ESI†); and enhanced electronegativity on the carbonyl oxygen (computational analysis, Fig. S7, ESI†). Together, these structural effects, likely due to intramolecular H-bonding (Fig. S8, ESI†), could promote enolization of C-4 carbonyl of **4** (or **13**) leading to enhanced ROS generation by these juglone derivatives in comparison with other analogues without a proximal hydroxyl group including the benzylated derivatives **8** and **9** (Fig. 1).

Compound **14**, the exclusive organic product during incubation of **13** did not generate $O_2^{-\bullet}$ or H_2O_2 in aerobic buffer (Tables S1 and S3, ESI†) and neither did it induce significant DNA damage (Fig. 2c). An increased intracellular fluorescence in the DCFH-DA-based assay conducted in the presence of *Mycobacterium smegmatis* MC^2155 (*Msm*) was observed (Fig. S4, ESI†). A quinone with a reduction potential in the range of −0.7 to −1.1 V would be predicted to be a candidate for reduction by enzymes such as NADPH:cytochrome P450 reductase[15] and CV analysis of **14** gave a reduction potential of −0.94 V (Fig. S9, ESI†). Together, these data are consistent with a bioreductive mode of activation of **14** to produce oxidative species (Scheme 1). Quinone **14** inhibited *Mtb* growth with a MIC of 1.56 μg mL^{-1} (Table 1, entry 14) supporting our hypothesis that direct generation of ROS by **13** (Fig. 1) in conjunction with intracellular production of oxidative species by redox cycling by **14** could result in inhibition of *Mtb* growth (Scheme 2).

The ROS generator **13** was not a significant inhibitor (IC_{50} > 25 μM) of normal human kidney (HEK) cells (Fig. S10, ESI†). This result is consistent with anti-cancer oxidative stress inducers which have shown selective toxicity towards cancers but spared normal cells.[5,6] The lead compound **13** (at 100 μg mL^{-1}) did not significantly inhibit several fast-growing Gram-positive and Gram-negative bacterial strains tested (Table S8, ESI†). The microbe selectivity of **13** parallels that of an artemisinin–mycobactin drug conjugate which has shown high *Mtb* inhibitory potency.[17]

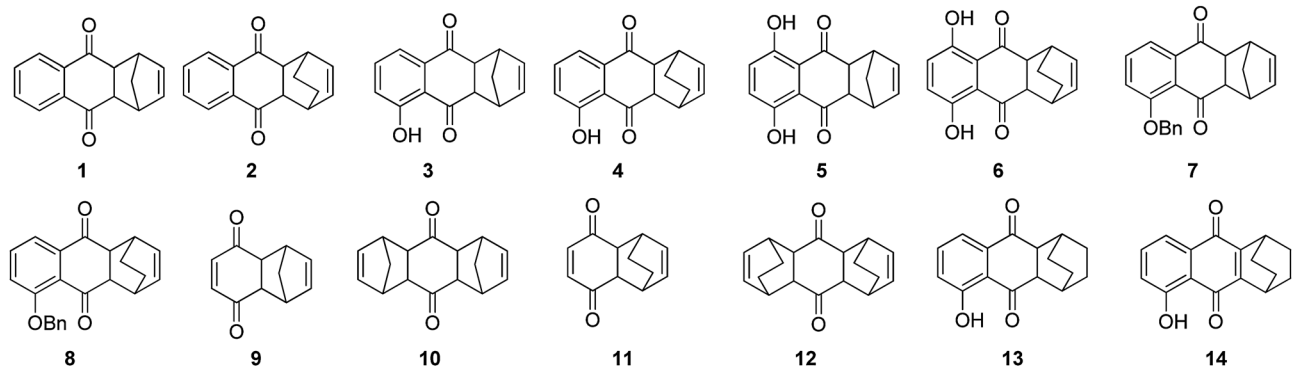

Fig. 1 Compounds **1–14**.

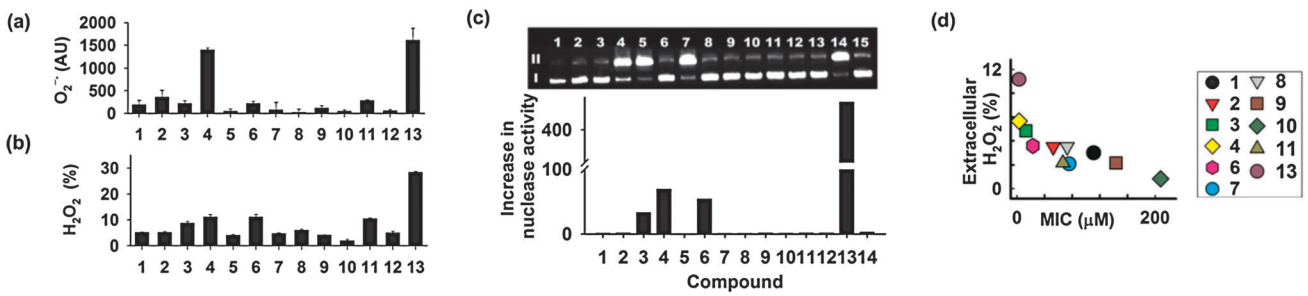

Fig. 2 (a) Superoxide ($O_2^{-\bullet}$) generated during incubation of **1–13** (5 μM) in pH 7.4 buffer at 37 °C for 30 min was estimated by a luminol-based chemiluminescence assay. Hypoxanthine/xanthine oxidase was used as a positive control in this assay. (b) H_2O_2 generated during incubation of **1–13** (5 μM) in pH 7.4 buffer at 37 °C for 30 min was estimated by a xylenol orange-based colorimetric assay; (c) nuclease activity of **1–14**: reaction mixtures (20 μL) contained 100 ng of form I DNA in pH 8.0 phosphate buffer (100 mM) and compound (50 μM) were incubated at 37 °C for 6 h: lane 1, untreated control; lane 2, **1**; lane 3, **2**; lane 4, **3**; lane 5, **4**; lane 6, **5**; lane 7, **6**; lane 8, **7**; lane 9, **8**; lane 10, **9**; lane 11, **10**; lane 12, **11**; lane 13, **12**; lane 14, **13**; lane 15, **14**. Nicked DNA is represented by II. A relative increase in nuclease activity is defined as the ratio of form II (cleaved) to form I (uncleaved) in comparison with untreated control (lane 1); (d) comparison of MICs determined against *Mycobacterium tuberculosis* and extracellular H_2O_2 yields during incubation of that compound with *Mycobacterium smegmatis* for 1 h and Spearman's correlation coefficient was found to be $\rho = -0.91$, *P*-value $< 10^{-5}$.

Table 1 Extracellular ROS generation, *Mycobacterium tuberculosis* growth inhibitory activity and calculated partition coefficients (clogPs)

Entry	Compd	MIC[a] (μg mL^{-1})	MIC (μM)	Extracellular H_2O_2[b] (%)	clogP[c]
1	**1**	25	111.0	3.6	2.43
2	**2**	12.5	52.4	4.2	2.99
3	**3**	3.13	13.0	5.8	2.76
4	**4**	0.76	3.0	6.8	3.32
5	**5**	>100	>350	1.9	2.72
6	**6**	6.25	23.1	4.3	3.28
7	**7**	25	75.6	2.5	4.29
8	**8**	25	72.5	4.2	4.85
9	**9**	25	143.5	2.6	0.43
10	**10**	50	208.0	1.0[d]	1.93
11	**11**	12.5	66.4	2.6	0.99
12	**12**	>100	>350	2.2[d]	3.04
13	**13**	0.76	3.0	11.0	3.81
14	**14**	1.56	6.1	3.8	4.52
15	Isoniazid	0.05	0.37	—	−0.67
16	Ethambutol	1.56	7.64	—	0.12
17	Pyrazinamide	6.25	50.8	—	−0.68

[a] Minimum inhibitory concentration (MIC) is the minimum concentration of the compound required to inhibit 99% of bacterial growth and was found against *Mycobacterium tuberculosis* $H_{37}R_v$ strain. [b] Extracellular H_2O_2 measured during incubation of **1–14** (50 μM) in the presence of *Msm* at 37 °C for 1 h estimated by an Amplex red-based fluorescence assay. [c] Calculated values using Chembiodraw Ultra. [d] Calculated based on 2 mol H_2O_2 from 1 mol of compound.

At the outset our goal was two-fold: one, to design, synthesize and study compounds that were capable of generating ROS; and two, to identify compounds with a range of ROS generation profiles by structural modifications to study the effects of varying ROS on *Mtb* growth. Having established that compounds **1–13** were ROS generators in buffer, we estimated ROS generated by **1–13** in the presence of cultured *Mycobacterium smegmatis* MC^2155 (*Msm*) and extracellular H_2O_2 was estimated using an Amplex Red-based fluorescence assay (Table 1). A good range of ROS in the presence of mycobacteria (1–11%) was observed with **13** being the best H_2O_2 generator (Table 1, entry 13). Statistical analysis between the compound's extracellular H_2O_2 yield in the aforementioned assay and the compound's measurable MIC against *Mtb* revealed a strong negative correlation (Fig. 2d) between these variables (Spearman's rank correlation coefficient $\rho = -0.91$, P-value $< 10^{-5}$). This result is indicative of ROS generating ability of the compound being important for inhibitory effects but without detailed mechanistic investigations, a conclusive connection cannot be established. However, previous studies show that the exquisite susceptibility of *Mtb* to isoniazid, a clinically used TB drug that in part acts through induction of oxidative stress, is attributable to inactivation of oxyR, a regulatory system that activates >20 anti-oxidant genes in response to ROS;[18] while oxyR is present in most actinobacteria, paradoxically, it is an inactive pseudogene in *Mtb* suggesting that a coherent response to induction of oxidative stress might be impaired.[19] Precursors of reactive species such as nitric oxide and sulfur dioxide have shown *Mtb* inhibitory activity.[11,16] Here, we demonstrate the feasibility of a tuberculosis drug design strategy based on compounds generating reactive oxygen species in order to perturb redox homeostasis.

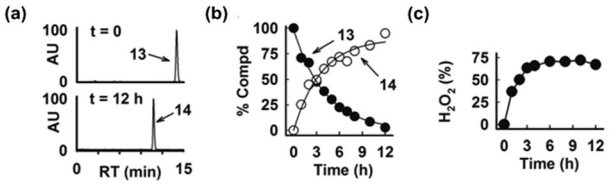

Fig. 3 (a) HPLC traces of incubation of **13** in pH 7.4 buffer for 12 h show complete conversion of **13** to **14**; (b) time courses of disappearance of **13** ($k_{13} = 0.24 \pm 0.01$ h^{-1}) and appearance of **14** (k_{14} was 0.28 ± 0.04 h^{-1}) based on HPLC analysis; (c) time course of H_2O_2 generated during incubation of **13** ($k_{HP} = 0.7$ h^{-1}) in pH 7.4 buffer.

This work was supported in part by Department of Biotechnology, India (BT/05/IYBA/2011). ATD acknowledges a research fellowship from Council for Scientific and Industrial Research (CSIR).

Notes and references

1 R. S. Wallis, W. Jakubiec, M. Mitton-Fry, L. Ladutko, S. Campbell, D. Paige, A. Silvia and P. F. Miller, *PLoS One*, 2012, **7**, e30479.
2 L. G. Dover and G. D. Coxon, *J. Med. Chem.*, 2011, **54**, 6157–6165.
3 A. Kumar, A. Farhana, L. Guidry, V. Saini, M. Hondalus and A. J. C. Steyn, *Expert Rev. Mol. Med.*, 2011, **13**, 1 (e39).
4 F. C. Fang, *Nat. Rev. Microbiol.*, 2004, **2**, 820–832.
5 L. Raj, T. Ide, A. U. Gurkar, M. Foley, M. Schenone, X. Li, N. J. Tolliday, T. R. Golub, S. A. Carr, A. F. Shamji, A. M. Stern, A. Mandinova, S. L. Schreiber and S. W. Lee, *Nature*, 2011, **475**, 231–234.
6 J. S. Bair, R. Palchaudhuri and P. J. Hergenrother, *J. Am. Chem. Soc.*, 2010, **132**, 5469–5478.
7 G. T. Wondrak, *Antioxid. Redox Signaling*, 2009, **11**, 3015–3069.
8 J. M. Campos-Martin, G. Blanco-Brieva and J. L. G. Fierro, *Angew. Chem., Int. Ed.*, 2006, **45**, 6962–6984.
9 H. Trung Pham, C. Marquetty, C. Pasquier and J. Hakim, *Anal. Biochem.*, 1984, **142**, 467–472.
10 C. Gay, J. Collins and J. M. Gebicki, *Anal. Biochem.*, 1999, **273**, 149–155.
11 S. R. Malwal, D. Sriram, P. Yogeeswari, V. B. Konkimalla and H. Chakrapani, *J. Med. Chem.*, 2012, **55**, 553–557.
12 J. A. Valderrama, O. Espinoza, M. F. Gonzalez, R. A. Tapia, J. A. Rodriguez, C. Theoduloz and G. Schmeda-Hirschmann, *Tetrahedron*, 2006, **62**, 2631–2638.
13 K. U. Ingold, T. Paul, M. J. Young and L. Doiron, *J. Am. Chem. Soc.*, 1997, **119**, 12364–12365.
14 J. Adamus, J. Gebicki, I. Ciebiada, E. Korczak and A. Denys, *J. Med. Chem.*, 1998, **41**, 2932–2933.
15 M. H. Livertoux, P. Lagrange and A. Minn, *Brain Res.*, 1996, **725**, 207–216.
16 R. Singh, U. Manjunatha, H. I. Boshoff, Y. H. Ha, P. Niyomrattanakit, R. Ledwidge, C. S. Dowd, I. Y. Lee, P. Kim, L. Zhang, S. Kang, T. H. Keller, J. Jiricek and C. E. Barry, 3rd, *Science*, 2008, **322**, 1392–1395.
17 M. J. Miller, A. J. Walz, H. Zhu, C. Wu, G. Moraski, U. Möllmann, E. M. Tristani, A. L. Crumbliss, M. T. Ferdig, L. Checkley, R. L. Edwards and H. I. Boshoff, *J. Am. Chem. Soc.*, 2011, **133**, 2076–2079.
18 C. D. den Hengst and M. J. Buttner, *Biochim. Biophys. Acta*, 2008, **1780**, 1201–1216.
19 E. Pagán-Ramos, S. S. Master, C. L. Pritchett, R. Reimschuessel, M. Trucksis, G. S. Timmins and V. Deretic, *J. Bacteriol.*, 2006, **188**, 2674–2680.

JOC The Journal of Organic Chemistry

Note

pubs.acs.org/joc

Substituent Effects on Reactive Oxygen Species (ROS) Generation by Hydroquinones

Allimuthu T. Dharmaraja, Charu Jain, and Harinath Chakrapani*

Department of Chemistry, Indian Institute of Science Education and Research Pune, Dr. Homi Bhabha Road, Pashan, Pune 411021, Maharashtra, India

Supporting Information

ABSTRACT: In order to understand the structural aspects of stabilization of hydroquinones and their ability to generate reactive oxygen species (ROS), we designed and synthesized a series of 6-aryl-2,3-dihydro-1,4-benzoquinones. These compounds equilibrate with the corresponding 6-aryl-1,4-dihydroxybenzenes in an organic medium; a linear free energy relationship analysis gave ρ = +2.37, suggesting that this equilibrium was sensitive to electronic effects. The propensity of the compound to enolize appears to determine ROS-generating capability, thus offering scope for tunable ROS generation.

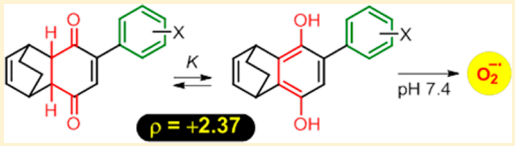

During aerobic respiration, inadvertent 1e transfer to molecular O_2 produces the superoxide radical anion $O_2^{-\bullet}$.[1,2] $O_2^{-\bullet}$ is converted to hydrogen peroxide (H_2O_2), which in the presence of trace metal ions through Fenton chemistry can generate the highly reactive hydroxyl radical $^\bullet$OH.[1−3] Together, $O_2^{-\bullet}$, H_2O_2 and $^\bullet$OH are considered as reactive oxygen species (ROS) and are central to redox biology, immune response, an understanding of the pathology of numerous diseases, including cancer, and aging.[4−6] Recently, a number of studies provide evidence for the use of ROS as a therapeutic.[4] For example, cancers have been reported to have impaired capability to maintain redox homeostasis[4] and are sensitive to small molecules capable of generating ROS.[7,8] Drug resistance in bacteria can be overcome by enhancement of ROS,[9] suggesting possible applications for ROS generators as an adjuvant that can enhance the efficacy of existing drugs.[10−16] However, the precise roles of ROS are yet to be completely understood[17] and the rate of ROS generation plays an important role in the observed biological effects.[11] Although multiple strategies can be used for ROS generation with variable rates, a single scaffold with control over ROS generation rates is not available.[18−20] Such a tool would allow us to study the differences in biological effects of varying ROS generation. Furthermore, due to comparable physicochemical properties offered by a single scaffold, development of one with diverse ROS generation profiles would be useful. We considered 6-aryl-2,3-dihydro-1,4-benzoquinones as a possible candidate scaffold for tunable ROS generation (Scheme 1). A mechanism for ROS generation from these compounds involves enolization as the first step that produces an aromatic 1,4-diol, which reacts with oxygen to produce $O_2^{-\bullet}$.[12] Placing substituents on the position adjacent to the carbonyl functional group might affect the propensity of the keto form to enolize. Being able to systematically alter the position of this equilibrium might offer opportunities to tune ROS generation. In addition to ROS generation, hydroquinones find frequent use as a functional group capable of transferring electrons[21−23] and are components of numerous bioactive natural products.[24−26] Understanding substituent effects on stabilizing the enol would hence enable us to better characterize the reactivity of this important functional group.

Scheme 1. Equilibration of 6-Aryl-2,3-dihydro-1,4-benzoquinones with Their Corresponding Diols, Which under Physiological Conditions React with Oxygen To Produce ROS

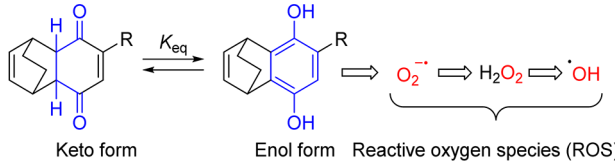

In order to synthesize the 6-aryl-2,3-dihydrobenzoquinone scaffold, substituted *p*-benzoquinones **15**−**26** were first synthesized using a silver nitrate catalyzed arylation of 1,4-benzoquinone (**14**) with functionalized arylboronic acids (Table S1 (Supporting Information), entries 1−12).[27] Next, **14**−**26**, containing electron-withdrawing and electron-donating groups, were independently reacted with 1,3-cyclohexadiene to produce the corresponding Diels−Alder adducts in yields ranging from 67 to 95% (Table 1, entries 1−13). A ^{1}H nuclear magnetic resonance (^{1}H NMR) spectroscopy study conducted on **2** showed that this compound exclusively existed in the keto form (**2a**), as evidenced by signals for the hydrogens of α and β (bridgehead) to the C═O, which appeared in the range 3.0−3.4 ppm (Figure S1 (Supporting Information)). A similar result was recorded for the 4-methyl as well as 4-methoxyphenyl derivatives **3** and **4** (Figure S1), suggesting no major effect of introduction of an electron-donating group on the position of the equilibrium (Table 1). Next, the ^{1}H NMR spectrum for the

Received: August 4, 2014
Published: September 10, 2014

dx.doi.org/10.1021/jo501796z | J. Org. Chem. 2014, 79, 9413−9417

Table 1. Synthesis of 1−13, Results of Keto−Enol Ratios Studied by ^{1}H NMR, Percent Compound Remaining in Buffer Calculated from HPLC Studies, and H_2O_2 Generated from 1−13 in Buffer

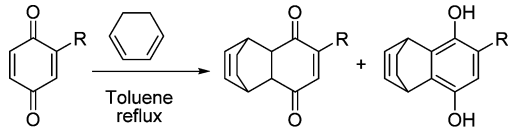

14-26 **1a-13a** **1b-13b**

entry	R	quinone	product	yield (%)	keto (%)[a]	enol (%)[a]	K_{eq}[b]	remaining (%)[c]	H_2O_2 (μM)[d]
1	H	**14**	**1a**	70	100	n.d.	0.0204[e]	32	1.16
2	Ph	**15**	**2a**	73	100	n.d.	0.0204[e]	74	1.66
3	4-MePh	**16**	**3a**	83	100	n.d.	0.0204[e]	60	0.75
4	4-MeOPh	**17**	**4a**	74	100	n.d.	0.0204[e]	86	1.07
5	4-BrPh	**18**	**5a + 5b**	81	93	7[f]	0.0753	25	0.85
6	4-ClPh	**19**	**6a + 6b**	95	62[f]	38	0.6129	52	3.67
7	4-FPh	**20**	**7a + 7b**	66	89	11	0.1235	57	2.65
8	4-AcPh	**21**	**8a + 8b**	84	74	26[f]	0.3513	17	2.44
9	4-NO_2Ph	**22**	**9b**	84	n.d.	100[f]	49[e]	9.6	1.59[g]
10	4-CHOPh	**23**	**10b**	81	n.d.	100[f]	49[e]	11.4	5.42
11	3-NO_2Ph	**24**	**11a + 11b**	67	27	73	2.703	18	3.55
12	3-CHOPh	**25**	**12b**	87	n.d.	100[f]	49[e]	40	3.55
13	2-MeOPh	**26**	**13a**	70	100	n.d.	0.0204[e]	70	0.45

[a]The percent keto and enol forms were estimated by ^{1}H NMR spectroscopy in $CDCl_3$ unless otherwise indicated (spectra were recorded on a 400 MHz NMR spectrometer). n.d. = not detected. [b]K_{eq} was estimated by the ratio of peaks correspnding to α- and β-hydrogens to the C=O (for the keto form) and the bridgehead hydrogens (for the enol form). n.d. = not detected. [c]The compound (1 mM) was incubated in pH 7.4 phosphate buffer for 60 min at 37 °C under ambient aerobic conditions, and HPLC was used to determine percnet compound remaining. [d]The compound (10 μM) was incubated in pH 7.4 phosphate buffer under ambient aerobic conditions for 60 min, and H_2O_2 was assayed by an Amplex Red fluorescence assay. [e]Estimated by considering 98% of the major tautomer. [f]Experiment was conducted in DMSO-d_6. [g]HPLC analysis of this reaction mixture showed multiple unidentified products, suggesting possible side reactions or collateral consumption of H_2O_2 likely contributing to the diminished yield of H_2O_2.

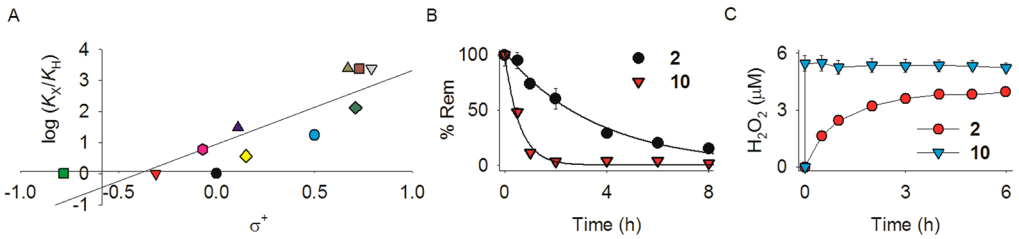

Figure 1. (a) Plot of log(K_X/K_H) for keto−enol equilibria of 2,3-dihydrobenzoquinones versus the Hammett substitution constant σ^+ [28] (reaction constant ρ = 2.37; R^2 = 0.7420). (b) Time course of decomposition of **2** (1 mM, k_2 = 0.28 h^{-1}, R^2 = 0.9875) and **10** (1 mM, k_{10} = 1.48 h^{-1}, R^2 = 0.9546) in acetonitrile (pH 7.4 phosphate buffer (1/1, v/v)) based on HPLC analysis. (c) Time course of H_2O_2 generated from **2** (10 μM) and **10** (10 μM) over 6 h in pH 7.4 phosphate buffer measured using Amplex Red based fluorescence assay.

4-bromo derivative **5** was recorded and this compound was found to exist predominantly in its keto form **5a**; however, a set of peaks at 4.2−4.5 ppm for the bridgehead hydrogens of the enol form **5b** was also observed (Figure S1). The major tautomer was the keto form **5a**, estimated as 93% (Table 1, entry 5). A similar result was recorded for **6**−**8** (Figure S1), whose equilibria were found to be 62−89% in favor of the keto tautomer (Table 1, entries 6−8).

Among the compounds with electron-withdrawing groups, the enol form was dominant and **9**, **10**, and **12** were found to exist nearly exclusively in the enol forms **9b**, **10b**, and **12b** while the 3-nitroaryl derivative **11** was 73% enol in DMSO-d_6 (Table 1, entries 9−12). The aryl derivative **13** with a 2-methoxy substituent was found to behave similarly to the 4-methoxy derivative **4**, and only the keto form **13a** could be detected (Table 1, entry 13).

On the basis of the ratios of the keto and enol forms, the equilibrium constant for enolization K_{eq} was calculated (Table 1). In order to understand substituent effects on the position of this equilibrium, using these K_{eq} values, a Hammett plot was constructed. A moderately linear correlation (R^2 = 0.6751) was observed with σ, and an overall reaction constant ρ of +3.6 was obtained (see the Supporting Information, Figure S2). The resonance contribution to the position of the equilibrium was estimated using a similar plot that was constructed with σ^+, and a ρ value of +2.37 was obtained, but with better linearity (R^2 = 0.7420, Figure 1a).[28] Previous reports of such equilibria in related β-diketones such as benzoylacetones and benzoylcyclohexanones indicate that the keto form is stabilized by electron-releasing groups.[29−31] Although the magnitude of the reaction constant ρ derived from σ^+ and equilibrium constants in the aforementioned studies was significantly lower (i.e. 0.6−0.9[29−31]) than the ρ value that we find in this study, the sign was positive, supporting similar trends in substituent effects on the stability of keto and enol forms.

dx.doi.org/10.1021/jo501796z | J. Org. Chem. 2014, 79, 9413−9417

Next, the electronic effect on the keto form's propensity to enolize was studied by exposing the compound to base, which would promote enolization. Compound **2**, which predominantly exists in the keto form **2a**, was exposed to NaOD (0.2 equiv) in DMSO-d_6, and the NMR spectrum was recorded after 15 min (see the Supporting Information, Figure S3). The formation of signals that were characteristic of the bridgehead hydrogens of the enolate was observed (indicated by arrows in Figure S3) with concomitant disappearance of the α-keto hydrogens. A similar experiment conducted with **4a** showed that, in the same time period, 62% of **4a** remained and complete enolization was observed in 1 h, suggesting that an electron-donating group on the aryl ring significantly lowered the rate of enolization (see the Supporting Information, Figure S4). A similar experiment conducted with **5** (93/7; **5a**/**5b**) and **8** (77/23; **8a**/**8b**) showed nearly complete enolization in 15 min (see the Supporting Information, Figures S5 and S6). These observations are consistent with electron-donating groups significantly decreasing the propensity of the hydroquinone to enolize.

Our data suggest that the enolization of 6-aryl-2,3-dihydrobenzoquinones is dependent on electronic effects and the ratio of keto and enol tautomers can be modulated by simple structural modifications on the aryl ring. Accordingly, compounds with dominant enol forms are expected to be more reactive in ambient aerobic buffer and vice versa. When **1a** was dissolved in pH 7.4 phosphate buffer/acetonitrile (1/1, v/v), we found nearly 32% of the compound remaining after 60 min (Table 1, entry 1). When a similar experiment was conducted with **2a**, 74% of the compound remained after 1 h (Table 1, entry 2). Curve fitting of percent **2a** remaining to a first-order reaction gave a rate constant of 0.28 h^{-1} (R^2 = 0.9875) and a half-life ($t_{1/2}$) of 2.49 h (Figure 1b). Compounds **3a** and **4a** with electron-donating groups were found to have comparable decomposition profiles after 1 h (Table 1, entries 3 and 4). In the cases of compounds **5**−**8** and **11**, which existed as mixtures of keto and enol forms in organic media, the percent remaining in these cases was calculated on the basis of the keto form and ranged from 18 to 57%, all lower in comparison with **2a** (Table 1, entries 5−8 and 11). Compounds **9b** and **10b** were 90% decomposed in 1 h, while 40% of the formyl derivative **12b** remained in the same time period (Table 1, entries 9, 10, and 12). Under these conditions, the first-order rate constant k = 1.48 h^{-1} (R^2 = 0.9546) was recorded for decomposition of **10b** (Figure 1b). The half-life of this compound was estimated as 0.47 h, which is lower in comparison with **2a** (Figure 1b).

In ambient aerobic buffer, the hydroquinone is expected to rapidly react with oxygen to produce the corresponding 1,4-benzoquinone (see the Supporting Information, Table S3, compounds **27**−**29**). Its keto tautomer, on the other hand, would have to first tautomerize to generate hydroquinone enolate in buffer, and a sequential one-electron transfer from the enolate to molecular oxygen produces ROS such as $O_2^{-\bullet}$ and H_2O_2 (Scheme S2, Supporting Information).[12,13] We studied superoxide ($O_2^{-\bullet}$) generated from **1**−**13** using a reported chemiluminescence assay,[32] and results of this assay confirmed that **1**−**13** were capable of generating $O_2^{-\bullet}$ in buffer (see the Supporting Information, Figure S12). Addition of an electron to $O_2^{-\bullet}$ would lead to the formation of H_2O_2, which was assayed using a commercially available Amplex Red reagent.[33,14] All compounds tested were found to generate H_2O_2, and in a majority of the cases, we found that the presence of an electron-withdrawing substituent enhanced ROS generation (Table 1, entries 1−13). This result is consistent with enolization being the critical step in ROS production; once formed, the enolate reacts rapidly with O_2 to generate ROS (Scheme 1). Hence, the keto−enol ratio in organic media was a good indicator of the ability to generate ROS in buffer, suggesting that enolization is the key step to control ROS generation by these compounds.[37] Finally, the tunability offered by this scaffold is illustrated by time courses of H_2O_2 generated by **2a**, which is gradual, and **10b**, which rapidly dissociates to generate ROS (Figure 1c). Taken together, we provide evidence for predictably tuning keto−enol tautomerism in dihydrobenzoquinones by varying substituent electronics and the position of this equilibrium significantly affects ROS generation.

EXPERIMENTAL SECTION

Compounds **1**,[34] **2**,[35] and **15**−**26**[27,36] have been previously reported, and analytical data that we recorded were consistent with the reported values.

General Procedure for Synthesis of Compounds 1a−13a. To a solution of 2-aryl-1,4-benzoquinone (1 mmol) in toluene (10 mL) was added freshly distilled 1,3-cyclohexadiene (2 mmol), and the mixture was refluxed. Upon complete consumption of the starting material (TLC analysis), the reaction mixture was evaporated to dryness under reduced pressure to obtain the crude product. The crude material was purified by silica gel column chromatography using an ethyl acetate (5 → 15%) and petroleum ether solvent system. This material was recrystallized in chloroform to obtain pure material.

General Procedure for Synthesis of 27−29. To a solution of 2,3-dihydro-1,4-benzoquinone (0.2 mmol) in tetrahydrofuran (THF, 5 mL) was added potassium carbonate (0.5 mmol, 2.5 equiv), and the reaction mixture was stirred at room temperature overnight. The reaction mixture was washed with 5 mL of deionized water and extracted with ethyl acetate (4 × 5 mL). The combined organic layer was dried (anhydrous Na_2SO_4, 5 g) and filtered, and the filtrate was evaporated under reduced pressure to obtain the crude product. The crude mixture was purified by a silica gel column by washing with ethyl acetate/petroleum ether (1/3 ratio, v/v). The organic solvent was evaporated under reduced pressure to obtain pure material.

6-(4-Methylphenyl)-1,4,4a,8a-tetrahydro-1,4-ethanonaphthalene-5,8-dione (3a). Starting from **16** (150 mg, 0.76 mmol), **3a** (174 mg, 66%) was isolated as a pale yellow solid: mp 116−118 °C; FT-IR (ν_{max}, cm^{-1}) 2927, 2861, 1743, 1681, 1653, 1516, 1462, 1208, 1029; ^{1}H NMR (400 MHz, $CDCl_3$) δ 7.30 (d, J = 8.2 Hz, 2H), 7.20 (d, J = 8.0 Hz, 2H), 6.74 (s, 1H), 6.15−6.31 (m, 2H), 3.21−3.27 (m, 2H), 3.15 (dd, J = 2.5, 9.3 Hz, 1H), 3.06 (dd, J = 2.5, 9.3 Hz, 1H), 2.37 (s, 3H), 1.69−1.76 (m, 2H), 1.34−1. 69 (m, 2H); ^{13}C NMR (100 MHz, $CDCl_3$) δ 199.6, 198.9, 151.7, 140.6, 137.7, 133.8, 133.4, 130.5, 129.3, 128.8, 50.7, 50.2, 35.6, 35.5, 24.8, 21.5; HRMS (ESI-TOF) for $[C_{19}H_{18}O_2 + Na]^+$ calcd 301.1204, found 301.1194. Anal. Calcd for $C_{19}H_{18}O_2$: C, 81.99; H, 6.52. Found: C, 81.71; H, 6.42.

6-(4-Methoxyphenyl)-1,4,4a,8a-tetrahydro-1,4-ethanonaphthalene-5,8-dione (4a). Starting from **17** (100 mg, 0.47 mmol), **4a** (101 mg, 74%) was isolated as an orange-yellow solid: mp 121−123 °C; FT-IR (ν_{max}, cm^{-1}) 2928, 2859, 1743, 1678, 1652, 1515, 1462, 1258, 1023; ^{1}H NMR (400 MHz, $CDCl_3$) δ 7.39 (d, J = 8.7 Hz, 2H), 6.90 (d, J = 8.7 Hz, 2H), 6.72 (s, 1H), 6.18−6.33 (m, 2H), 3.82 (s, 3H), 3.23 (s, 2H), 3.13 (dd, J = 2.1, 9.3 Hz, 1H), 3.05 (dd, J = 2.1, 9.3 Hz, 1H), 1.72 (d, J = 6.9 Hz, 2H), 1.38 (d, J = 7.8 Hz, 2H); ^{13}C NMR (100 MHz, $CDCl_3$) δ 199.5, 199.2, 161.4, 151.0, 136.7, 133.8, 133.4, 130.5, 125.6, 114.1, 55.5, 50.8, 50.1, 35.5, 35.4, 24.9; HRMS (ESI-TOF) for $[C_{19}H_{18}O_3 + Na]^+$ calcd 317.1153, found 317.1149. Anal. Calcd for $C_{19}H_{18}O_3$: C, 77.53; H, 6.16. Found: C, 77.64; H, 5.82.

6-(4-Bromophenyl)-1,4,4a,8a-tetrahydro-1,4-ethanonaphthalene-5,8-dione (5a). Starting from **18** (500 mg, 1.9 mmol), **5** (531 mg, 81%) was isolated as a pale yellow solid: mp 132−134 °C; FT-IR (ν_{max}, cm^{-1}) 3531, 2920, 2873, 1741, 1651, 1460, 1339, 1201, 1073; ^{1}H NMR (400 MHz, $CDCl_3$) δ 7.50−7.54 (m, 2H), 7.24−7.27

dx.doi.org/10.1021/jo501796z | J. Org. Chem. 2014, 79, 9413−9417

(m, 2H), 6.69−6.77 (m, 1H), 6.19−6.28 (m, 2H), 3.23 (dd, J = 2.5, 5.0 Hz, 2H), 3.15 (d, J = 2.5 Hz, 1H), 3.13 (d, J = 2.5 Hz, 1H), 1.66−1.79 (m, 2H), 1.33−1.46 (m, 2H); ^{13}C NMR (100 MHz, $CDCl_3$) δ 199.3, 198.4, 150.5, 138.4, 133.9, 133.4, 132.3, 132.1, 131.8, 130.9, 130.5, 124.8, 50.6, 50.2, 35.6, 35.5, 24.8; HRMS (ESI-TOF) for $[C_{18}H_{15}BrO_2 + Na]^+$ calcd 365.0152, found 365.0152. Anal. Calcd for $C_{18}H_{15}BrO_2$ calcd. C, 62.99; H, 4.41. Found, C, 63.21; H, 4.09. Note: NMR data presented here are for the major isomer.

6-(4-Chlorophenyl)-1,4,4a,8a-tetrahydro-1,4-ethanonaphthalene-5,8-dione (6a). Starting from **19** (300 mg, 1.4 mmol), **6** (391 mg, 95%) was isolated as a yellow solid: mp 149−151 °C; FT-IR (ν_{max}, cm^{-1}) 3581, 3422, 3055, 2952, 2869, 1742, 1653, 1467, 1259, 1040; ^{1}H NMR (400 MHz, DMSO-d_6) δ 7.41−7.45 (m, 4H), 6.82 (s, 1H), 6.12−6.23 (m, 2H), 3.23 (dd, J = 2.4, 9.5 Hz, 1H), 3.01−3.13 (m, 3H), 1.67 (d, J = 8.2 Hz, 2H), 1.20−1.40 (m, 2H); ^{13}C NMR (100 MHz, DMSO-d_6) δ 199.2, 198.4, 150.4, 138.4, 133.9, 133.4, 130.6, 130.2, 129.4, 128.7, 113.3, 63.8, 50.6, 50.2, 35.6, 35.5, 25.0, 24.8 (a mixture of keto (62%) and enol (38%) tautomers); HRMS (ESI-TOF) for $[C_{18}H_{15}ClO_2 + Na]^+$ calcd 321.0658, found 321.0656. Note: NMR data presented here are for the major isomer.

6-(4-Fluorophenyl)-1,4,4a,8a-tetrahydro-1,4-ethanonaphthalene-5,8-dione (7a). Starting from **20** (300 mg, 1.48 mmol), **7** (277 mg, 66%) was isolated as a yellow semisolid: FT-IR (ν_{max}, cm^{-1}) 3567, 2961, 1742, 1695, 1652, 1513, 1462, 1220, 1157; ^{1}H NMR (400 MHz, $CDCl_3$) δ 7.36−7.41 (m, 2H), 7.03−7.12 (m, 2H), 6.72 (s, 1H), 6.24 (dd, J = 3.4, 4.3 Hz, 2H), 3.22−3.27 (m, 2H), 3.14 (dd, J = 2.5, 9.3 Hz, 1H), 3.06 (dd, J = 2.5, 9.3 Hz, 1H), 1.67−1.78 (m, 2H), 1.32−1.43 (m, 2H); ^{13}C NMR (100 MHz, $CDCl_3$) δ 199.3, 198.6, 165.2, 162.7, 150.4, 138.2, 133.9, 133.3, 131.0, 130.9, 115.8, 115.6, 113.5, 50.6, 50.2, 35.6, 35.5, 24.8; HRMS (ESI-TOF) for $[C_{18}H_{15}FO_2 + Na]^+$ calcd 305.0953, found 305.0957. Note: NMR data presented here are for the major isomer.

6-(4-Acetylphenyl)-1,4,4a,8a-tetrahydro-1,4-ethanonaphthalene-5,8-dione (8a). Starting from **21** (500 mg, 2.2 mmol), **8** (566 mg, 84%) was isolated as a yellow solid: mp 127−128 °C; FT-IR (ν_{max}, cm^{-1}) 3563, 2980, 2862, 1742, 1659, 1519, 1461, 1354, 1170, 1044; ^{1}H NMR (400 MHz, $CDCl_3$) δ 7.95 (dd, J = 2.1, 8.4 Hz, 2H), 7.46 (dd, J = 1.8, 8.3 Hz, 2H), 6.76 (d, J = 2.2 Hz, 1H), 6.25 (dd, J = 2.5, 4.8 Hz, 2H), 3.04−3.30 (m, 4H), 2.59 (d, J = 2.2 Hz, 3H), 1.73 (d, J = 7.4 Hz, 2H), 1.38 (d, J = 8.1 Hz, 2H); ^{13}C NMR (100 MHz, $CDCl_3$) δ 199.3, 198.3, 197.6, 150.6, 144.4, 139.1, 134.0, 133.4, 129.2, 129.1, 128.4, 127.5, 50.6, 50.2, 35.7, 35.5, 26.8, 24.8; HRMS (ESI-TOF) for $[C_{20}H_{18}O_3 + Na]^+$ calcd 329.1153, found 329.1154. Anal. Calcd for $C_{20}H_{18}O_3$: C, 78.41; H, 5.92. Found: C, 78.09; H, 5.57. Note: NMR data presented here are for the major isomer.

NMR Data of Enol Tautomer, 6-(4-Acetylphenyl)-1,4-dihydro-1,4-ethanonaphthalene-5,8-diol (8b). ^{1}H NMR (400 MHz, DMSO-d_6) δ 8.73 (s, 1H), 7.99 (s, 1H), 7.91 (d, J = 8.3 Hz, 2H), 7.57 (d, J = 7.8 Hz, 2H), 6.42−6.49 (m, 3H), 4.39 (s, 1H), 4.26 (s, 1H), 2.54 (s, 3H), 1.40 (d, J = 8.1 Hz, 2H), 1.28 (d, J = 9.6 Hz, 2H); ^{13}C NMR (100 MHz, DMSO-d_6) δ 198.05, 145.1, 145.0, 140.9, 135.8, 135.6, 135.0, 134.2, 132.0, 129.9, 128.4, 126.1, 113.7, 33.7, 33.3, 27.2, 25.4, 25.3; HRMS (ESI-TOF) for $[C_{20}H_{18}O_3 + H]^+$ calcd 307.1334, found 307.1330.

6-(4-Nitrophenyl)-1,4-dihydro-1,4-ethanonaphthalene-5,8-diol (9b). Starting from **22** (100 mg, 0.41 mmol), **9b** (64 mg, 47%) was isolated as a pale yellow semisolid: FT-IR (ν_{max}, cm^{-1}) 3517, 3452, 2936, 2869, 1741, 1653, 1517, 1460, 1196, 1021; ^{1}H NMR (400 MHz, DMSO-d_6) δ 8.79 (s, 1H), 8.17−8.20 (m, 3H), 7.69 (d, J = 8.7 Hz, 2H), 6.49 (s, 1H), 6.44−6.46 (m, 2H), 4.40 (s, 1H), 4.26 (s, 1H), 1.40 (d, J = 7.6 Hz, 2H), 1.27 (d, J = 9.9 Hz, 2H); ^{13}C NMR (100 MHz, DMSO-d_6) δ 172.8, 166.1, 147.3, 146.1, 145.2, 140.9, 135.7, 135.6, 134.4, 132.9, 130.7, 125.0, 123.6, 113.6, 33.7, 33.4, 25.3, 25.1; HRMS (ESI-TOF) for $[C_{18}H_{15}NO_4 + H]^+$ calcd 310.1079, found 310.1078.

6-(4-Formylphenyl)-1,4-dihydro-1,4-ethanonaphthalene-5,8-diol (10b). Starting from **23** (150 mg, 0.71 mmol), **10b** (168 mg, 81%) was isolated as a pale yellow solid: mp 193−195 °C; FT-IR (ν_{max}, cm^{-1}) 3568, 2930, 2862, 1743, 1684, 1598, 1551, 1520, 1461, 1266, 1067, 1020; ^{1}H NMR (400 MHz, DMSO-d_6) δ 9.96 (s, 1H), 8.73 (s, 1H), 8.03 (s, 1H), 7.86 (d, J = 8.2 Hz, 2H), 7.65 (d, J = 8.1 Hz, 2H), 6.37−6.58 (m, 3H), 4.40 (s, 1H), 4.26 (s, 1H), 1.40 (d, J = 7.9 Hz, 2H), 1.28 (d, J = 8.9 Hz, 2H); ^{13}C NMR (100 MHz, DMSO-d_6) δ 193.2, 146.6, 145.1, 140.9, 135.7, 135.6, 134.5, 134.3, 132.3, 130.3, 129.7, 126.0, 113.7, 33.7, 33.3, 25.4, 25.3; HRMS (ESI-TOF) for $[C_{19}H_{16}O_3 + H]^+$ calcd 293.1177, found 293.1173.

6-(3-Nitrophenyl)-1,4-dihydro-1,4-ethanonaphthalene-5,8-diol (11b). Starting from **24** (100 mg, 0.46 mmol), **11** (96 mg, 67%) was isolated as a yellow solid: mp 163−165 °C; FT-IR (ν_{max}, cm^{-1}) 3615, 2928, 1741, 1688, 1517, 1462, 1339, 1272, 1154; ^{1}H NMR (400 MHz, DMSO-d_6) δ 8.78 (s, 1H), 8.27−8.32 (m, 1H), 8.17 (s, 1H), 8.07 (dd, J = 1.8, 8.1 Hz, 1H), 7.82−7.88 (m, 1H), 7.62 (t, J = 8.0 Hz, 1H), 6.46 (dd, J = 9.1, 12.9 Hz, 3H), 4.39 (s, 1H), 4.26 (s, 1H), 1.40 (d, J = 8.0 Hz, 2H), 1.22−1.31 (m, 2H); ^{13}C NMR (100 MHz, DMSO-d_6) δ 199.2, 198.4, 148.8, 148.0, 145.2, 141.6, 140.8, 139.2, 136.1, 135.9, 135.7, 135.6, 135.4, 134.3, 134.1, 132.4, 130.4, 130.0, 124.9, 124.7, 124.3, 124.2, 121.4, 113.5, 50.4, 50.1, 34.8, 33.7, 33.3, 25.4, 25.3, 24.7, 24.6 (a mixture of keto/enol (27/73) tautomers); HRMS (ESI-TOF) for $[C_{18}H_{15}NO_4 + Na]^+$ calcd 332.0899, found 332.0898. Note: NMR data presented here are for the major isomer.

6-(3-Formylphenyl)-1,4-dihydro-1,4-ethanonaphthalene-5,8-diol (12b). Starting from **25** (400 mg, 1.88 mmol), **12b** (477 mg, 87%) was isolated as a yellow solid: mp 158−160 °C; FT-IR (ν_{max}, cm^{-1}) 3455, 3323, 2913, 2865, 1833, 1742, 1675, 1514, 1459, 1288, 1146, 1071; ^{1}H NMR (400 MHz, DMSO-d_6) δ 10.00 (s, 1H), 8.72 (s, 1H), 8.00 (s, 1H), 7.97 (s, 1H), 7.76 (dd, J = 1.4, 7.6 Hz, 2H), 7.56 (t, J = 7.6 Hz, 1H), 6.45−6.48 (m, 3H), 4.40 (s, 1H), 4.27 (s, 1H), 1.40 (d, J = 7.8 Hz, 2H), 1.29 (d, J = 9.4 Hz, 2H); ^{13}C NMR (100 MHz, DMSO-d_6) δ 193.9, 145.1, 141.0, 140.7, 136.5, 135.8, 135.7, 135.7, 134.2, 131.7, 130.8, 129.3, 127.8, 125.9, 113.7, 33.7, 33.3, 25.4, 25.3; HRMS (ESI-TOF) for $[C_{19}H_{16}O_3 + H]^+$ calcd 293.1177, found 293.1170. Anal. Calcd for $C_{19}H_{16}O_3$: C, 78.06; H, 5.52. Found: C, 77.66; H, 5.31.

6-(2-Methoxyphenyl)-1,4,4a,8a-tetrahydro-1,4-ethanonaphthalene-5,8-dione (13a). Starting from **26** (200 mg, 0.93 mmol), **13a** (193 mg, 70%) was isolated as an orange-yellow solid: mp 143−145 °C; FT-IR (ν_{max}, cm^{-1}) 2927, 2856, 1743, 1655, 1518, 1462, 1256, 1167, 1019; ^{1}H NMR (400 MHz, $CDCl_3$) δ 7.37 (ddd, J = 1.8, 7.3, 8.3 Hz, 1H), 7.08 (dd, J = 1.8, 7.4 Hz, 1H), 6.94−6.99 (m, 1H), 6.90 (d, J = 8.3 Hz, 1H), 6.65 (s, 1H), 6.16−6.39 (m, 2H), 3.76 (s, 3H), 3.13−3.26 (m, 3H), 3.07 (dd, J = 2.7, 9.2 Hz, 1H), 1.66−1.78 (m, 2H), 1.34−1. 46 (m, 2H); ^{13}C NMR (100 MHz, $CDCl_3$) δ 198.3, 196.8, 155.8, 151.5, 138.0, 133.1, 131.8, 130.2, 128.8, 122.9, 119.9, 110.2, 54.5, 49.4, 49.1, 34.1, 33.8, 24.1, 23.4; HRMS (ESI-TOF) for $[C_{19}H_{18}O_3 + Na]^+$ calcd 317.1153, found 317.1149. Anal. Calcd for $C_{19}H_{18}O_3$: C, 77.53; H, 6.16. Found: C, 77.19; H, 6.04.

6-Phenyl-1,4-dihydro-1,4-ethanonaphthalene-5,8-dione (27). Starting from **2a** (50 mg, 0.19 mmol), **27** was isolated as a yellow semisolid (41 mg, 83%): FT-IR (ν_{max}, cm^{-1}) 2928, 2817, 1648, 1585, 1488, 1337, 1011; ^{1}H NMR (400 MHz, $CDCl_3$) δ 7.33−7.48 (m, 5H), 6.68 (s, 1H), 6.33−6.50 (m, 2H), 4.39 (dd, J = 1.7, 18.5 Hz, 2H), 1.50 (dd, J = 4.8, 6.0 Hz, 2H), 1.35−1.44 (m, 2H); ^{13}C NMR (100 MHz, $CDCl_3$) δ 183.7, 182.8, 148.6, 148.5, 144.4, 134.0, 133.2, 132.8, 132.1, 131.7, 130.9, 124.5, 34.2, 33.8, 24.8, 24.7; HRMS (ESI-TOF) for $[C_{18}H_{14}O_2 + H]^+$ calcd 263.1072, found 263.1063.

6-(4-Methoxyphenyl)-1,4-dihydro-1,4-ethanonaphthalene-5,8-dione (28). Starting from **4a** (50 mg, 0.17 mmol), **28** was isolated as an orange semisolid (19 mg, 38%): FT-IR (ν_{max}, cm^{-1}) 2924, 1649, 1563, 1511, 1460, 1340, 1240, 1181, 1028; ^{1}H NMR (400 MHz, $CDCl_3$) δ 7.32−7.54 (m, 2H), 6.84−7.02 (m, 2H), 6.64 (s, 1H), 6.31−6.50 (m, 2H), 4.27−4.47 (m, 2H), 3.83 (s, 3H), 1.42−1.53 (m, 2H), 1.31−1.41 (m, 2H); ^{13}C NMR (100 MHz, $CDCl_3$) δ 184.1, 183.6, 161.1, 148.5, 148.3, 144.8, 134.0, 133.9, 131.0, 130.6, 125.7, 114.0, 55.4, 34.2, 33.7, 24.8, 24.7; HRMS (ESI-TOF) for $[C_{19}H_{16}O_3 + H]^+$ calcd 293.1177, found 293.1174.

6-(4-Acetylphenyl)-1,4-dihydro-1,4-ethanonaphthalene-5,8-dione (29). Starting from **8a** (50 mg, 0.16 mmol), **29** (31 mg, 62%) was isolated as a yellow semisolid: FT-IR (ν_{max}, cm^{-1}) 2929, 2872, 1682, 1650, 1602, 1460, 1359, 1268, 1142, 1041; ^{1}H NMR (400 MHz, $CDCl_3$) δ 7.91−7.99 (m, 2H), 7.51−7.56 (m, 2H), 6.72 (s, 1H), 6.40−6.44 (m, 2H), 4.35−4.43 (m, 2H), 2.61 (s, 3H), 1.49−1.54 (m,

dx.doi.org/10.1021/jo501796z | J. Org. Chem. 2014, 79, 9413−9417

2H), 1.37−1.41 (m, 2H); ^{13}C NMR (100 MHz, $CDCl_3$) δ 197.7, 183.6, 182.6, 148.6, 144.5, 137.8, 137.6, 134.0, 133.8, 132.9, 129.7, 128.5, 128.4, 128.3, 34.2, 33.8, 26.8, 24.8, 24.7; HRMS (ESI-TOF) for $[C_{20}H_{16}O_3 + H]^+$ calcd 305.1177, found 305.1172.

^{1}H NMR Experiment for Studying Enolization Potential. A stock solution of sodium deuteroxide (NaOD) in DMSO-d_6 was prepared by mixing 10 μL of 30 wt % NaOD in D_2O with 490 μL of DMSO-d_6. The ^{1}H NMR spectrum was recorded for **2** (10 mg) in DMSO-d_6 (0.6 mL) at 25 °C. To a solution of **2** in DMSO-d_6 (0.6 mL) was added 0.2 equiv of NaOD (10 μL from the aforementioned stock solution) at room temperature (25 °C), and after 15 min the ^{1}H NMR spectrum was recorded on a 400 MHz NMR spectrometer. By following similar experimental conditions the ^{1}H NMR experiments for **4**, **5**, **8**, and **10** were carried out.

Stability Studies using HPLC. A stock solution of compound (10 mM) was diluted to 1 mM in pH 7.4 phosphate buffer (100 mM)/acetonitrile ACN (1/1 ratio, v/v) and incubated at 37 °C over a period of 2−8 h. The reaction mixture was filtered (0.22 μm) and injected (25 μL) in a high-performance liquid chromatograph (HPLC) attached with a diode-array detector (the detection wavelength was 254 nm) and a Zorbax SB C-18 reversed-phase column (250 mm × 4.6 mm, 5 μm). A mobile phase of water/acetonitrile was used with a run time of 25 min: multistep gradient technology with a flow rate of 1 mL/min starting with 50/50 for 0−5 min, 40/60 for 5−10 min, 30/70 for 10−15 min, 20/80 for 15−20 min, 50.50 for 20−23 min, and 50/50 for 23−25 min.

Superoxide Detection by Luminol Assay.[32] 5-Amino-2,3-dihydro-1,4-phthalazinedione solution (Luminol, 4 mM) was prepared in 30 mM aqueous sodium hydroxide and stored under ice. To a microwell plate was added a stock solution of the compound (2 μL of 1 mM) to phosphate buffer (100 mM pH 8.0, 193 μL) followed by Luminol (5 μL, final 100 μM in 200 μL) in six repeats. The resulting mixture was incubated at 37 °C for 25 min, and chemiluminescence was measured using a microtiter plate reader.

Estimation of Hydrogen Peroxide.[33] A solution of the test compound (1 μL, 1 mM, 10 μM final concentration) was added to 25 mM pH 7.4 phosphate buffer (45 μL), and the mixture was incubated at 37 °C for 60 min. To the incubated reaction mixture was added 50 μL of a premixed solution of 10-acetyl-3,7- dihydroxyphenoxazine or Amplex Red (prepared by following the manufacturer's protocol from Invitrogen), and this mixture was incubated at room temperature for 25 min before measuring the fluorescence using a microtiter plate reader (excitation 550 nm; emission 590 nm).

■ ASSOCIATED CONTENT

Ⓢ Supporting Information

Tables and figures giving NMR spectra, HPLC traces, and yield data for **15**−**29**. This material is available free of charge via the Internet at http://pubs.acs.org.

■ AUTHOR INFORMATION

Corresponding Author

*E-mail for H.C.: harinath@iiserpune.ac.in

Notes

The authors declare no competing financial interest.

■ REFERENCES

(1) Fang, F. C. *Nat. Rev. Microbiol.* **2004**, *2*, 820.
(2) Finkel, T.; Holbrook, N. J. *Nature* **2000**, *408*, 239.
(3) Ernster, L.; Dallner, G. *Biochim. Biophys. Acta* **1995**, *1271*, 195.
(4) Trachootham, D.; Alexandre, J.; Huang, P. *Nat. Rev. Drug Discovery* **2009**, *8*, 579.
(5) Lopez-Lazaro, M. *Cancer Lett.* **2007**, *252*, 1.
(6) Szatrowski, T. P.; Nathan, C. F. *Cancer Res.* **1991**, *51*, 794.
(7) Bair, J. S.; Palchaudhuri, R.; Hergenrother, P. J. *J. Am. Chem. Soc.* **2010**, *132*, 5469.
(8) Dharmaraja, A. T.; Dash, T. K.; Konkimalla, V. B.; Chakrapani, H. *MedChemComm* **2012**, *3*, 219.
(9) Kohanski, M. A.; Dwyer, D. J.; Hayete, B.; Lawrence, C. A.; Collins, J. J. *Cell* **2007**, *130*, 797.
(10) Li, Y.; Zhang, W.; Niu, J.; Chen, Y. *ACS Nano* **2012**, *6*, 5164.
(11) Brynildsen, M. P.; Winkler, J. A.; Spina, C. S.; MacDonald, I. C.; Collins, J. J. *Nat. Biotechnol.* **2013**, *31*, 160.
(12) Dharmaraja, A. T.; Alvala, M.; Sriram, D.; Yogeeswari, P.; Chakrapani, H. *Chem. Commun.* **2012**, *48*, 10325.
(13) Dharmaraja, A. T.; Chakrapani, H. *Org. Lett.* **2014**, *16*, 398.
(14) Khodade, V. S.; Dharmaraja, A. T.; Chakrapani, H. *Bioorg. Med. Chem. Lett.* **2012**, *22*, 3766.
(15) Foti, J. J.; Devadoss, B.; Winkler, J. A.; Collins, J. J.; Walker, G. C. *Science* **2012**, *336*, 315.
(16) Khodade, V. S.; Sharath Chandra, M.; Banerjee, A.; Lahiri, S.; Pulipeta, M.; Rangarajan, R.; Chakrapani, H. *ACS Med. Chem. Lett.* **2014**, *5*, 777−781.
(17) Liu, Y.; Imlay, J. A. *Science* **2013**, *339*, 1210.
(18) Aitken, R. J.; Buckingham, D.; Harkiss, D. *J. Reprod. Fertil.* **1993**, *97*, 441.
(19) Boveris, A.; Martino, E.; Stoppani, A. O. M. *Anal. Biochem.* **1977**, *80*, 145.
(20) McCord, J. M.; Fridovich, I. *J. Biol. Chem.* **1968**, *243*, 5753.
(21) Rathore, R.; Kochi, J. K. *J. Org. Chem.* **1995**, *60*, 4399.
(22) Rathore, R.; Kumar, A. S.; Lindeman, S. V.; Kochi, J. K. *J. Org. Chem.* **1998**, *63*, 5847.
(23) Curreli, M.; Li, C.; Sun, Y.; Lei, B.; Gundersen, M. A.; Thompson, M. E.; Zhou, C. *J. Am. Chem. Soc.* **2005**, *127*, 6922.
(24) da Costa, G. M.; de Lemos, T. L. G.; Pessoa, O. D. L.; Monte, F. J. Q.; Braz-Filho, R. *J. Nat. Prod.* **1999**, *62*, 1044.
(25) De Rosa, S.; De Giulio, A.; Iodice, C. *J. Nat. Prod.* **1994**, *57*, 1711.
(26) Koren-Goldshlager, G.; Klein, P.; Rudi, A.; Benayahu, Y.; Schleyer, M.; Kashman, Y. *J. Nat. Prod.* **1996**, *59*, 262.
(27) Fujiwara, Y.; Domingo, V.; Seiple, I. B.; Gianatassio, R.; Del Bel, M.; Baran, P. S. *J. Am. Chem. Soc.* **2011**, *133*, 3292.
(28) Hansch, C.; Leo, A.; Taft, R. W. *Chem. Rev.* **1991**, *91*, 165.
(29) Sardella, D. J.; Heinert, D. H.; Shapiro, B. L. *J. Org. Chem.* **1969**, *34*, 2817.
(30) Campbell, R. D.; Gilow, H. M. *J. Am. Chem. Soc.* **1960**, *82*, 5426.
(31) Campbell, R. D.; Harmer, W. L. *J. Org. Chem.* **1963**, *28*, 379.
(32) Trung Pham, H.; Marquetty, C.; Pasquier, C.; Hakim, J. *Anal. Biochem.* **1984**, *142*, 467.
(33) Zhou, M.; Diwu, Z.; Panchuk-Voloshina, N.; Haugland, R. P. *Anal. Biochem.* **1997**, *253*, 162.
(34) Eastgate, M. D.; Buono, F. G. *Angew. Chem., Int. Ed.* **2009**, *48*, 5958.
(35) Porter, R. F.; Rees, W. W.; Frauenglass, E.; Wilgus, H. S.; Nawn, G. H.; Chiesa, P. P.; Gates, J. W. *J. Org. Chem.* **1964**, *29*, 588.
(36) Deb, A.; Manna, S.; Maji, A.; Dutta, U.; Maiti, D. *Eur. J. Org. Chem.* **2013**, *2013*, 5251.

Organic LETTERS

Letter

pubs.acs.org/OrgLett

A Small Molecule for Controlled Generation of Reactive Oxygen Species (ROS)

Allimuthu T. Dharmaraja and Harinath Chakrapani*

Indian Institute of Science Education and Research Pune, Dr. Homi Bhabha Road Pashan, Pune 411 008, Maharashtra, India

Supporting Information

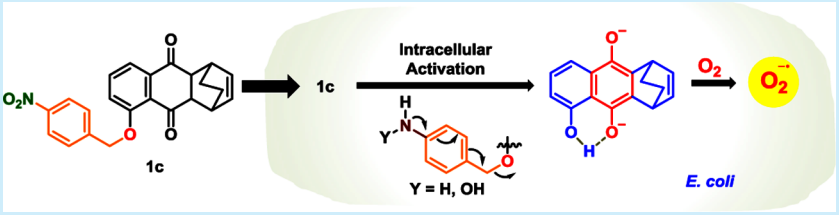

ABSTRACT: Due to the short half-life of reactive oxygen species (ROS) such as a superoxide radical, controlled and localized generation of ROS is challenging. Here, we report a rationally designed small-molecule **1c** that generates ROS only when triggered by a bacterial enzyme. We provide evidence for **1c** predictably enhancing the intracellular superoxide radical in a model bacterium. Spatiotemporal control over ROS generation offered by **1c** should help better understand stress responses in bacteria to increased ROS.

Nearly all organisms inadvertently produce superoxide $O_2^{\bullet-}$, by 1-electron transfer to oxygen during respiration.[1] $O_2^{\bullet-}$ is subsequently converted to hydrogen peroxide H_2O_2, which through the Fenton reaction generates the highly reactive $^{\bullet}OH$.[1] Together, these reactive oxygen species (ROS) can damage vital cellular components and are hence deployed by the immune system to counter infectious pathogens. Several recent studies have shown that ROS can sensitize infectious bacteria to clinical antibiotics suggesting the possible therapeutic utility for ROS. Due to a weak pipeline of antibiotics in preclinical development and the global emergence of antibiotic resistance, methodologies for selectively enhancing intracellular ROS including $O_2^{\bullet-}$ might help better understand[2] and evaluate the therapeutic potential of ROS.[3]

Due to its short life, $O_2^{\bullet-}$ must be produced *in situ* by reaction with oxygen for use in biochemical studies. Hence, either small organic molecules that spontaneously generate $O_2^{\bullet-}$ or enzymatic methods that process a substrate to generate $O_2^{\bullet-}$ are used.[4] For example, a combination of hypoxanthine and xanthine oxidase (X + XO) where hypoxanthine is metabolized by XO predominantly produces $O_2^{\bullet-}$ in the proximity of cells.[4] Any $O_2^{\bullet-}$ that is produced must diffuse across a lipid bilayer to exert its effects. However, $O_2^{\bullet-}$ is not highly permeable at neutral pH and such a method may not be useful for enhancing intracellular ROS.[5] Small molecules such as paraquat or menadione, which require bioactivation for $O_2^{\bullet-}$ production, have often been used but at elevated concentrations that can potentially complicate mechanistic interpretations (see Supporting Information, Chart S1).[3] Thus, a cell permeable small molecule that can predictably and exclusively increase $O_2^{\bullet-}$ within cells is not available. Herein, we report a small molecule that is activated by a bacterial enzyme to generate $O_2^{\bullet-}$ that is well suited to simulate increased ROS in bacteria.

5-(4-Nitrobenzyloxy)-1,4,4a,9a-tetrahydro-1,4-ethanoanthracene-9,10-dione (**1c**) was considered as a cell-permeable $O_2^{\bullet-}$ generator (Scheme 1).[6] The 4-nitrobenzyl group is a known substrate for *E. coli* nitroreductase (NTR), a commonly expressed oxygen-insensitive bacterial enzyme that reduces a broad range of aromatic nitro compounds to amines.[7] Reduction of the nitro group might lead to a rearrangement leading to the departure of **1a**, which has been previously reported to generate $O_2^{\bullet-}$ in ambient aerobic buffer through a keto−enol tautomerism as the first step (Scheme 1). Enolization of the carbonyls in **1a** is promoted by a proximal H-bonding hydroxyl group, and as a consequence, ROS generation by this compound was enhanced in comparison with an analogous benzylated derivative **1b** (Scheme 1). Hence, similarly in the case of **1c**, where intramolecular H-bonding is not possible, enolization is disfavored and this compound is predicted to be a poor $O_2^{\bullet-}$ generator in buffer.

Compound **1c** was synthesized from **1a** by reaction with 4-nitrobenzylbromide (Supporting Information, Scheme S1). During the incubation of **1c** in ambient aerobic buffer, increased $O_2^{\bullet-}$ was observed only in the presence of NTR as determined by a luminol-based chemiluminescence assay (Figure 1a and 1b).[8] An HPLC-based dihydroethidium (DHE) assay was used to independently assess $O_2^{\bullet-}$ production (Figure 1c). During incubation of **1c** in the presence of NTR, the nearly complete disappearance of DHE with concomitant formation of 2-hydroxyethidium (2-OH-E^+)

Received: November 15, 2013
Published: December 27, 2013

Scheme 1. Design of a Cell Permeable ROS Generator[a]

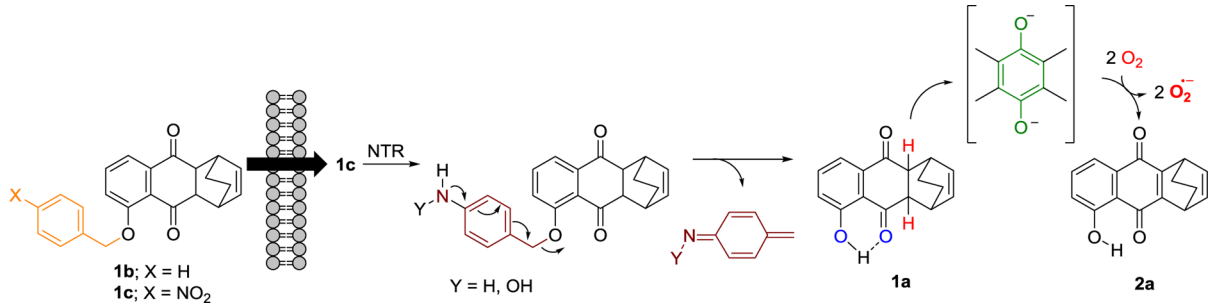

[a]The 4-nitrobenzyl derivative **1c** is a substrate for nitro reduction, which would convert **1c** to the active ROS producing **1a**. When this transformation is catalyzed by *E. coli* nitroreductase (NTR), exclusive intracellular accumulation of ROS is predicted.

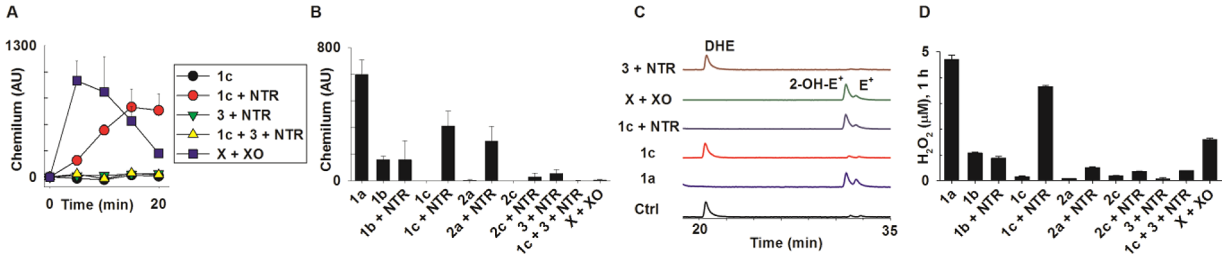

Figure 1. Estimation of ROS in ambient aerobic aqueous buffer. + NTR implies *E. coli* nitroreductase and NADPH; X + XO: hypoxanthine and xanthine oxidase were used. (a) Chemiluminescence measurement upon reaction with luminol as a measure of $O_2^{\bullet-}$ production was carried out with various compounds (10 μM) and combinations in pH 8.0 buffer. (b) Results of the above assay conducted after 30 min; (c) A HPLC-based dihydroethidium (DHE) assay was used to infer generation of $O_2^{\bullet-}$ after incubation of compounds (100 μM) in pH 8.0 buffer for 3 h. 2-Hydroxyethidium (2-OH-E^+), which is exclusively formed by the reaction of $O_2^{\bullet-}$ with DHE, elutes at 30.9 min, and ethidium E^+, which is formed by nonspecific oxidation of DHE, elutes at 31.7 min. (d) The amount of hydrogen peroxide generated during incubation of 10 μM of each compound in pH 7.4 was estimated using an Amplex Red fluorescence assay.

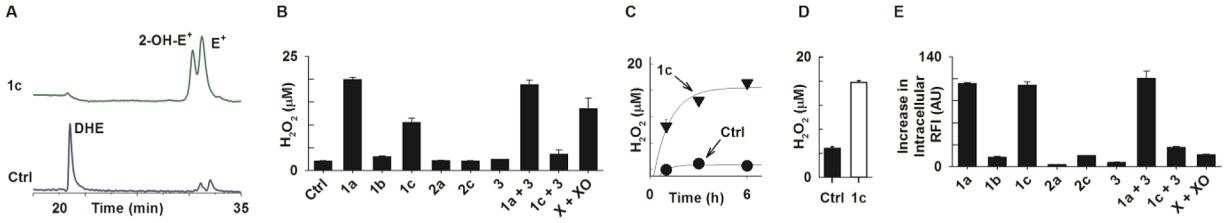

Figure 2. ROS generation during incubation with *E. coli*: (a) HPLC traces of assay for intracellular $O_2^{\bullet-}$ production using a hydroethidine (DHE) assay. Incubation with **1c** (250 μM) was for 30 min; DHE levels indicate unoxidized dye while 2-OH-E^+ formed is an indicator for $O_2^{\bullet-}$ production and E^+ is indicative of an increase in oxidative species. Ctrl: untreated bacteria. (b) Extracellular H_2O_2 generated during incubation of *E. coli* with compounds (100 μM) for 1 h was estimated using an Amplex Red fluorescence assay. Ctrl: untreated bacteria. (c) H_2O_2 generation during incubation of *E. coli* with **1c** (100 μM) was recorded during 6 h as described above. A first-order rate constant for ROS production was calculated as 0.96 h^{-1}. Ctrl: untreated bacteria. (d) *E. coli* treated with **1c** (100 μM) for 1 h; centrifugation and removal of the supernatant followed by resuspension of bacteria in fresh media. H_2O_2 generated after incubation of bacteria for 3 h was recorded as described above. Ctrl: untreated bacteria. (e) A 2,7-dichlorodihydrofluorescein-diacetate ($DCFH_2$-DA)-based fluorescence assay was used to estimate oxidative species generated intracellularly in *E. coli*. Increase in relative fluorescence intensity (RFI) with respect to DMSO (0.5%).

was observed, thus, confirming the intermediacy of $O_2^{\bullet-}$ (Figure 1c).[9] H_2O_2 is produced by $1e^-$ transfer to $O_2^{\bullet-}$, and we estimated H_2O_2 using an Amplex Red fluorescence assay.[10] In the absence of NTR, negligible H_2O_2 was produced during incubation of **1c** (10 μM), but in the presence of NTR, a yield of 3.65 μM H_2O_2 was recorded after 1 h (Figure 1d). 4-Nitrobenzyl benzoate **3** (Chart S1), which is a substrate for NTR but should not produce ROS during its metabolism by this enzyme, was synthesized using a reported procedure.[11] Compound **3** (100 μM) was metabolized by NTR, and as predicted no evidence for $O_2^{\bullet-}$ or H_2O_2 was found (Figure 1) indicating that possible products of metabolism of the 4-nitrobenzyl group were incapable of generating ROS. When **1c** and **3** (10 equiv) were coincubated in the presence of NTR, diminished $O_2^{\bullet-}$ and H_2O_2 were produced possibly due to inhibition of turnover of **1c** to **1a** (Figure 1). Under similar experimental conditions, the amounts of $O_2^{\bullet-}$ and H_2O_2 generated by **1a** and **1b** were consistent with previously reported data (Figure 1b and 1d).[6]

Next, the possibility of the use of **1c** as a tool for predictably enhancing intracellular $O_2^{\bullet-}$ in bacteria was examined. The production of $O_2^{\bullet-}$ in *E. coli* was estimated using a DHE assay that is selective for intracellular $O_2^{\bullet-}$ (Figure 2a).[9] The bacterial control showed unreacted DHE with negligible oxidized DHE (Figure 2a), but in the presence of **1c**, the formation of 2-OH-E^+ was observed with concomitant loss of DHE suggestive of

dx.doi.org/10.1021/ol403300a | Org. Lett. 2014, 16, 398−401

$O_2^{\bullet-}$ production intracellularly (Figure 2a). Due to the difficulty in accurately quantifying $O_2^{\bullet-}$ using the DHE assay, measurement of H_2O_2, which provides a quantitative basis for assessing ROS production, was carried out. During incubation of *E. coli* with **1c** (100 μM), a yield of 10.5 μM H_2O_2 after 1 h was recorded (Figure 2b). The formation of H_2O_2 was nearly completely abrogated when **1c** was cotreated with **3** (10 equiv), a substrate for intracellular nitroreductases including NTR (Figure 2b).

Treatment of *E. coli* with **3** did not increase H_2O_2 and this compound did not inhibit ROS generation by **1a** (Figure 2b), suggesting that **3** inhibited the metabolism of **1c** to **1a**. A time course for ROS generation during incubation of *E. coli* with **1c** showed an increase in H_2O_2 levels during 6 h, which is consistent with temporally controlled enhancement in intracellular ROS (Figure 2c).

Next, a series of experiments to test if **1c** was metabolized only intracellularly in bacteria to enhance levels of ROS were carried out. *E. coli* was incubated with **1c** for 1 h, which was followed by removal of media, and cells were resuspended in fresh media: under these conditions, any **1c** that does not permeate cells would be removed and any H_2O_2 produced would be due to intracellular activation. The difference in yields of H_2O_2 obtained during this experiment (Figure 2d) and during a bolus treatment of **1c** (Figure 2b) was minimal, which supports intracellular metabolism to produce ROS as the major pathway. Next, *E. coli* was grown overnight and the cell-free media was incubated with **1c**: any reductases secreted might activate **1c** to produce ROS. However, no significant increase in H_2O_2 was found even after 3 h suggesting that extracellular activation of **1c** was not important (see Supporting Information, Figure S3).

Next, the intermediacy of hydroxyl radical $^{\bullet}$OH was assessed by a supercoiled plasmid DNA cleavage assay. When cotreated with Fe(II), the ROS generator **1c** produced nicks only in the presence of NTR, supporting the use of this protocol for enhancement of ROS (Figure S4). For cellular assays, the ability of **1c** to increase intracellular oxidative species including $^{\bullet}$OH was studied.[12] Incubation of *E. coli* with dichlorofluorescein-diacetate, $DCFH_2$-DA, followed by treatment with **1c** resulted in an increased intracellular fluorescence attributable to oxidative species (Figure 2e).[13] In addition, formation of ethidium (E^+) in the DHE assay is suggestive of an increased oxidative intracellular environment caused by **1c** (Figure 2a).

Taken together, our data suggest that the use of **1c** predictably increases ROS in bacteria. Compound **1c** was next compared with the X + XO protocol. The time course of X + XO indicates that a burst of $O_2^{\bullet-}$ is produced while **1c** + NTR showed a gradual increase in ROS during this time period (Figure 1a). Thus, for biochemical studies, the use of **1c** + NTR might simulate gradual ROS production. In cell-based assays, the ability of X + XO to increase intracellular ROS was diminished in comparison with **1c** (see Supporting Information, Figure S1).[14] Thus, **1c** complements the existing repertoire of ROS generators while offering distinct advantages such as cell permeability and temporal control.

Two possible pathways for metabolism of **1c** to generate $O_2^{\bullet-}$ were considered (Scheme 2). First, NTR-induced reduction of the nitroaryl group should produce an amine or hydroxylamine, which might initiate a deprotection cascade to produce **1a** (Scheme 1). Under chemoreductive conditions ($Zn/HCOONH_4$) in pH 7.4 buffer, complete consumption of

Scheme 2. Proposed Mechanisms for ROS Generation during Incubation of 1c in Buffer in the Presence of NTR

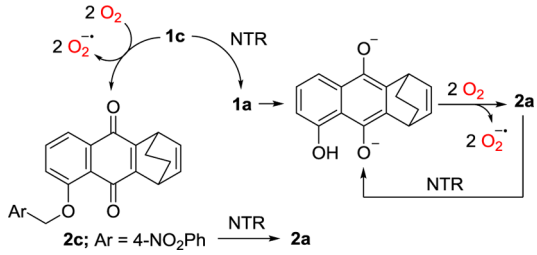

1c with concomitant formation of **1a** as the major product was observed (Figure S5).

Mass spectrometric analysis of this reaction mixture (Figure S6) revealed the formation of an amine and hydroxylamine byproducts (Scheme 1), which is consistent with a reduction–rearrangement cascade.[15] When **1c** was treated with NTR and NADPH, mass spectrometric analysis revealed the formation of **2a**, again consistent with the proposed mechanism.

Incubation of **1a** in aerobic buffer generated $O_2^{\bullet-}$ (Figure 1b and 1c) and produced **2a** as the major organic product (Figure S7). The role of intramolecular H-bonding is apparent in the large difference in the rate of conversion of **1c** to **2c** (<20% conversion after 18 h) and the oxidation of **1a** to **2a**, which was nearly complete in the same time period (Figure S7). The quinone **2a** is also a candidate for ROS generation in the presence of bioreductive enzymes including NTR. However, our cellular assays showed that **2a** did not produce ROS (Figure 2b and 2d) perhaps due to the diminished rates of redox cycling of this compound intracellularly.[16] This observation also implies that once **1a** converts to **2a**, no further ROS is produced suggesting that **1c** might produce up to 2 mol of $O_2^{\bullet-}$ per mol of compound (Scheme 2).[17] An alternate ROS producing pathway occurred during conversion of **1c** to **2c**, which in turn can be cleaved in the presence of NTR to produce **2a** (Scheme 2). If this was a major pathway, ROS generation from **1c** neither would depend on NTR nor should be inhibited by **3**. However, ROS generation by **1c** is significant only in the presence of NTR and was nearly completely inhibited by **3** in both test tube and cellular assays (Figures 1 and 2). In addition, the nitrobenzyl derivative **2c** was a poor ROS generator (Figures 1 and 2). Thus, ROS generation by direct conversion of **1c** to **2c** appears to be minor. Although biocatalytic reduction of **1c** by NTR requires NADPH as a cofactor, our observation that treatment of *E. coli* with **3** resulted in no significant increase of H_2O_2 (Figure 2b) suggests that such perturbations of NADPH levels (estimated millimolar concentrations) do not result in ROS generation.[18]

Recently, compounds that potentiate ROS in bacteria were proposed as adjuvants, which are small molecules that may not have significant antimicrobial properties themselves but when cotreated with antibiotics can reduce effective dosages and minimize side effects.[4,19] As few drug candidates with novel mechanisms are in the pipeline, the development of adjuvants assume importance.[18] The ROS generator **1c** did not inhibit *E. coli* growth (Table S5), but this compound significantly sensitized bacteria to aminoglycosides supporting possible applications of ROS as an adjuvant to this class of antibiotics (Table S6).[20]

In conclusion, we report that **1c** is capable of predictably increasing intracellular levels of ROS in a model bacterium. To our knowledge, this is the first report of a rationally designed

dx.doi.org/10.1021/ol403300a | *Org. Lett.* 2014, 16, 398–401

enzyme activated $O_2^{\bullet-}$ generator that is suitable for enhancing ROS in bacteria. It is anticipated that **1c** would facilitate the understanding of bacterial responses to ROS, mechanisms of antibiotic action, and the therapeutic potential of ROS. The use of **1c** to predictably enhance ROS in bacteria other than *E. coli* is expected to depend on the expression levels of NTR and on the uptake of this small molecule. These studies are underway in our laboratory.

■ ASSOCIATED CONTENT

Supporting Information

Synthesis, characterization data, assay protocols, and associated data. This material is available free of charge via the Internet at http://pubs.acs.org.

■ AUTHOR INFORMATION

Corresponding Author

*E-mail: harinath@iiserpune.ac.in.

Notes

The authors declare no competing financial interest.

■ ACKNOWLEDGMENTS

The authors thank IISER Pune and the Department of Biotechnology, Ministry of Science and Technology, India (BT/PR6798/MED/29/636/2012; BT/05/IYBA/2011) for financial support. A.T.D. acknowledges a research fellowship from the Council for Scientific and Industrial Research (CSIR).

■ REFERENCES

(1) (a) Fang, F. C. *Nat. Rev. Microbiol.* **2004**, *2*, 820. (b) Imlay, J. A. *Nat. Rev. Microbiol.* **2013**, *11*, 443. (c) Fang, F. C. *Nat. Biotechnol.* **2013**, *31*, 415.

(2) (a) Keren, I.; Wu, Y.; Inocencio, J.; Mulcahy, L. R.; Lewis, K. *Science* **2013**, *339*, 1213. (b) Liu, Y.; Imlay, J. A. *Science* **2013**, *339*, 1210. (c) Ezraty, B.; Vergnes, A.; Banzhaf, M.; Duverger, Y.; Huguenot, A.; Brochado, A. R.; Su, S. Y.; Espinosa, L.; Loiseau, L.; Py, B.; Typas, A.; Barras, F. *Science* **2013**, *340*, 1583.

(3) (a) Kohanski, M. A.; Dwyer, D. J.; Hayete, B.; Lawrence, C. A.; Collins, J. J. *Cell* **2007**, *130*, 797. (b) Foti, J. J.; Devadoss, B.; Winkler, J. A.; Collins, J. J.; Walker, G. C. *Science* **2012**, *336*, 315. (c) Brynildsen, M. P.; Winkler, J. A.; Spina, C. S.; MacDonald, I. C.; Collins, J. J. *Nat. Biotechnol.* **2013**, *31*, 160.

(4) (a) McCord, J. M.; Fridovich, I. *J. Biol. Chem.* **1968**, *243*, 5753. (b) Lynch, R. E.; Fridovich, I. *J. Biol. Chem.* **1978**, *253*, 4697. (c) Ingold, K. U.; Paul, T.; Young, M. J.; Doiron, L. *J. Am. Chem. Soc.* **1997**, *119*, 12364.

(5) (a) Korshunov, S. S.; Imlay, J. A. *Mol. Microbiol.* **2002**, *43*, 95. (b) Zenno, S.; Koike, H.; Tanokura, M.; Saigo, K. *J. Biochem.* **1996**, *120*, 736.

(6) Dharmaraja, A. T.; Alvala, M.; Sriram, D.; Yogeeswari, P.; Chakrapani, H. *Chem. Commun.* **2012**, *48*, 10325.

(7) (a) Zenno, S.; Koike, H.; Tanokura, M.; Saigo, K. *J. Biochem.* **1996**, *120*, 736. (b) Race, P. R.; Lovering, A. L.; Green, R. M.; Ossor, A.; White, S. A.; Searle, P. F.; Wrighton, C. J.; Hyde, E. I. *J. Biol. Chem.* **2005**, *280*, 13256.

(8) Trung Pham, H.; Marquetty, C.; Pasquier, C.; Hakim, J. *Anal. Biochem.* **1984**, *142*, 467.

(9) (a) Zhao, H.; Joseph, J.; Fales, H. M.; Sokoloski, E. A.; Levine, R. L.; Vasquez-Vivar, J.; Kalyanaraman, B. *Proc. Natl. Acad. Sci. U.S.A.* **2005**, *102*, 5727. (b) Zielonka, J.; Vasquez-Vivar, J.; Kalyanaraman, B. *Nat. Protoc.* **2008**, *3*, 8. (c) Georgiou, C. D.; Papapostolou, I.; Grintzalis, K. *Nat. Protoc.* **2008**, *3*, 1679.

(10) (a) Zhou, M.; Diwu, Z.; Panchuk-Voloshina, N.; Haugland, R. P. *Anal. Biochem.* **1997**, *253*, 162. (b) Khodade, V. S.; Dharmaraja, A. T.; Chakrapani, H. *Bioorg. Med. Chem. Lett.* **2012**, *22*, 3766−3769.

(11) Sharma, K.; Sengupta, K.; Chakrapani, H. *Bioorg. Med. Chem. Lett.* **2013**, *23*, 5964.

(12) Due to its extremely short half-life and indiscriminate reactivity, *in vivo* detection of the hydroxyl radical is challenging and the specificity of previously used fluorescence assays for $^{\bullet}$OH has been questioned (see ref 1c).

(13) Wardman, P. *Free Radical Biol. Med.* **2007**, *43*, 995.

(14) In cellular assays at comparable concentrations with menadione, despite several attempts, nonspecific decomposition of DHE without formation of 2-OH-E^+ or E^+ was observed (Figure S1).

(15) Attempts to isolate these amine byproducts were unsuccessful and instead produced **1a** or **2a** as the major product.

(16) The precise rationale for this observation is unclear, but steric hindrance might hamper the accessibility of the quinone ring to reductive enzymes.

(17) Intracellular ROS generation yield and rate are dictated by the efficiency and kinetics of metabolism of **1c** by NTR in *E. coli*.

(18) Kumar, S. R.; Imlay, J. A. *J. Bacteriol.* **2013**, *2*, 2.

(19) Ruben Morones-Ramirez, J.; Winkler, J. A.; Spina, C. S.; Collins, J. J. *Sci. Transl. Med.* **2013**, *5*, 190ra81.

(20) A Clinical and Laboratory Standards Institute (CLSI) recommended protocol was used to determine the minimum inhibitory concentration (MIC) against *E. coli* (Table S5). No significant inhibition of bacterial growth by **1c** was observed at elevated concentrations (MIC >100 μM) suggesting that perhaps ROS alone is well tolerated by *E. coli*. However, when gentamycin was cotreated with **1c** (50 μM), an 8-fold decrease in MIC for this antibiotic was observed suggesting that a lower antibiotic dosage was required to obtain similar efficacy.

MedChemComm

Cite this: *Med. Chem. Commun.*, 2012, **3**, 219

www.rsc.org/medchemcomm

CONCISE ARTICLE

Synthesis, thiol-mediated reactive oxygen species generation profiles and anti-proliferative activities of 2,3-epoxy-1,4-naphthoquinones†

Allimuthu T. Dharmaraja,[a] Tapan K. Dash,[b] V. Badireenath Konkimalla*[b] and Harinath Chakrapani*[a]

Received 14th September 2011, Accepted 17th October 2011
DOI: 10.1039/c1md00234a

Here, we report that thiol-mediated decomposition of 2,3-epoxy-1,4-naphthoquinones to generate peroxide, a reactive oxygen species (ROS), could be modulated by changing the substitution pattern on the aryl ring and the epoxide. Epoxides which generated higher amounts of peroxide upon reaction with thiols were better inhibitors of human leukaemia (THP1) cell proliferation.

1,4-Naphthoquinone-based epoxides are constituents of a number of natural products with medicinal properties.[1,2] For example, 2,3-epoxysesamone[3,4] and frenolicin[5–12] have shown anti-bacterial, anti-fungal and/or anti-proliferative activities (Fig. 1).

The biological activity of 2,3-epoxy-1,4-naphthoquinones is in part attributable to the reactivity of the epoxide ring towards nucleophiles.[13] For example, 2,3-epoxy-2,3-dihydro-1,4-naphthoquinone (**1a**) is a target for reaction with nucleophiles such as thiols.[14] Thiols such as glutathione (GSH) are critical for maintenance of redox homeostasis and depletion of thiols could induce cellular stress and trigger cell death.[15,16] Furthermore, under aerobic conditions, addition of GSH to **1a** has been shown to generate the reactive oxygen species (ROS) peroxide anion (O_2^{2-}) by redox cycling.[14] ROS such as peroxide, superoxide ($O_2^{\cdot-}$) and hydroxyl radical (˙OH) are generated during immune response to combat pathogens[17] and these reactive species cause cellular stress by damaging biomacromolecules such as proteins, DNA and lipids.[18–25] Recently, Vitamin K3-epoxide (Fig. 1) was shown to generate ROS intracellularly to induce oxidative stress in human glioma cells.[33]

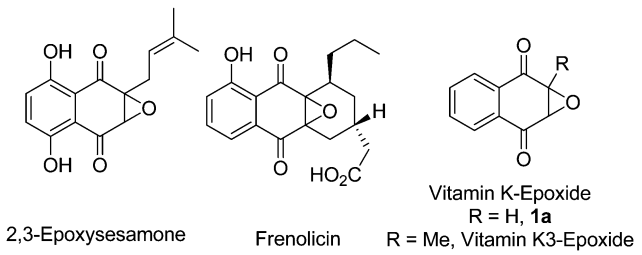

Fig. 1 Some naturally occurring 1,4-naphthoquinone-based epoxides.

The relationship between ROS and cancer is complex.[26–28] Several reports indicate that ROS prevented differentiation of certain cancers.[29,30] However, other studies show that ROS such as peroxide can inhibit proliferation of cancer cells by induction of apoptosis.[31,32] Here, we proposed to synthesize a series of 2,3-epoxy-1,4-naphthoquinones and evaluate their reactivity with biologically relevant nucleophiles, their ROS generation profiles, and their ability to inhibit human leukaemia cell proliferation. We hypothesized that modulating rates of epoxide-opening by systematic variation of substituents around the epoxide and the aryl ring of 2,3-epoxy-1,4-naphthoquinone could affect their propensity for reaction with nucleophiles, ROS generation profiles, and biological properties (Fig. 2). Introduction of an electron withdrawing group in proximity to the epoxide functionality of 2,3-epoxy-1,4-naphthoquinone could enhance the reactivity of the epoxide with nucleophiles and perhaps affect peroxide generation; conversely, an electron-donating group might diminish the rate of this process. A series of compounds with a range of peroxide generation profiles would permit us to study the effects of modulating rates of peroxide generation on *in vitro* human leukaemia cell proliferation.

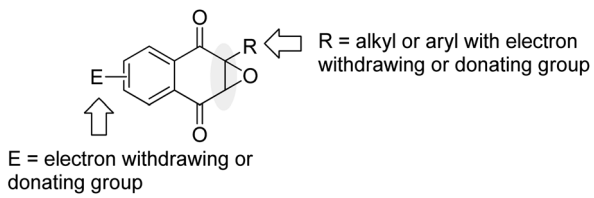

Fig. 2 Proposed scaffold for systematically modulating epoxide reactivity of quinone epoxides. E = electron withdrawing or donating groups; R = methyl or aryl groups.

[a]*Department of Chemistry, Indian Institute of Science Education and Research (IISER) Pune, Pune, 411 008, Maharashtra, India. E-mail: harinath@iiserpune.ac.in; Fax: +91-20-2589-9790; Tel: +91-20-2590-8090*
[b]*School of Biological Sciences, National Institute of Science Education and Research (NISER), Bhubaneswar, 751 005, Orissa, India. E-mail: badireenath@niser.ac.in; Fax: +91-674-230-4070; Tel: +91-674-230-4121*

† Electronic supplementary information (ESI) available: Compound characterization data and assay procedures with relevant plots. CCDC reference numbers [CCDC NUMBER(S)]. For ESI and crystallographic data in CIF or other electronic format see DOI: 10.1039/c1md00234a

2,3-Epoxy-1,4-naphthoquinones are synthesized by epoxidation of the corresponding 1,4-naphthoquinones.[34] 1,4-Naphthoquinone (**1**) was nitrated to produce 5-nitro-1,4-naphthoquinone (**2**) and 6-nitro-1,4-naphthoquinone (**3**) in 78% and 9% yields, respectively (Scheme 1).[35,36] An electron donating amino group on the aryl ring could be obtained by reduction of **2** with Sn/HCl to afford **4** in a nearly quantitative yield (Scheme 1).[37]

5-Hydroxy-1,4-naphthoquinone (juglone, **5**), which was synthesized using a reported reaction, was reacted with bromoethane in the presence of Ag_2O to afford **6** in 87% yield (Table 1, entry 1).[38] The reaction of **5** with benzyl bromides under similar conditions produced **7** and **8** in 98% and 96% yields, respectively (Table 1, entries 2 and 3). Menadione or Vitamin K3 (**9**) and plumbagin (**10**) were obtained from commercial sources. Benzylation of **10** produced **11** in 99% yield (Table 1, entry 4). Next, 2-phenyl-1,4-naphthoquinone was synthesized in 90% yield using a Pd-catalyzed Suzuki coupling of 2-bromo-1,4-naphthoquinone with phenylboronic acid (Table 2, entry 1).[39] Coupling of aryl boronic acids containing electron withdrawing groups with 2-bromo-1,4-naphthoquinone produced the desired products **13–15** in diminished yields in comparison with **12** (28–52%, Table 2, entries 2–4).[39–41] Compounds **16–19** with electron donating substituents on the aryl ring were isolated in yields ranging from 78 to 93% (Table 2, entries 5–8), which were comparable or better than the yield of **12** under similar reaction conditions.[39–41]

Epoxidation of **1** was carried out using sodium hypochlorite to produce the corresponding epoxide **1a** in 88% yield (Table 3, entry 1).[42] Compounds **2–8** were completely reacted in 30 min upon treatment with hypochlorite to produce the epoxides **2a–8a** in moderate to good yields (Table 3, entries 2–8).[43,44] X-Ray diffraction analysis of **5a** revealed the presence of intramolecular H-bonding between the 5-hydroxyl group and 4-carbonyl group (see the ESI†).

Quinones **9–11** were epoxidized with hypochlorite to produce the corresponding products **9a–11a** in yields ranging from 45 to 89% (Table 3, entries 9–11). 2-Phenyl-1,4-naphthoquinone was the slowest (120 min) in undergoing epoxidation in comparison with all other compounds prepared in this study (Table 3, entry 12). Other 2-aryl epoxides were synthesized in yields ranging from 52 to 93% (Table 3, entries 13–19). Additional evidence for the structure of **19a** was obtained by X-ray crystallographic analysis of this compound (see the ESI†).

Compound **1a** was reacted with various biologically relevant nucleophiles in pH 7.4 buffer. This compound was found to be reactive with thiols such as cysteine (Cys) and glutathione (GSH) with nearly 70% of **1a** decomposed within 5 min (Fig. 3). Compound **1a** was unreactive towards other amino acids (10 eq.) tested such as methionine, arginine and tyrosine with >90% of **1a**

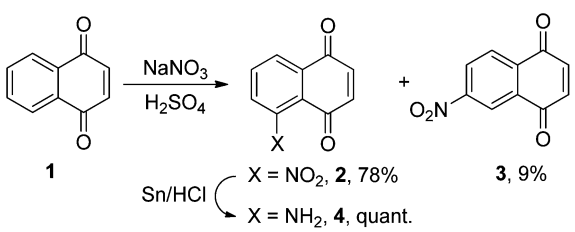

Scheme 1 Synthesis of **2**, **3** and **4**.

Table 1 Synthesis of derivatives of juglone (**5**) and plumbagin (**10**)

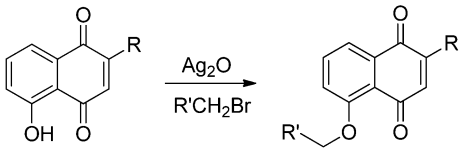

Entry	Quinone	R	R′	Product	Yield
1	**5**	H	Me	**6**	87
2	**5**	H	Ph	**7**	98
3	**5**	H	4-CF_3Ph	**8**	96
4	**10**	Me	Ph	**11**	99

remaining after 7 h. In the presence of 10 eq. of nucleobases, the epoxide was also nearly completely recovered after 24 h. Taken together, these results suggested that **1a** was highly selective towards reaction with thiols.

Next, in order to estimate the reactivity of other epoxides prepared in this study with thiols, we chose similar conditions as those used in our previous experiment with **1a** and glutathione (1 eq.). The 2,3-epoxy-2,3-dihydro-1,4-naphthoquinones **2a–8a** all reacted to varying extents under these conditions (Fig. 3). As predicted, an electron withdrawing nitro group enhanced the reaction rate with GSH (Fig. 3). In the case of **2a**, 12% remained after 5 min while 6% of **3a** remained during the same time period (Table 4, entries 2 and 3).

In the presence of an electron donating amino group (**4a**), the reaction rate was diminished in comparison with **1a** with 68% **4a** still remaining after 5 min (Table 4, entry 4). 26% of the juglone derivative **5a** remained after 5 min, which was comparable to **2a** suggesting that the hydroxyl group had no major effect on the modulating rate of epoxide opening (Table 4, entry 5). Replacement of the H in the hydroxyl with ethyl or benzyl groups (**6a**, **7a** or **8a**) resulted in diminished reactivity with GSH in comparison with **5a** or **1a** suggesting that the intramolecular H-bonding in **5a** played a role in accelerating epoxide opening by

Table 2 Synthesis of 2-aryl-1,4-naphthoquinones

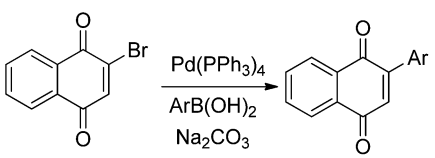

Entry	Ar	Product	Time/h	Yield (%)
1	Ph	**12**	1.5	90
2	3-NO_2Ph	**13**	12	28
3	4-AcPh	**14**	10	43
4	4-FPh	**15**	5	52
5	4-Me	**16**	10	78
6	2-OMe	**17**	24	82
7	3-OMe	**18**	7	93
8	4-OMe	**19**	7	81

Table 3 Synthesis of 2,3-epoxy-1,4-naphthoquinones

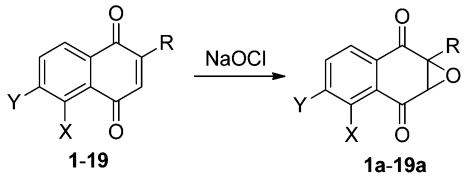

1-19 **1a-19a**

Entry	Quinone	Time/min	Epoxide	X	Y	R	Isolated yield (%)
1	**1**	5	**1a**	H	H	H	88
2	**2**	20	**2a**	NO_2	H	H	67
3	**3**	15	**3a**	H	NO_2	H	88
4	**4**	30	**4a**	NH_2	H	H	43
5	**5**	5	**5a**	OH	H	H	68
6	**6**	25	**6a**	OEt	H	H	68
7	**7**	15	**7a**	OBn	H	H	81
8	**8**	35	**8a**	$OCH_2(4\text{-}CF_3Ph)$	H	H	82
9	**9**	15	**9a**	H	H	Me	89
10	**10**	30	**10a**	OH	H	Me	65
11	**11**	60	**11a**	OBn	H	Me	45
12	**12**	120	**12a**	H	H	Ph	97
13	**13**	25	**13a**	H	H	$3\text{-}NO_2Ph$	81
14	**14**	30	**14a**	H	H	4-AcPh	74
15	**15**	20	**15a**	H	H	4-FPh	52
16	**16**	15	**16a**	H	H	4-Me	78
17	**17**	40	**17a**	H	H	2-OMe	82
18	**18**	25	**18a**	H	H	3-OMe	93
19	**19**	45	**19a**	H	H	4-OMe	81

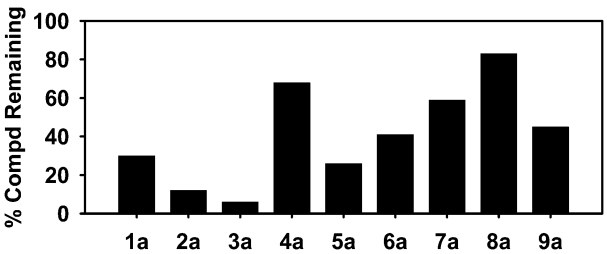

Fig. 3 Reactivity of 2,3-epoxy-1,4-naphthoquinones **1a–9a** towards thiols as measured by % compound remaining after 5 min of reaction with GSH (1 eq.) in pH 7.4 buffer.

GSH (Table 4, entries 6–8). Thus, these results suggested that although remote, substitution on the aryl ring appeared to have a significant effect on the rate of reactivity of the epoxide with thiols.

Addition of a methyl group at the 2-position of 2,3-epoxy-1,4-naphthoquinone (as in **9a**) resulted in diminution of reactivity with GSH (Table 4, entry 9; Fig. 4). This result was consistent with previous reports where the rate of reaction of **9a** with GSH was found to be diminished in comparison with **1a**. Addition of a 5-hydroxyl (**10a**) group to Vitamin K3-epoxide did not have a major effect on reactivity with thiols (Table 4, entry 10). However, the presence of a 5-benzyloxy group (**11a**) resulted in a diminution in reactivity with GSH with 94% of **11a** remaining after 5 min (Table 4, entry11).

Next, the effect of introduction of an aryl group on the 2-position of 2,3-epoxy-1,4-naphthoquinone on reactivity with thiols was studied. Reaction of **12a** with GSH in 5 min was comparable with that of **9a** under similar reaction conditions (Table 4, entry 12). An increased reactivity was seen in the case of electron withdrawing substituents on the aryl ring (Table 4, entries 13–15). Electron donating groups did not have a major effect on the reactivity of 2-aryl epoxides with thiols (Table 4, entries 16–19).

Reaction of **1a** with glutathione has been previously reported to generate peroxide through the intermediacy of quinol **1b**; reaction of **1b** with molecular oxygen produces peroxide and **1c** as the major organic product (Scheme 2).[14] In our hands, compound **1a** (100 μM) produced 4.4 μM peroxide during 30 min in the presence of 5 eq. GSH in aerobic pH 7.4 buffer supplemented with oxygen (Table 4, entry 1).[46] The presence of an electron withdrawing nitro substituent enhanced the amount of peroxide generated with **2a** producing 5.2 μM of peroxide (Table 4, entry 2). The 6-nitro derivative **3a**, which reacted the fastest with GSH amongst the analogues tested, produced 8.34 μM of peroxide under similar reaction conditions, which was nearly double the amount of peroxide generated by **1a** under similar conditions (Table 4, entry 3). The derivative **4a** with an electron-donating amino group produced diminished amounts of peroxide in comparison with **1a** (Table 4, entry 4). The juglone derivative **5a** formed 5.64 μM of peroxide in the same time period, which was comparable with peroxide generated from **2a** under similar conditions (Table 4, entry 5). Derivatives **6a–8a** with electron donating ether substituents produced negligible amounts of peroxide (Table 4, entries 6–8). Taken together, these results suggested that thiol-mediated peroxide generation profiles from 2,3-epoxy-2,3-dihydro-1,4-naphthoquinones can be modulated by changing substituents on the aryl ring (Fig. 4).

Table 4 Glutathione-mediated compound decomposition, peroxide yield upon reaction with GSH, *in vitro* anti-proliferative activity and calculated partition coefficients of 2,3-epoxy-1,4-naphthoquinones

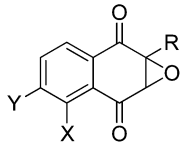

1a-19a

Entry	Compd	X	Y	R	% Compd remaining[a]	Peroxide yield/μM[b]	IC_{50}/μM[c]	*c* log *P*[d]
1	**1a**	H	H	H	30	4.40	6.3	0.44
2	**2a**	NO_2	H	H	12	5.20	3.6	0.21
3	**3a**	H	NO_2	H	6	8.34	2.3	0.21
4	**4a**	NH_2	H	H	68	1.68	>50	0.36
5	**5a**	OH	H	H	26	5.64	11.2	0.77
6	**6a**	OEt	H	H	41	1.68	9.6	1.10
7	**7a**	OBn	H	H	59	1.60	28	2.29
8	**8a**	$OCH_2(4\text{-}CF_3Ph)$	H	H	83	1.68	>50	3.18
9	**9a**	H	H	Me	45	1.52	13.6	0.35
10	**10a**	OH	H	Me	64	1.60	22.8	1.28
11	**11a**	OBn	H	Me	94	1.58	>50	2.81
12	**12a**	H	H	Ph	44	1.44	>50	2.13
13	**13a**	H	H	$3\text{-}NO_2Ph$	29	1.40	>50	1.88
14	**14a**	H	H	4-AcPh	16	1.36	>50	1.57
15	**15a**	H	H	4-FPh	32	1.36	11.7	2.27
16	**16a**	H	H	4-Me	66	1.48	20.4	2.63
17	**17a**	H	H	2-OMe	54	1.28	12.4	2.05
18	**18a**	H	H	3-OMe	43	1.46	>50	2.05
19	**19a**	H	H	4-OMe	37	1.40	11.6	2.05
20	Doxorubicin[e]	—	—	—	—	—	0.11	—

[a] Reaction of the compound with 1 eq. GSH was conducted in pH 7.4 and % compound remaining after 5 min was estimated using HPLC analysis. Values represented are an average of two independent runs. [b] The compound (100 μM) was reacted with 5 eq. GSH in the presence of oxygen and peroxide formed after 30 min of reaction was estimated using a xylenol orange-based colorimetric assay. Values represented are an average of two independent runs. [c] 50% Inhibitory activity of compounds was determined against human monocytic leukaemia THP1 cells using a standard cell viability assay. [d] Calculated using ChemBiodraw Ultra 12.0. [e] Reported value for IC_{50} of Doxorubicin against THP1 cells was 0.05 μM.[45]

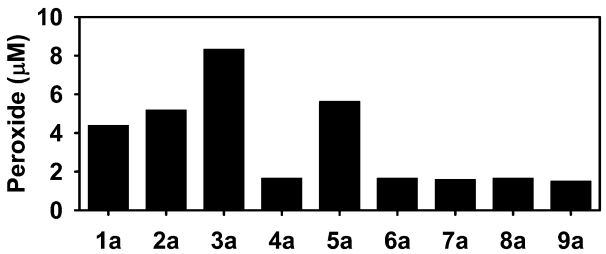

Fig. 4 Reaction of **1a–9a** (100 μM) with glutathione (5 eq.) and oxygen produced peroxide as estimated by a xylenol orange-based colorimetric assay. Peroxide measurement was done after 30 min.

However, rationalizing the differences in amounts of peroxide generated requires further characterization and study but a possible contributor to differences in peroxide levels would be the reactivity of an intermediate of type **1b** with oxygen, which might be affected by sterics and electronics of the aryl ring (Scheme 2).

Addition of GSH to **9a** produces **9c** as the major product; the mechanism proposed for the formation of **9c** was addition of GSH to form **9b**; elimination of water from **9b** produces **9c** as a major organic product (Scheme 3).[14,47] Peroxide generation from **9a** was reported as negligible in comparison with **1a** and the mechanism of peroxide generation is complicated and has been proposed to involve radical intermediates.[14] When we reacted **9a**

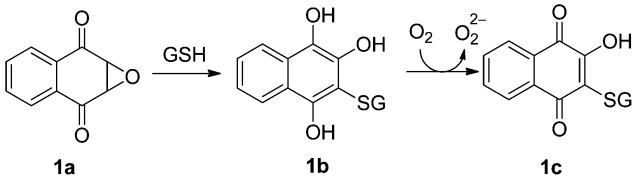

Scheme 2 2,3-Epoxy-2,3-dihydro-1,4-naphthoquinone reacts with thiols in the presence of oxygen to generate peroxide.

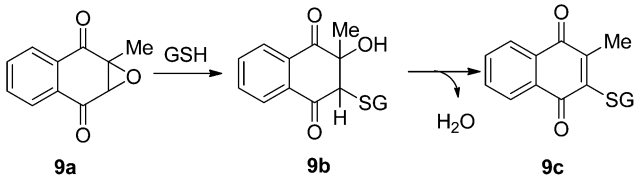

Scheme 3 2-Methyl-2,3-epoxy-1,4-naphthoquinone (**9a**) reacts with thiols to produce 2-methyl-3-glutathionyl-1,4-naphthoquinone (**9c**).

with GSH, we also found diminished amounts of peroxide formed in comparison with **1a** under similar reaction conditions (Table 4, entry 9; Fig. 4).

Furthermore, in all the cases tested, compounds with a substituent on the epoxide ring, irrespective of the nature of the substituent, produced negligible amounts of peroxide (Table 4, entries 10–19). Thus, 2-substituted 2,3-epoxy-1,4-naphthoquinones' biological effects might be primarily due to reactions with thiols whereas some of their corresponding 2,3-epoxy-2,3-dihydro-1,4-naphthoquinones might act by both thiol alkylation and peroxide generation.

Next, the efficacy of these compounds as anti-proliferative agents against THP1 human monocytic leukaemia cells[29,30] was determined using a standard cell viability assay.[48] Compound **1a** was found to be a good inhibitor of THP1 cells with IC_{50} determined as 6.3 μM (Table 4, entry 1). Compound **2a** which produced comparable amounts of peroxide and reacted faster with GSH than **1a** was found to have good anti-proliferative activity with IC_{50} of 3.6 μM (Table 4, entry 2). The most thiol-reactive 6-nitro derivative, **3a** which also produced the highest amount of peroxide, was the best inhibitor of proliferation of THP1 cells with an IC_{50} of 2.3 μM (Table 4, entry 3). The 5-amino derivative **4a** was found to be inactive at 50 μM (Table 4, entry 4). IC_{50}s of the juglone derivatives **5a–7a** ranged from 9.6 to 28 μM; **8a** was found to be inactive at 50 μM (Table 4, entries 5–8). 2-Substituted 2,3-epoxy-1,4-naphthoquinones were also tested for their ability to inhibit proliferation of THP1 cells (Table 4, entries 9–19). The IC_{50} for Vitamin K3-epoxide **9a** was found to be 13.6 μM (Table 4, entry 9). This IC_{50} value was comparable to the reported IC_{50} of 15.7 μM against human glioma cells.[33] The 2-aryl-derivatives were all marginally good or poor inhibitors of proliferation of THP1 cells (Table 4, entries 10–19).[49] Doxorubicin, a clinically used anti-cancer drug was used as a positive control in this assay; IC_{50} of this compound against THP1 cells was determined as 0.11 μM (Table 4, entry 20), which was comparable to a reported IC_{50} of 0.05 μM against the same cell line.[45]

An earlier study showed that in cultured human fibroblast cells, increased peroxide concentrations resulted in a higher proportion of cells in apoptosis.[50] Our study shows that compounds with enhanced peroxide generation in 30 min upon reaction with GSH were better inhibitors of leukaemia cell proliferation (Table 4, entries 1–3).[29] For example, **3a** was the best inhibitor in the series prepared and this compound also generated the highest amount of peroxide amongst the compounds studied in this work (Table 4). Compound **11a**, which was the least reactive amongst the compounds tested, did not show any inhibitory activity at 50 μM against THP1 cells (Table 4). Generation of ROS intracellularly in glioma cells leading to apoptosis with activation of ROS-dependent extracellular-regulated protein kinase (ERK) and c-Jun *N*-terminal kinase (JNK) was recently reported.[33] Thus, the inhibitory activity of epoxides prepared in this study might be due to peroxide-mediated apoptosis induction. Fosfomycin, a broad spectrum antibiotic used for the treatment of urinary tract infections, and terreic acid,[51–57] a quinone-based epoxide, were found to inhibit a bacterial cell wall biosynthetic enzyme, UDP-*N*-acetylglucosamine enol-pyruvyl transferase (or MurA) through covalent modification of Cys115-thiol by reaction with the epoxide group. Being catalytically active, modification of this cysteine resulted in inactivation of the enzyme and associated pathways. Thus modification of cysteine residues of proteins that could be critical for cell survival and growth might be a mechanism of action of the epoxides prepared in this study. Further mechanistic studies are currently underway to characterize molecular targets and study the possible role of ROS generation from these epoxides as mechanisms of stress induction in human leukaemia cells.

Table 5 *In vitro* anti-proliferative activities against human embryonic kidney 293 cells (HEK) and human monocytic leukaemia cells (THP1)

Entry	Compd	IC_{50} (μM, HEK)[a]	IC_{50} (μM, THP1)[b]	SI[c]
1	**1a**	18.9	6.3	3
2	**2a**	12.4	3.6	3.4
3	**3a**	55.4	2.3	24
4	Doxorubicin	0.7	0.11	6.4

[a] Human embryonic kidney 293 cells (HEK). [b] Human monocytic leukaemia (THP-1) cells. [c] IC_{50} (HEK)/IC_{50} (THP1).

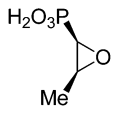

Fosfomycin

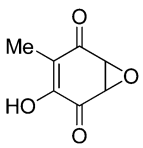

Terreic Acid

Finally, the anti-proliferative activity of compounds **1a–3a** against human embryonic kidney cells (HEK293) was determined: the IC_{50}s of **1a–3a** were in excess of 10 μM (Table 5, entries 1–3).

The compound with the best selectivity index, SI = IC_{50} (HEK)/IC_{50} (THP1), was **3a** whose SI was 24 suggesting that this compound was selective in inhibiting cancer cells. It is noteworthy that **3a** had a higher SI than Doxorubicin under similar assay conditions (Table 5, entry 4). Thus, we report several 2,3-epoxy-1,4-naphthoquinones with inhibitory potency higher than Vitamin K3-epoxide; in particular 6-nitro-2,3-epoxy-2,3-dihydro-1,4-naphthoquinone (**3a**) shows promise as an anti-cancer agent and future mechanistic studies will focus on this compound.

Acknowledgements

The authors thank IISER Pune, NISER Bhubaneshwar, and the Department of Science and Technology (DST) India for funding (grant number SR/FT/CS-89/2010). ATD acknowledges a research fellowship from Council for Scientific and Industrial Research (CSIR).

Notes and references

1 B. A. Adeniyi, M. F. Robert, H. Chai and H. H. Fong, *Phytother. Res.*, 2003, **17**, 282–284.
2 L. B. Alake, *Planta Med.*, 1994, **60**, 477.
3 T. Furumoto, *Biosci., Biotechnol., Biochem.*, 2009, **73**, 2535–2537.
4 A. F. Hasan, T. Furumoto, S. Begum and H. Fukui, *Phytochemistry*, 2001, **58**, 1225–1228.
5 Q. Li, C. Khosla, J. D. Puglisi and C. W. Liu, *Biochemistry*, 2003, **42**, 4648–4657.

6 D. C. Kossor, S. Han, F. W. Kemp, R. W. Slauter, D. Serota, D. Rajaskarian, N. Milner, A. Davidovich and J. D. Bogden, *J. Nutr.*, 2001, **131**, 3247–3250.
7 R. E. Armer, C. J. Dutton, B. R. Fenner, S. D. Greenwood, K. T. Hall and A. J. Rudge, *Bioorg. Med. Chem. Lett.*, 1998, **8**, 139–142.
8 M. J. Bibb, D. H. Sherman, S. Omura and D. A. Hopwood, *Gene*, 1994, **142**, 31–39.
9 K. Tsuzuki, Y. Iwai, S. Omura, H. Shimizu and N. Kitajima, *J. Antibiot.*, 1986, **39**, 1343–1345.
10 S. Omura, K. Tsuzuki, Y. Iwai, M. Kishi, S. Watanabe and H. Shimizu, *J. Antibiot.*, 1985, **38**, 1447–1448.
11 Y. Iwai, A. Kora, Y. Takahashi, T. Hayashi, J. Awaya, R. Masuma, R. Oiwa and S. Omura, *J. Antibiot.*, 1978, **31**, 959–965.
12 G. A. Ellestad, M. P. Kunstmann, H. A. Whaley and E. L. Patterson, *J. Am. Chem. Soc.*, 1968, **90**, 1325–1332.
13 M. H. Potashman and M. E. Duggan, *J. Med. Chem.*, 2009, **52**, 1231–1246.
14 A. Brunmark and E. Cadenas, *Free Radical Biol. Med.*, 1989, **6**, 149–165.
15 J. S. Armstrong, K. K. Steinauer, B. Hornung, J. M. Irish, P. Lecane, G. W. Birrell, D. M. Peehl and S. J. Knox, *Cell Death Differ.*, 2002, **9**, 252–263.
16 J. S. Armstrong and D. P. Jones, *FASEB J.*, 2002, **16**, 1263–1265.
17 H. J. Forman and M. Torres, *Am. J. Respir. Crit. Care Med.*, 2002, **166**, 4S–S8.
18 S. R. Atilano, M. Chwa, D. W. Kim, N. Jordan, N. Udar, P. Coskun, J. V. Jester, D. C. Wallace and M. C. Kenney, *Cornea*, 2009, **28**, 426–433.
19 K. Krohn, J. Maier and R. Paschke, *Nat. Clin. Pract. Endocrinol. Metab.*, 2007, **3**, 713–720.
20 N. H. Kim and J. H. Kang, *J. Biochem. Mol. Biol.*, 2006, **39**, 452–456.
21 R. Prasad, S. R. Kumar and S. Kumar, *Indian J. Exp. Biol.*, 2006, **44**, 377–380.
22 P. Daroui, S. D. Desai, T. K. Li, A. A. Liu and L. F. Liu, *J. Biol. Chem.*, 2004, **279**, 14587–14594.
23 C. Gonzalez, O. Najera, E. Cortes, G. Toledo, L. Lopez, M. Betancourt and R. Ortiz, *Environ. Mol. Mutagen.*, 2002, **39**, 33–42.
24 A. B. Petersen, R. Gniadecki, J. Vicanova, T. Thorn and H. C. Wulf, *J. Photochem. Photobiol., B*, 2000, **59**, 123–131.
25 W. J. Meehan, J. P. Spencer, D. E. Rannels, D. R. Welch, E. T. Knobbe and G. K. Ostrander, *Environ. Mol. Mutagen.*, 1999, **33**, 273–278.
26 H. Sauer, M. Wartenberg and J. Hescheler, *Cell. Physiol. Biochem.*, 2001, **11**, 173–186.
27 Y.-M. Go, J. J. Gipp, R. T. Mulcahy and D. P. Jones, *J. Biol. Chem.*, 2004, **279**, 5837–5845.
28 M. Sattler, T. Winkler, S. Verma, C. H. Byrne, G. Shrikhande, R. Salgia and J. D. Griffin, *Blood*, 1999, **93**, 2928–2935.
29 S. Kusmartsev and D. I. Gabrilovich, *J. Leukocyte Biol.*, 2003, **74**, 186–196.
30 Q. Ding, T. Jin, Z. Wang and Y. Chen, *J. Leukocyte Biol.*, 2007, **81**, 1568–1576.
31 M. Valko, C. J. Rhodes, J. Moncol, M. Izakovic and M. Mazur, *Chem.-Biol. Interact.*, 2006, **160**, 1–40.
32 S. S. Leonard, G. K. Harris and X. Shi, *Free Radical Biol. Med.*, 2004, **37**, 1921–1942.
33 J. Wu, C.-C. Chien, L.-Y. Yang, G.-C. Huang, M.-C. Cheng, C.-T. Lin, S.-C. Shen and Y.-C. Chen, *Chem.-Biol. Interact.*, 2011, **193**, 3–11.
34 A. Rashid and G. Read, *J. Chem. Soc. C*, 1967, 1323–1325.
35 D. W. Cameron, G. I. Feutrill and A. F. Patti, *Aust. J. Chem.*, 1980, **33**, 1805–1816.
36 N. Maugel and B. B. Snider, *Org. Lett.*, 2009, **11**, 4926–4929.
37 R. L. Betts, S. T. Murphy and C. R. Johnson, *Tetrahedron: Asymmetry*, 2004, **15**, 2853–2860.
38 M. Yoshizawa, Y. Takeyama, T. Okano and M. Fujita, *J. Am. Chem. Soc.*, 2003, **125**, 3243–3247.
39 M. T. Molina, C. Navarro, A. Moreno and A. G. Csaky, *Org. Lett.*, 2009, **11**, 4938–4941.
40 O. M. Demchuk and K. M. Pietrusiewicz, *Synlett*, 2009, **7**, 1149–1153.
41 A. J. Shand and R. H. Thomson, *Tetrahedron*, 1963, **19**, 1919–1937.
42 J. A. Valderrama, M. F. Gónzalez and C. Torres, *Heterocycles*, 2003, **60**, 2343–2348.
43 S. Colona, N. Gaggero, A. Manfredil, M. Spadoni, L. Casella, G. Carrea and P. Pasta, *Tetrahedron*, 1988, **44**, 5169–5178.
44 J. A. G. Valderrama, M. Florencia and T. Cristián, *Heterocycles*, 2003, **60**, 2343–2348.
45 P. Verhaeghe, N. Azas, M. Gasquet, S. Hutter, C. Ducros, M. Laget, S. Rault, P. Rathelota and P. Vanellea, *Bioorg. Med. Chem.Lett.*, 2008, **18**, 396–401.
46 Y. S. Cho, H. S. Kim, C. H. Kim and H. G. Cheon, *Anal. Biochem.*, 2006, **351**, 62–68.
47 I. Wilson, P. Wardman, T.-S. Lin and A. C. Sartorelli, *J. Med. Chem.*, 1986, **29**, 1381–1384.
48 D. A. Scudiero, R. H. Shoemaker, K. D. Paull, A. Monks, S. Tierney, T. H. Nofziger, M. J. Currens, D. Seniff and M. R. Boyd, *Cancer Res.*, 1988, **48**, 4827–4833.
49 J. Montoya, A. Varela-Ramirez, M. Shanmugasundram, L. E. Martinez, T. P. Primm and R. J. Aguilera, *Biochem. Biophys. Res. Commun.*, 2005, **335**, 367–372.
50 C. Bladier, E. Wolvetang, P. Hutchinson, J. de Haan and I. Kola, *Cell Growth Differ.*, 1997, **8**, 589–598.
51 H. Han, Y. Yang, S. H. Olesen, A. Becker, S. Betzi and E. Schonbrunn, *Biochemistry*, 2010, **49**, 4276–4282.
52 Y. Kawakami, S. E. Hartman, E. Kinoshita, H. Suzuki, J. Kitaura, L. Yao, N. Inagaki, A. Franco, D. Hata, M. Maeda-Yamamoto, H. Fukamachi, H. Nagai and T. Kawakami, *Proc. Natl. Acad. Sci. U. S. A.*, 1999, **96**, 2227–2232.
53 T. Subramanian, K. M. Namasivayam and E. R. Shanmugasundaram, *Toxicol. Lett.*, 1982, **10**, 249–253.
54 H. Yamamoto, K. Moriyama, H. Jinnouchi and K. Yagishita, *Jpn. J. Antibiot.*, 1980, **33**, 320–328.
55 J. C. Sheehan and Y. S. Lo, *J. Med. Chem.*, 1974, **17**, 371–372.
56 R. G. Owens, R. E. Welty and G. B. Lucas, *Anal. Biochem.*, 1970, **35**, 249–258.
57 G. Read, D. W. Westlake and L. C. Vining, *Biochem. Cell Biol.*, 1969, **47**, 1071–1079.

